The Influence of pH on the Binding of Immunoglobulin G to *Staphylococcal* Protein A

A thesis submitted in partial fulfilment of the requirements for the degree of Master of Engineering in Chemical and Process Engineering

Ben Thomas Plummer

University of Canterbury

2013

Abstract

The interaction between Protein A and Immunoglobulin G (IgG) was studied at a variety of pH values using a surface plasmon resonance (SPR) device, which provides real time kinetic data without labelling or molecular alteration. This study was carried out due to the large scale use of Protein A affinity chromatography for the purification of IgG for pharmaceutical purposes, and is one of the most costly steps in the purification process. The results produced were largely in line with those produced in previous literature with binding remaining strong between pH 7.4 and 5.0, although the association rate decreased as pH decreased. Below pH 5.0, the rate of IgG elution markedly increased, with pH 3.5 showing near full elution seconds after the association phase of the SPR interaction finished. Problems were encountered with non-specific binding between the SPR sensor chip and IgG occurring under a variety of conditions, requiring various remedies. However, no complete interactions were successfully carried out under pH 5.0, so the results obtained below this value were obtained by binding at pH 7.4 and then elution at the desired pH.

The data showed binding behaviour that was most successfully explained by a three-site model, each with a binding ratio of 1:1. The binding ratio is questionable given that Protein A and IgG typically bind at a ratio of 1:2 but may be explained by the sites being independent of one another and thus no secondary attachment is observed. A variety of models were fitted to the data but only two- and three-site models fitted the experimental data, with the three-site model being a more accurate and robust fit across pH changes. A multiple site model seems intuitively correct given the six different binding sites that Protein A has for interaction with IgG. The models produced have potential applications in a larger model of Protein A affinity chromatography, although a number of additional factors would need to be taken into account, such as mass transfer effects and the IgG concentration gradient.

Acknowledgements

I would like to thank Professor Conan Fee for his guidance and support throughout this project. I would also like to thank him for taking me on and giving me a project when I initially expressed my interest but lack of direction almost two years ago. Thanks to Dr. Simone Dimartino, who provided many insights from his time working with immunoglobulins and his upbeat manner always made for enjoyable to converse and work with him. Professor Giorgio Carta also has my gratitude for his groundwork and help at the beginning of the project.

Next, my parents need many thanks for their financial and emotional support for my return to study in a rather unstable city. I hope to be able to repay their investment in my six years of tertiary education soon. I also need to thank my brother for providing perspective and empathy during my study.

Finally, I need to thank Rayleen Fredericks-Short, without her help I would have been lost in the lab. My fellow postgraduates; Balaji, Kannan, Prasanna and Neha, also derserve thanks for their suggestions and support. The students and staff of Biology's fifth floor helped make my lunches more interesting, and more bizarre, for which I am grateful. My friends and girlfriend, Emma, helped keep my life in balance and gave me an outlet away from University, for which I am grateful.

Contents

Abstract i

Acknowledgements iii

Contents v

Abbreviations vii

List of Figures and Tables viii

Chapter 1: Introduction 1

1.1 Structure and Characteristics of Immunoglobulin G 1
1.2 Structure and Characteristics Of Protein A 3
1.3 Surface Plasmon Resonance 4
1.4 Protein A Affinity Chromatography 8
1.5 Project Objectives 11
1.6 Scope and Organisation of Thesis 11

Chapter 2: Literature Review 12

2.1 Protein A and Immunoglobulin G Interactions 12
2.2 Elution Conditions for Immunoglobulin G from a Protein A Affinity Column 13
2.3 Protein A Affinity Media Varieties 16
2.4 Immunoglobulin G Therapeutics 22
2.5 Industrial Production of Monoclonal Antibodies 24

Chapter 3: Modelling Equations and Programs 28

3.1 Reaction Equations 28
3.2 Langmuir Equations 30
3.3 Analysis Software 33

Chapter 4: Experimental Materials and Methodolgy 39

4.1 Materials and Equipment 39
4.2 Buffer and Sample Preparation 41
4.3 Initial Experiments for the Determination of Optimal Parameters 42
4.4 Kinetic Experiments 46

4.5 Low pH Experiments **46**

4.6 Data Analysis **46**

Chapter 5: Results **47**

5.1 Initial Optimisation Results **47**

5.2 Kinetic Experiment Results **51**

5.3 Immunoglobulin G Binding in PBST **58**

Chapter 6: Discussion **64**

6.1 HTG Chip Immobilisation and Interactions **64**

6.2 Models **66**

6.3 Experimental Conditions **68**

6.4 Kinetic Results **70**

6.5 Low pH Experiments **72**

Chapter 7: Conclusions **75**

Chapter 8: Recommendations **77**

Chapter 9: References **78**

Appendix A: Sample Models **81**

Appendix B: Full models used in Results **86**

B.1: Data from Kinetic Experiments **87**

B.2: Data From IgG in PBST Experiments **175**

Abbreviations

Anti-TNF	Anti-tumour necrosis factor
E. Coli	Escherichia Coli
EDAC	1-ethyl-3-(3-dimethylaminopropyl)carbodiimide
EDTA	Ethylenediaminetetraacetic acid
EGF	Epidermal growth factor (HER2 is an EGF)
ELISA	Enzyme-Linked Immunosorbent Assay
EMEA	European Medicines Agency
FDA	United States Food and Drug Administration
His-tag	Histidine tag made up of a long chain of histidines
HPLC	High Performance/Pressure Liquid Chromatography
IgG	Immunoglobulin G
mAb	Monoclonal antibody
MES	2-(*N*-morpholino)ethanesulfonic acid
MW	Molecular weight
NHS	N-hydroxy succinimide
PBST	Phosphate buffered saline with Tween-20
PEG	Polyethylene-glycol
ProA	Staphylococcal Protein A
RU	Resonance Units (the measurement unit of SPR devices)
SDS	Sodium dodecyl sulfate
SPR	Surface Plasmon resonance, may refer to device or phenomena

List of Figures and Tables

Figure 1.1: Basic structure of immunoglobulin G. 1) The Fab region. 2) The Fc region (constant region). 3) The heavy chain (blue). 4) The light chain (green). 5) Antigen binding site. 6) Hinge region. –S-S- indicates the disulfide bonds that hold the sections together. 2

Figure 1.2: The different subclasses of IgG in humans. 3

Figure 1.3: Structure of Z-domain an analogue of the B-domain (one of the five domains in protein A) used for IgG purification. 4

Figure 1.4: Schematic of the measuring element of an SPR device. 5

Figure 1.5: Indirect ligand binding via an antibody linker. 7

Figure 1.6: The three interaction stages using a SPR. A) Blank (buffer) stage. B) Association/interaction stage. C) Dissociation/elution stage. Each curve ("sensorgram") represents a different analyte concentration. 8

Figure 1.7: Basic setup and action of an affinity chromatography system. 9

Figure 2.1: IgG with significant regions labelled. 13

Table 2.1: The properties of Bio-rad's Protein A affinity media (1). 17

Table 2.2: The properties of Millipore's Protein A affinity media (2, 3). 18

Table 2.3: The properties of GE's Protein A affinity media (4). 18

Table 2.4: The properties of Invitrogen's Protein A affinity media (5). 19

Table 2.5: Pierce Protein A media properties (6). 20

Table 2.6: Hahn et al chosen Protein A media (7). 21

Table 2.7: Approved and commercialised mAb therapeutics (8). 23

Table 2.8: mAb manufacturing facilities size and cost between 2000 and 2009 (9). 25

Figure 2.2: mAb facility production size from 2000-2009 (9). 26

Figure 2.3: Basic process for purification of pharmaceutical mAbs (10). 27

Table 2.9: Cost of mAb production (10). 27

Table 2.10: Breakdown of mAb purification costs based on unit operation and materials (10). 27

Figure 3.1: A bivalent model of IgG and Protein A using ProteOn software. The data is a dilution series (each step is half the previous) of IgG and a blank. The dashed lines are the model. 34

Figure 3.2: Data output screen of Scrubber. 35

Figure 3.3: A screenshot of a ClampXP optimised model of the interaction between IgG and Protein A. 36

Figure 3.4: A visual flow diagram from Stella for the interaction mechanism between IgG and Protein A. 38

Figure 4.1: The ProteOn XPR36. 1) The chip. 2) Sample chamber containing rack and autosampler. 3) Running Buffer Chamber. 40

Figure 5.1: An example of the data initially obtained from the GLC chip. Protein A immobilised at 0.5 µg/ml and IgG injected at 160 µg/ml. 48

Figure 5.2: Non-specific binding of IgG across all channels on the HTG chip; only Flow cell 1 had Protein A immobilised on it. 49

Figure 5.3: IgG-Protein A interaction on the HTG chip with 20 mM imidazole in PBST (pH7.4). A simple first order model was used because this best fitted the action. 49

Figure 5.4: Three different flow rates of IgG interacting with Protein A in uniform conditions. 50

Figure 5.5: A 2:1 binding ratio (IgG:Protein A) model, single site. Red is the model, black the data. 52

Figure 5.6: A good two-site (on the Protein A) model with single-binding. Red is the model, black the data. 52

Figure 5.7: Another two-site model but not as accurate as in Figure 5.6. Red is the model, black is the data. 53

Figure 5.8: Three-site, single-binding model using the same data as Figure 5.5. Red is the model, black is the data. 53

Figure 5.9: The three-site model, single-binding, using the same data as Figure 5.6. Red is the model, black is the data. 54

Figure 5.10: Two-site, dual-binding model. Red is the model, black is the data. 54

Figure 5.11: Association/adsorption constant for IgG-Protein A interactions in running buffer. ka1 is the highest and ka3 the smallest in the set of three constants obtained from each interaction. 55

Figure 5.12: Dissociation constant for IgG-Protein A interactions in running buffer. kd1, kd2 and kd3 are the dissociation rates that go with ka1, ka2 and ka3 respectively. 56

Figure 5.13: Rate constants for IgG-Protein A interactions in running buffer. K1, K2 and K3 represent ka1, ka2 and ka3 respectively. 56

Figure 5.14: Average of all the association constants in each separate run and each pH. 57

Figure 5.15: Average of all dissociation constants in each separate run and each pH. 57

Figure 5.16: Average of all rate constants for each separate run and each pH. 58

Figure 5.17: Dissociation constants for IgG-Protein A interactions binding in PBST (pH 7.4). kd1, kd2 and kd3 are the dissociation rates that go with ka1, ka2 and ka3 respectively. 59

Figure 5.18: Rate Constants for IgG-Protein A interactions binding in PBST (pH 7.4). K1, K2 and K3 represent ka1, ka2 and ka3 respectively. 59

Figure 5.19: Average of dissociation constants per run and pH for IgG in PBST (pH7.4). 60

Figure 5.20: Average of rate constants per run and pH for IgG in PBST (pH 7.4). 60

Figure 5.21: Protein A-IgG interaction at pH 4.5 with IgG in PBST at pH 7.4. Data is black, model is red. 61

Figure 5.22: Protein A-IgG interaction at pH 4.0 with IgG in PBST at pH 7.4. Data is black, model is red. 62

Figure 5.23: Protein A-IgG interaction at pH 3.5 with IgG in PBST at pH 7.4. Data is black, model is red. 62

Figure 5.24: A-IgG interaction at pH 3.0 with IgG in PBST at pH 7.4. Data is black, model is red. 63

Figure A.1: The Stella model from Figure 3.4 reproduced for ease of use. 82

Figure A.2: Screen shot of an Excel model. 83

Figure A.3: A screen shot of the Model tab in ClampXP. 84

Figure A.4: A screen shot of the Data tab in ClampXP. 85

Figures B.1 to B.128: Run [run number], channel [channel number] model and graph. 87-213

Tables B.1 to B.128: Run [run number], channel [channel number] model parameters. 87-213

Chapter 1: Introduction

Monoclonal antibodies, particularly Immunoglobulin G, are used extensively in the treatment of a variety of diseases in both humans and animals, including bowel, lung and breast cancer as well as Crohn's disease and rheumatoid arthritis. Monoclonal antibodies can be produced in a variety of ways, with mammalian cell culture the most popular current method, while transgenic plants and animals showing promise for the future. Regardless of how the mAb is produced it is generally expressed at low concentrations and in the presence of a large number of impurities. Protein A (or Protein A fragment) affinity chromatography is almost universally used as one of the first steps in mAb purification due to its high specificity and yields, removing the majority of impurities in a single step. However, Protein A chromatography is expensive with the media costing upwards of NZ$10,000 per litre. IgG is also highly valuable with production costs exceeding $1000 per gram in some circumstances. Given these costs and the benefits that IgG therapeutics possess any improvement on the purification is of great value. An unfortunate side-effect of the strong affinity between Protein A and IgG is that harsh conditions, usually low pH, are required for elution, which can damage IgG. The IgG is highly valuable given due to the high production costs and thus minimising the loss of IgG in the process is crucial to decreasing the price of these potentially life-saving drugs. Therefore it is the aim of this research is to better understand the effects of pH, and to a lesser extent salt concentration, on the binding between IgG and Protein A.

1.1 Structure and Characteristics of Immunoglobulin G

IgG is produced both in human and animals by white blood cells and makes up 75% of the antibodies in human serum. IgG is a simple antibody in the form of a Y-shape as shown in Figure 1.1, with the various different regions labelled. IgG is made up of four polypeptide chains, two identical heavy chains of approximately 50 kDa (60 kDa for IgG3) and two identical light chains of 25 kDa to make up the full 150 kDa (170 kDa for IgG3) structure(11). The chains are held together by disulfide bonds and non-covalent interactions (such as hydrogen bonds and electrostatic interactions). The antigen binding site (region 3 in Figure 1.1) is altered to fit receptors on pathogenic cells by the immune system. This allows IgG to be used to target an almost unlimited variety of diseases, which has resulted in the production of IgG grow every year since its potential was first discovered. The Fc region can

also be removed (leaving only the Fab fragment) or have other molecules attached to provide different therapeutic effects without affecting the binding mechanism between the IgG and pathogen.

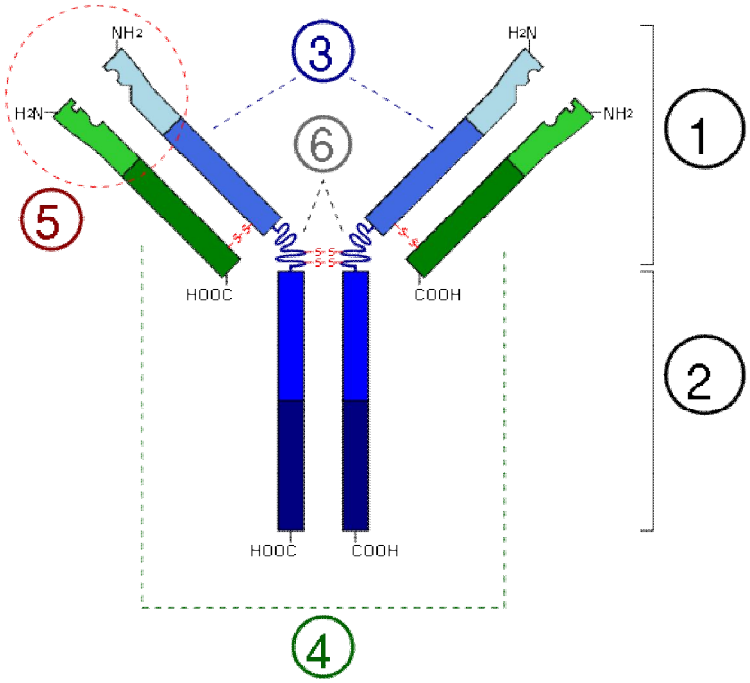

Figure 1.1: Basic structure of immunoglobulin G. 1) The Fab region. 2) The Fc region (constant region). 3) The heavy chain (blue). 4) The light chain (green). 5) Antigen binding site. 6) Hinge region. –S-S- indicates the disulfide bonds that hold the sections together.

There are four human IgG subclasses known as IgG1 to IgG4 and their structures shown are in Figure 1.2. They are named based on their abundance in human serum, e.g. IgG1 is the most abundant and IgG4 is the least abundant. The Fc (constant) region is 95% similar across all subclasses allowing most IgG to be purified by Fc region interactions, such as those that occur with Protein A (11). IgG3 shows the greatest structural variation with the heavy chains each being 10 kDa larger which affects the Fc region binding, causing IgG3 to have no significant interaction with protein A.

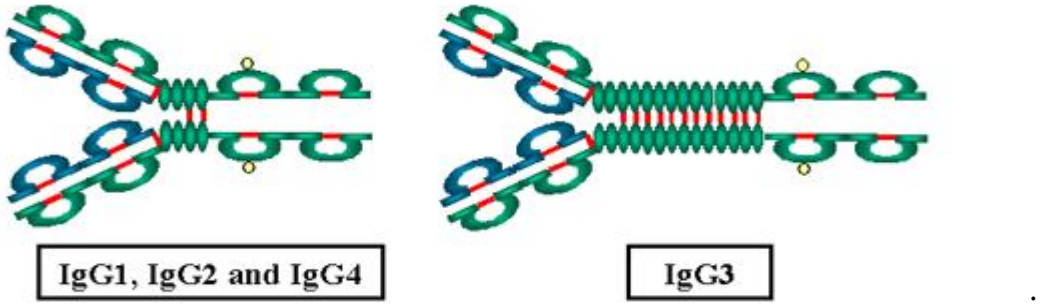

Figure 1.2: The different subclasses of IgG in humans.

1.2 Structure and Characteristics of Protein A

Protein A is a cell wall protein found on the pathogenic bacteria *Staphylococcus Aureus*. The reasons for the strong affinity between IgG and Protein A is that *Staphylococcus Aureus* produces Protein A as a counter-measure against IgG to thwart the immune response against the *Staphylococcus* (12). Protein A is a 42 kDa (13) or 56 kDa (14) consisting of four (13) or five (15) repeating regions (known as the A-E domains) that bind to the Fc region of IgG. The D domain also shows some limited Fab binding (16) through weak interactions with the heavy chain, although this interaction is considerably weaker than the Fc-binding interactions (17). The multiple binding sites ensure that regardless of the method of surface immobilisation it will always be able to bind IgG. Protein A shows an extended shape containing a number of α-helices (13), shown in Figure 1.3, which allows it to bind two IgG molecules when in solution (18, 19), despite being around one-third the size of IgG. The repeating units are highly homologous, showing similar amino acid sequences and allowing each unit to bind with the Fc region on IgG (20). These units also show multiple binding sites for the cell wall of *Staphylococcus Aureus* as expected.

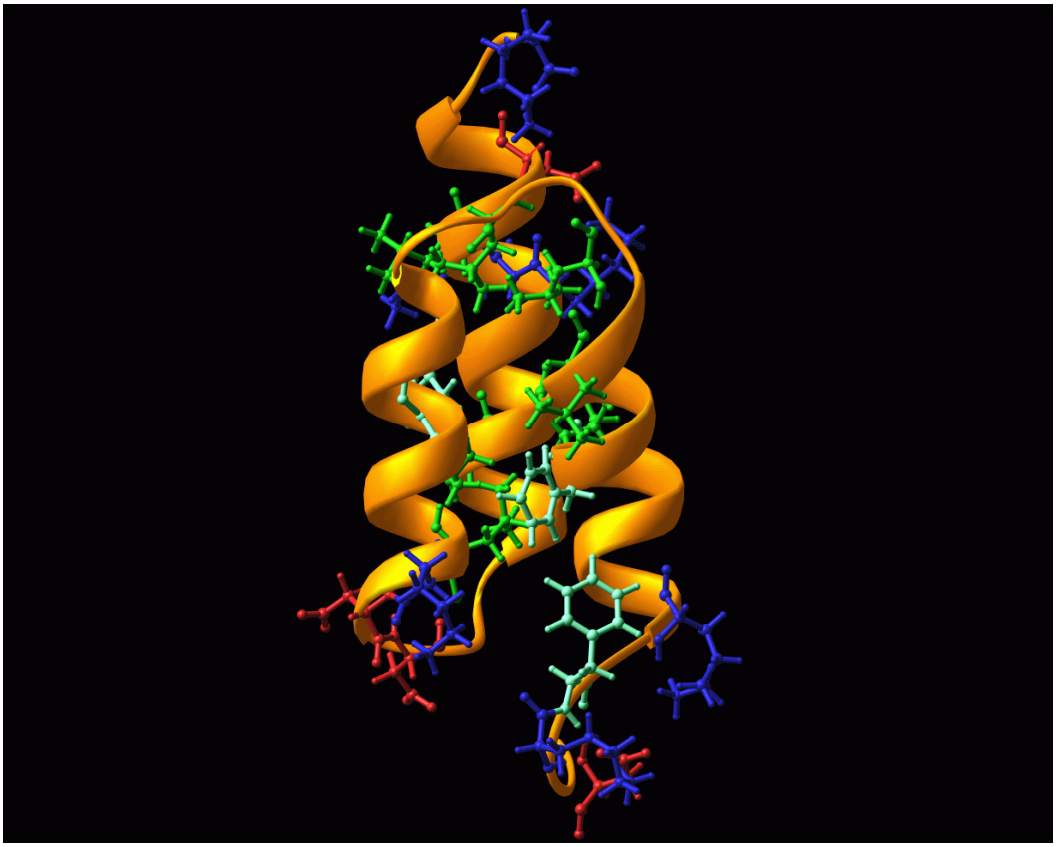

Figure 1.3: Structure of Z-domain an analogue of the B-domain (one of the five domains in protein A) used for IgG purification.

Protein A has a number of other properties that make it a useful tool in affinity chromatography. It is stable over a wide range of pH (2-11) and is able to refold after treatment with a denaturating agent like guanidine or urea (21). It is easy to produce, either via cultures of the native *Stapholoccocus Aureus* or by recombinant cultures of *E. Coli*. Protein A also holds up well when cleaned with 0.5 M sodium hydroxide, showing only a minor loss of activity and no increase in leakage into the eluate (22). This stability ensures Protein A's use in affinity chromatography, because long-term repeated use is an important economic consideration when it comes to purification methods, particularly high-cost ones like affinity chromatography.

1.3 Surface Plasmon Resonance

For this research a ProteOn™ XPR36 (Bio-Rad Laboratories, Hercules, CA, USA) protein interaction array system was used to measure the interactions between the IgG and Protein A in real time without any markers or alteration to the molecules. This system is a surface

plasmon resonance (SPR) device that uses polarised light to measure molecule interactions on a metallic surface (23, 24), allowing for real time reaction kinetics to be determined with a high level of accuracy. The system uses a setup similar to HPLC (making it a good analogue for this project) with a stationary phase of surface bound molecules (the ligand) interacting with another molecule (the analyte) in a mobile liquid phase. The ligand is bound on a thin metallic (usually gold but silver and aluminium can also be used) surface that sits atop a glass prism. The light from the device passes through one edge of the prism, before reflecting off the metal surface and exiting out the other side of the prism. A diagram of the chip setup and operation is shown in Figure 1.4.

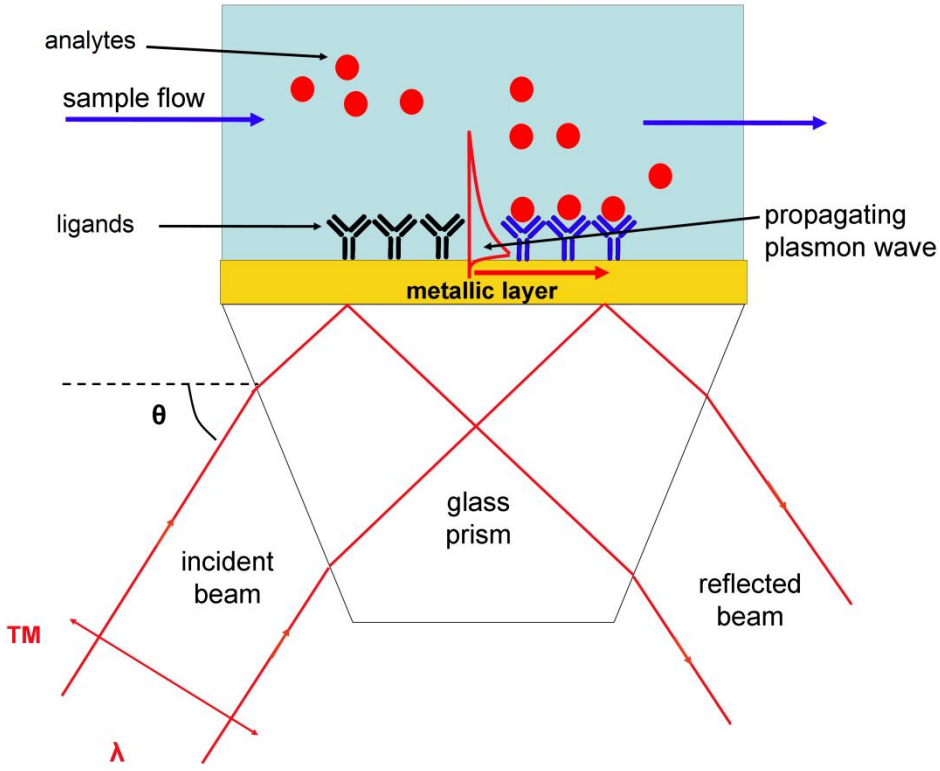

Figure 1.4: Schematic of the measuring element of an SPR device.

SPR devices work by emitting the polarised light at an exact angle (shown as θ in Figure 1.4) and measuring the reflected beam over a range of angles. The change in the angle of the lowest intensity of reflected light is proportional to the change in refractive index, which is affected by the amount of molecules within 200 nm of the metallic surface (24). This is caused by the SPR phenomena; when light strikes a thin metallic surface some of the energy is transferred to the surface, creating a plasmon wave (23). The amount of energy absorbed is affected by the conditions on the other side of the metallic surface. The prism is used to

increase the wave number of the light and hence the light impulse to generate a greater response. This is all carried out via computer allowing for the highest level of precision and the ability to take multiple readings per second for extremely accurate data. The output data is given as response units (RU) which can be converted into concentration by the following equation (25):

$$\gamma = \frac{R * 10^{-6}}{MW}$$

where: γ = Surface concentration on chip (mol/m^2)

R = Response (RU)

MW = Molecular weight (g/mol)

The ligand is not directly bound to the metallic layer, as in most cases that would greatly reduce the functionality in reactions of the ligand. An alginate, dextran or polyethylene-glycol layer (26) is generally employed to provide the binding surface for the ligand. The ligand is most frequently bound by direct coupling with the polymer layer via amine, carbohydrate or thiol coupling. However direct bonding can reduce activity as the binding is usually non-specific and can hinder analyte access to reaction sites. A number of indirect binding systems exist, including histidine-tag binding that works in the same way as immobilised metal affinity chromatography, or using antibodies as a linker molecule to ensure the ligand is perfectly positioned, as shown in Figure 1.5.

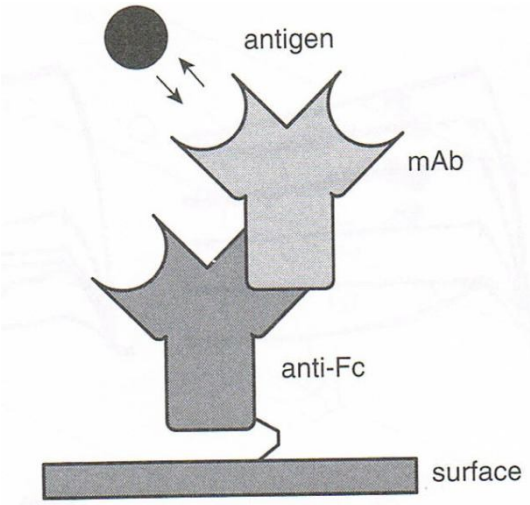

Figure 1.5: Indirect ligand binding via an antibody linker.

SPR is an effective system for measuring molecular interactions for a number of reasons. As previously mentioned SPR devices provide real time data, giving a complete picture of how the reaction is occurring, unlike ELISA or a simple reaction vessel, where only snapshots of the reaction can be taken. The other advantage of the SPR system is that no modification of the molecules is required, unlike systems that use fluorescence, which means the interaction between the ligand and analyte will match normal reaction conditions as closely as possible. The downside of this is that SPR lacks specificity and any molecule that adheres to the surface will generate a response. This necessitates careful preparation of samples to ensure as little chance of impurities as possible. The alginate layer causes the interactions to inexactly replicate surface binding, while also not perfectly replicating free solution binding. However, previous studies have found that, within experimental error, SPR methods replicate free solution methods (16). The final advantage of SPR is that it can monitor a number of interactions at the same time, the XPR36 allows six different ligands to be bound onto their own individual channel and six analytes to be passed across at one time hence allowing a possible 36 interactions at once. Other commercially available systems have a similar number of interaction sites but some go as high as 400 sites (Biacore Flexichip Kinetic Analysis system, Little Chalfont, United Kingdom).

Each interaction performed on the SPR follows a specific form made up of three stages, as shown in Figure 1.6. The first step is simply to run some buffer over the chip to establish a

baseline, which forms the basis for comparison with the remaining steps. In the second stage (association/binding stage) the analyte sample is injected across the chip and the interaction occurs, with the flow rate and length of injection controlled by the user. The final stage (dissociation/elution stage) returns the chip to running buffer for a user-defined amount of time. The association and dissociation phases are used to determine the kinetics of the interaction. The regeneration and blank steps that are used between interactions follow a similar form, with the sample injection between to buffer stages (although they are generally equally short).

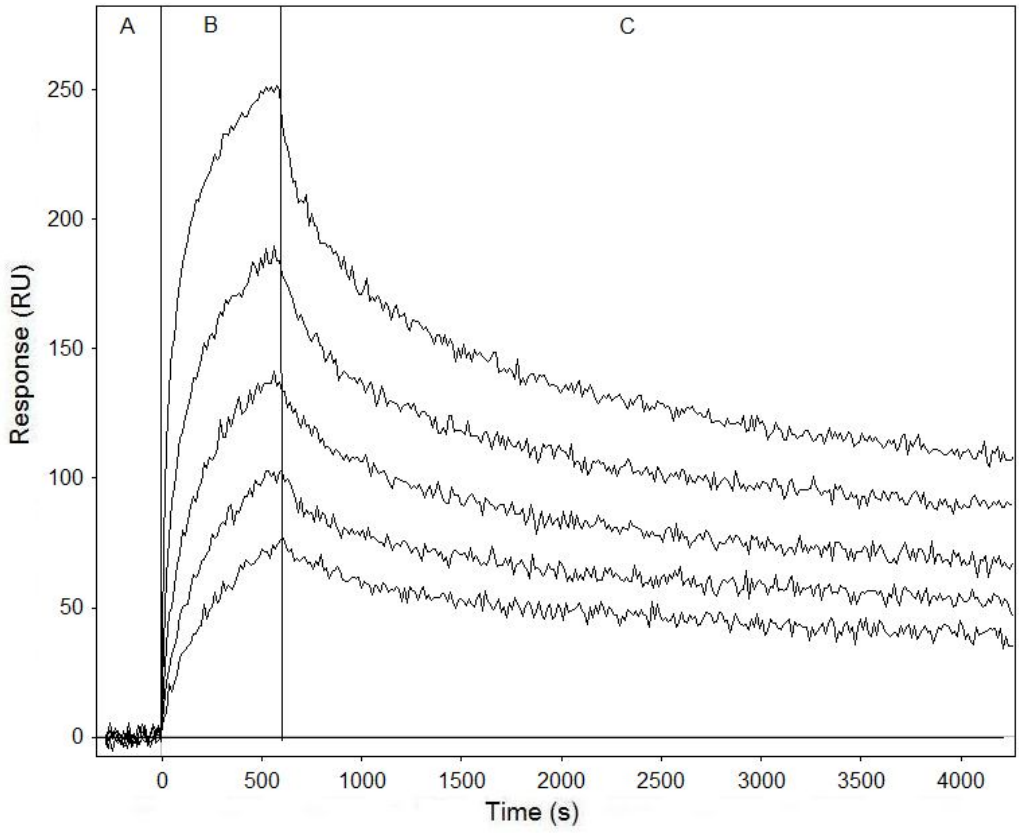

Figure 1.6: The three interaction stages using a SPR. A) Blank (buffer) stage. B) Association/interaction stage. C) Dissociation/elution stage. Each curve ("sensorgram") represents a different analyte concentration.

1.4 Protein A Affinity Chromatography

Protein A and a variety of derivatives are regularly used in affinity chromatography to purify IgG. This is evident by the large number of manufacturers and products available, from Bio-

rad's UNOsphere SUPrA™ media through Millipore's Prosep®-Va media to GE's Mab Select Range, all of which use Protein A or a Protein A derivative and sell for upwards of NZ$10,000/l. The growing use of monoclonal antibodies (IgG, IgD and IgE) for therapeutic purposes has provided a large market for the Protein A media, with at least 23 different mAbs currently in use (8) and hundreds in development (27).

Affinity chromatography follows the standard liquid chromatography form, being comprising a column filled with a solid stationary phase through which a mobile liquid phase flows (28). The stationary phase is made up of multiple beads (usually roughly spherical in shape) upon which the ligand is bound. The ligand is selected for its specificity of binding for a desired product; in this case the ligand is protein A and the product IgG. Often the beads contain pores or channels to increase the amount of surface area for increased ligand binding. The beads can be made out of any of a number of materials, often with polymers, agarose and glass. The stationary phase can be called the matrix or the medium/media. The basic setup and performance of affinity media is shown in Figure 1.7.

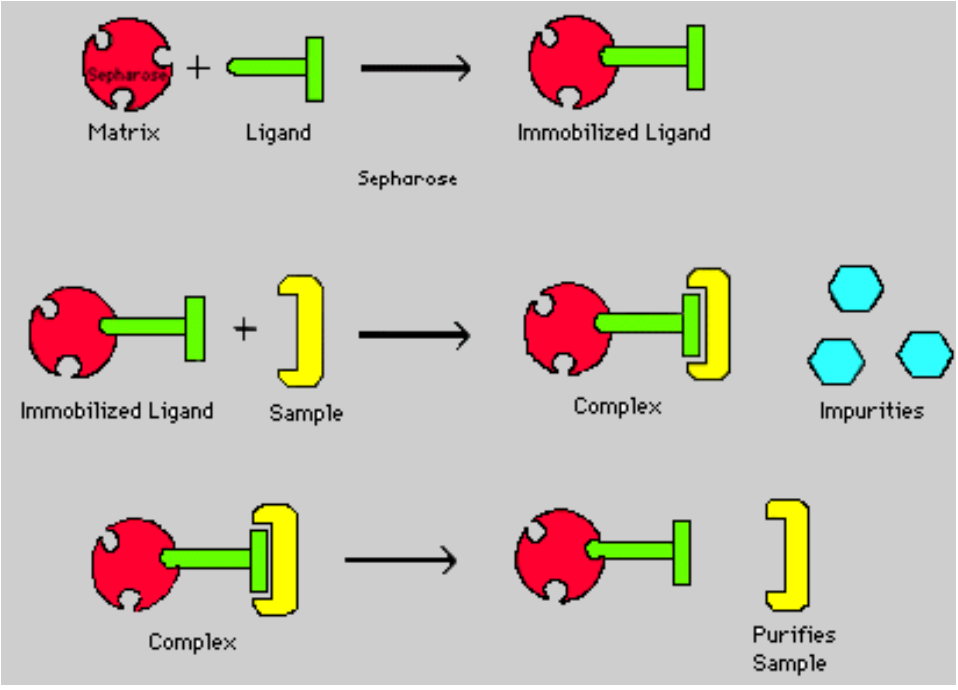

Figure 1.7: Basic setup and action of an affinity chromatography system.

Any liquid chromatography process contains a number of steps for product separation. The first step is to equilibrate the column, usually by running a buffer similar or identical to the buffer containing the product. The next step is to run the product through for capture onto the media. This is followed by washing with the original buffer and then the elution step, where the buffer is contains a modifier component to change (pH, conductivity, organic content or other properties) using either a step change or a gradient to elute the product(s). Finally a cleaning step is performed to remove any remaining product or impurities from the column, and this step is usually done with a high conductivity, strong acid or base.

Currently most processes use harsh conditions, with buffers with a pH of 3 or less to elute IgG off the Protein A column. This can lead to aggregation and degradation of IgG making it useless for therapeutic purposes (29). While this damage can be minimised with good operational practices it would be preferable to find a solution that reduces or eliminates the damage to the IgG, especially given the significant value of even small amounts of therapeutic IgG. The harsh pH is used to ensure the complete elution, because of the perceived strength of the interaction between IgG and Protein A and the difficulty of fully removing bound IgG that the interaction causes. Determinig whether this level of acidity is truly required for elution is the subject of this thesis.

A number of purification alternatives exist to a Protein A column. Protein G and Protein L are similar in effect to Protein A, with strong antibody affinity. Protein G is the more similar of the two; binding to the Fab and Fc regions of IgG and often used in combination with Protein A to enhance overall binding. Native Protein G also binds albumin but this binding is usually eliminated in its recombinant forms. Protein A does not bind IgG3, which is one reason it is used in combination with Protein G (which does). A combination of non-affinity chromatographic techniques can also be used for purification but this is unpopular due to the greater number of steps needed to replicate the purification achieved in one Protein A step.

1.5 Project Objectives

The increasing growth of monoclonal antibody therapeutics and their reliance on Protein A affinity chromatography as a means of purification makes understanding the interaction between IgG and Protein A important to ensure that existing and new drugs are as cheap as possible to allow the greatest number of people and animals to benefit from them. While a great deal of work has been done on the various binding sites and their mechanisms, there seems to be little research examining how the complete molecules interact (specifically their association and dissociation constants) and how that interaction is effected by pH changes. This project intends to fill that gap by using a SPR device to examine the interactions between IgG and Protein A over a range of pH conditions. Other current (unpublished work) by Professor Giorgio Carta (University of Virginia) and colleagues shows variation between the elution pH of mAbs and that of the elution buffer used, which calls into question established methods for elution. IgG is sensitive to low pH and can degrade under normal (pH 3) elution conditions causing loss of product. By examining the interaction kinetics over a range of pH it is hoped that a more optimal solution can be found that allows elution while decreasing or eliminating product degradation.

1.6 Scope and Organisation of Thesis

The current knowledge of the interactions between IgG and Protein A as well as their effects on wider process considerations are presented in the next chapter. Chapter 3 describes the equations and models used for analysing the experimental data and the software programs that best utilise them. The methodology and materials used for the experiments are fully discussed in Chapter 4, with the experimental results given in Chapter 5. Chapter 6 discusses the results of the experiments. Conclusions are given in Chapter 7, while the recommendations for any further work or alternative uses of the data are given in Chapter 8. The Appendices will contain the full data sets and their models with all associated details.

Chapter 2: Literature Review

Research of the current literature was undertaken to survey the existing knowledge of Protein A and IgG interactions. Focus was given to elution conditions and techniques used, with special attention paid to salt type, additives and pH. The current product lines of Protein A affinity media were also examined to determine the favoured characteristics of the media and how this research will apply to them. The range of IgG therapeutics was also investigated to determine the direction of the market and future relevance of this research.

2.1 Protein A and Immunoglobulin G Interactions

The interactions between Protein A and IgG have only really been studied in detail between fragments with either other fragments or an entire molecule. While this has produced some incredibly detailed data and insights about certain interactions, it still leaves the overall mechanism of interaction between the two molecules largely unknown. The knowledge regarding these individual interactions is difficult to apply to whole molecule interactions, as the studies do not take account of steric factors or whether the individual parts act alone or in combination. There has also been significant work on the interaction within an affinity column or in free solution but none have examined the effects as they occur, instead taking only snapshots of certain points to determine certain properties. These studies give us some knowledge of the interactions but leave a significant gap in the knowledge that this study attempts to fill in terms of multiple interaction conditions.

The interaction between the B domain of Protein A and the Fc region of IgG has been studied in some depth. As mentioned in Chapter 1, Protein A exhibits an extended shape with a number of α-helices. The B domain is made up of two (30) or three (31) of these helices with the rest of the molecule folded irregularly. The B domain interacts with both the CH2 and CH3 regions of the Fc fragment (shown in Figure 2.1). The bond is formed primarily through hydrophobic interactions between the two fragments. While this study (30) also found a second bond this was put down to interaction caused by the crystallographic method. This was an early study into the interactions between protein A and IgG that first elucidated the binding mechanism behind the interaction between the two molecules.

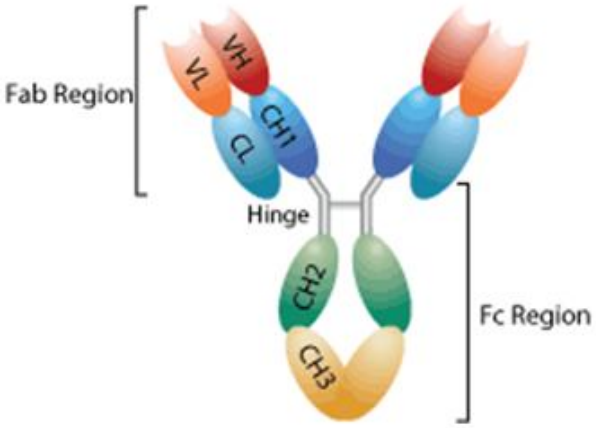

Figure 2.1: IgG with significant regions labelled.

Another, more recent study (32), examined the same interaction between Domain B and the Fc region of IgG (the whole molecule was used for this), this time using a quartz crystal microbalance (QCM). While this could not determine the exact nature of the binding it could determine the adsorption (ka) and desorption (kd) rate constants as well as the maximum amount adsorbed. A simple 1:1 binding ratio was found, but at higher surface densities, a single IgG could be bound by multiple B fragments. The rate constants determined will be compared later with the results of this thesis but while some similarities are possible, it is likely that these constants will be different to those obtained due to being only a single part of a greater moleule.

2.2 Elution conditions for Immunoglobulin G from a Protein A Affinity Column

A great deal of research has been done into increasing the pH required for effective elution of IgG from Protein A. Initial studies in the area established the pH gradient convention that is now the basis of all elutions of IgG from Protein A. From there, a variety of methods for increasing the pH have been investigated, such as altering the Protein A, matrix effects, varying the elution buffer and heat elution. These methods have had mixed success but even the more effective methods have had limited uptake, generally because of the cost of using relatively unproven methods. Ultimately, the industry remains focused on simple pH-based approaches to elution, using proven buffers at standard conditions.

One of the early studies (33) into elution proved the efficacy of a simple pH gradient for elution. Using a Superose column with immobilised Protein A, a pH gradient from 8 to 3 was used to elute IgG. This research also showed that using a pH gradient could be used to at least partially separate the different IgG isotypes. The eluted IgG was also extremely pure, a feature of current Protein A affinity chromatography. This study established the basis for IgG purification that has remained largely unchanged for 30 years. The most improvement that has occurred in that time has been in the Protein A media, with higher flows and binding capacities achievable, which is discussed in Section (2.3).

Once the basic procedure was well established, research began into improving the process with engineering of Protein A to the fore. An early study by Bottomley et al (34) in this area focused on altering the B domain of Protein A. The B domain was altered in one case by C-terminal truncation and in other cases by site-directed mutagenesis. The truncation proved the most effective, showing IgG2 elution at pH 5.0 and IgG1 elution at pH 4.1. By adding some site-directed mutagenesis to the truncation full elution was achievable at pH 5.0. The two site directed mutants failed as one eluted too easily and was lost under wash conditions, while the other showed almost no change, eluting at pH 3.2. The most significant problem with such alterations is that the decrease in affinity they cause reduces dynamic binding capacity. This trade-off means protein alteration is useful but on a large scale loses much of its appeal due to the increase in production time and/or chromatography media that it causes.

Another study (35) focused on a B domain alteration, using a synthetic analogue known as the Z domain, shown previously in Figure 1.3. The alterations were made by site directed mutagenesis to form two mutants, both with decreased helix size, to evaluate the importance of the helices effects on binding. The mutants also had decreased chemical and thermal stability compared to the original Z domain. Both mutants showed improved elution properties with 97% and 93% of the IgG eluted at pH 4.5 compared with just 70% for the parent molecule. While this kind of protein engineering shows good results, the side-effects again decrease its desirability with chemical and thermal stability important for long term use, the ability to effectively clean any media and ensuring leaching of the column is minimal.

To address some of the issues associated with native protein/mutants Teng et al (36) synthesised a variety of ligands that mimicked some of the properties of Protein A, while at the same time having greater chemical stability. Of the mimetics tested one stood out, with IgG capture of 99% and a yield of 98% when bound on a column. It also was able to bind human IgG3, unlike Protein A, and a similar variety of mammalian IgGs as Protein A. Unfortunately, the mimetic's strong affinity for IgG means that the elution conditions required were even harsher than for Protein A with a pH below 2.9 required. However, the chemical stability was extremely good, with no significant loss of performance after 7 days (>140 hours) in 1 M sodium hydroxide. This suggests stability for more than 500 wash cycles under normal process conditions. Given the large cost of Protein A media such stability can be of great value for large scale manufacturers.

Heat elution is another possibility; however it has so far not been used with a Protein A derivative. Heat elution is possible with *Streptococcal* M proteins, which are unstable at low temperatures and completely unfold above 40 ºC (37). The unfolding is reversed simply by reducing the temperature to below 40 ºC. This study used Protein H from streptococcus pyogenes, which can bind a single IgG. Protein H unfolds and loses its affinity for IgG between 30 and 35ºC, thus making elution simple, with no change of buffer required. These temperatures are not extreme enough to damage the IgG and mutagenesis could be used to isolate the IgG binding domain. The structure of such proteins could also be used to develop a Protein A derivative with similar properties, or the two proteins could be grafted together. This process does still present challenges on a process scale, with uniformly heating a large scale column potentially challenging and also the high cost of the media. However, this area seems to warrant further investigation.

The last elution method of significance has been identified in a number of studies (38-40) and examines the use of arginine in the elution buffer. Arakawa et al (38) were the first to identify arginine as a useful eluent due to its use in protein refolding to prevent aggregation. It was found that 0.5 M arginine increased the recovery of IgG4 from 46 to 92% at pH 3.8 (compared to 0.1 M citrate buffer). At pH 4.1 citrate recovery dropped to 18% while arginine

remained high at 82%. Recovery was also observed to increase with the concentration of arginine; using 0.5 M arginine at pH 4.3 only recovered 48% but with 2.0 M arginine at pH 4.4 recovery was 84%. IgG1 also responded well going from 6% to 38% and onto 77% recovery with 0.1 M citrate, 0.5 M arginine and 2 M arginine respectively. These findings were expanded upon by the same group (39) to determine the active part of arginine and if other molecules held the same properties. Of the molecules tested actyl-arginine and agmatine, both arginine derivatives, were found to be comparable to arginine for elution purposes. Of the amino acids tested only histidine showed any effect and was still less effective than arginine. Guanidine hydrochloride was also effective but increased antibody aggregation. The last study (40) studied the exact interaction between the arginine, IgG and Protein A using computer models. It determined that arginine's positively and negatively charged N and C terminals, plus the guandinium group, fuel interactions with polar, charged and aromatic groups. This allows arginine to crowd out the Protein A interaction with IgG aiding elution and also preventing aggregation by the same effect.

2.3 Protein A Affinity Media Varieties

As mentioned in the introduction, a number of manufacturers produce a large variety of Protein A media. The media vary in a number of ways; bead size, bead structure, surface binding mechanism and alteration of the Protein A. This can all be altered to produce better results for a given set of conditions. This is most evident in the differentiation between process scale and laboratory scale media, with one engineered to produce reasonable separation at high flows and pressures while the other is designed to produce excellent product resolution but with lower flow and pressure limits. This difference is achieved by finer media, which decreases the flow because of the smaller spaces between the media, while increasing the binding capacity due to the greater surface area. Dynamic binding capacity is also usually reduced for higher flow systems due to the beads requiring greater strength through increased cross-linking, which tends to limit their surface area and hence ligand density. It should be noted that this is by no means a complete list of all available Protein A media. The four manufacturers listed are larger companies that produce multiple kinds of media usable at process scale. Of the smaller manufacturers investigated many produced media that was largely comparable to one of those listed here.

Bio-rad Laboratories (Hercules, CA, USA) produces three different protein A affinity media: UNOsphere SUPrA, Affi-Gel Protein A and Affi-Prep Protein A (1). The basic properties of these media are shown in Table 2.1. It is clear from the product data that the UNOsphere and Affi-Prep media are better for a process scale, with higher flow rates attainable due to their more robust matrix materials. UNOsphere also shows the benefits of recombinant Protein A, with more than twice the binding capacity of the other two media and the ability to purify a range of mAbs (not just IgG). UNOsphere and Affi-gel are roughly similar in price (~NZ$2000 for 25 ml) while the Affi-Prep costs almost twice that (NZ$3553 for 25 ml). Affi-Prep is likely the most expensive because it can support the highest flows (up to 2000 cm/hr). Flow rate, along with binding capacity, are amongst the most important characteristics on a process scale due to relatively slow flow rates that can be achieved in chromatography compared to other process steps such as filtration or centrifugation and the bottle neck that this creates in processes.

Table 2.1: The properties of Bio-rad's Protein A affinity media (1).

Name	Matrix	Functional Group	Specificity	Capacity (Dynamic)*	Pressure Limit/ Flow rate	Working pH
UNOsphere SUPrA	Highly cross-linked polyacrylamide polymer	Recombinant protein A	Antibodies/ Immunoglobulins	25 to 30 mg/ml	100-600cm/h	3-11
Affi-Gel Protein A	Cross-linked agarose	Protein A 2mg/ml	IgG	6 to 15 mg/ml	1 bar	2-10
Affi-Prep Protein A	Pressure stable polymer	Protein A 2mg/ml	IgG	7 to 12 mg/ml	70 bar	2-10

* Based on human IgG at 10% breakthrough.

Millipore also has three different Protein A media but they are less varied than those produced by Bio-rad. The products and their key characteristics are shown in Table 2.2. Similar to the UNOsphere media the ProSep media operates at a maximum flow rate of approximately 600 cm/h but the binding capacities given greatly exceed those of their Bio-rad rivals. Porous glass also has some advantages as a matrix material as it is uncompressible and is unaffected by almost any condition extremes, e.g. pH, salt, organic solvents etc. The pore size of the media is also carefully controlled to allow greater contact time for particles below a certain size, thus allowing for greater optimisation depending on the desired product. While pore size in polymers can also be controlled it is generally less exact due to their more

varied nature. The disadvantage of porous glass is that the uncontrolled, on-spherical particle shapes pack into a non-uniform bed, generally increasing dispersion.

Table 2.2: The properties of Millipore's Protein A affinity media (2, 3).

Name	Matrix	Functional Group	Specificity	Capacity (Dynamic)*	Pressure Limit/ Flow rate	Working pH
ProSep Ultra Plus	60µm porous glass	Recombinant protein A	mAbs	45 to 55 mg/ml	10 bar	1-8.5
ProSep-vA Ultra	Porous glass 700Å pores	Native protein A	mAbs	40 to 55 mg/ml	10 bar	1-8.5
ProSep-vA High Capacity	Porous glass 1000Å pores	Native protein A	mAbs	20 to 30 mg/ml	10 bar	1-8.5

* Based on human IgG at 10% breakthrough.

By far the largest range of products belongs to GE Life Sciences with 9 different types of Protein A media, as shown in Table 2.3. GE's matrix of choice is agarose with an average bead diameter between 75 and 90µm. Three different forms of protein A are used: native, recombinant and a derivative. The Protein A derivative allows for the highest binding capacity of any manufacturer's media (MabSelect SuRe LX) without reducing maximum the maximum flow rate. GE's media has good binding capacity but relatively low pressure limits and thus more limited maximum flow rates.

Table 2.3: The properties of GE's Protein A affinity media (4).

Name	Matrix	Functional Group	Specificity	Capacity (Dynamic)*	Pressure Limit/ Flow rate	Working pH
MabSelect	85µm highly cross-linked agarose	Recombinant Protein A (E. Coli)	mAbs	>30 mg/ml	<200 kPa <500 cm/h	3-10
MabSelect SuRe	85µm highly cross-linked agarose	Alkali-stabilized Protein A-derived (E.coli)	mAbs	>30 mg/ml	<200 kPa <500 cm/h	3-12
MabSelect SuRe LX	85µm highly cross-linked agarose	Alkali-stabilized Protein A-derived (E.coli)	mAbs	60 mg/ml	<200 kPa <500 cm/h	3-12
MabSelect Xtra	75µm highly cross-linked agarose	Recombinant Protein A (E. Coli)	mAbs	>30 mg/ml	<200 kPa <300 cm/h	3-10
nProtein A Sepharose 4 Fast Flow	90µm 4% cross-linked agarose	Native Protein A (S. aureus)	mAbs	>30 mg/ml	<100 kPa <250 cm/h	3-9
Protein A	Paramagnetic,	Native Protein	mAbs	27 mg/ml	Not	Not

Mag Sepharose Xtra	spherical, highly cross-linked agarose particles	A (S. aureus)			specified	specified
Protein A Sepharose CL-4B	90µm 4% cross-linked agarose	Native Protein A (S. aureus)	mAbs	20 mg/ml	<150 cm/h	3-9
rmp Protein A Sepharose Fast Flow	90µm 4% cross-linked agarose	Recombinant Protein A (E. Coli)	mAbs	>35 mg/ml	<100 kPa <250 cm/h	3-10
rProtein A Sepharose Fast Flow	90µm 4% cross-linked agarose	Recombinant Protein A (E. Coli)	mAbs	50 mg/ml	<100 kPa <250 cm/h	3-10

* Based on human IgG at 10% breakthrough.

Invitrogen produces six different Protein A affinity media but only two can be bought in amounts large enough for process scale, which are shown in Table 2.4. These media are largely similar in pressure limit and dynamic capacity to those produced by Millipore. However, Invitrogen uses a complex polymer to achieve strengths similar to those of the glass beads used by Millipore, with the same maximum flow as Bio-rad's Affi-Prep media that also uses a polymer matrix.

Table 2.4: The properties of Invitrogen's Protein A affinity media (5).

Name	Matrix	Functional Group	Specificity	Capacity (Dynamic)*	Pressure Limit/ Flow rate	Working pH
POROS MabCapture A	Cross-linked poly(styrene-divinylbenzene)	Recombinant Protein A	mAbs	40 to 50 mg/ml	10 bar 2000 cm/h	2-10
POROS A 50µm	Cross-linked poly(styrene-divinylbenzene)	Recombinant Protein A	mAbs	30 to 38 mg/ml	10 bar 2000 cm/h	2-10

* Based on human IgG at 10% breakthrough.

Pierce Protein Biology Products (part of Thermo Fisher Scientific) produces a wide range of Protein A media, as well as mixed Protein A and Protein G media. Table 2.5 shows the four kinds of Protein A media Pierce produces, all of which are also produced as mixed Protein A and G with the same properties other than binding capacity. The dynamic binding capacities (using human IgG) for the Protein A/G mix are 25mg/ml, 7mg/ml, 20mg/ml, 28mg/ml for the Plus Agarose, Agarose, Ultralink and UltraLink Plus, respectively. The agarose media is largely similar to those produced by GE while the Ultralink media is most like Bio-rad's UNOsphere media.

Table 2.5: Pierce Protein A media properties (6).

Name	Matrix	Functional Group	Specificity	Capacity (Dynamic)*	Pressure Limit/ Flow rate	Working pH
Protein A Plus Agarose	6% Cross-linked Agarose	Native Protein A	mAbs	>34 mg/ml	<1.5 bar 30 cm/h	2-14
Recombinant Protein A Agarose	6% Cross-linked Agarose	Recombinant Protein A	mAbs	15 to 17 mg/ml	<1.5 bar 30 cm/h	2-14
Protein A Agarose	6% Cross-linked Agarose	Native Protein A	mAbs	12 to 19 mg/ml	<1.5 bar 30 cm/h	2-14
Protein A UltraLink Resin	Highly Cross-linked Polyacrylamide	Native Protein A	mAbs	16 mg/ml	6.9 bar 3000 cm/h	1-13
Protein A Plus UltraLink Resin	Highly Cross-linked Polyacrylamide	Native Protein A	mAbs	30 mg/ml	6.9 bar 3000 cm/h	1-13

* Based on human IgG at 10% breakthrough.

By comparing the various media from all the manufacturers a number of conclusions can be drawn. On a process scale average bead diameter must be approximately between 40 and 100µm. While agarose (the most established material) remains popular, a number of alternative media materials are now in use and perform as well as or better than agarose in many cases. Native Protein A remains in use for a number of media, but it is clear that in order to reach the highest binding capacities recombinant Protein A or a derivative is required. The different media show a range of dynamic binding capacities from 6 to 60 mg/ml, but the majority fall between 20 and 50 mg/ml. While the flow rates vary greatly between media the extremely high flows need to be treated with a level of suspicion, because while it may be possible to have a flow rate above 500 cm/h there is always a trade off between flow rate and binding capacity due to the influence of residence time. Thus, while 2000 cm/h might be achievable on a 20 cm column the residence time would only be 36 seconds and barely any binding would have time to occur. The dynamic binding capacities quoted were for between 3 and 6 minutes, which limits the flow rate in standard columns of between 15 and 25 cm to 300 to 500 cm/h respectively.

In 2003 Hahn et al (7) produced a comparative study of 15 different Protein A media, shown in Table 2.6. Of these products most still exist either in the same or an improved form and have appeared in the previous product tables. This study used polyclonal IgG and between 0.5 and 2 ml of media in a 2.5 cm tall column, which are not the desired parameters but

should still give some insight into the performance of the media. Mabselect was found to be the best (highest binding capacity) at 50 and 100 cm/h (residence time greater than 1.5 minutes) while Poros 50 A was found to be the best at higher flows. This study also found that at 200 cm/h or above (less than 45 s residence time) five types of media showed no binding whatsoever. This fits with the data provided by manufacturers and reinforces the fact that the ability to achieve high flows is often limited not by the pressure but the binding capacity. Furthermore, the authors noted that the desired residence time had a large effect on the best media for the job with Poros 50 A performing better when residence time was less than 3 minutes but rPrA Sepharose Fast flow the better option for any longer residence time.

Table 2.6: Hahn et al chosen Protein A media (7).

Name	Manufacturer	Matrix	Mean Particle Diameter (μm)	Ligand Density (mg/ml)
rProtein A Sepharose Fast Flow	Amersham Biosciences (now GE Life Sciences)	Cross-linked agarose	90	4-6
Protein A Sepharose 4 Fast Flow	GE Life Sciences	Cross-linked agarose	90	4-6
MabSelect	GE Life Sciences	Cross-linked agarose	85	N/A
IPA-500	RepliGen Corp.	Cross-linked agarose	90	N/A
Protein A Ceramic HyperD F	Biosepra	Polyacrylamide gel in ceramic macro-bead	50	4-5
Prosep-A High Capacity	Millipore	Porous Glass	75	N/A
Prosep-rA High Capacity	Millipore	Porous Glass	75	N/A
Poros 50 A High Capacity	PerSeptive Biosystems (now Invitrogen)	Polystyrene-divinylbenzene	50	N/A
UltraLink Immobilised Protein A Plus	Pierce	Polymeric	60	N/A
UltraLink Immobilised	Pierce	Polymeric	60	N/A

Protein A				
Affi-Gel Protein A	Bio-rad	Cross-linked agarose	N/A	2
Affi-Prep Protein A	Bio-rad	Polymeric	N/A	2
Protein A Agarose 4XL	Affinity Chromatography Ltd	Cross-linked agarose	N/A	N/A
Protein A Cellthru 300	Sterogen Bioseparations	N/A	200-300	N/A
AF-Protein A Toyopearl 650 M	Tosoh Biosep	Polymethacrylate	80	N/A

Hahn et al did another study in 2006 (41) into the long term effects of industrial scale purification on protein A media. Only three media were used for this study; MabSelect SuRe, MabSelect Xtra and Prosep-vA Ultra. The media was tested after 50 consecutive purification cycles (equilibration, binding, elution and cleaning) to determine any loss of performance or additional leakage from the column. None of the media showed a loss of purification performance over the test period. MabSelect SuRe showed the least leakage with less than 4 ppm in any run. Xtra had leakage between 5-35 ppm with no noticeable increase with number of runs while Prosep was generally less than 40 ppm, but in later cycles did show some larger outlying results. Overall this study showed that Protein A media is relatively stable over multiple cycles and this stability is improving with the matrix and ligand advances.

2.4 Immunoglobulin G Therapeutics

There are at least 23 different mAb therapeutics in use, that treat a variety of different diseases, shown in Table 2.7. Of the therapeutics shown, 17 utilise IgG which illustrates the importance of IgG, and its purification process, in the pharmaceutical industry. These therapeutics are potentially just the tip of the iceberg with many more in development (27) and a bright future with the rise of transgenic animals and crops to potentially provide cheaper upstream costs. IgG's ability to specifically target undesirables allows for targeted treatment of a huge range of diseases and lower doses to decrease negative side effects and speed recovery.

Table 2.7: Approved and commercialised mAb therapeutics (8).

Generic Name	Molecule type	Disease(s) Treated	Company	Approval Status
Golimumab	Human Anti-TNFα	Rheumatoid arthritis, active psoriatic arthritis and active ankylosing spondylitis	Centocor	2009 FDA 2009 EMEA
Certolizumab	Pegylated humanized Fab fragment IgG1 TNF-α	Crohn's disease	UCB Pharma	2008 FDA
Eculizumab	Humanized IgG2/4κ that binds to C5	Chronic orphan blood disorder and paroxysmal nocturnal hemoglobinuria	Alexion Pharmaceuticals	2007 FDA 2007 EMEA
Ranibizumab	Recombinant humanized IgG1κ mAb Fab	Neovascular age-related macular degeneration	Genentech/ Novartis	2006 FDA 2007 EMEA
Panitumumab	Human, IgG2κ, anti-EGF receptor	Metastatic colorectal cancer	Amgen/ Abgenix	2006 FDA 2007 EMEA
Natalizumab	Recombinant Humanized IgG4κ	Crohn's disease, Multiple Sclerosis	Biogen IDEC	2004 FDA 2006 EMEA
Nimotuzumab	Humanized IgG1 anti-EGF receptor	Epithelial cancer	YM Biosciences/ Biocon	2005 China 2006 India
Bevacizumab	Humanized IgG1 anti-VEGF	Metastatic colorectal cancer	Genentech/ Roche	2004 FDA 2005 EMEA
Omalizumab	Humanized (anti-IgE Fc)	Allergy	Genentech/ Novartis	2003 FDA 2005EMEA
Cetuximab	Chimeric IgG1κ anti-EGF receptor	Epidermal growth factor receptor expressing metastatic colorectal cancer	ImClone/ Bristol-Myers Squibb	2004 FDA 2004 EMEA
Efalizumab	Humanized Ig anti-CD11a	Psoraisis	Genentech/ Roche	2003 FDA 2004 EMEA
I-131 tositumomab	Murine, IgG2aλ anti-CD20, radiolabeled (I-131)	Non-Hodgkin's lymphoma	Corixa/ GlaxoSmithKline	2003 FDA
Ibritumomab tiuxetan	Murine, IgG1κ, anti-CD20, radiolabeled (Y-90)	Non-Hodgkin's lymphoma	IDEC Pharmaceuticals	2002 FDA 2004 EMEA

Adalimumab	Human anti-TNFα	Crohn's disease, rheumatoid arthritis, ankylosing spondylitis	Abbott Laborartories	2002 FDA 2003 EMEA
I-131 ch-TNT	Chimeric IgG1κ, anti-DNA associated antigens, radiolabeled (I-131)	Advanced lung cancer	Shanghai Medipharm Biotech	2003 China
Alemtuzumab	Humanized, IgG1κ, anti CD52	Chronic lymphocytic leukaemia	Millenium/ ILEX Partners	2001 FDA 2001 EMEA
Gemtuzumab ozogamicin	Humanized, IgG4κ, anti-CD33, immunotoxin	Relapsed acute myeloid leukaemia	Celltech/Wyeth	2000 FDA
Infliximab	Chimeric anti-TNFα	Rheumatoid arthritis, Crohn's disease	Centocor	1998 FDA 1999 EMEA
Trastuzumab	Humanized, IgG1κ, anti-ER2	HER2 over-expressing metastatic breast cancer	Genentech	1998 FDA 2000 EMEA
Palivizumab	Humanized anti-F-protein	Respiratory Syncitial viral disease	MedImmune	1998 FDA 1999 EMEA
Basiliximab	Chimeric anti-IL-2 receptor	Kidney transplant rejection	Novartis	1998 FDA 1998 EMEA
Rituximab	Chimeric, IgG1κ, anti-CD20	Relapsed non-Hodgkin's lymphoma	IDEC/ Genentech	1997 FDA 1998 EMEA
Daclizumab	Humanized anti-IL-2 receptor	Refactory unstable angina, Allograft rejection	Hoffmann-LaRoche	1997 FDA 1999 EMEA
Abciximab	Chimeric Fab fragment, IgG1 IIb/IIIa glycoprotein	Inhibits platelet aggregation following angioplasty	Centocor/ Eli Lilly & Co.	1994 FDA
Muromomab	Murine, IgG2a anti-CD3	Acute rejection of organ transplantation	Ortho Biotech	1986 FDA 1987 EMEA

2.5 Industrial Production of Monoclonal Antibodies

The industrial process for the production of monoclonal antibodies generally adheres to a set structure with some minor variation in production and purification techniques. The main form of production is by mammalian cell culture although transgenic livestock and plants have increasing potential due to the cost savings they provide. A variety of purification techniques

are used in the process with the most costly being the various chromatography steps used because of the high cost of the media required.

The growth of mAbs in pharmaceuticals has seen a large increase in the number and size of production facilities as shown in Table 2.8 and Figure 2.2. The table also shows the significant cost of such facilities, which in turn affects the cost of the pharmaceutical products. The graph shows an increase in facility area over the years while the bioreactor size shows more gradual growth. This is likely due to advances in culture methods allowing larger production from cultures while facility size must increase to allow for greater purification capacity.

Table 2.8: mAb manufacturing facilities size and cost between 2000 and 2009 (9).

Manufacturing Facility	Date Facility Completed	Capital Investment (US$M)	Area (sq ft)	Bioreactor Capacity (L)
Genentech – Vacaville, CA, USA	2000	250	310000	96000
Imclone – Branchburg, NJ, USA	2001	53	80000	30000
Biogen – NC, USA	2001	175	245000	90000
Boehringer ingelheim expansion – Biberach Germany	2003	315	-	90000
Lonza biologics expansion – Portsmouth, NH, USA	2004	207	270000	60000
Amgen – West Greenwich, RI, USA	2005	500	500000	180000
Genentech – Oceanside, CA, USA	2005	380	470000	90000
Imclone – Branchburg, NJ, USA	2005	260	250000	99000
Biogen – Hillerod, Denmark	2007*	350	366000	90000
Lonza biologics – Tuas, Singapore	2009*	250	-	80000
Genentech expansion – Vacaville, CA, USA	2009*	600	380000	200000

*Expected Completion date

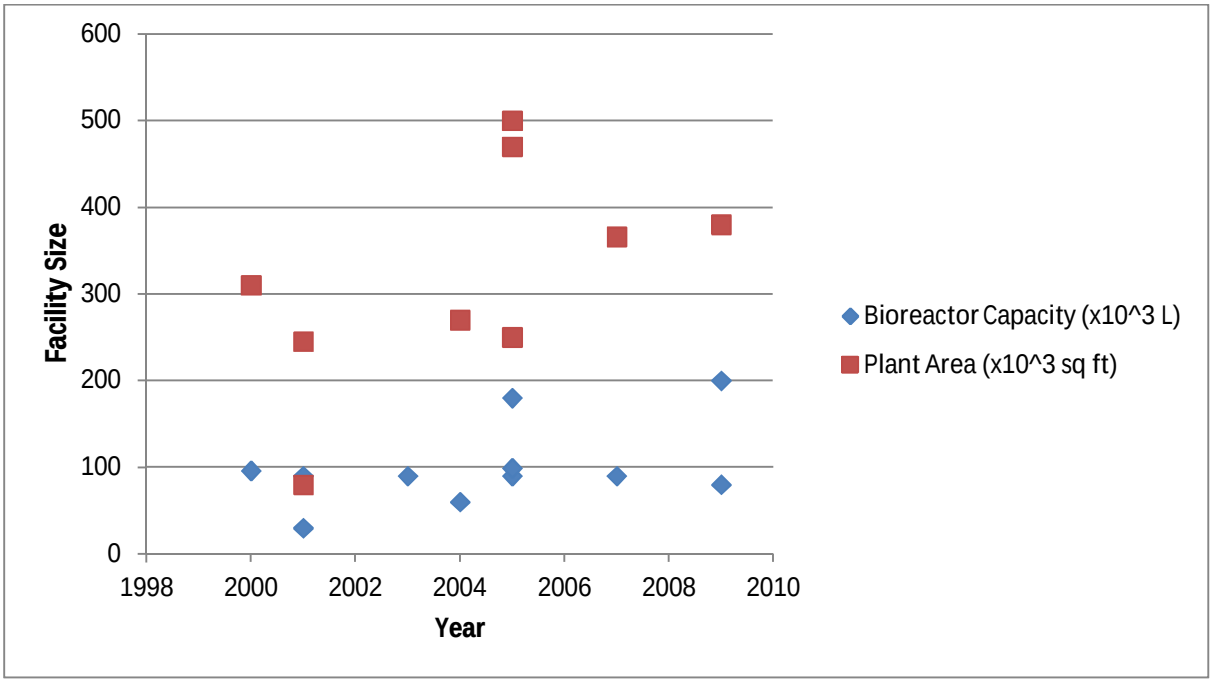

Figure 2.2: mAb facility production size from 2000-2009 (9).

The basic process for production and purification of pharmaceutical mAbs (10) is shown in Figure 2.3. The process is defined in six steps, all of which, excepting cell culture, are different purification steps, although two are chromatographic processes and two filtration processes. The production costs for a sample case (10ton/yr production facility) have been examined based on the process steps as shown in Tables 2.9 and 2.10 (10). The cost of raw materials for purification make up a significant part of the cost of goods for the drug product as well as contributing to the facility costs (purification needs infrastructure and floor space), which can be seen in Table 2.9. Breaking down the purification material costs by step (Table 2.10) it can be seen that Protein A chromatography media makes up half of these costs. This highlights the importance of understanding the IgG-Protein A interaction in economic terms given the high costs of these drugs vital to the survival of many.

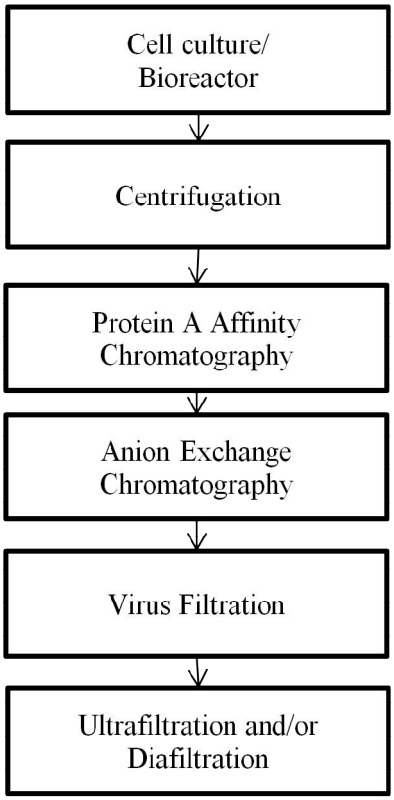

Figure 2.3: Basic process for purification of pharmaceutical mAbs (10).

Table 2.9: Cost of mAb production (10).

Total Cost of Goods Estimate (drug product)	US$/g
Upstream (medium cost of $8/L)	2
Purification raw material costs	4
Facility depreciation	5
Staff salaries	5
Fill-finish cost per vial	10
Total COGs (1g/vial)	**26**

Table 2.10: Breakdown of mAb purification costs based on unit operation and materials (10).

Purification costs per unit operation	US$/g	Top Five Raw Material Costs	US$M/yr
Harvest (centrifugation and clarification)	1.02	Protein A resin	13.1
Affinity Chromatography (Protein A)	2.03	0.2µm prefilters	5.6
Anion-exchange Chromatography	0.35	VRF Membrane	4.4
Virus Removal Filter	0.50	Buffer for harvest and ProA	3.6
Ultra/Dia-filtration	0.12	ProA step wash salt	3.5
Total cost of purification	**4.02**	**Total Purification Process Cost**	**40.2**

Chapter 3: Modelling Equations and Programs

Molecular interactions are heavily studied and there are a large number of ways to produce models for such interactions. There are a variety of equations used to model interactions, depending upon the kind of interaction and the environment that it is occurring in. Once the type of interaction is established, a number of different programs can be used to model the interaction. These vary from ground up models where all the equations, parameters and data points must be entered by the user to more specialised software that have the models mostly built and require only certain aspects to be defined.

3.1 Reaction Equations

There are a variety of equations used to describe the reactions and interactions between molecules (42). One of the first considerations is the phase of the reactants; as reactants in different phases limit the reaction to the interface between the phases. However, as all the experiments in this thesis are carried out with both reactants in aqueous solution, even the immobilised Protein A (see description of SPR, Chapter 2) this area will be ignored. Other considerations are temperature, concentration of reactants, pressure, and presence of catalysts and/or inhibitors. Pressure in a liquid system does not have a large effect on the interaction, as it does not cause a significant alteration in the dynamics of the molecules within the system unlike a gaseous system. Thus, pressure does not need to be accounted for, in the absence of orders of magnitude changes. The remaining factors can all have significant effects and must be controlled or accounted for during experimentation.

Temperature has a large effect on reactions, particularly when using biological molecules as a significant temperature shift can completely stop a reaction due to the breakdown of the molecules. Biological reactions are often limited to between 1ºC and 40ºC as they are aqueous and prone to heat degradation beyond body temperatures. Between these temperatures, reactions are subject to the Arrhenius equation (Equation 1), which is defined empirically for each different reaction. Given that the equation is empirically defined, to use the equation the values need to be obtained from the literature or by experimental work. Alternatively, if the reactions are all performed at the same temperature then no correction of

the rate constant is required and the values are unnecessary. Fortunately, the XPR36 and other SPR devices are temperature-controlled for consistency of results, allowing the Arrhenius relationship (Eqtn[1]) to be ignored.

$$k = Ae^{-E_a/(k_B T)} \quad [1]$$

where: k = the rate constant for the reaction

A = the pre-exponential factor

E_a = the activation energy of the reaction

k_B = the Boltzmann constant

T = temperature in Kelvin

The remaining factors determine the equation that is used for the reaction. If there is no catalyst or inhibitor then the Langmuir equation can be used to describe the system. The Langmuir equation assumes a limited number of binding sites on a set number of molecules, usually adsorbed onto a surface. This equation is useful for SPR binding and similar systems such as HPLC and ELISA. The initial equation (Equation 2) gives the equilibrium constant, which occurs when the reaction rate is zero. From this the equation can be rearranged to give a rate equation (Equation 4) at equilibrium. The rate equation can then be used to model an interaction or be modelled from an interaction. This can also be done by combining two standard rate equations for the association and dissociation (not shown here).

$$K = \frac{[AB]}{[A][B]} \quad [2]$$

$$K = \frac{k_a}{k_d} = \frac{[AB]}{[A][B]} \quad [3]$$

$$r = 0 = k_a[A][B] - k_d[AB] \quad [4]$$

where: K = the equilibrium constant

$[X]$ = concentration of species X

k_a = the association constant

k_d = the dissociation constant

r = reaction rate

The presence of a catalyst can be dealt with in a number of ways for the purposes of reaction modelling. Either the standard rate equation can be applied, and the difference between the rate constants can be compared with and without catalyst, or a more specialised equation can be applied. In biochemistry enzymes are the most frequent catalysts and are described by the Michaelis-Menten equation as shown in Equation 5. This equation assumes a single reactant/substrate binding one catalyst to convert to a product. Inhibition is dealt with in a similar fashion with K_m becoming K_m^{app} in the Michaelis-Menten equation which is described in Equation 6. Where Michaelis-Menten does not apply empirical results coupled with the standard rate equation can be used to study the effect of the inhibition.

$$r = \frac{R_{max}[S]}{K_m + [S]} \quad [5]$$

$$K_m^{app} = K_m\left(1 + \frac{[I]}{K_i}\right) \quad [6]$$

Where: R_{max} = the maximum rate achievable when the catalyst is saturated with substrate

$[S]$ = substrate (reactant) concentration

K_m = the Michaelis constant is the substrate concentration at half R_{max}

K_m^{app} = the Michaelis constant when inhibition occurs

$[I]$ = inhibitor concentration

K_i = the inhibitor's dissociation constant

3.2 Langmuir Equations

Langmuir equations are suitable for the interaction between IgG and Protein A because they are the only molecules that act in the binding mechanism and the immobilised protein A acts similarly to a molecule in free solution. The first equation to be tested was a simple single interaction between the IgG and Protein A with a 1:1 binding ratio. The interaction and rate equations for this are shown below in Equations 1 and 2 respectively. This is the simplest

form a kinetic equation can take and is common for chemical reactions and reactions involving smaller biological molecules.

$$IgG + ProA \leftrightarrow IgGProA \quad [1]$$

$$r_{IgGProA} = k_a * [IgG] * [ProA] - k_d * [IgGProA] \quad [2]$$

where: $r_{IgGProA}$ = the change in concentration of IgGProA complex over time

k_a = the association constant between IgG and protein A

k_d = the dissociation constant between IgG and protein A

[x] = the concentration of a given species

Greater complexity is simple to add to the standard equations if different ratios or additional binding sites are present. Equations 3 to 6 show the equations for a 3:1 binding ratio between IgG and Protein A. These equations can easily be expanded to any number ratio of x:1 with Equations 4 and 6 remaining the same at either end and additional equations in the middle taking the same form as Equation 4. For IgG and Protein A a 2:1 ratio is likely, as noted in the literature (18, 19) with anything higher than this unlikely due to the steric inhibition caused by the large size of IgG compared with Protein A. There is also some possibility of multiple Protein A's binding to a single IgG (32) but as long as the surface density of Protein A is limited, this should not have a significant effect.

$$IgG + ProA \leftrightarrow IgGProA + IgG \leftrightarrow IgG2ProA + IgG \leftrightarrow IgG3ProA \ldots. \quad [3]$$

$$r_{IgGProA} = k_{a1} * [IgG] * [ProA] - k_{d1} * [IgGProA] - k_{a2} * [IgG] * [IgGProA] + k_{d2} * [IgG2ProA] \quad [4]$$

$$r_{IgG2ProA} = k_{a2} * [IgG] * [IgGProA] - k_{d2} * [IgG2ProA] - k_{a3} * [IgG] * [IgG2ProA] + k_{d3} * [IgG3ProA] \quad [5]$$

$$r_{IgG3ProA} = k_{a3} * [IgG] * [IgG2ProA] - k_{d3} * [IgG3ProA] \quad [6]$$

Another source of complexity arises from the multiple binding sites on Protein A allowing for a number of different binding mechanisms. The basic equations for this are Equations 7 and 8 when the binding ratio is 1:1. These can be expanded to a multiple binding model through Equations 9 through 11. Multiple binding sites combined with multiple binding represents one of the most complicated, but likely, models that could be required for the interaction of IgG and Protein A. When such a model is implemented careful checking is required to ensure all factors and pathways have been accounted for. A disadvantage of using multiple binding sites is that each new site introduced to the model is effectively introducing another fitting parameter, which can obscure the simplest mechanistic understanding. Generally, the simplest fitted model that can adequately explain the data is the most likely to reflect reality.

$$IgG + ProA \leftrightarrow IgGProA_x \quad [7]$$

$$r_{IgGProA_x} = k_{ax} * [IgG] * [ProA] - k_{dx} * [IgGProA_x] \quad [8]$$

$$IgG + IgGProA_x \leftrightarrow IgG2ProA_{xy} \quad [9]$$

$$IgG + IgGProA_y \leftrightarrow IgG2ProA_{xy} \quad [10]$$

$$r_{IgG2ProA_{xy}} = k_{axy} * [IgG] * [IgGProA_x] + k_{ayx} * [IgG] * [IgGProA_y] - k_{dxy} * [IgG2ProA_{xy}] - k_{dyx} * [IgG2ProA_{xy}] \quad [11]$$

There are a number of other considerations that could potentially affect the model but not the interaction equations. A mass transport limited system would affect the reaction by limiting the amount of IgG available to interact as shown in Equations 12 and 13. If there are mass transport effects, it will be clear from the data based on interactions at different flow rates. Another potential effect is IgG aggregation, which could reduce the amount of IgG available for interaction with the Protein A, as shown in Equations 14 and 15. Aggregation is known to occur under a variety of conditions (29), but is unlikely to have a large effect on the current experiments for most of the conditions used.

$$IgG^* \leftrightarrow IgG \quad [12]$$

$$r_{IgG} = k_{m,in} * [IgG^*] - k_{m,out} * [IgG] \quad [13]$$

Where: IgG^* = IgG in free solution

IgG = IgG within reaction zone

$k_{m,in/out}$ = the transport constant for movement in/out

$$IgG + IgG \leftrightarrow 2IgG \quad [14]$$

$$r_{2IgG} = k_{a,ag} * [IgG] - k_{d,ag} * [2IgG] \quad [15]$$

3.3 Analysis Software

A number of different software programs were used to ensure accuracy and verify results when performing the modelling of the interactions. The XPR36 has its own software (ProteOn Manager) for data output and some data analysis. Scrubber (Biologic Software, Canberra, Australia) performs many of the same functions as the inbuilt XPR36 software but with greater user control and also can provide limited modelling ability. ClampXP (Biologic Software, Canberra, Australia) is a modelling program that allows for user defined reaction equations and uses the output data from Scrubber. Stella (Isee Systems, Lebanon, NH, USA) is a program that can model dynamic systems by finite difference, with the user creating the system and defining virtually every aspect therein. Microsoft Excel (Microsoft, Redmond, WA, USA) can also be used as a data modelling program and could also be used to refine the data but this would be relatively time consuming compared to the more specialised programs.

The ProteOn Manager software (Bio-Rad, Hercules, CA, USA) that comes with the ProteOn XPR36 provides raw, processed and analysed data outputs in both graphical and numerical form. The raw data can be tidied up in a number of ways using ProteOn software. Blank channels and/or samples can be referenced to remove pH, salt and non-specific binding effects from the data. Interspot (the empty space between the ligand channels) referencing can be used in a similar manner to blank or control channels. Artifact (large aggregates, air bubbles etc that appear as large spikes on the output graphs) removal is also possible but only automatically by the program (not manually). Alignment of the start and end of the injection curves is possible either manually or using the auto-correcting magic wand tool. Baseline alignment to zero is also only available through the program tools. All these tools allow the elimination of unwanted effects on the data, allowing the interaction between IgG and Protein A to be isolated and studied. Once this has occurred, the program can then model the reaction

in a variety of ways. The processed data can be modelled with a simple 1:1 binding ratio Langmuir model or a 2:1 bivalent model (as shown below in Figure 3.1) with a mass-transfer limited model and an equilibrium model as well. The models are done almost exclusively by the program, with analyte concentration and injection start and end times being the only user controlled parameters. Overall, the ProteOn software is largely controlled by automated algorithms buried within the program itself, making it easy to use but difficult to control or alter when it is not performing as desired.

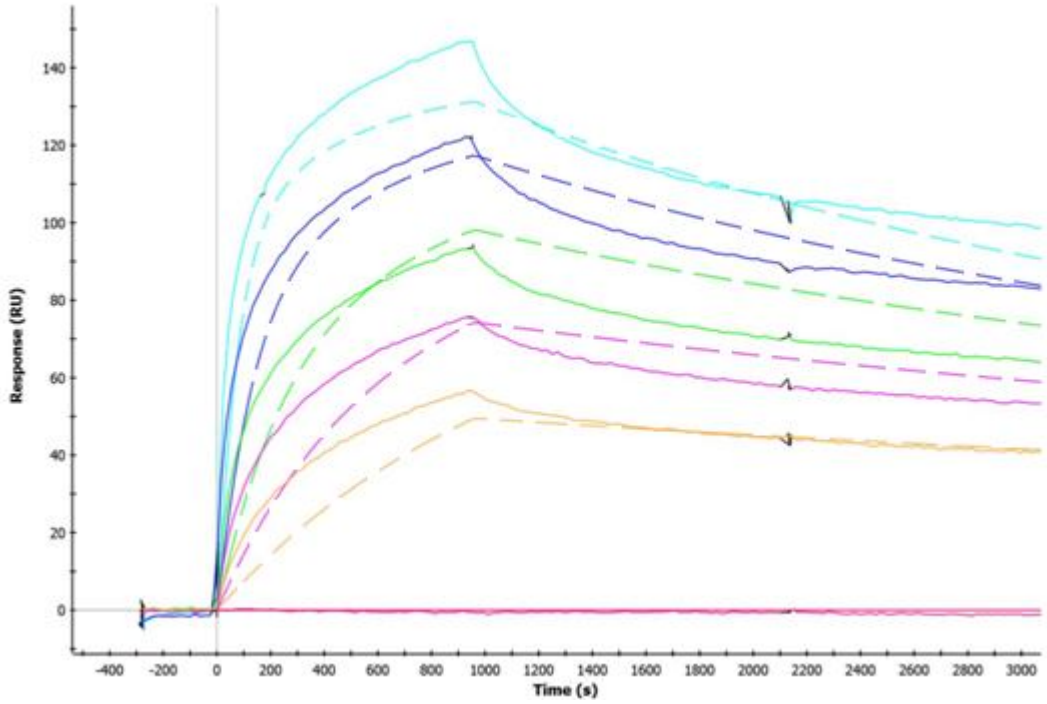

Figure 3.1: A bivalent model of IgG and Protein A using ProteOn software. The data is a dilution series (each step is half the previous) of IgG and a blank. The dashed lines are the model.

Scrubber was developed for Biacore systems but has a ProteOn version. It is largely similar in function to the ProteOn Manager software, providing most of the same data refining functions, as shown by the output data shown in Figure 3.2 below. The main difference between the two programs when it comes to data refining is the amount of user control allowed, with Scrubber providing almost complete user control, compared with the far more constrained ProteOn software. Injection alignment, referencing, baseline alignment and artefact removal are all available, with additional functions allowing cropping and removal of

any specific data points or sets. Scrubber also provides basic kinetic modelling but is limited to simple 1:1 binding kinetics. It also provides a statistical analysis of the amount bound and saturation. Scrubber's greater user control allows better control of the processed data but does make it more time consuming. The modelling package remains inadequate for anything beyond the most basic interaction model (1:1 binding), whereas ClampXP provides additional versatility.

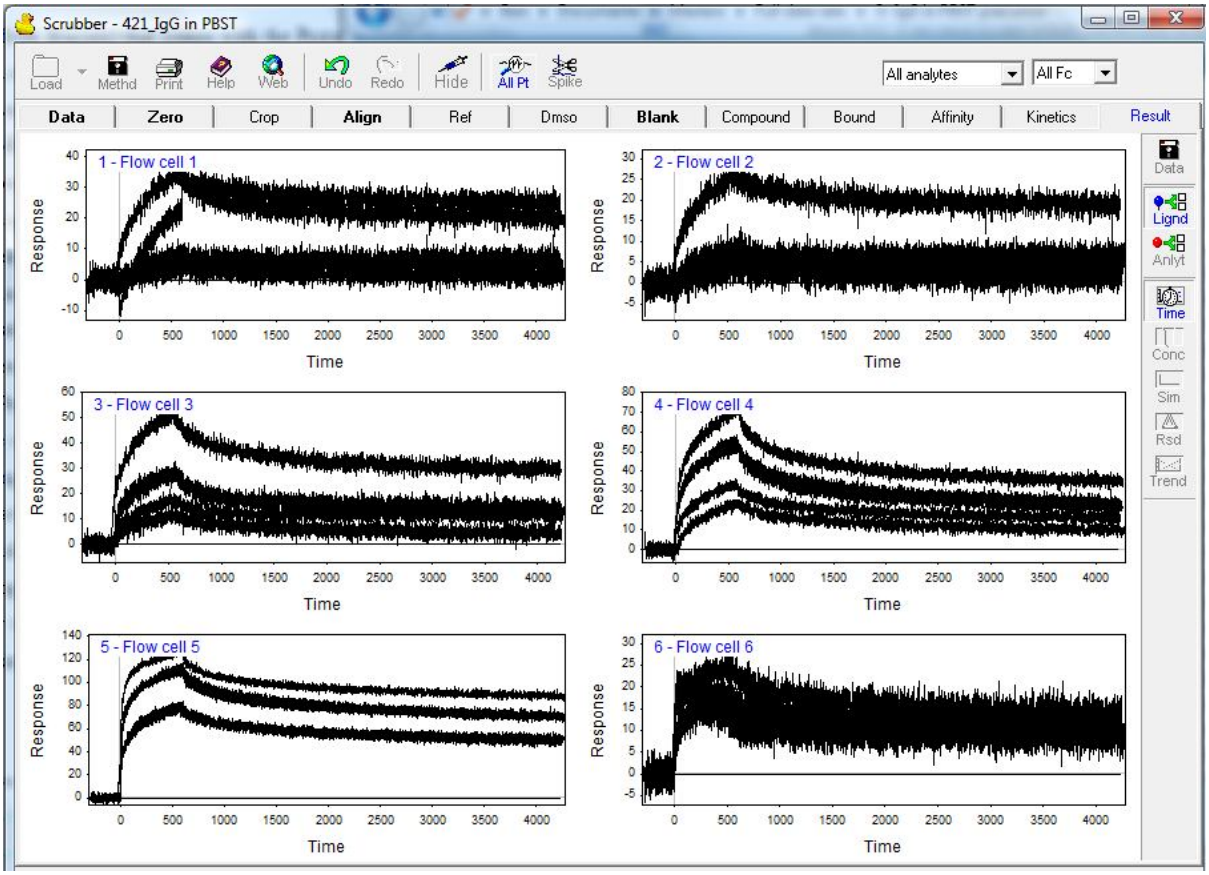

Figure 3.2: Data output screen of Scrubber.

ClampXP (Biologic Software, Canberra, Australia) is an interaction modelling program that combines data with user-defined equations to produce virtually any model desired by the user. It is designed to integrate with Scrubber by taking the processed data and providing a better fit than Scrubber can achieve. The program allows as many compounds and reactions as the user desires to define, although it is limited to two reactants and one product within any single reaction. The program is based on Langmuir kinetics, with user inputs for association

and dissociation constants for each reaction. The user chooses the parameters they wish to be fitted for the model, with virtually all values able to be fitted. ClampXP then runs the model against the data and optimises the desired parameters until convergence is reached or the user stops the simulation, as shown in Figure 3.3 below. Error outputs are given for each parameter and the overall fit. Monte Carlo simulation can be used in addition to the standard simulation. ClampXP will stop if it detects an irrelevant parameter so that parameter can be removed or re-evaluated. All these factors make ClampXP easy to use and very effective for modelling interactions from an SPR, which is why it was chosen as the main modelling program for this thesis.

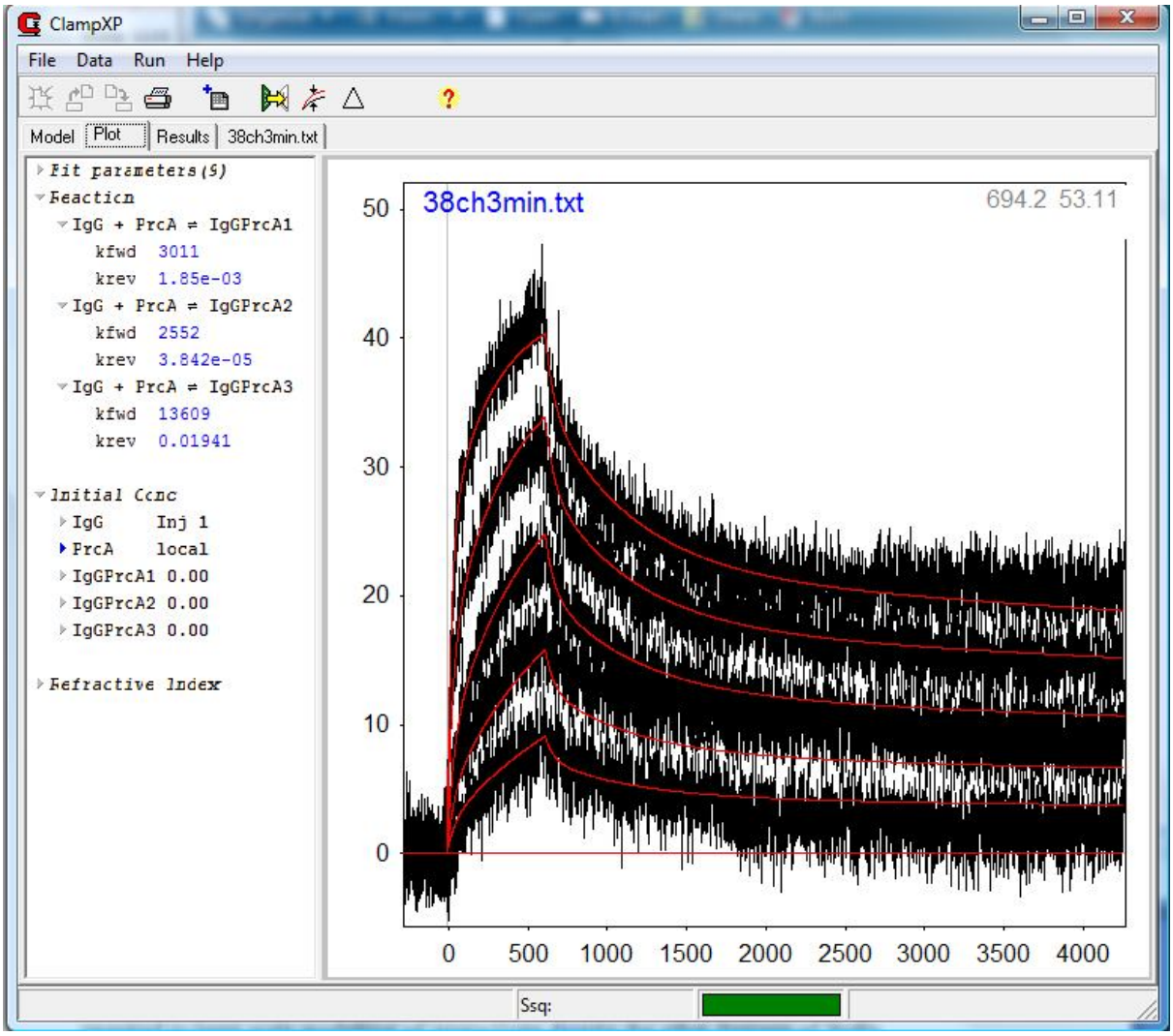

Figure 3.3: A screenshot of a ClampXP optimised model of the interaction between IgG and Protein A.

Stella (Isee Systems, Lebanon, NH, USA) is a standalone program that can be used for modelling of interactions, due to its versatility. The program works through visual flow diagrams, with variables and equations each defined in their own separate units, as shown in Figure 3.4. In the diagram (Figure 3.4) the boxes represent stocks of the individual compounds and fill or empty depending on their concentration. The thick arrows represent reaction pathways (flows), each with a user-defined equation, while the small arrows represent the parameter values used in those equations. As an example, the thick arrow going from the box labelled "bivalent binding" to the ligand site A box is labelled "Bivalent Dissociation to A" and contains the equation $r = k_{db}[IgG2ProA]$ and hence has small arrows from the kdb constant and the bivalent binding box. The full model is shown and explained in Appendix A. The visual aspect can make it easier to conceptualise and follow the progression of the reactions and their constituents within the system. Unfortunately, it is a great deal more difficult to optimise the model when fitting the data, as there is no inbuilt function in the program and no direct way to match a data set and the model produced. The model data could easily be broken down and examined in parts easily to see the effect of any one mechanism or compound and data was easily available from output tables. Ultimately, the lack of an optimisation function makes this program unsuited to large scale modelling of interactions, despite the useful conceptualisation features of Stella.

Microsoft Excel (Microsoft, Redmond, WA, USA) is a spreadsheet program with a large variety of add-ons and even the ability to code new programs when using Visual Basic. While Excel is not designed specifically for the purpose of modelling interactions its flexibility allows for enough user control to create virtually any model desired. Raw or processed data can be used in Excel from Scrubber or ProteOn Manager. All data points can be viewed on the spreadsheet or easily plotted on a graph, which allows full user control to examine, alter or remove any of the data. Any model can be used if the user knows how to create it. By setting up an error/difference column between the data and the model the solver add-in can be used to optimise the results by minimising the error. Euler's method can be applied to the Langmuir rate equations to produce a model in Excel (which can be checked for accuracy by decreasing the step size). This makes Excel effective for modelling interactions but somewhat time-consuming. Excel was used to verify some of the results gained from ClampXP for this thesis because of the complexities of dealing with the large data sets and setting up the models.

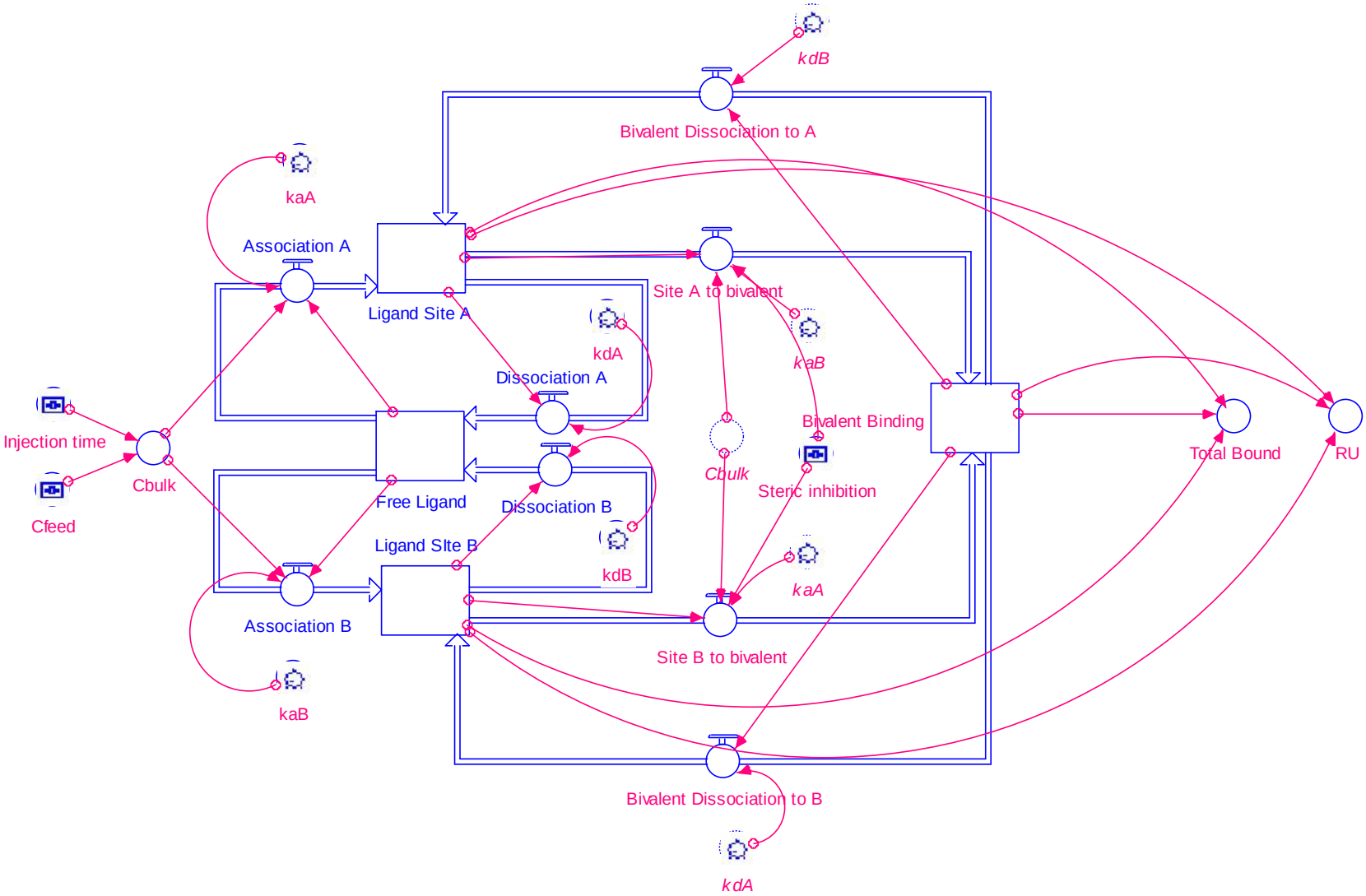

Figure 3.4: A visual flow diagram from Stella for the interaction mechanism between IgG and Protein A.

Chapter 4: Experimental Materials and Methodology

Virtually all experimental work was done on the ProteOn XPR36. A great deal of optimisation was needed before the experiments produced useful data and ongoing problems with the interaction and SPR system. All work was performed in the Biological Sciences building, fifth floor laboratory at the University of Canterbury.

4.1 Materials and Equipment

All the IgG used was polyclonal, from human serum, reagent grade ≥95% pure (product code I4506), obtained from Sigma-Aldrich (St. Louis, MO, USA). Two forms of Protein A were used. The first, from Sigma-Aldrich, was recombinant Protein A, expressed in E. Coli (from Cowan strain, MW 45kDa), reagent grade ≥95% pure (product code P7837). The second, from Sino Biological (Beijing, China), was also recombinant Protein A, expressed in E. Coli (MW 34kDa), reagent grade ≥95% pure (catalogue code 10600-P07E) but had a his-tag in place of the cell wall anchoring section of the protein. A variety of analytical grade chemicals were used for the experiments, including sodium chloride, sodium dihydrogen orthophosphate, disodium hydrogen orthophosphate, sodium hydroxide, sodium acetate, citric acid, acetic acid, hydrochloric acid, glycine, sodium dodecyl sulfate, tween-20, EDTA, ethanolamine hydrogen chloride, nickel sulfate, potassium dihydrogen orthophosphate, EDAC, NHS and imidazole. These chemicals were made up into a variety of buffers using purified (Milli-Q) water.

An Eppendorf (Hamburg, Germany) Centrifuge 5415 R was used for sample centrifugation to ensure the amount of aggregate was minimised. The NanoDrop 1000 (Thermo Fisher Scientific, Waltham, MA, USA) was used to check the concentration of IgG and Protein A in solutions before use in the SPR. A XCell4 Surelock Midi-Cell Electrophoresis System (Life Technologies, Carlsbad, CA, USA) was used for electrophoresis gels to ensure the IgG and Protein A were in native forms and not denatured. Purified water was sourced from a Millipore (Billercia, MA, USA) Milli-Q Direct 16 system, which after buffer preparation was filtered through 0.2µm vacuum filters to ensure sample purity and minimise contamination.

Buffers were sonicated for 15 minutes (Digitech Systems, Kolkata, India) to remove dissolved gas from solution.

The XPR36 operates as described in Chapter 1. The chip is where the interactions take place on a thin gold surface coated with alginate with six “vertical” and six “horizontal” channels etched into the chip. Actually both flow directions are in the horizontal plane but flow channels are in sets of six, oriented at right angles to one another. The sets of channels are referred to, for convenience, as “vertical” ligand (L) channels and “horizontal” analyte (A) channels, due to their apparent orientation if viewed with the chip held up in front of the eye. The chip is maintained under a flowing solution while in the SPR, with a running buffer supply requiring frequent refill/replacement when running. There are two pumps (A and B) that allow for changing of running buffer during a run or additional capacity for extended runs. The sample chamber can either contain microplates with approximately 350µl wells or 1.5ml sample vials but the instrument simultaneously draws up samples in sets of six (one per channel). The machine is shown below in Figure 4.1.

Figure 4.1: The ProteOn XPR36. 1) The chip. 2) Sample chamber containing rack and autosampler. 3) Running Buffer Chamber.

4.2 Buffer and Sample Preparation

The most frequently used buffer was phosphate buffered saline with Tween-20 pH 7.4, which contains sodium chloride (137 mM), potassium chloride (3 mM), disodium hydrogen orthophosphate (10 mM), potassium dihydrogen orthophosphate (2 mM) and Tween-20 (a non-ionic detergent) at 0.005%. PBS is made to mimic physiological conditions with Tween-20 added to improve SPR performance by reducing salt deposits. The PBST buffers used at pH 7.0, 6.5 and 6.0 were modified to improve buffer stability employing only sodium salts. Disodium hydrogen orthophosphate was used at 12.2, 6.3 and 2.46 mM, respectively, with sodium dihydrogen orthophosphate used at 7.8, 13.7 and 17.54 mM to maintain phosphate at 20 mM. The sodium chloride and Tween-20 concentrations were the same as above in all buffers. All phosphate buffers were made up to the desired pH by the addition of hydrochloric acid and/or sodium hydroxide.

Most of the other buffers were simpler in composition. The acetate buffers used were made to the desired concentration using sodium acetate with acetic acid and sodium hydroxide added to obtain the desired pH. When used as a running buffer in the SPR sodium chloride and Tween-20 were added as above. Similarly, the glycine-HCl, EDTA and MES buffers were made up from their named component with hydrochloric acid/sodium hydroxide added to reach the desired pH. The glycine-HCl was almost always made up with glycine at 10 mM, at pH 2.0, as it was used as the regeneration solution for the GLC chip. The imidazole, when not added to other buffers was simply made up to concentration in water. The EDAC and NHS were also made up in water.

The IgG was made up from the lyophilized powder into stock solutions of >1 mg/ml in PBST (pH 7.4) for the initial experiments and then saline solution (137 mM) for the kinetic experiments so as not to affect the buffer significantly when mixed. The lyophilized IgG was stored at 4 ºC and the stock solutions were stored at -80 ºC in 750 or 1000 µl amounts. When used the stock IgG was stored at 4 ºC for no more than a week and never refrozen. The Protein A was always made up in PBST (pH 7.4), for stability, at concentrations between 0.1 and 0.6 mg/ml. The stock solutions were stored at either -20 ºC or -80 ºC with the products (Sigma and Sino) both stored at -20 ºC. The Protein A was immobilised at such low

concentrations (<0.01 mg/ml) that the effect of the PBST buffer was negligible on the buffer used for immobilisation (MES or sodium acetate). Due to the minimal amounts of Protein A required the stock samples were used immediately and not stored or refrozen. When making up the stock solutions a microbalance was used to approximately measure the amount of powder before mixing up the solution. The solution was then centrifuged for 5 minutes at 13,000 rpm and 4 ºC to separate insoluble components. The solution was then tested on the NanoDrop 1000 to get an accurate concentration. Solutions were centrifuged every day they were in use and concentration was tested when first defrosted. All products were tested using SDS-PAGE (in the XCEll4 Surelock Midi-Cell), in both native and reduced forms, to ensure they were intact and behaving as expected. All experiments performed on the XPR36 were temperature controlled with both the chip and the sample plates held at 25 ºC.

4.3 Initial Experiments for the Determination of Optimal Parameters

SPR devices are highly sensitive and to get the best results careful preparation of buffers and samples is crucial, along with rigorous testing to determine the best conditions for studying the interaction (e.g. ligand concentration, analyte concentration, buffer salt concentration, immobilisation method). The basic conditions and parameters are well established for chromatographic columns but these will not necessarily be perfectly reproducible or workable for an SPR and any deviations need to be noted to ensure the results remain valid to the large scale chromatographic processes.

A range of chips, upon which the Protein A can be immobilised, are available for the XPR36 with a variety of properties. Of the seven options (43) for the chip, high capacity varieties (HTE, GLM, GLH) can be immediately eliminated as reaction kinetics are more accurate at lower concentrations (26) because this limits aggregation of the analyte and ligand. Next, the LCP chip can be eliminated as it is for capturing lipid assemblies not proteins. That leaves the GLC, HTG and NLC chips, which immobilise the ligand by amine coupling, His-tag affinity and biotin affinity respectively. The HTG and NLC chips provide site-specific binding, giving a consistent ligand orientation but requiring the ligand to be altered for binding to occur. The GLC chip's binding mechanism is not site-specific but gives randomly oriented ligands. Because the NLC and HTG chip offer similar advantages it was decided to

experiment with the HTG and GLC chips to determine the best option for the full experiments.

The GLC chip was therefore tested first with a variety of concentrations of Protein A (10 to 0.01 µg/ml) initially applied, based on molecular weight and previous experimentation.

Pre-Conditioning:

Before immobilisation was performed the chip was pre-conditioned by passing 0.5% SDS, 50 mM sodium hydroxide and 100 mM hydrochloric acid solutions across the chip consecutively at 100 µl/min for 60 seconds. After eight blank/buffer (PBST) runs (to remove any residue), at 100 µl/min for 60 seconds, the chip can be immobilised. PBST was used because virtually all interactions between IgG and Protein A are carried out in PBS at a pH between 7.0 and 8.0.

Ligand Immobilisation:

Immobilisation was performed according to the standard amine coupling protocol suggested by Bio-Rad. EDAC (133 mM) and NHS (33 mM) were mixed and applied to the chip to activate the surface and allow binding to occur at 30 µl/min for 300 seconds. The Protein A was then applied to the chip in a sodium acetate solution (10 mM, pH 4.0), at 30 µl/min for 300 seconds, as acidic conditions are necessary for amine coupling to occur. Finally, any remaining active sites were blocked by the application of ethanolamine-HCl (1 M, pH 8.5) at 30 µl/min for 300 seconds. Once more, eight buffer runs were performed to remove any residual chemicals. Once the immobilisation was complete IgG could be applied and the interaction was studied.

HTG Chip Immobilisation:

The immobilisation procedure for the HTG chip followed similar lines with a pre-conditioning step to begin. The pre-conditioning was the same as for the GLC with the

addition of an EDTA (300 mM, pH 8.5) step after the original steps followed by the eight buffer runs. The HTG chip was activated by the application of nickel sulfate (10 mM) in MES buffer (10 mM, pH 6.0) at 30 µl/min for 120 seconds, with the Protein A following also in MES buffer at 30 µl/min for 300 seconds. The Protein A was applied at the same concentrations (10µg/ml and 5 µg/ml) as on the GLC chip. There was no deactivation step as the $NiSO_4$ comes off naturally and small amounts of $NiSO_4$ are not of great concern as the IgG does not have any histidine chains to cause significant interaction. The eight buffer runs are then carried out before the IgG interactions were initiated, to wash away any residual Protein A or $NiSO_4$.

Regeneration and Blanks:

The interactions runs were separated by regeneration and blank runs to ensure they were consistent and did not affect each other. After each interaction step at least 180 seconds of regeneration occurred to ensure complete removal of any remaining IgG from the chip surface. These were followed by four to eight buffer runs comprising at least 480 µl of buffer over 480 seconds in total. These runs were to ensure uniformity of conditions between interactions by washing away any residues left by the previous steps. These steps ensured the pH, salt concentration and ligand concentration remained as consistent as possible. If the buffer was changed a system flush was performed with the new buffer followed by four to eight buffer steps, the same as after an interaction. This did not change between the initial and kinetic experiments.

For both chips, a number of initial runs were carried out with a variety of IgG concentrations (between 1 µM and 3 nM) to determine the best range of concentrations for clear and accurate results. Flow rate (25-200 µl/min limited by the XPR36), contact time (limited by the sample size) and dissociation time were also varied to examine any associated affects. PBST buffer (pH 7.4) was used as the blank and for the interaction between IgG and Protein A for the majority of the runs. Imidazole (10-30 mM) was added to the PBST for some of the runs on the HTG chip to decrease non-specific binding. The regeneration step was varied to determine the most effective regeneration buffer and showed some variation between chips with Glycine-HCl (10 mM, pH 2.0) and sodium acetate (10-100 mM, pH 2.0 and 3.0) used

for both and Imidazole (100 mM) and EDTA (300 mM, pH 8.5) used on the HTG chip only. These initial runs were useful in highlighting any issues with the chips or buffer conditions that they were performed under. Once complete these runs provided a clear picture as how to best perform the experiments for analysis and modelling.

4.4 Kinetic Experiments

From the initial experiments the best experimental parameters were found to provide the best data for analysis. The GLC chip was chosen as it was more robust and easiest to work with. The Protein A immobilisation was lowered by using dilute EDAC (13.3 mM) and NHS (3.3 mM) and decreasing the concentration of Protein A to 1 and 0.5 µg/ml. Contact time between the IgG and Protein A was maximised by using the lowest flow rate (25 µl/min for 720 seconds for the IgG) to provide the clearest picture of the interaction's mechanisms. Dissociation time was set at 60 minutes to provide enough time for the dissociation rate to be clear. Glycine-HCl (10 mM, pH 2.0) was chosen as the regeneration solution because it provided the most effective elution, along with sodium acetate (10 mM, pH 2.0), and was the easiest to make up.

After the baseline parameters were established as above, data could be gathered for analysis. To determine the effect of pH on the interaction it was decided to perform runs initially at pH 7.4 and then from pH 7.0 down in steps of 0.5 to pH 3.0 (the frequently quoted elution point of IgG from Protein A), with additional experiments at closer intervals if required. At each pH, at least six interactions were performed to ensure consistency of results and that even multiple errors would not invalidate results. PBST was used from pH 7.4 to pH 6.0 with sodium acetate (20 mM) buffered with saline (after initial problems encountered with non-specific interactions without saline) from pH 6.0 down to pH 3.0. Both buffers were used at pH 6.0 to ensure there was no significant effect when changing the buffer. For the six input samples a serial dilution of IgG was used (with the highest concentrations at 1.0667, 1.5, 3.0 and 0.5 µM) for the first five samples with a blank buffer sample making up the final sample. In all cases an empty channel (either untouched or first activated with EDAC/NHS then deactivated with ethanolamine) was present on the chip, along with any bound channels to provide a reference, along with the blank sample, for comparison. The sensorgram for the

reference channel was subtracted from those for the ligand channels, to eliminate SPR responses caused by buffer change (changes in refractive index or some non-specific background interactions) rather than actual ligand-analyte interactions.

4.5 Low pH Experiments

Due to the elution of IgG from Protein A occurring between pH 3.0 and 4.0 it was impossible to attain consistent results at the lower pH values when the IgG was applied to the chip in the running buffer. To attain some data at the lower pH values, the IgG was first bound on in PBST at pH 7.4, then eluted under the desired (low pH) value. These experiments were expanded to all pH values to determine if the data collected was valid when compared with the data from the IgG binding in running buffer. These experiments were performed under the same conditions as those in running buffer.

4.6 Data Analysis

The data from the experiments was taken in raw form and processed using the Scrubber program described in Chapter 3. In all cases the baseline and injection time were aligned and any artefacts removed. However, the referencing varied between runs depending on what occurred during the run and what effect it had on the desired data. Some examples of this are when a channel or the blank sample was compromised and did not represent a true blank interaction. Alternatively, if the data was referenced against all three references (interspot, channel and sample) the slight variations that occured across each reference reduced the differences in the data to tiny amounts or add excessive noise. The processed data was then inserted into ClampXP for modelling using Langmuir equations. A variety of models were attempted to determine the nature of the interaction. Mass transfer and a simple 1:1 single site binding mechanism were ruled out because the curves did not fit with the data with the behaviours associated with these phenomena. This left multiple site and higher binding ratios to be worked through to determine the most accurate model. Aggregation was ignored as there was little evidence to suggest such a phenomenon was occurring and it would be difficult to quantify even if did (because of the constant flow of the IgG sample where it would be occurring).

Chapter 5: Results

This chapter provides the collated data from the experiments with selected examples to illustrate the significant points. The full results, containing all runs used in the data sets, are shown in Appendix B. All of the data, except where mentioned, shown both here and in Appendix B was processed because few practical observations can be made from the raw data.

5.1 Initial Optimisation Results

The initial results from the GLC chip were promising but obtaining the desired concentration of Protein A was challenging. The starting concentrations of 10 and 5 µg/ml of Protein A produced responses above 1000 RU during the IgG interactions. Even lowering the concentrations to 1 and 0.5 µg/ml produced responses above 500 RU, which remain higher than desirable due to aggregation and mass transfer becoming more likely at higher concentrations. The EDAC and NHS used in the immobilisation were then diluted 10 times to produce lower responses. Figure 5.1 shows what the initial results looked like after processing with the highest IgG concentration, reaching over 350 RU. While these results were significantly higher than the desired 200 RU they could still be modelled and they were clear and required little processing. It should be noted that this is a concentration of 0.5 µg/ml of immobilised Protein A with the IgG dilution series starting at 1.0667 µM (0.16 mg/ml). To bring the responses into the best range the concentrations were dropped to 0.1, and 0.05 or 0.01 µg/ml.

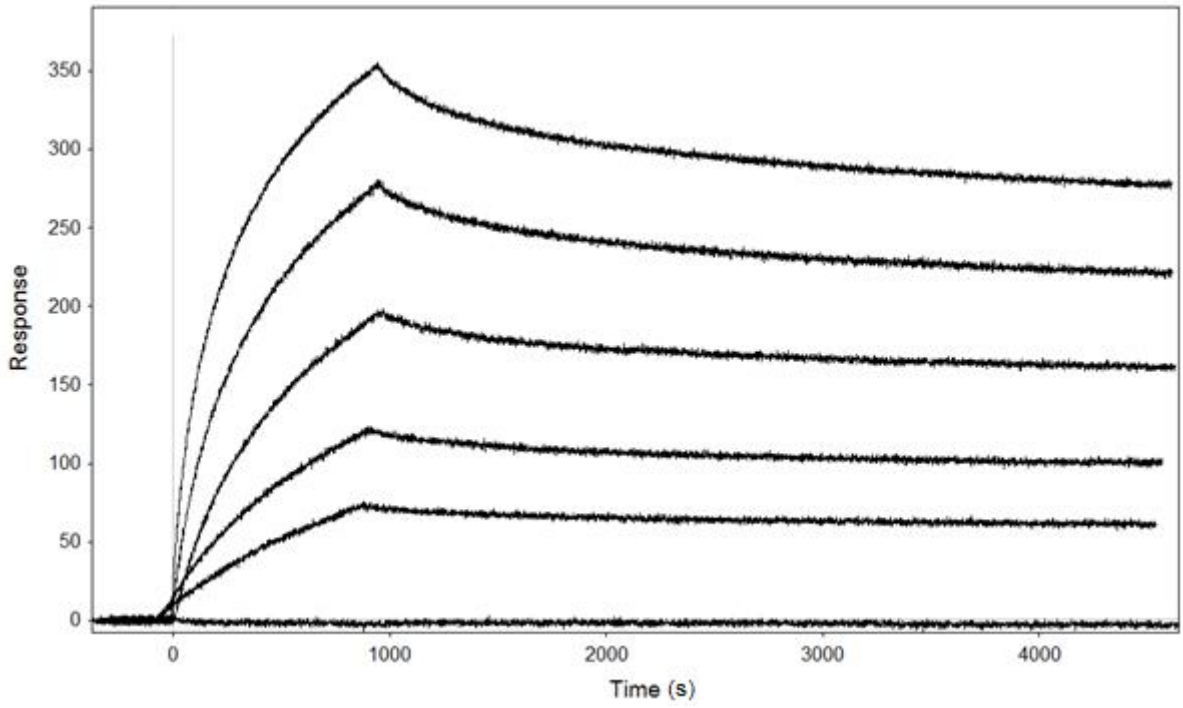

Figure 5.1: An example of the data initially obtained from the GLC chip. Protein A immobilised at 0.5 µg/ml and IgG injected at 160 µg/ml.

The HTG chip was not so promising, with the basic protocol proving insufficient to produce clear results across a range of IgG concentrations. Non-specific interactions occurred across the chip when IgG was passed across as shown by Figure 5.2. The non-specific binding can be removed by referencing against a blank channel but difficulties remained in getting data that could be accurately modelled, as shown in Figure 5.3. This lead to the addition of imidazole to decrease non-specific binding, which met with mixed success. The concentration of imidazole required to fully reduce the non-specific binding depended on the concentration of IgG. Initially, 20 mM imidazole was used with 64 µg/ml of IgG and it was effective in reducing non-specific binding for the lower concentrations of IgG in the dilution series, but the highest two concentrations maintained some non-specific binding. However, at 100 mM, imidazole is used to remove the Protein A from the chip, which suggests its use could be damaging to the Protein A even in small quantities. This was further reinforced by the rapid degradation ligand that was seen when using the HTG chip. In an attempt to reduce this degradation, the IgG was reduced to 2 µg/ml and the imidazole to 15 mM but problems remained even at such low concentrations. While there was some potential in using an HTG chip the results did not compare favourably with those attained from the GLC chip.

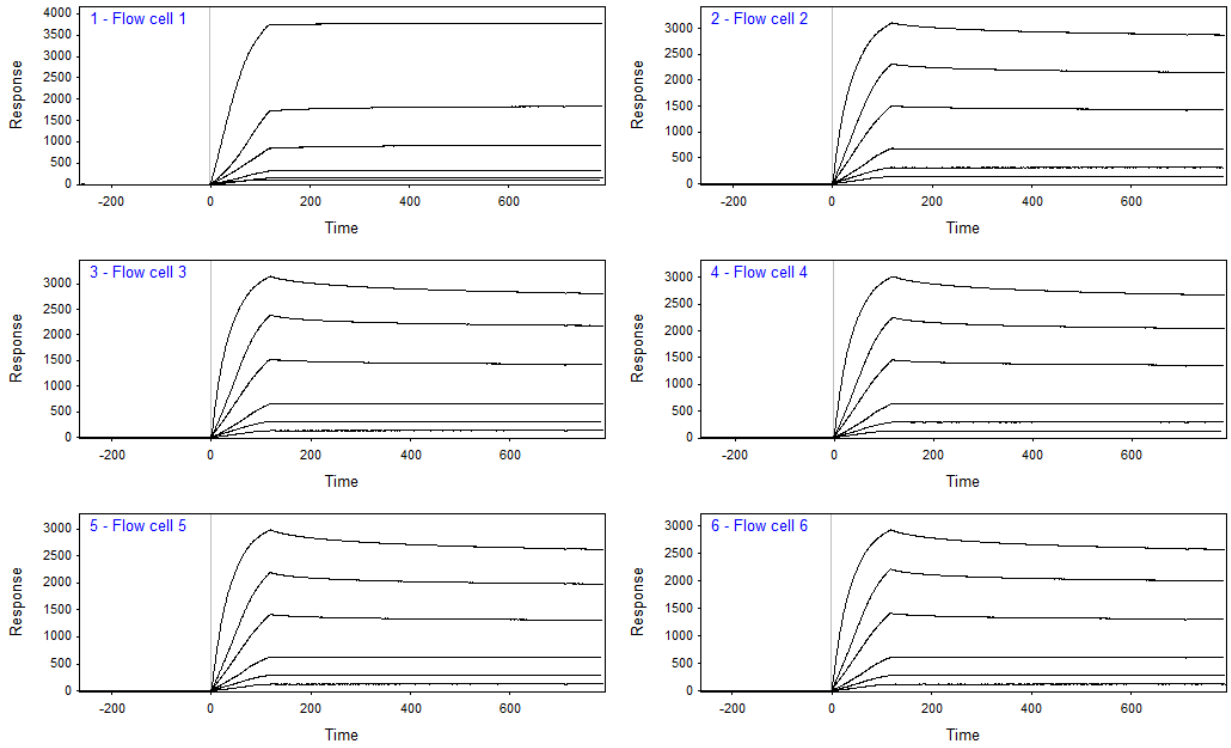

Figure 5.2: Non-specific binding of IgG across all channels on the HTG chip; only Flow cell 1 had Protein A immobilised on it.

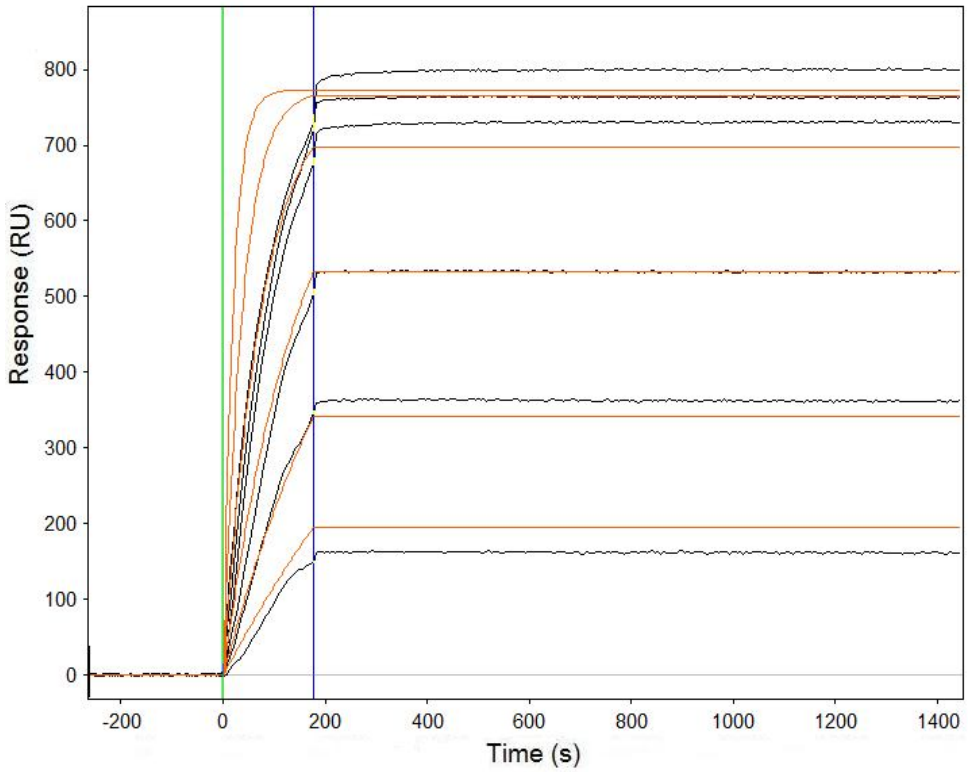

Figure 5.3: IgG-Protein A interaction on the HTG chip with 20 mM imidazole in PBST (pH7.4). A simple first order model was used because this best fitted the action.

The flow rate was varied to identify any mass transfer effects that could be occurring. Three flow rates were used, 25, 100 and 200 µl/min (the minimum, middle and maximum flow rates the XPR36 can achieve). Each was run using a 250 µl sample for 600, 150 and 75 seconds respectively. The combined runs can be seen in Figure 5.4, following the same adsorption line at all flow rates. Each flow rate was tested three times for consistency and any combination produced would look like Figure 5.4. This suggests that there were no mass transfer effects and the process is not limited by any factors other than the interaction itself, as desired.

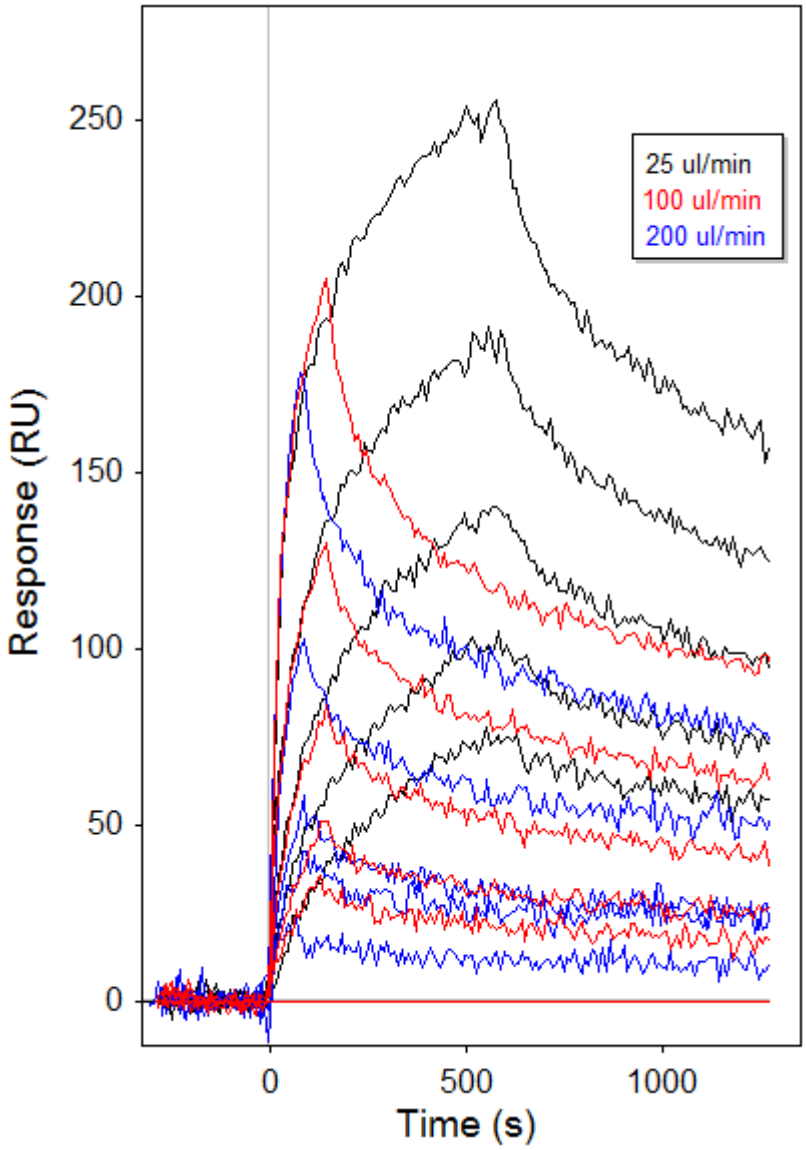

Figure 5.4: Three different flow rates of IgG interacting with Protein A in uniform conditions.

5.2 Kinetic Experiment Results

A number of different models were tested against the data to determine the most accurate and robust model. Mass transfer was ruled out as shown above and a simple 1:1 model does not curve in the way these data do. Models were then tested by steadily adding complexity until an adequate fit could be found. A 2:1 binding ratio was then attempted as this seemed likely given Protein A's ability to bind two IgG, an example of this is shown in Figure 5.5. Next a single-binding two-site model was tested, with mixed results as shown in Figures 5.6 and 5.7. A three-site single binding model was also tested, shown in Figures 5.8 and 5.9 for comparison with Figures 5.6 and 5.7. Finally a two-site, double-binding (2:1 IgG:Protein A) model was tested, shown in Figure 5.10. This model was harder to fit (hence the different data set) as ClampXP finds the additional complexity unnecessary and stops fitting until the parameter is removed. No further models were tested, as it became clear that further complexity did not improve the fit of the model. The three-site single-binding model was chosen to go forward with, as it was robust and effective at modelling the large amount of data gathered.

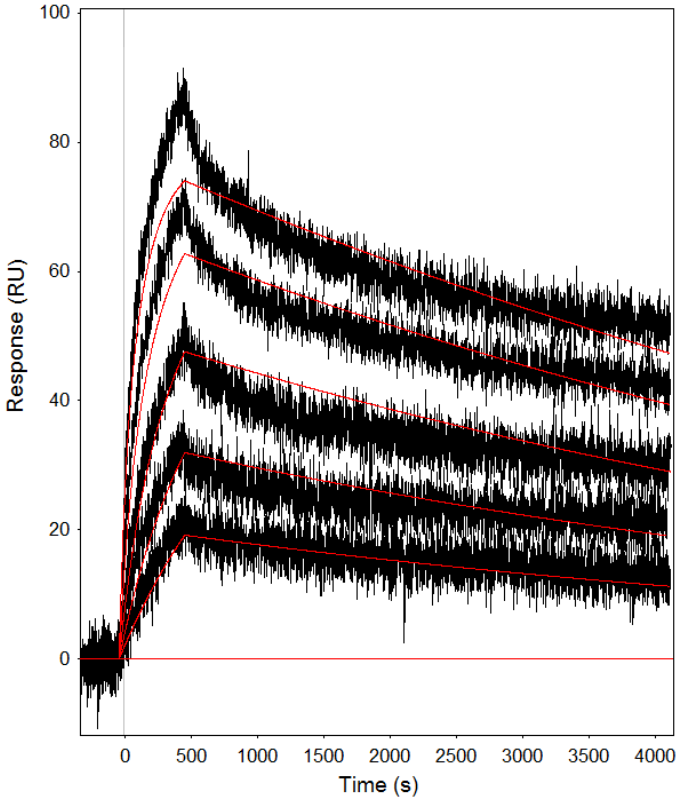

Figure 5.5: A 2:1 binding ratio (IgG:Protein A) model, single site. Red is the model, black the data.

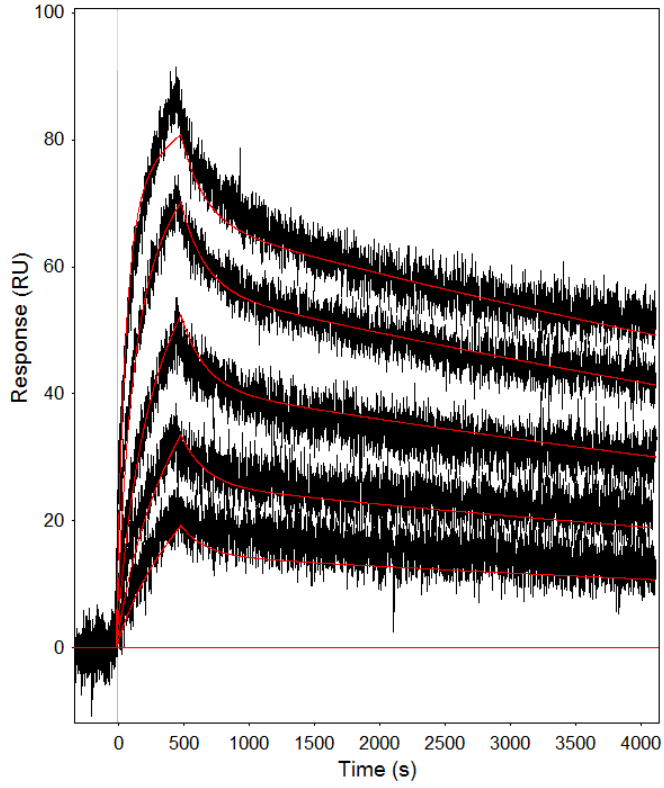

Figure 5.6: A good two-site (on the Protein A) model with single-binding. Red is the model, black the data.

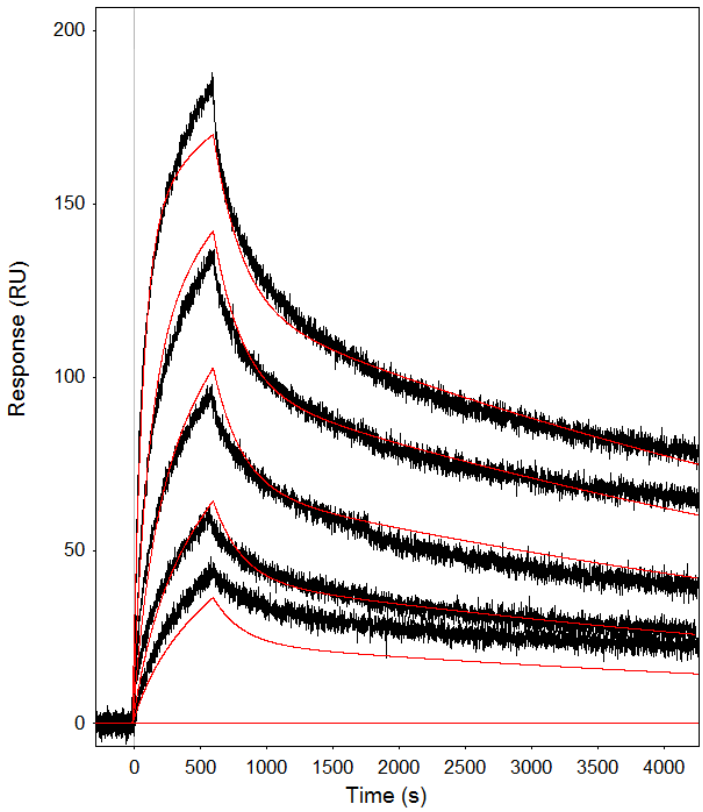

Figure 5.7: Another two-site model but not as accurate as in Figure 5.6. Red is the model, black is the data.

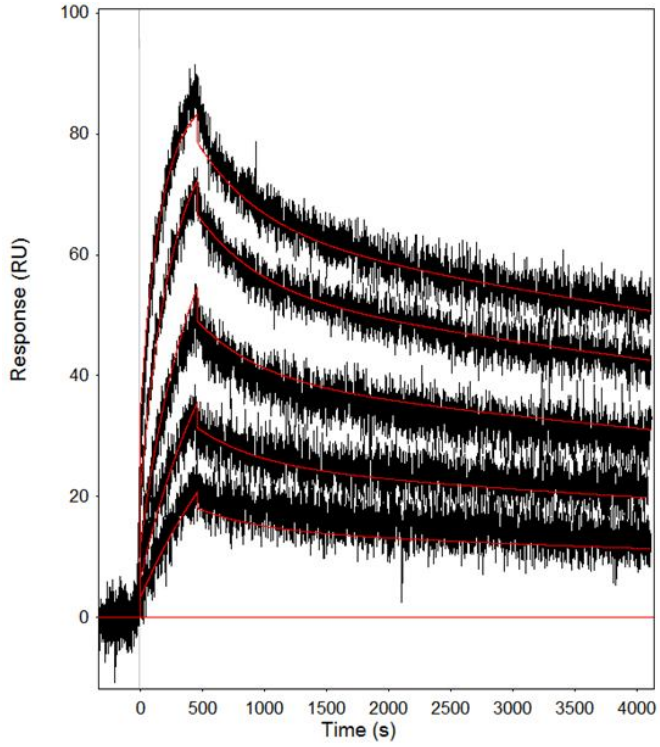

Figure 5.8: Three-site, single-binding model using the same data as Figure 5.5. Red is the model, black is the data.

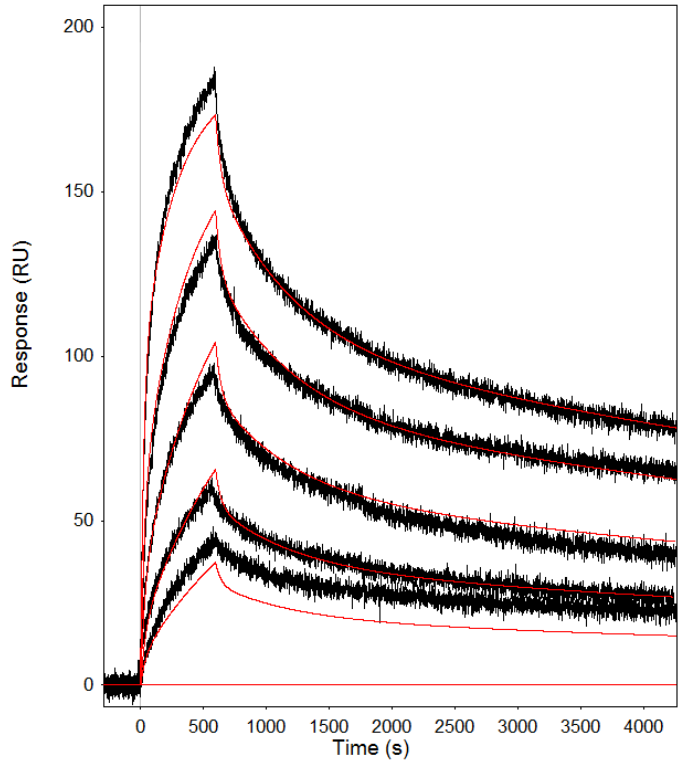

Figure 5.9: The three-site model, single-binding, using the same data as Figure 5.6. Red is the model, black is the data.

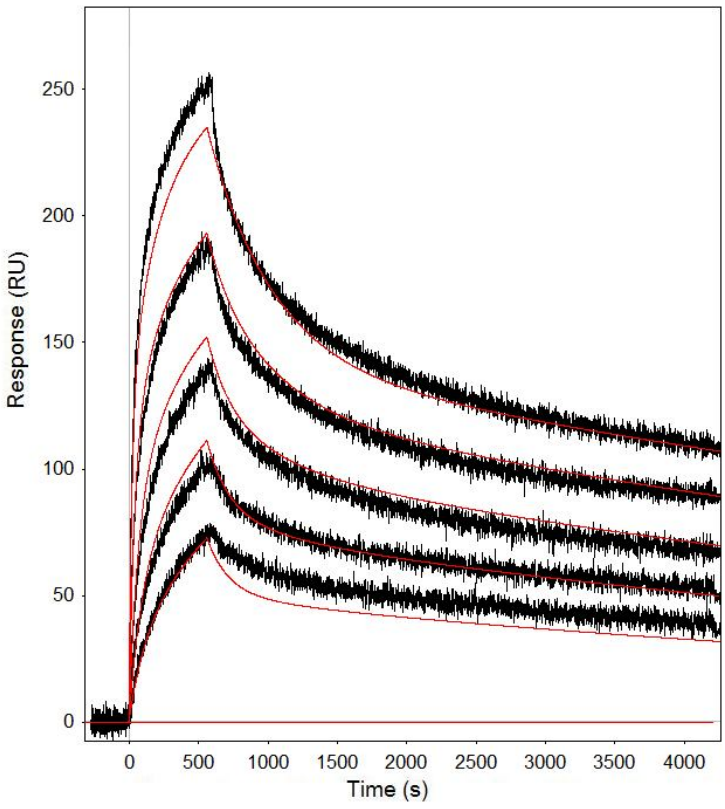

Figure 5.10: Two-site, dual-binding model. Red is the model, black is the data.

Once the model was established and the data collected and collated, the larger scale analysis of trends across the pH range could be examined. Unfortunately, below pH 5.0 it became extremely difficult to determine interaction kinetics because the IgG was strongly interacting with the chip surface and the Protein A and IgG interaction was weakened. At pH 5.0 and above a large amount of data was obtained and analysed. Figures 5.11, 5.12 and 5.13 show the association, dissociation and rate (association over dissociation) constants obtained from the experiments between pH 5.0 and 7.4. The averages of these can be seen in Figures 5.14 to 5.16, which make the overall trends somewhat easier to see. The association and dissociation rates show a downward trend from pH 7.4 to 5.0, however the rate constants remain relatively steady.

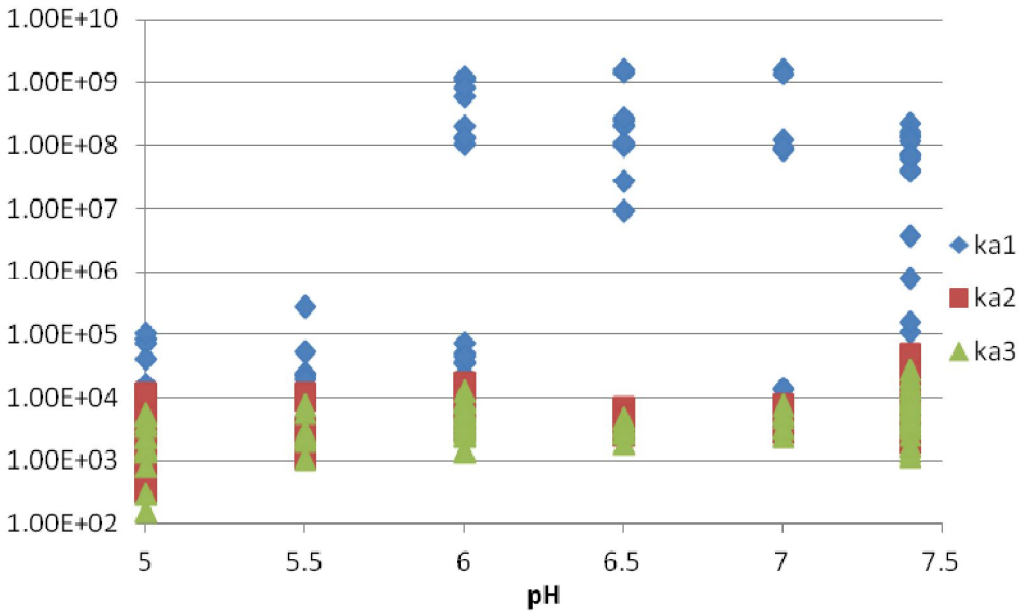

Figure 5.11: Association/adsorption constant for IgG-Protein A interactions in running buffer. ka1 is the highest and ka3 the smallest in the set of three constants obtained from each interaction.

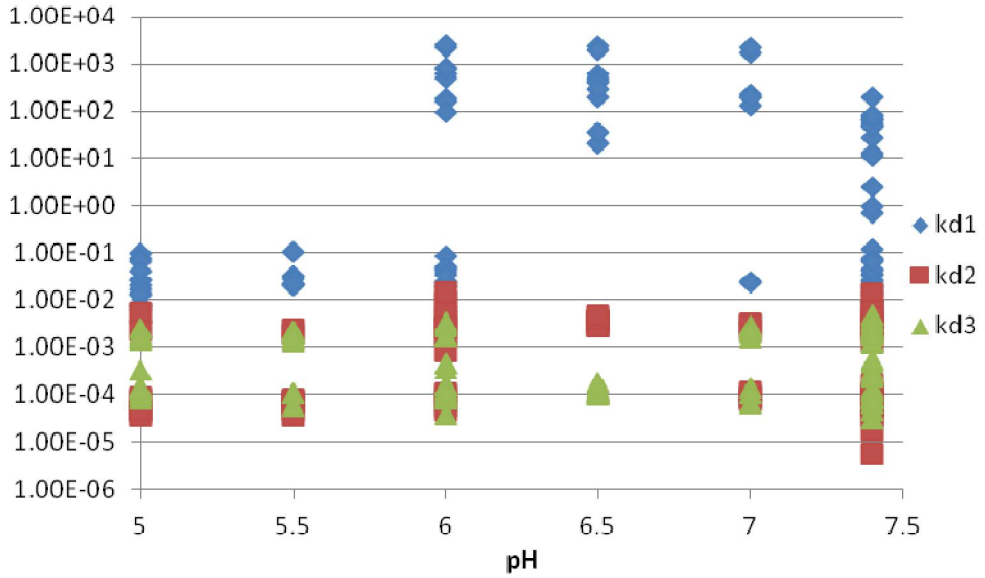

Figure 5.12: Dissociation constant for IgG-Protein A interactions in running buffer. kd1, kd2 and kd3 are the dissociation rates that go with ka1, ka2 and ka3 respectively.

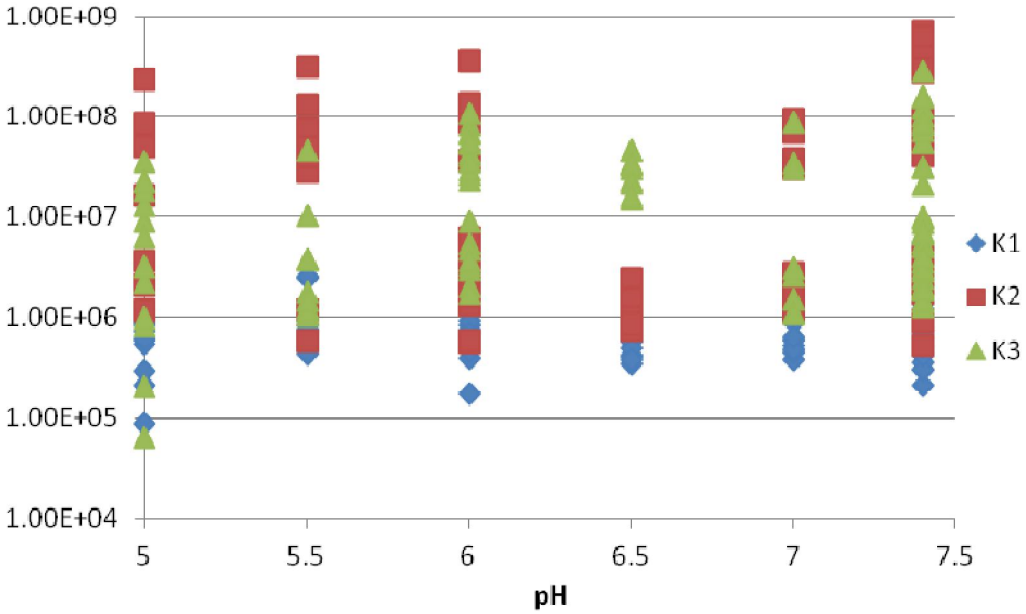

Figure 5.13: Rate constants for IgG-Protein A interactions in running buffer. K1, K2 and K3 represent ka1, ka2 and ka3 respectively.

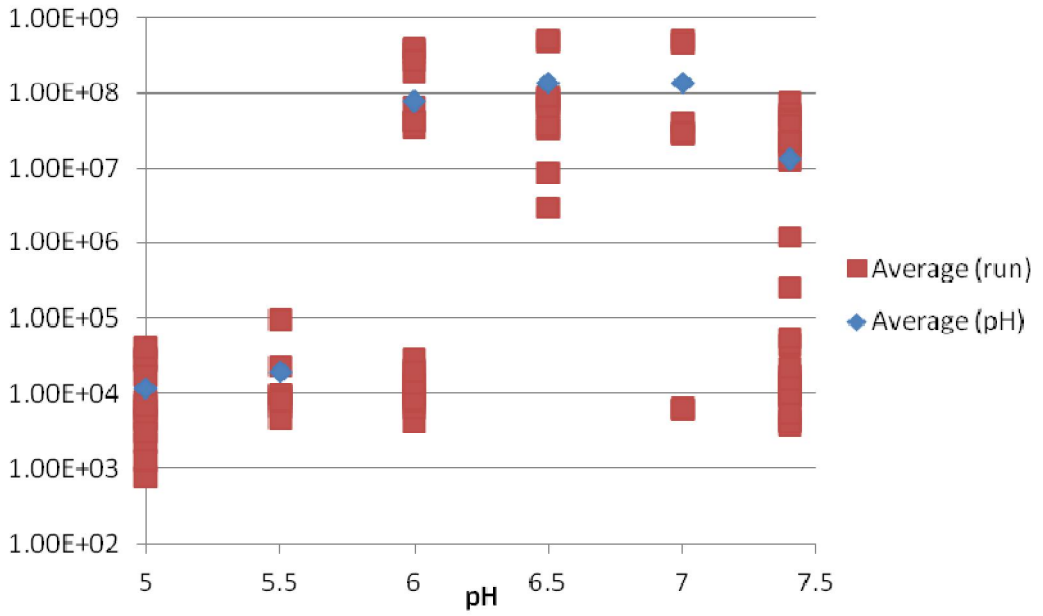

Figure 5.14: Average of all the association constants in each separate run and each pH.

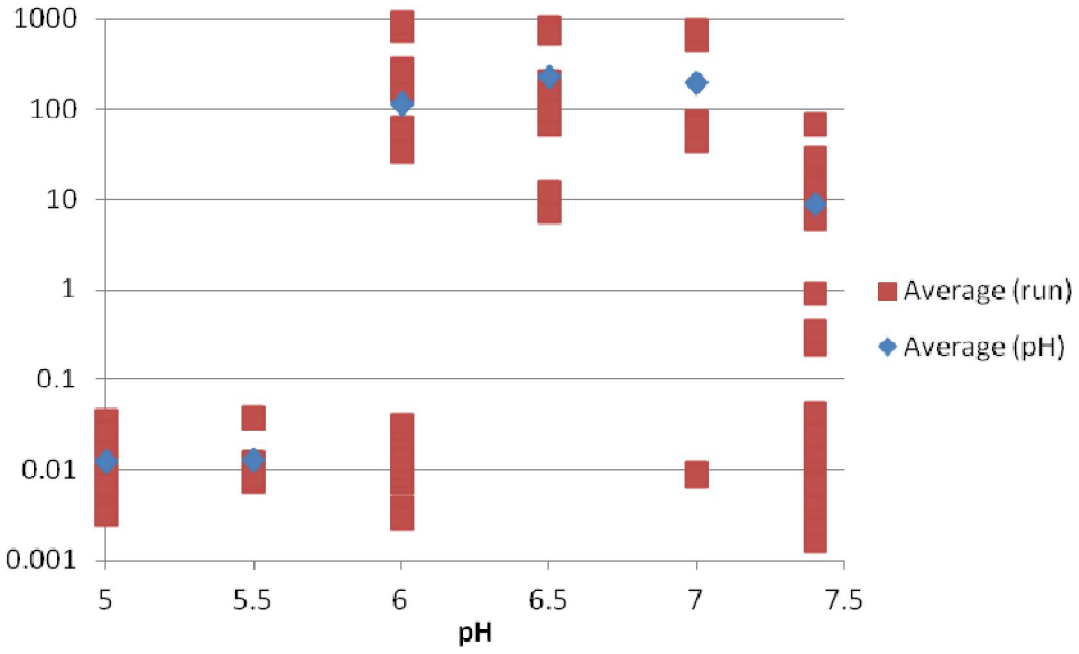

Figure 5.15: Average of all dissociation constants in each separate run and each pH.

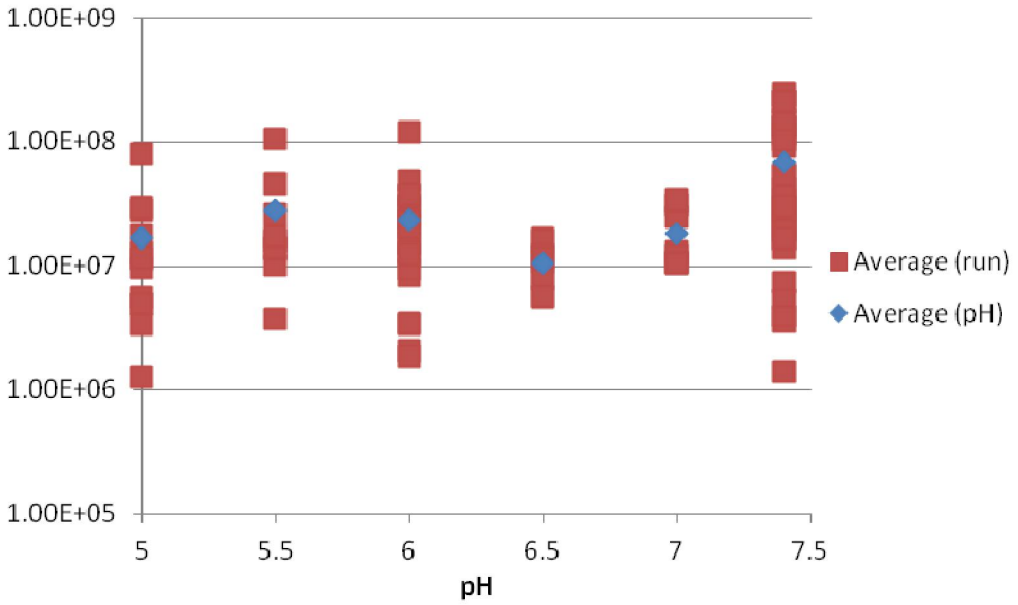

Figure 5.16: Average of all rate constants for each separate run and each pH.

5.3 Immunoglobulin G Binding in PBST

The difficulty of measuring pH less than 5 with the IgG in running buffer forced a rethink of how to measure the rates at low pHs. Because the binding phase is not as important at these levels (in practice, binding would not be expected at this pH so purificaition would be run at a pH value closer to neutral), the focus was moved to the elution phase, only, at low pH, while PBST (pH 7.4) was used to bind the IgG. Even with this strategy it was difficult to obtain consistent results below pH 4.0. IgG in PBST (pH 7.4) was used across the full range of pH to provide a basis for comparison with the IgG in buffer experiments. Figures 5.17 to 5.19 show the association, dissociation and rate constants respectively, for the experiments. While the association constant is not of any real purpose it is shown as it was used in the model because it affects the dissociation constant. The average values of each constant are also shown in Figures 5.20 to 5.22 to see what overall trends exist. The trends shown are somewhat similar to those of the IgG in buffer, with a slight decline from pH 6.5 to 5.0 for the dissociation rates. Below pH 5.0 a steady increase in dissociation constants occurs. However, the rate constants remain relatively steady between pH 5.0 and 7.0, but show a steady decline from pH 5.0 down to 3.0. This is in line with expectations of decreasing affinity as pH decreases.

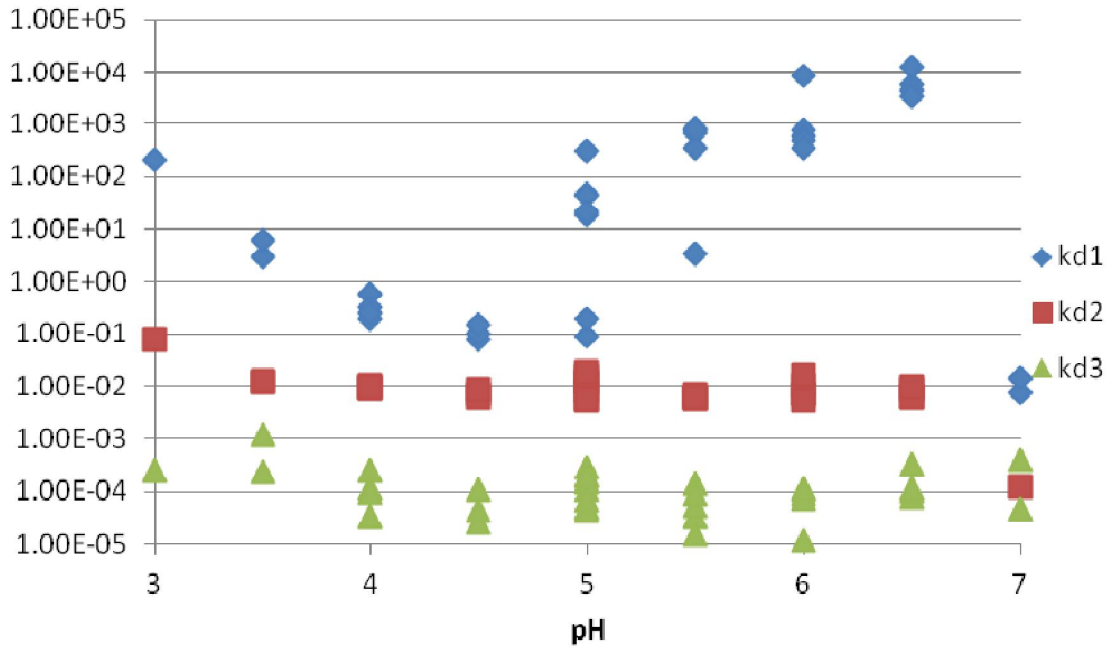

Figure 5.17: Dissociation constants for IgG-Protein A interactions binding in PBST (pH 7.4). kd1, kd2 and kd3 are the dissociation rates that go with ka1, ka2 and ka3 respectively.

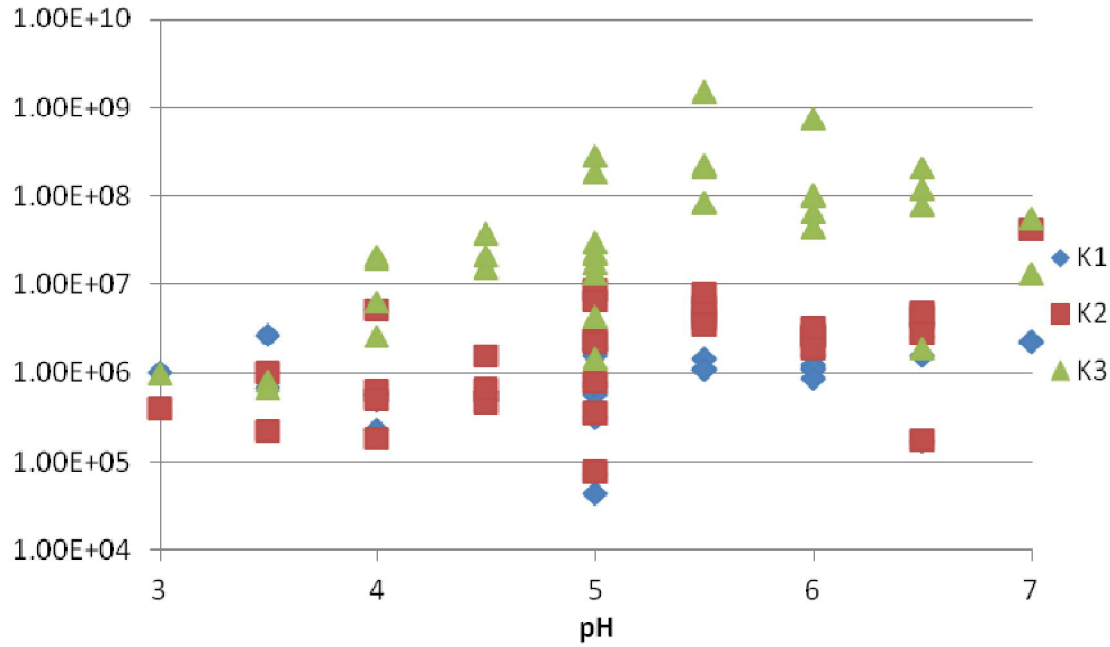

Figure 5.18: Rate Constants for IgG-Protein A interactions binding in PBST (pH 7.4). K1, K2 and K3 represent ka1, ka2 and ka3 respectively.

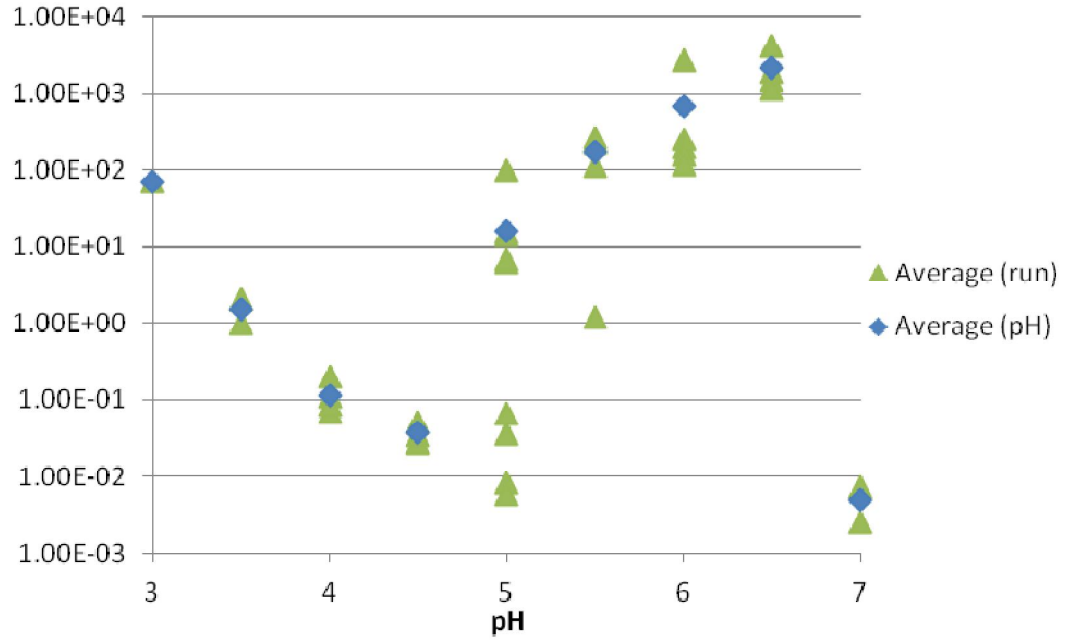

Figure 5.19: Average of dissociation constants per run and pH for IgG in PBST (pH7.4).

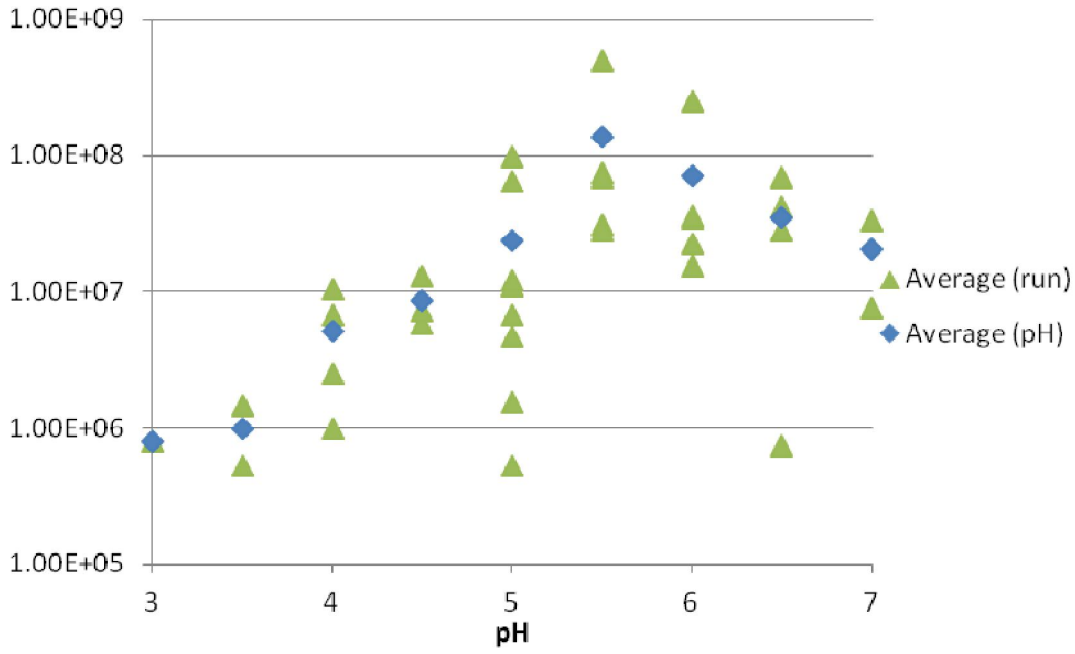

Figure 5.20: Average of rate constants per run and pH for IgG in PBST (pH 7.4).

The behaviour of the IgG-Protein A interaction changes significantly below pH 5.0, as demonstrated by the difficulty producing results when attempting the reaction in buffer. The difference between the buffer and IgG in PBST (pH 7.4) is stark and produces inflated values

from the model to cope with the two different parts of the interaction, as shown in Figures 5.23 to 5.26. As the pH descends the model struggles to accurately reproduce the association phase because of the fast dissociation that occurs once the injection is finished (Figures 5.25 and 5.26, especially). These graphs show that a significant portion of the IgG dissociates quickly at pH 4.5 and the fraction that remains bound decreases with the pH. This largely fits with what is expected given a previous study (33) found IgG2 elutes at around pH 4.0 and IgG1 follows at pH 3.0.

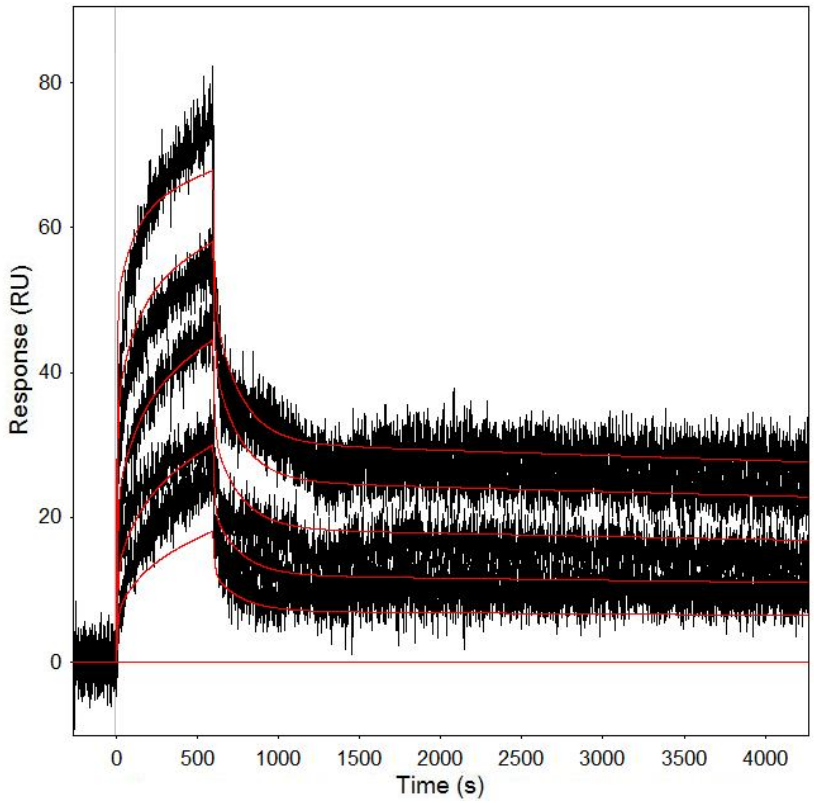

Figure 5.21: Protein A-IgG interaction at pH 4.5 with IgG in PBST at pH 7.4. Data is black, model is red.

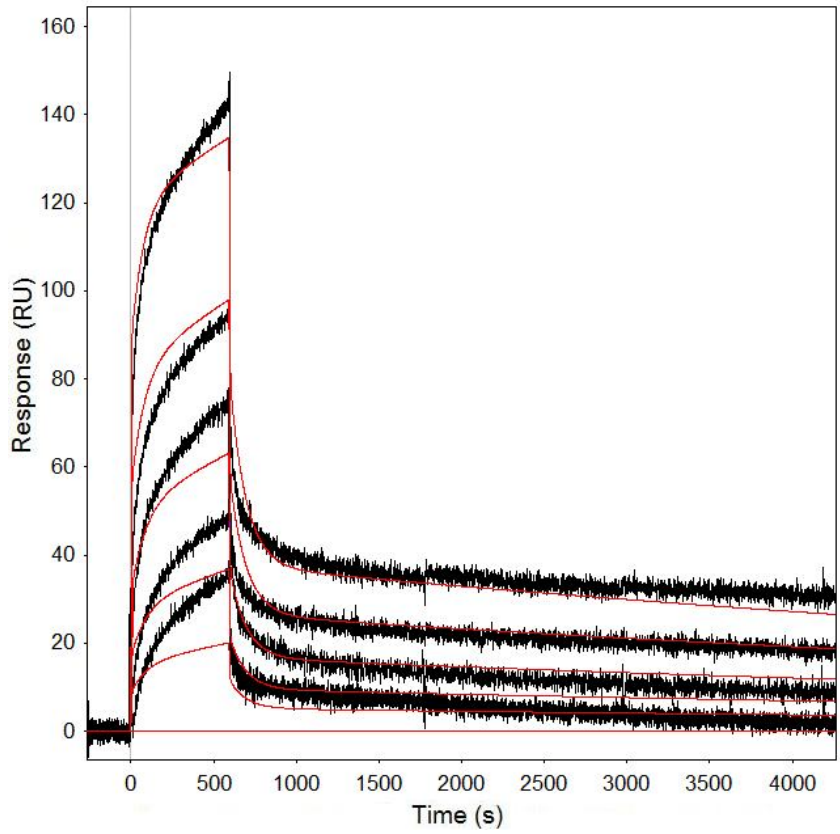

Figure 5.22: Protein A-IgG interaction at pH 4.0 with IgG in PBST at pH 7.4. Data is black, model is red.

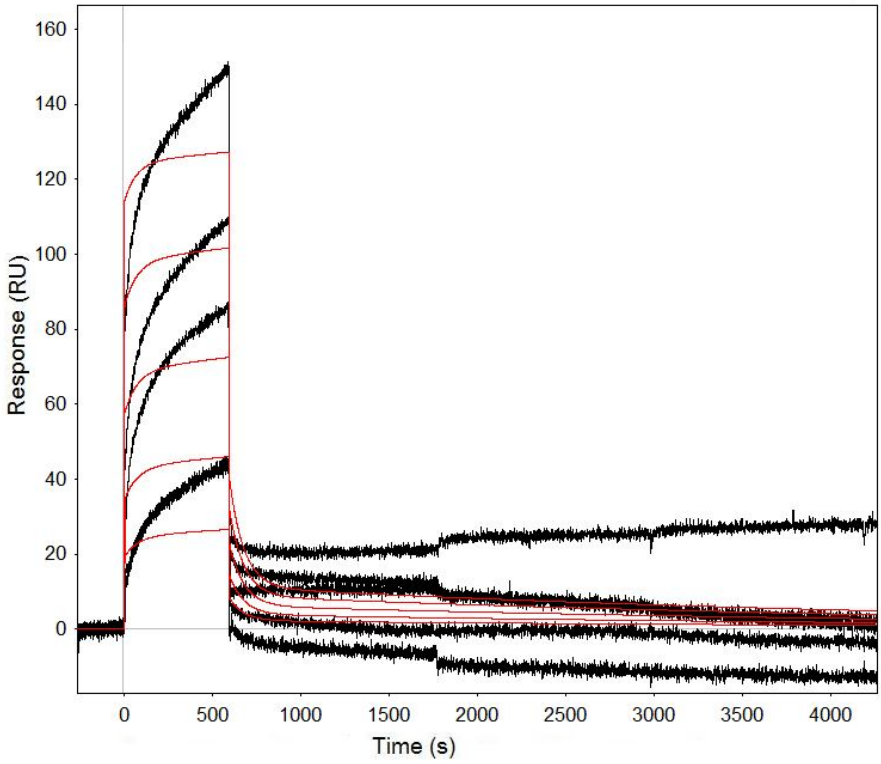

Figure 5.23: Protein A-IgG interaction at pH 3.5 with IgG in PBST at pH 7.4. Data is black, model is red.

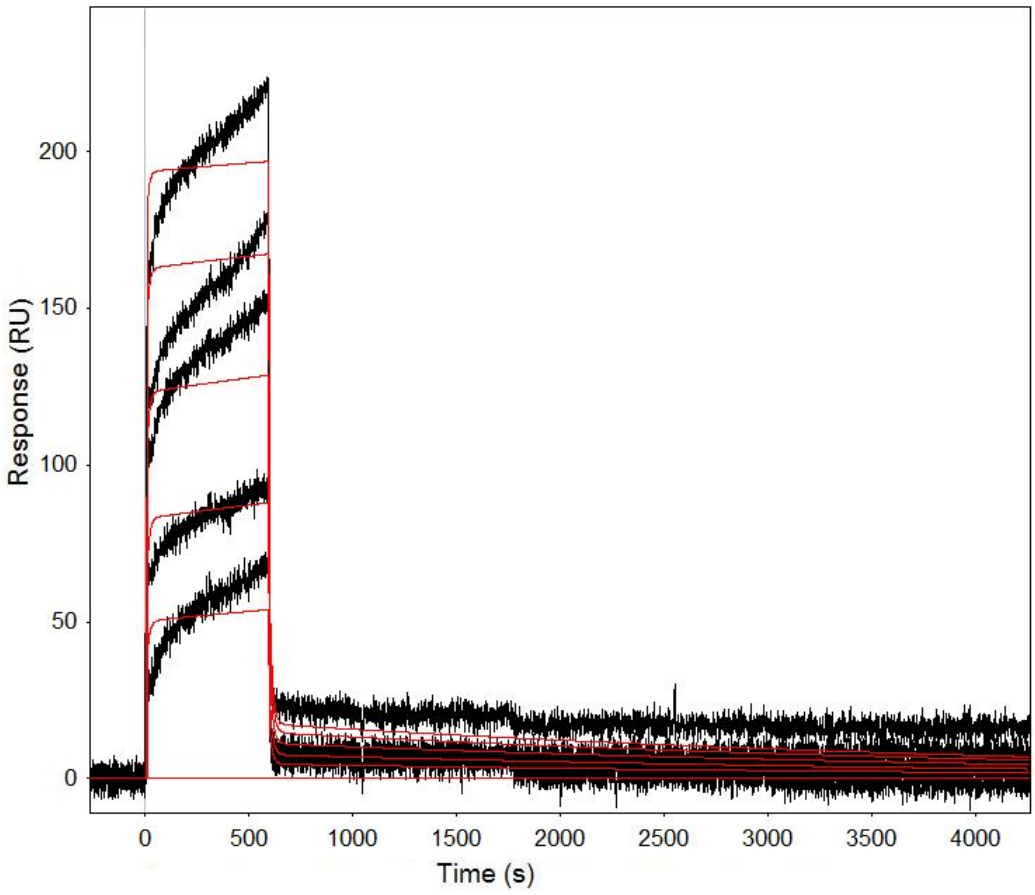

Figure 5.24: A-IgG interaction at pH 3.0 with IgG in PBST at pH 7.4. Data is black, model is red.

Chapter 6: Discussion

Many problems and challenges were encountered throughout with a variety of solutions attempted, with varying success. Whether the solutions used were appropriate and, with the benefit of hindsight, whether better options existed will be discussed here. The validity of all methods and results will also be examined to determine what can be taken from this study.

6.1 HTG Chip Immobilisation and Interactions

As mentioned in the results the HTG chip produced high non-specific binding (Figure 5.2) when the IgG was interacted with the Protein A, which seemed to affect the accuracy of the data obtained. This led to the HTG chip being discarded for any further experimentation, as the GLC chip gave much better responses without significant alteration to the chip conditions. However, Bio-Rad has performed Protein A-IgG interactions on a His-tag chip with some success (44). This leads to questions about how each study was performed and the results between the two were dramatically different.

The method of immobilisation of the Protein A is important for this comparison, because this could immediately produce significant differences between this project and Bio-Rad's work. Both studies immobilised Protein A over 300 seconds onto the chip, which gave a response of roughly 2500 RU. Not only that, but the conditioning and activation steps were also identical in both studies. Furthermore, when the experiments did not produce the desired results the ligand was re-immobilised to try and increase the interaction effect, and make it distinguishable from the non-specific binding. The uniformity between the two studies suggests that the difference in achieving clear results was not due to the immobilisation procedure. This leaves the interaction conditions as the likely cause of the disparity.

The interaction conditions were also close to uniform between the two, with PBST (pH 7.4) used as the running buffer in both cases. Bio-Rad's results are near perfect in terms of behaviour, whereas, in our hands, interaction failed to line up with the expected behaviour over a dilution series. This suggests that the sample preparation was potentially poor as that would cause the concentrations to be inexact and not fit the prediction. However, the

problems persisted over a number of runs using different samples, which makes the consistency of such an error less likely, though still possible. Also given that these errors were not an issue when subsequently using the GLC chip, sample preparation errors are less likely. This does potentially suggest a fault in the chip. Another potential factor is the regeneration solution used, as this was not fully determined on the HTG chip at the time of this work. Bio-Rad used 50 mM NaOH as their regeneration solution, while this project tested a variety of solutions for regeneration, with a focus on low pH, as this was effective for elution in chromatography and on the GLC chip. However, all regeneration solutions were at least pH 3.0, which was shown in the results as leading to almost complete elution within seconds, with at most 10% of the IgG remaining bound. While this might have had some effect, it should not have been significant, especially because none of the interactions showed saturation had occurred and any remaining IgG would be included in the baseline when a new run was performed. This also would not explain the poor results of the first run after initialisation.

The addition of imidazole to the buffer was not performed by Bio-Rad but it is a recommended method for reducing non-specific interactions on the HTG chip. The imidazole had the desired effect for the most part but, as noted, did not remove all of the non-specific interactions at higher concentrations of IgG. Despite this improvement, the same problems with the processed data remained. Adding imidazole also raised other questions, given its properties and how these are used. The first question is whether the imidazole affects the IgG-Protein A interaction as well as the non-specific interactions and if so, how significant is that effect? The second question, which has already been mentioned, is what effects the imidazole has on the immobilised Protein A, given its use for stripping ligands from the HTG chip? To answer these questions a great deal of testing would need to be undertaken, which seemed non-productive when the simple alternative of using the GLC chip was available. Ultimately, resolving the problems with the HTG chip were abandoned because the GLC chip already met the requirements of the experiments. It appears that the random orientation of the Protein A had no significant drawbacks. (Further information was sought on the experimental procedures used for (44) by direct contact with the original authors but none was provided.)

6.2 Models

The three-site single-binding model was chosen to model the entire result set because it produced good fits and was robust across the majority of the data. However, it should be noted that for a number of models ClampXP found the third site unnecessary and a two-site model was used instead. The model does not necessarily identify the true nature of the interaction but, along with the existing literature, the nature of the interaction is further elucidated. A site directed binding of the Protein A to the chip could perhaps help improve the understanding of the mechanisms of the interaction, because this would eliminate any effects caused by the polymer layer interfering with the binding.

Protein A contains five Fc binding sites that are largely similar in terms of structure but the way in which the larger structure of Protein A affects this is unknown. There also exists the ability for Protein A to interact with the Fab region, although this interaction is much weaker (16, 17). Just one of the five interaction sites with IgG has been studied (30) and that interaction was studied in isolation (i.e. using only a fragment of Protein A). This leaves the exact binding mechanisms largely unknown. It is well known that each Protein A molecule can bind two IgG molecules (18), which provides one limitation on the binding mechanism. Given the structural similarities of the five sites (13) it seems probable that the binding mechanisms of each are also similar and perhaps could even be expressed as uniform in terms of the reaction constants. This project suggests this is not the case, because the binding is too complex to be expressed even as a double-binding single-site model. However, given that five sites exist and potentially just two need to be expressed in a model, there does seem to be some evidence that the five sites share similarities. There is also the possibility that the sites work in groups of two and/or three to form two binding sites for the IgG. If the Protein A does act as a two-site double-binder, then there are steric effects to consider that could affect the binding of the second IgG. These factors must be applied when considering each model and its likely representation of the IgG-Protein A interaction.

The three site single binding model can be explained in a number of ways that fit with the existing knowledge. The first and simplest explanation is that the Protein A contains three different binding sites that can individually bind one IgG, which prevents the other sites from

binding IgG likely due to the random orientation of the Protein A on the chip or the short duration of the contact time. The second explanation is that again there are three sites but double binding can occur, however the three sites are independent of one another and the addition of double binding equations or parameters is unnecessary. The third explanation is that there are only two sites, but double binding can occur and the second binding is affected by the first and a third parameter set compensates for this effect. Other explanations of greater complexity could undoubtedly be put forward, but these four simple explanations give reasonable scope and further complexity, without added accuracy, is undesirable in the model. Of these explanations no one possibility seems particularly more likely than any other. There are almost certainly two sites and a third effect exists that needs to be accounted for. This seems likely because the two site model fits the data with a good level of accuracy but the model can still be improved upon. What the exact nature of the third effect is harder to identify as a significant number of possibilities exist and it could be a single effect or a combination of many.

A single site binding model, regardless of the number of IgG that can be bound, does not adequately account for the behaviour the interaction produces. A single site single binding model can be applied when the interaction period is short and the IgG concentration is significantly lower than the Protein A concentration as demonstrated by Bio-Rad (44). This is likely because of the dominance of the higher affinity site over the shorter time periods and in greater availability. Single binding models do not work at higher binding numbers because the first IgG bound must be the last to elute, which forces the first binding to have a low dissociation to match the interaction behaviour in the elution stage. This low dissociation limits how large the first association constant can be to bind the right amount of IgG for the elution stage. This causes the model to rise too slowly in the association phase; hence the model cannot match the data in both the association and elution phases. Ultimately, this prevents any single site model from being accurate and forces the introduction of additional binding sites.

Models with greater complexity than the three site single binding did not significantly increase the accuracy of the model and were discarded. When modelling any system the aim is to produce a model of sufficient accuracy and the least complexity for a number of reasons.

Low complexity makes models faster to simulate and easier to understand for users. Added complexity for minor increases in accuracy can lead to models that are affected by data noise or minor factors that lead to erroneous conclusions about the data's behaviour. For some of the data sets the higher order models show increases in model accuracy but are unnecessary for the majority of the data. This gives a clear indication that the additional parameters do not give a true representation of the interaction's mechanism. The one higher order model that may accurately represent the interaction is the two-site double-binding model. As discussed the two sites could be largely independent of each other causing only minor steric hindrance to the second binding. Due to the minor nature of the hindrance it could be adequately represented by a single parameter set (the third site) when the true action is present at both sites. While this is possible, without knowing with certainty that it is occurring there is no point representing it and even if it is occurring it is accounted for in some manner.

6.3 Experimental Conditions

The conditions under which the experiments were performed had significant effects on the results that were produced. This is particularly obvious in the case of binding in sodium acetate buffer, where the addition of saline significantly decreased non-specific interactions enough to allow for proper interpretation of the results. A variety of other conditions affect the interaction and the subsequent data obtained and for that reason must be carefully controlled to ensure the validity of the results.

As mentioned previously, temperature affects the rate of reaction as described by the Arrhenius equation, making it imperative to be controlled to ensure consistent data. To remove the need to calculate the effect of the temperature all experiments were performed at 25 ºC. This temperature was chosen as Protein A chromatography is generally performed at room temperature as there seems to be no significant benefit to performing it at any higher or lower temperature, although above approximately 40 ºC degradation of IgG occurs. Given that the IgG-Protein A interaction usually occurs at body temperature it is possible that the interaction would be stronger/faster at those conditions than at room temperature but no published study has been done to validate this hypothesis. Given the affinity of IgG and Protein A at room temperature, it has not been necessary to try and increase the affinity and,

because heating/cooling of chromatographic equipment can be costly and difficult, the interaction temperature has not warranted investigation.

The buffer makeup produced significant effects in the experiments and was one of the most difficult experimental conditions to optimise. The choice of buffer was based on those used previously in the literature with PBS being used almost universally for the interaction between pH 7.0 and 8.0, it was the obvious choice for the higher pH buffers. For the lower pHs a number of different buffers had been used with the most common being glycine-HCl, acetate and citrate buffers. There has been no significant comparative study of buffer effects either on binding or elution, with the only studies to have any kind of buffer focus being those comparing citrate buffers with and without arginine (38, 40). There is also some older work on the use of magnesium chloride in buffers to improve elution (45) but this is not commonly used in more recent times. Sodium acetate was arbitrarily chosen from the more common lower pH buffers and for the initial testing. Once the non-specific binding was dealt with by the addition of saline to the buffer, acetate buffer performed effectively enough that no further consideration was given to the buffer use, until the kinetic and low pH experiments were complete. Both PBST and acetate buffers were used at pH 6.0 (see Appendix B) to see if there was any significant effect caused by the change but none were observed.

The binding time was relatively simple to optimise but bears analysis to ensure the experiments validity and provide guidance for any future work. The binding time is of interest because duration can significantly affect the behaviour of the binding. Bio-Rad (44) created data that could be modelled as a simple first-order interaction by using an abundance of immobilised Protein A and a short interaction time (90 seconds). The current work, however, produced data that was definitely not a first order interaction by limiting the Protein A and using extended interaction times (600 seconds). This study is seeking to provide knowledge for Protein A chromatography in industry and thus must match those conditions as far as possible. The most efficient use of any chromatography column is for binding to last until breakthrough of [usually] 10% of the desired compound occurs, to ensure the column is efficiently used and to minimise the number of runs needed for a full batch to be processed or to minimise the size (and cost) of column required. As noted above (in Chapter 2), the minimum residence time for IgG in a Protein A column is two minutes for effective binding

to take place and, generally, multiple column volumes of sample will be passed through before breakthrough occurs. This suggests that at an absolute minimum, a two-minute interaction is required, with longer times better representing the whole process. Given that columns are generally saturated this also requires time for the majority of the Protein A sites to be saturated with IgG, which also requires longer time periods on the SPR or high concentrations of IgG compared with Protein A. It is difficult to model an entire column because the interactions will be different through the length of the column and these will also change with time, however, it is possible to replicate a single section. The binding time was limited by the SPR control software and hardware, with the injection limited to 400 µl (14 minutes injection time) by the software and 275 µl (11 minutes injection time) by the wells on the micro-plate. To prevent any air in the SPR, 10 minutes (600 seconds) was chosen as the binding time.

The elution time was also important for providing an effective analogue to a chromatography column. Instead of trying to exactly replicate the elution time needed through a column the elution time was optimised with the goal of having steady elution at the end of the time so any required extrapolation would be simple. The easiest way to achieve this was to use a relatively long elution time to ensure that any weak binding had already eluted and only the stronger bindings remained. An hour was chosen as the elution time after some experimentation, as this provided more than enough time for the weak non-specific interactions to elute and the stronger binding (and, hence, more slowly eluting) molecules to dominate the action. Half an hour would probably have been sufficient but there was no large detriment to a longer elution time, while the data from the longer elution can be decreased to provide data for a shorter elution time if that is so desired in the model.

6.4 Kinetic Experiments

The models for the kinetic experiments show a number of trends within each pH set and across the pH range. The limited pH range that these experiments were able to be reliably performed in limits what can be taken from the experiments, but a number of behaviours remain of interest for further assessment. The three interaction constants give some indications of how the interaction occurs and how this changes with the pH.

One noticeable feature of the interaction constants is that the highest association constants, and their dissociation constants (also the highest), have the lowest (generally) rate constant of the three constants. The largest constants generally make up the third site with the first two, largely resembling the constants attained when using a two-site model. The behaviour of the third site is mostly caused by the model needing to account for the sharp rise during the association stage and sharp drop off at the start of the dissociation stage that is not fully characterised by the other two sites. This explains why the third site has the lowest rate constant, as it is accounting for the smallest part of the data's behaviour. The third site had consistently the highest error of the three sites (see Appendix B), which is likely due to the small influence it has on the overall model and hence the least precision is needed to create its effect.

Over the pH range (5.0 to 7.4) a number of trends are apparent from the interaction constants. The rate constants remain roughly constant, averaging between $1x10^7$ and $1x10^8$ as shown in Figure 5.16. This suggests that the interaction is not significantly affected by pH in this range. This fits with results from previous studies that found the elution points of the IgG subclasses to be between pH 5.0 and pH 3.0, with IgG1 mostly eluting at pH 4.1, while IgG2 eluted at first at pH 4.9 and again at pH 3.5 (33). This suggests that binding is at least retained until pH 4.0 and therefore it is likely that the interaction will continue to occur until the pH nears this point, with the possibility of the interaction continuing past this point only for IgG1. The dissociation and association constants do show some variation over this pH range with a significant drop in the average between pH 6.0 and 5.5. This drop is largely due to the decrease in the third site rate constant mentioned above. However, the drop is consistent between the two constants, causing it to have little effect on the rate constant. This change indicates that the curve becomes smoother after pH 6.0 because the association and dissociation is slower. This smoothing of the curve suggests that the saturation point is being approached (but some weaker interactions are continuing) at both pH values but it is achieved faster at the higher pH.

There were a number of difficulties when trying to produce consistent results below pH 5.0 with the IgG in running buffer. An overwhelming amount of non-specific binding occurred below pH 5.0, masking the Protein A-IgG interaction. This is likely caused by the alginate layer of the chip becoming charged, as this is the pH range used for immobilisation. These interactions still occurred even on a channel that was first activated with EDAC and NHS, before being deactivated with ethanolamine-HCl, which implies that the interactions cannot be completely removed through pre-treatment of the chip. A potential solution to this problem would be to increase the sodium chloride concentration, as this proved effective when non-specific binding occurred when the buffer was changed from PBST (pH 6.0) to sodium acetate (pH 6.0). Higher salt concentrations could have an impact on the interaction but the results would still give some idea of the behaviour of the interaction at lower pH. Additionally, the IgG starts to degrade at lower pH, leading to an increased number of artefacts breaking up the interaction data. The only way to combat this degradation would be to minimise the time the IgG spends in the buffer by preparing samples immediately before injection across the chip. Instead of dealing with these problems the decision was taken to inject the IgG in PBST (pH 7.4) to study the dissociation, which admittedly compromises the association values attained from such experiments. This new method was applied across the full pH range desired (3.0-7.4) to see what effect this had on the interaction constants when compared with those applied in buffer.

6.5 Low-pH Experiments

This set of experiments bears a great deal of similarity to the chromatographic purification of IgG using Protein A media. The application of IgG was performed in PBST at pH 7.4 to ensure effective binding, which was followed by elution using the desired buffer at a lower pH. This method was used because it was based on the behaviour of the system that this study seeks to help elucidate fully. This approach does make the modelling of the data more difficult, due to the two conditions used, as well as making the results less useful in predicting overall behaviour. Despite those reservations, some useful observations can still be drawn in regard to the dynamic of the elution over the pH range.

The interaction constants show behaviour that at first appears somewhat unusual but upon closer inspection larger fits with the expected behaviour as the pH decreases. Figure 5.18 and 5.20 show how the rate constants change with the pH, showing a steady decreased from pH 5.5 down to pH 3.0. This decrease is expected as the pH drops the binding should get weaker and elution should occur faster. Oddly, the rate constants increase as pH decreases from pH 7.0 to 5.5, which may be due to the need for the association constant (not shown because the binding occurs at pH 7.4 and the values are not a true representation of the mechanism) to increase more than the dissociation constant increases in order to maintain the same amount of IgG bound in the association stage. This effect may only be present from pH 7.0 to 5.5, because below this point the running buffer may start affecting the binding, because of sample/buffer contamination caused by mixing in the SPR or residue on the chip. From pH 4.5 down, a steady increase in the dissociation constants occur as the IgG more rapidly dissociates from the Protein A. At pH 7.0 the rate constant seems in line with the overall trends, but the dissociation constants are significantly lower than the next data set. These results were the last obtained and the data had some problems (see Appendix B) that may have been caused by chip degradation. Only two runs were at pH 7.0 were included as the other six runs data was too flawed for modelling.

The first basis for comparison is between previously reported elution points and the behaviour observed in these experiments. Figures 5.21 to 5.24 show the behaviour of the IgG when exposed to pH 4.5 to pH 3.0. At pH 4.5 approximately 40% of the IgG remains bound after 10 minutes of elution, which decreases to 30% at pH 4.0. At pH 3.5 and 3.0 elution speeds up considerably with just 13% and 10% left after one minute of elution. The literature suggests that IgG elutes between pH 5.0 and pH 3.0 (33), which fits with these observations. The difference between pH 3.5 and 3.0 is small in terms of remaining IgG but in a full scale chromatography column there may be benefits to using the lower pH, such as sharper elution peaks and the dilution of the elution buffer, from mixing with the residual binding buffer, would not affect elution greatly. Of the three binding sites used in the models there was clear variation in their association/dissociation constants with one site binding much stronger (having the lowest dissociation constant) than the others. This site was the only one to retain the IgG for any significant period during elution as expected from the earlier experiments.

The next comparison is between the interaction constants of these experiments and the previous kinetic experiments. Looking at the rate constant averages between pH 5.0 and 7.0 (Figures 5.16 and 5.20) for both forms of interaction they are roughly consistent with both having a pH average between $1x10^7$ and $1x10^8$ excepting the IgG in PBST at pH 5.5 which is slightly larger. However, the buffer experiments are more consistent between pH values, whereas the IgG in PBST values seem to peak at pH 5.5 and fall away either side of this point. This variation is minor and the likely causes were discussed above. The dissociation constants do not show such uniformity between the two experimental forms, which can be seen in Figures 5.15 and 5.19. The dissociation constants averages for the kinetic experiments show a step change between pH 6.0 and 5.5 with the other values consistent above and below this point. The averages for the IgG in PBST experiments, on the other hand, show a steady downward slope from pH 6.5 to 5.0 (the outlying point at pH 7.0 was discussed previously). The dissociation constants behaviour in the kinetic experiments averaged between 100 and 1000 between pH 7.0 and 6.0, which then drops to 0.01 for pH 5.5 and pH 5.0. The IgG in PBST experiments have larger numbers trending down, from over 1000 to 10, between pH 6.5 and 5.0. This consistency is explained by the higher association constants that the low-pH experiments produced (Appendix B), causing behaviour of the rate constants in the two experiment sets to be similar, with the higher values in the IgG in PBST largely cancelling each other out. Based on these comparisons, and the previous analysis of the kinetic data, it is clear that in the pH range of 5.0 to 7.0 there are only minor effects on the interaction, mostly relating to association and dissociation speed. It is possible that lower concentrations of IgG would further elucidate the effect of pH in this range as slowing the interaction could prevent binding saturation.

Chapter 7: Conclusions

This project has provided some insights into the binding properties of Protein A and IgG but there is still a great deal that remains to do. Given the importance of IgG in treating a variety of diseases and the crucial role that Protein A affinity chromatography plays in the purification process it is surprising that this area has not be studied previously in any depth. The interaction possesses complexity with the six different binding sites on the Protein A (five for the Fc section and one for the Fab section) and a proven binding ratio of 2:1 IgG to Protein A. However, the models produced from the data in this thesis are not overly complex with a two-site model proving adequate for most of the data, with a third site being desirable for greater accuracy. Ultimately, the interaction between the two molecules proved less challenging to interpret than experimentally producing accurate data below pH 5.0 did.

The data and models produced from the experiments fit with the results from previous studies, while also providing further insights into the exact nature of the interaction. At pH 5.0 to 7.4 the Protein A and IgG have a strong interaction that dissociates very slowly, while some weaker interactions are clearly present as well. A number of explanations exist that match this behaviour, such as the Fab binding site, which has been noted as comparatively weak in previous studies, and steric inhibition causing weaker binding, highly likely due to IgG being three times the size of Protein A. Below pH 5.0, more significant elution begins to occur and rapidly accelerate as the pH descending to almost instant elution of almost 90% of the IgG at pH 3.5. This is in line with previous studies that found similar elution behaviour using pH gradients. The data and models potentially have applications for modelling a chromatographic system although the scale up would be challenging and additional factors, such as mass transfer effects, would need to be taken into account.

A number of areas warrant further investigation, that were not addressed by this project, in order for the binding kinetics to be fully understood. The interaction below pH 5.0 is the first place to start with a number of options existing for further attempts. The first option is a change of platform away from SPR so that the non-specific interactions will no longer be a problem, although few systems exist that can so easily record real time interactions in a similar manner to SPR. If the SPR is persevered with, then an increase in saline concentration

is a potential solution, given the effect it had in this project. A change of chip is also an option, although given the difficulties experienced with the HTG chip, it seems an unlikely solution. If saline is increased then some consideration must be given to the salt effects on the interaction, and a study of different salts and their concentrations should be considered. Salt effects remain mostly unexplored and warrant further investigation regardless of the use of saline. This study seems unique at this point in time and attempts at replication could prove useful in dealing with problems, investigating various effects and confirming or refuting the data and models that have been produced.

Chapter 8: Recommendations

This project has highlighted many areas for future work with the following areas of most promise:

- Attempt low pH (<5.0) runs in running buffer with higher sodium chloride concentrations to try and combat the non-specific binding that occurs.
- A comparison between buffers made up of different salts should be performed. This initially could be done at a small selection of pH with further work occurring in areas of interest.
- A comparison between buffer concentrations could also be performed in a similar manner.
- Use the models from this project to create a larger scale model for chromatography columns in order to optimise elution conditions.

Chapter 9: References

1. Protein A Media: Process Separations: Bio-rad. Bio-rad; 2012 [cited 2012 05/12/2012]; Bio-rad's Protein A affinity media product page]. Available from: http://www.bio-rad.com/evportal/en/NZ/evolutionPortal.portal?_nfpb=true&_pageLabel=productsPage&catID=1b2de6df-d19b-477e-9bdc-8296179da1b5.
2. Kemp G, Hamilton G, Quinones-Garcia I, McCue J, Mann F, Low D, et al. Meeting the Demands in Process-scale Antibody Purification for High Capacity and Throughput. Millipore; 2002 [cited 2012 05/12/2012]; Available from: http://www.millipore.com/techpublications/tech1/biophexprosepa.
3. Prosep® Ultra Plus Affinity Chromatography Media: Operating Instructions2008 05/12/2012. Available from: http://www.millipore.com/userguides.nsf/a73664f9f981af8c852569b9005b4eee/0f5ed6367a02d615852575ac00461350/$FILE/00104755PU.pdf.
4. GE Healthcare Life Sciences: Antibody Affinity Chromatography. GE Healthcare; 2012 [cited 2012 07/12/2012]; Available from: http://www.gelifesciences.com/webapp/wcs/stores/servlet/catalog/en/GELifeSciences/products/AlternativeProductStructure_17357/.
5. POROS® MabCapture™ A Media

POROS® A 50 µm Bulk Media. Invitrogen; 2012 [10/12/2012]; Available from: http://products.invitrogen.com/ivgn/product/4374728

http://products.invitrogen.com/ivgn/product/9555913.
6. Piercenet: Protein A Resins and Kits. Thermo Fisher Scientific; 2012 [14/12/2012]; Available from: http://www.piercenet.com/browse.cfm?fldID=01010306.
7. Hahn R, Schlegel R, Jungbauer A. Comparison of protein A affinity sorbents. Journal of Chromatography B-Analytical Technologies in the Biomedical and Life Sciences. 2003;790(1-2):35-51.
8. ElBakri A, Nelson PN, Abu Odeh RO. The state of antibody therapy. Human Immunology. 2010;71(12):1243-50.
9. Farid SS. Process economics of industrial monoclonal antibody manufacture. Journal of Chromatography B-Analytical Technologies in the Biomedical and Life Sciences. 2007;848(1):8-18.
10. Kelley B. Very large scale monoclonal antibody purification: The case for conventional unit operations. Biotechnology Progress. 2007;23(5):995-1008.
11. Mayer G. Immunoglobulins - Structure and Function. In: Male D, Brostoff J, Roth DB, Roitt I, editors. Immunology. 7th ed. Maryland Heights, Missouri, USA: Mosby-Elsevier; 2006.
12. Goodyear CS, Silverman GJ. Death by a B cell superantigen: In vivo V-H-targeted apoptotic supraclonal B cell deletion by a staphylococcal toxin. Journal of Experimental Medicine. 2003;197(9):1125-39.
13. Bjork I, Bengt-Ake P, Sjoquist J. Some Physicochemical Properties of Protein A from Staphylococcus Aureus. European Journal of Biochemistry. 1972;29:579-84.
14. Shuttleworth HL, Duggleby CJ, Jones SA, Atkinson T, Minton NP. Nucleotide-Sequence Analysis of the Gene for Protein-A from Staphylococcus-Aureus Cowan-1 (NCTC8530) and Its Enhanced Expression in Escherichia-Coli. Gene. 1987;58(2-3):283-95.
15. Moks T, Abrahmsen L, Nilsson B, Hellman U, Sjoquist J, Uhien M. Staphylococcal protein A consists of five IgG-binding domains. European Journal of Biochemistry. 1986;156(3):637-43.
16. Ljungberg UK, Jansson B, Niss U, Nilsson R, Sandberg BEB, Nilsson B. The interaction between different domains of staphylococcal protein a and human polyclonal IgG, IgA, IgM and F(ab')2: Separation of affinity from specificity. Molecular Immunology. 1993;30(14):1279-85.
17. Bouvet JP. Immunoglobulin-Fab Fragment-Binding Proteins. International Journal of Immunopharmacology. 1994;16(5-6):419-24.

18. Yang L, Biswas ME, Chen P. Study of binding between protein a and Immunoglobulin G using a surface tension probe. Biophysical Journal. 2003;84(1):509-22.
19. Sjoquist J, Meloun B, Hjelm H. Protein A Isolated from Staphylococcus aureus after Digestion with Lysostaphin. European Journal of Biochemistry. 1972;29(3):572-8.
20. Sjodahl J. Structural Studies on 4 Repetitive Fc-Binding Regions in Protein-A from Staphylococcus-Aureus. European Journal of Biochemistry. 1977;78(2):471-90.
21. Huse K, Bohme HJ, Scholz GH. Purification of antibodies by affinity chromatography. Journal of Biochemical and Biophysical Methods. 2002;51(3):217-31.
22. Hale G, Drumm A, Harrison P, Phillips J. Repeated Cleaning of Protein-A Affinity Column with Sodium-Hydroxide. Journal of Immunological Methods. 1994;171(1):15-21.
23. Homola J. Surface plasmon resonance based sensors. Wolfbeis O, editor. Berlin: Springer; 2006.
24. Phillips K, Cheng Q. Molecular Biomethods Handbook. Dordrecht: Springer; 2008.
25. Marquart A. How to do BiaCalculations2011 23-01-2013. Available from: http://www.sprpages.nl/images/SPRDownloads/BiaCalculations.pdf.
26. Rich RL, Papalia GA, Flynn PJ, Furneisen J, Quinn J, Klein JS, et al. A global benchmark study using affinity-based biosensors. Analytical Biochemistry. 2009;386(2):194-216.
27. Low D, O'Leary R, Pujar NS. Future of antibody purification. Journal of Chromatography B-Analytical Technologies in the Biomedical and Life Sciences. 2007;848(1):48-63.
28. Poole CF. The Essence of Chromatography. Amsterdam, Boston: Elsevier; 2003.
29. Calmettes P, Cser L, Rajnavolgyi E. Temperature and pH-Dependence of Immunoglobulin-G Conformation. Archives of Biochemistry and Biophysics. 1991;291(2):277-83.
30. Deisenhofer J. Crystallographic Refinement and Atomic Models of a Human Fc Fragment and Its Complex with Fragment-B of Protein-A from Staphylococcus-Aureus at 2.9-A and 2.8-A Resolution. Biochemistry. 1981;20(9):2361-70.
31. Gouda H, Torigoe H, Saito A, Sato M, Arata Y, Shimada I. 3-Dimensional Solution Structure of the B-Domain of Staphylococcal Protein-A - Comparisons of the Solution and Crystal-Structures. Biochemistry. 1992;31(40):9665-72.
32. Mitomo H, Shigematsu H, Kobatake E, Furusawa H, Okahata Y. IgG binding kinetics to oligo B protein A domains on lipid layers quartz-crystal immobilized on a 27 MHz microbalance. Journal of Molecular Recognition. 2007;20(2):83-9.
33. Leibl H, Erber W, Eibl MM, Mannhalter JW. Separation of Polysaccharide-Specific Human Immunoglobulin-G Subclasses using a Protein-A Superose Column with a pH Gradient Elution System. Journal of Chromatography. 1993;639(1):51-6.
34. Bottomley SP, Sutton BJ, Gore MG. Elution of Human-IgG From Affinity Columns Containing Immobilized Variants of Protein-A. Journal of Immunological Methods. 1995;182(2):185-92.
35. Gulich S, Uhlen M, Hober S. Protein engineering of an IgG-binding domain allows milder elution conditions during affinity chromatography. Journal of Biotechnology. 2000;76(2-3):233-44.
36. Teng SF, Sproule K, Husain A, Lowe CR. Affinity chromatography on immobilized "biomimetic" ligands synthesis, immobilization and chromatographic assessment of an immunoglobulin G-binding ligand. Journal of Chromatography B. 2000;740(1):1-15.
37. Osmark P, Cedervall T, Pieters K, Akerstrom B. Heat elution chromatography of immunoglobulins. Protein Expression and Purification. 2003;30(2):301-3.
38. Arakawa T, Philo JS, Tsumoto K, Yumioka R, Ejima D. Elution of antibodies from a Protein-A column by aqueous arginine solutions. Protein Expression and Purification. 2004;36(2):244-8.
39. Ejima D, Yumioka R, Tsumoto K, Arakawa T. Effective elution of antibodies by arginine and arginine derivatives in affinity column chromatography. Analytical Biochemistry. 2005;345(2):250-7.
40. Shukla D, Zamolo L, Cavallotti C, Trout BL. Understanding the Role of Arginine as an Eluent in Affinity Chromatography via Molecular Computations. Journal of Physical Chemistry B. 2011;115(11):2645-54.

41. Hahn R, Shimahara K, Steindl F, Jungbauer A. Comparison of protein A affinity sorbents III. Life time study. Journal of Chromatography A. 2006;1102(1-2):224-31.
42. Pilling MJ, Seakins PW. Reaction Kinetics. Oxford, England: Oxford University Press; 1995.
43. ProteOn Sensor and Maintenance Chips. Bio-Rad Laboratories; 2013 [cited 2013 January 14th]; Available from: http://www.bio-rad.com/prd/en/NZ/LSR/PDP/051c70a2-ff01-4fbb-8c77-37975c1870a1/ProteOn-Sensor-and-Maintenance-Chips.
44. Rabkin E, Yosef N, Bronner V, Zafir-Lavie I, Shezifi D, Nimri S. The ProteOn HTG Sensor Chip: Novel Surface for Stable Capture of Histidine-Tagged Proteins for Protein-Protein Interaction Analysis. Bio-Rad Bulletin [Internet]. 2012; (6132). Available from: http://www.bio-rad.com/webroot/web/pdf/lsr/literature/Bulletin_6132.pdf.
45. Tsang VCW, Wilkins PP. Optimum Dissociating Condition for Immunoaffinity and Preferential Isolation of Antibodies with High Specific Activity. Journal of Immunological Methods. 1991;138(2):291-9.

Appendix A: Sample Models

The models were discussed briefly in Chapter 3 but require further explanation in order to recreate them and/or determine their accuracy. The ProteOn Manager software is self-explanatory and easy to use and does not require further explanation in order for the models used in this thesis to be recreated. Scrubber is also simple to use, and as it was not used to model the data, will not be further explained. Stella and Excel will be the focus of this section due to their more challenging nature, with ClampXP also being expanded upon to a less extent.

Stella uses more visual models as shown in Figure 3.4 (and again in Figure A.1) with the equations operating in the background. The best way to describe the machinations of Stella is to explain how this model (Figure A.1) works. The thick blue arrows represent physical changes, while the thin pink arrows represent an influence/part of an equation. Beginning at the left side of the figure are the injection time and feed concentration of IgG (Cfeed), these are simple parameters set by the user. These parameters determine the value of the bulk concentration of the IgG in solution, being equal to the feed concentration for the duration of the injection, and then being set to zero after the injection period has finished. The “Free Ligand” (Protein A), “Ligand Site A” (IgG bound to Protein A only at the first site) and “Ligand Site B” (IgG bound to Protein A only at the second site) boxes all represent the concentration/reservoir of their components. The free ligand is set initially to the concentration of the Protein A on the chip, approximated from the response created by IgG binding that occurred during the experiments. The two binding sites are set to zero initially as no IgG has been bound. During the interaction the free ligand reacts with the IgG in bulk solution along the two pathways to form one of the bound complexes. The “Association A” and “Association B” circles represent the association reaction and are here set to Langmuir equations. These equations are affected by the association constants shown as “kaA” and “kaB” circles. Similarly, the dissociation pathways are shown with the appropriate equations and parameters. The no name equations represent the association and dissociation reactions for the bivalent/dual-binding of Protein A and IgG. The dashed line circles with parameter names represent the exact parameters named but are ghosts to provide model clarity. A steric inhibition factor was also used for the bivalent binding, as shown. The concentrations of each contribute to the total bound and RU circles that represent the output variables of the model.

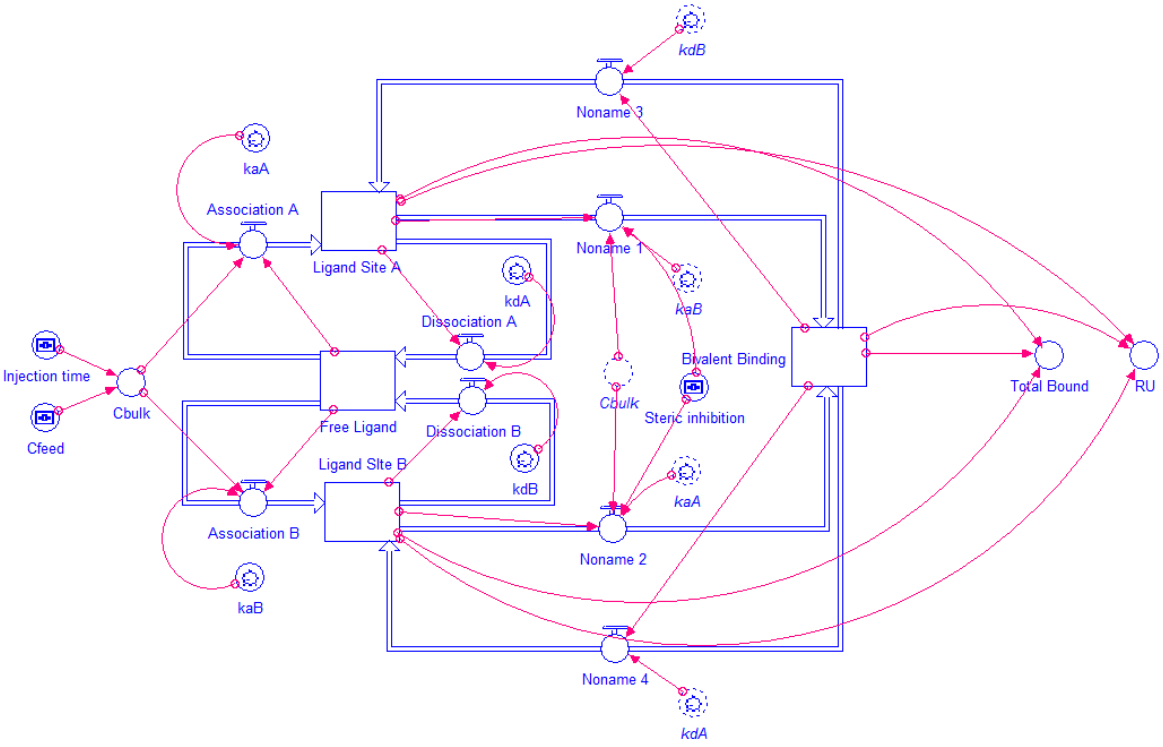

Figure A.1: The Stella model from Figure 3.4 reproduced for ease of use.

Stella runs all these equations and variables as finite difference equations based on a user-defined time step. The variables produced can be displayed as a table and/or a graph. One advantage of Stella is that any variable can be easily tracked by setting up the appropriate output variable in the model. The great disadvantage of Stella, as mentioned in Chapter 3, is that it does not possess any optimisation algorithms, so any data modelling must be optimised by the user, which is a slow process for the large data sets produced by the SPR.

Excel was set up to use Langmuir equations in a finite difference model in a similar manner to Stella. Figure A.2 shows a screen shot of part of an excel model; on the left is the experimental data, with the model on the right. Above the model, the parameters and their values are listed, while the IgG concentration (molar) and injection start and stop times (seconds) are above the data. The model shown is a dual-binding single-site model, hence, only two sets of rate constants. The time displayed shows that a measurement is taken every 0.9 seconds, which is used as the time step in the model. Langmuir equations are used with each value being determined based on the concentrations from the previous step. A squared

error is easily introduced by simply adding a column to the right of RU that takes the model value minus the data value squared to get the error. The solver function can then be used to minimise the sum of the errors by varying the model parameters to optimise the model. The data can be represented as a graph simply by using the graph function in Excel. While Excel is highly versatile it does require a great deal of time because of the control it affords. An example of this is the identification of the injection points and altering of the model equations at these points to account for the change in conditions. When these tasks have to be repeated five times per run (as the times are not perfectly aligned across all the data sets), for over one hundred runs this can become extremely time consuming and a faster program becomes desirable.

Vers 3.5b Data			Pro A conc	26	uM		
Conc1	6.67E-08			Model			
Start1	0		ka1	20000	ka2	30000	
Stop1	2855.3		kd1	0.00005	kd2	0.009	
Injn	1						
Cell	3			Data 1			
Time7	Data7			PA conc	IgGPA conc	IgG2PA Conc	RU
4.0496	-1.3341			0.000006	0	0	0
4.9496	-1.3292			0.000006	0	0	0
5.8496	3.6061			0.000006	0	0	0
6.7496	0.5799			5.99E-06	7.20E-09	0.00E+00	0.108000054
7.6496	1.394			5.99E-06	1.44E-08	1.30E-11	0.216060048
8.5496	-0.736			5.98E-06	2.15E-08	3.87E-11	0.324177992
9.4496	4.0143			5.97E-06	2.87E-08	7.72E-11	0.432351916
10.3496	3.7993			5.96E-06	3.58E-08	1.28E-10	0.540579873
11.2496	2.0872			5.96E-06	4.29E-08	1.92E-10	0.648859937
12.1496	0.1757			5.95E-06	4.99E-08	2.67E-10	0.7571902
13.0496	2.9765			5.94E-06	5.70E-08	3.55E-10	0.865568779

Figure A.2: Screen shot of an Excel model.

ClampXP again uses finite difference models employing Langmuir equations to model the experimental data. Figures A.3 and A.4 show the input tabs of Clamp and the parameters set by the user. In Figure A.3 every compound/molecule of the interaction is listed, this particular model is using a two-site, dual-binding model. The IgG has been set as injected ("Inj" tick box), while the Protein A is set as the ligand/local ("Lcl" tick box), with the remaining IgG-Protein A complexes having their initial concentration set at zero. The

complexes also have a response factor (“R factor”), which is the amount of response they generate when compared with the ligand. The response factor is set to three for the single-binding complexes because IgG is roughly three times the size of Protein A. The dual-binding complexes have a response of six because of the second IgG. The reactions are also set on this page, by setting the reacting molecules and reaction constants. The reaction constants must be given an initial value, however, if the fit box is selected they will be optimised when the model is executed. Figure A.4 shows the data tab where the initial concentration of the ligand is set (the value entered is in terms of RU). Again, by selecting the fit box the parameter will be optimised during the modelling. The injection concentrations and times are also set in this tab by selecting one of the needle buttons on the left hand side. Once the model is set up the execution is fast and rapidly optimises all the desired parameters. The models can be used on multiple data sets allowing a single model to be used for any number of experimental runs. The simplicity of setting up the model, the ability to use a single model across multiple runs and the ease of optimisation make ClampXP the most efficient program for modelling large numbers of experimental data sets.

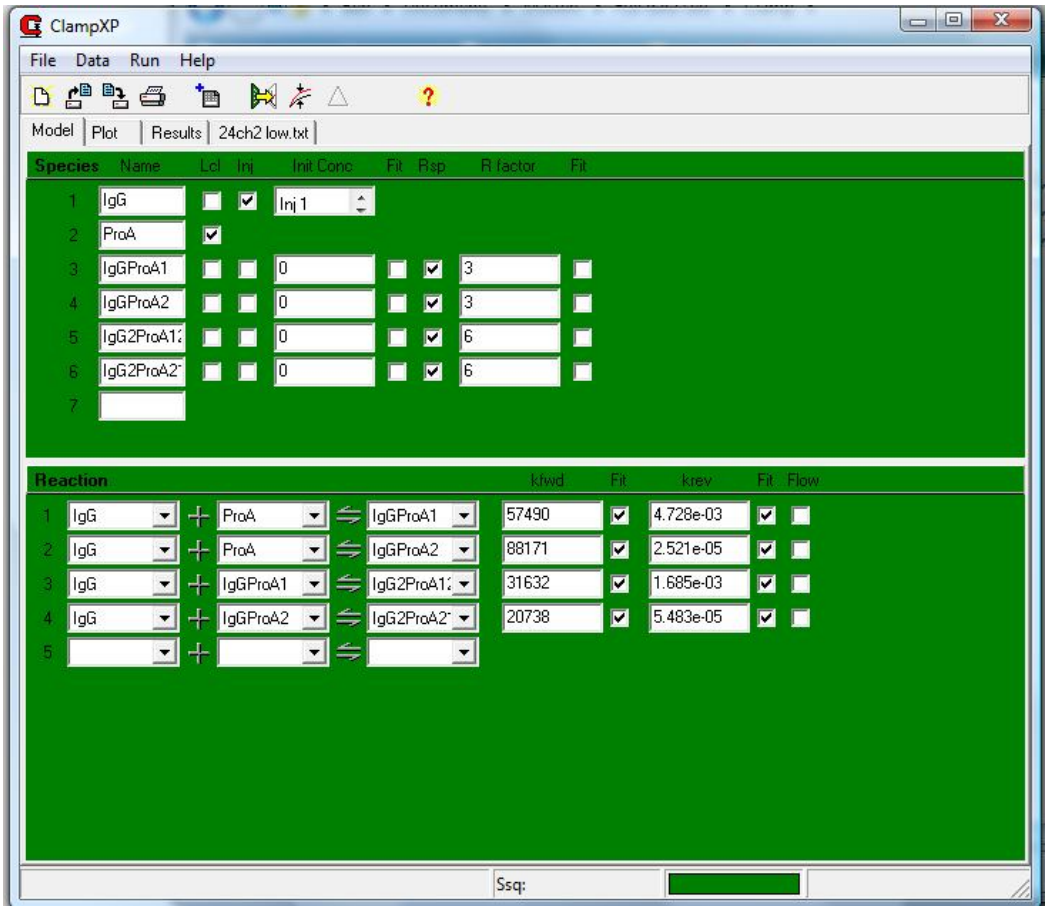

Figure A.3: A screen shot of the Model tab in ClampXP.

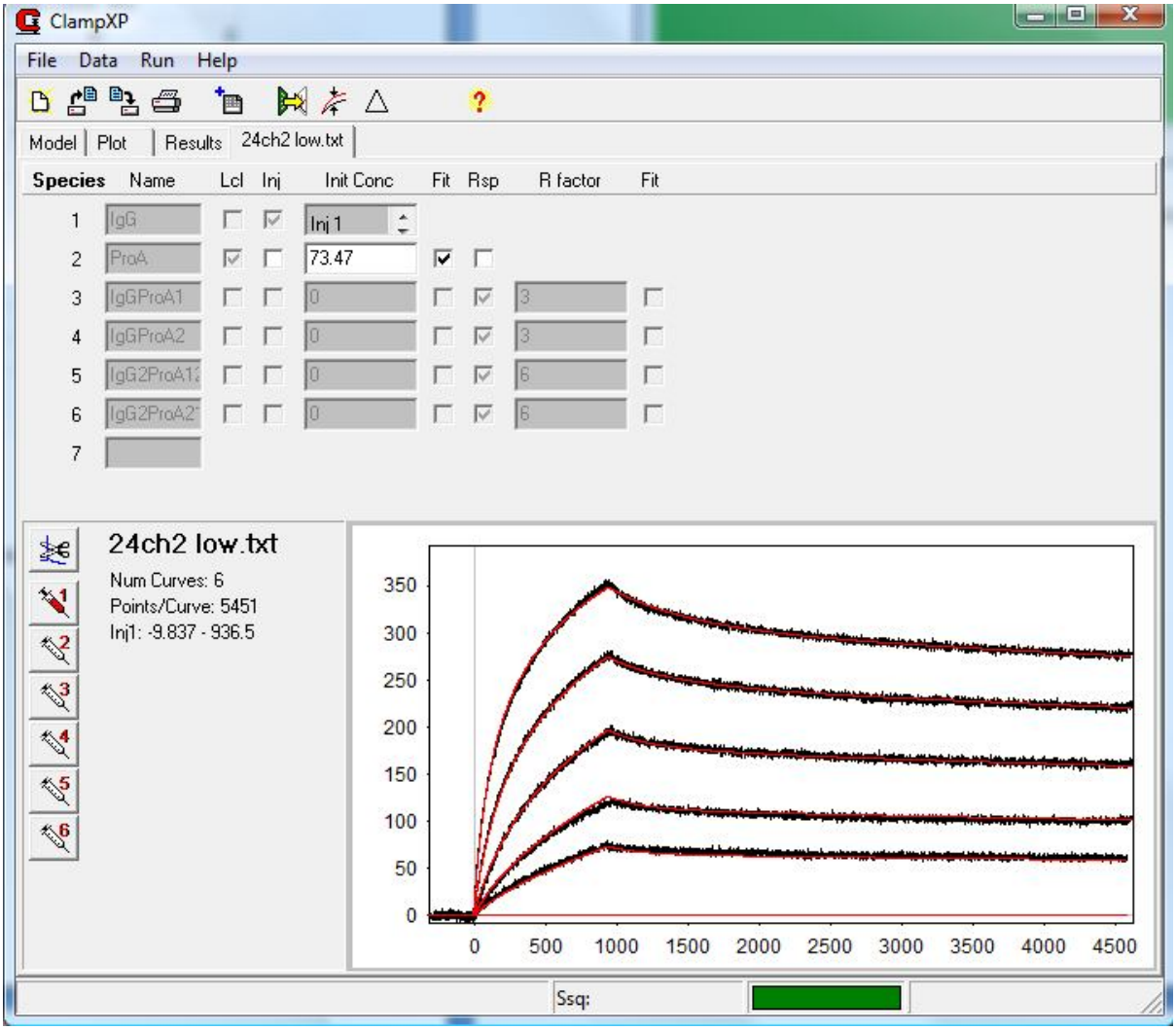

Figure A.4: A screen shot of the Data tab in ClampXP.

Appendix B: Full Models Used in Results

This appendix shows the complete result sets used in the results section. Each individual run will be set out with the highest concentration of IgG in the dilution series, buffer makeup, pH of the reaction and residual sum of squared errors for the data and model, followed by the graph showing the model (red) and data (black). A table of the constants from the reaction and the associated errors will also be shown. The results used for the kinetic experiments will be presented in the first section with the second section containing the results from the IgG in PBST runs. For the IgG in PBST runs all binding took place in PBST at pH 7.4 as noted before with the buffer conditions and pH representing only the elution part of the reaction. Each run will be denoted using a run and channel number, the run number is largely meaningless as it comes from the number of steps used on a particular chip (causing the numbers to reset when the chip was changed), while the channel does provide a basis for comparison as different channels had different concentrations of Protein A immobilised on them.

B.1: Data from the Kinetic Experiments

Run 24, channel 2: Performed at pH 7.4 in PBST, at an IgG concentration of 0.0667 µm. Residual sum of squared errors (RSSE) is 2.522.

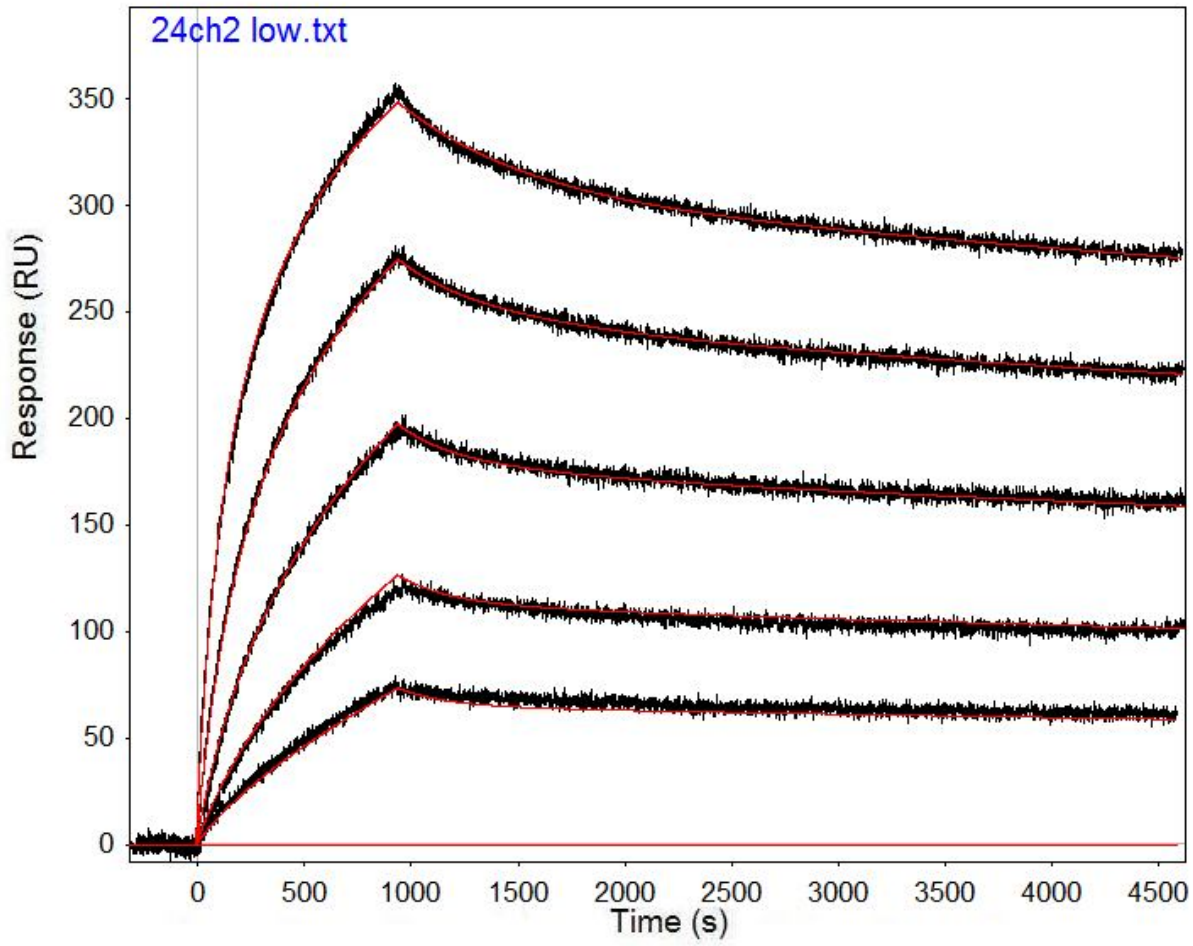

Figure B.1: Run 24 channel 2 model and data graph.

Table B.1: Run 24 channel 2 model parameters.

	kfwd1	krev1	kfwd2	krev2	kfwd3	krev3	ProA (RU)
Value	57490	4.73E-03	88171	2.52E-05	31632	1.69E-03	73.47
Error (abs)	543.5	5.82E-05	216.2	2.97E-07	356.2	2.69E-05	0.1501
Error (%)	0.95	1.23	0.25	1.18	1.13	1.60	0.20

Run 24, channel 3: Performed at pH 7.4 in PBST, at an IgG concentration of 0.0667 µm. RSSE is 2.215.

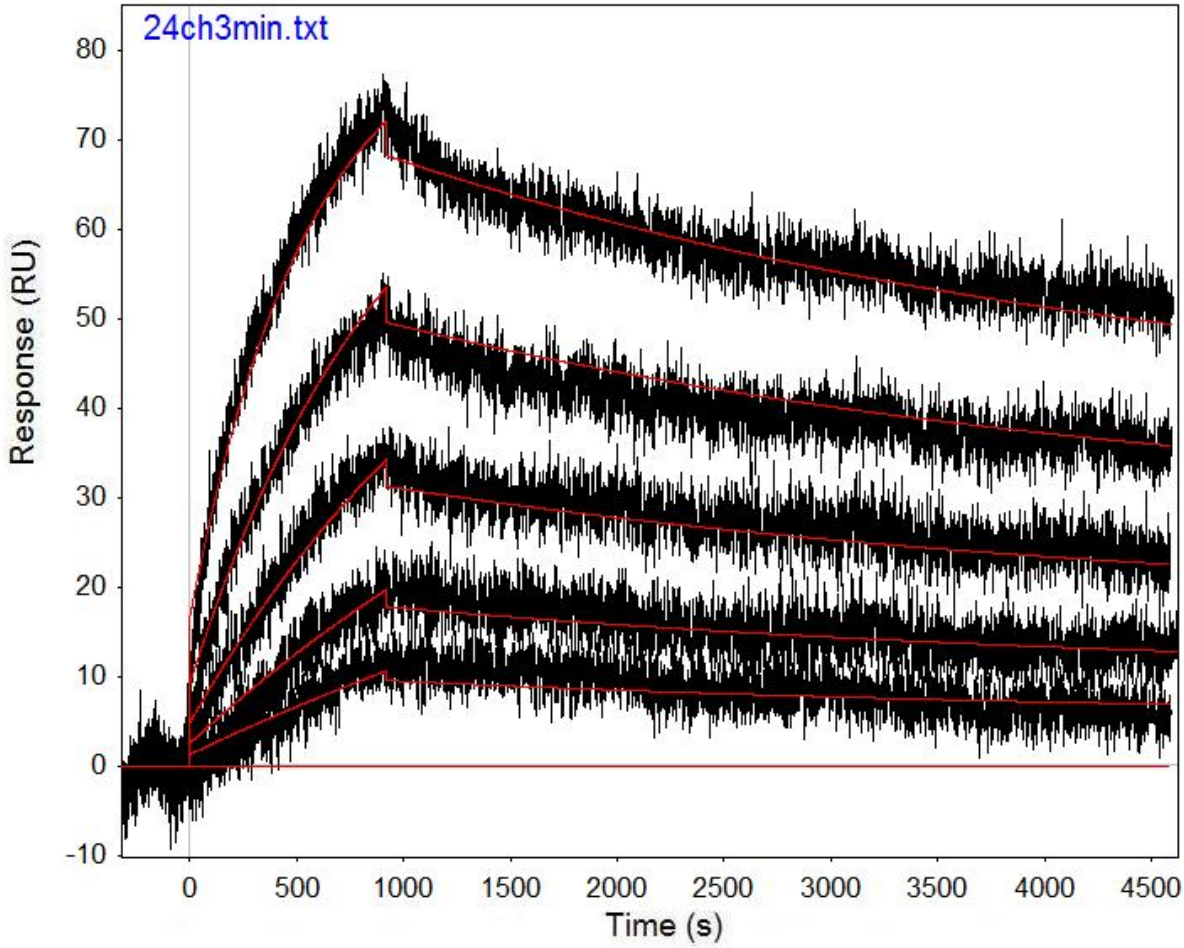

Figure B.2: Run 24 channel 3 model and data graph.

Table B.2: Run 24 channel 3 model parameters.

	kfwd1	krev1	kfwd2	krev2	kfwd3	krev3	ProA (RU)
Value	16401	0.00E+00	14999	2.69E-04	39710000	1.18E+01	29.83
Error (abs)	8224	5.16E-05	8157	1.02E-04	39650000	1.18E+01	0.04947
Error (%)	50.14		54.38	37.94	99.85	99.83	0.17

Run 39, channel 2: Performed at pH 7.4 in PBST, at an IgG concentration of 0.133 µm. RSSE is 12.74.

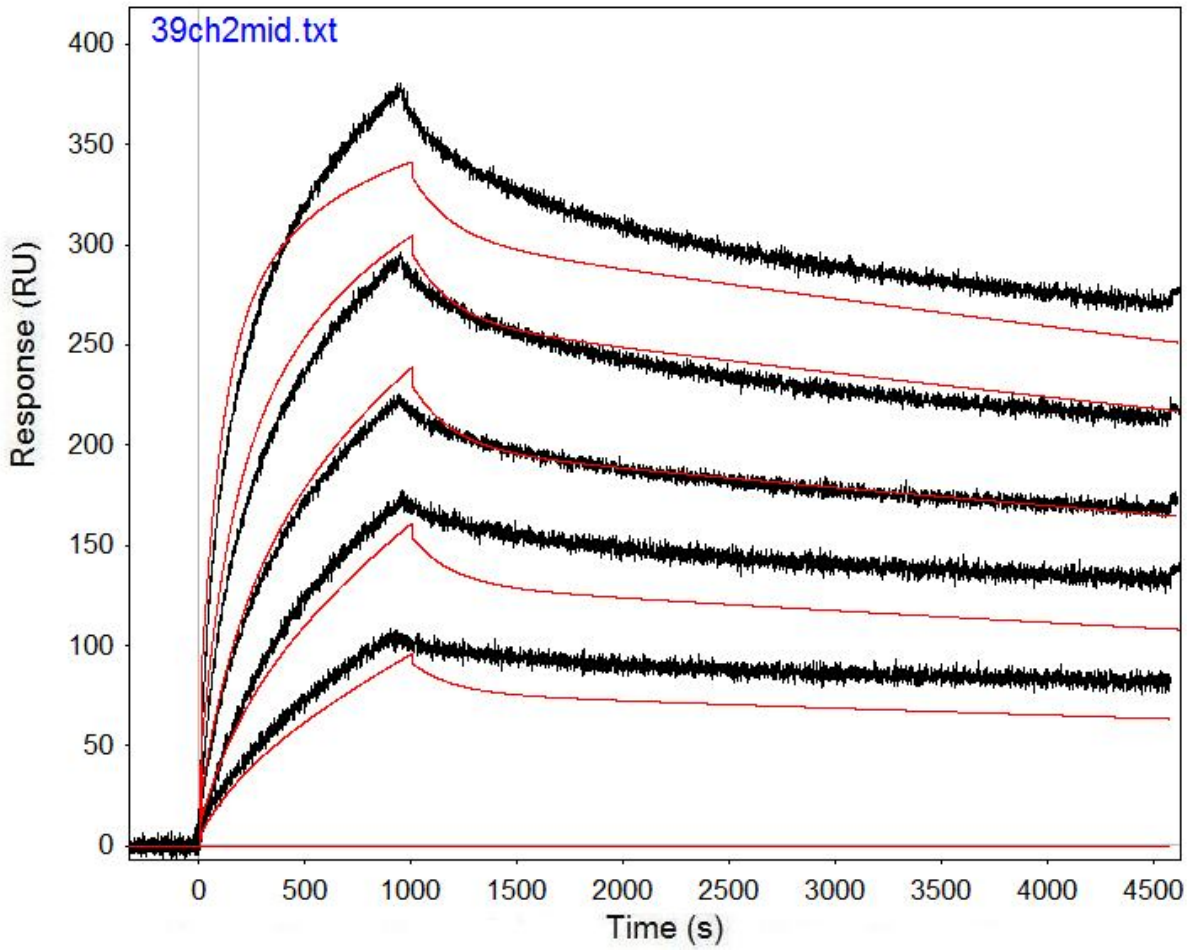

Figure B.3: Run 39 channel 2 model and data graph.

Table B.3: Run 39 channel 2 model parameters.

	kfwd1	krev1	kfwd2	krev2	kfwd3	krev3	ProA (RU)
Value	27038	5.00E-03	33953	5.42E-05	1.48E+08	7.12E+01	120.6
Error (abs)	821	1.33E-04	146	5.65E-07	3.14E+09	1.51E+03	0.1408
Error (%)	3.04	2.66	0.43	1.04	2125.76	2126.40	0.12

Run 39, channel 3: Performed at pH 7.4 in PBST, at an IgG concentration of 0.133 µm. RSSE is 3.551.

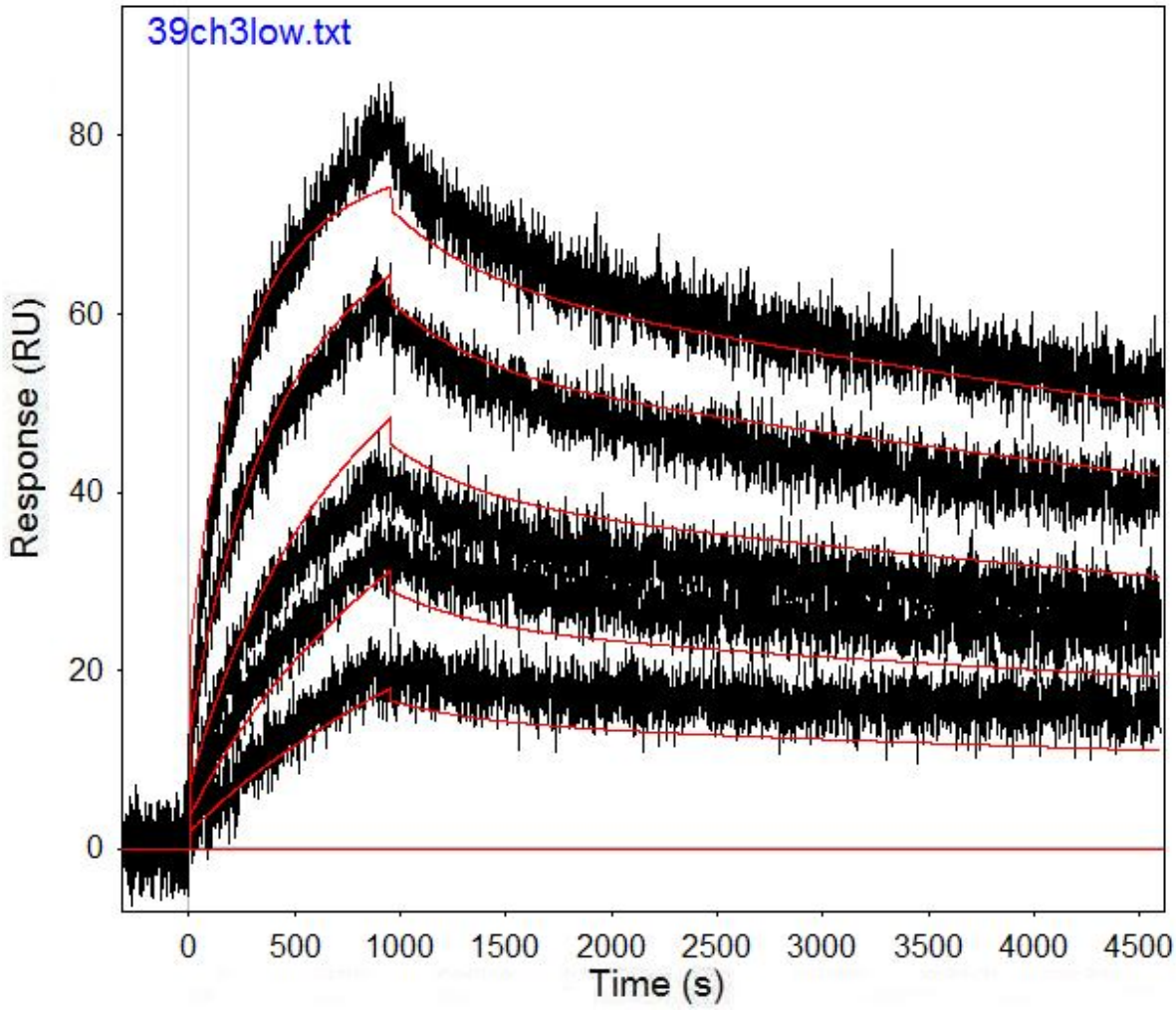

Figure B.4: Run 39 channel 3 model and data graph.

Table B.4: Run 39 channel 3 model parameters.

	kfwd1	krev1	kfwd2	krev2	kfwd3	krev3	ProA (RU)
Value	11813	0.00238	26069	6.77E-05	1.65E+08	58.25	27.07
Error (abs)	339.1	0.000103	139.3	1.35E-06	2.89E+09	1023	0.04373
Error (%)	2.870566	4.315126	0.534351	2.000887	1756.527	1756.223	0.1615441

Run 46, channel 3: Performed at pH 7.4 in PBST, at an IgG concentration of 0.133 µm. RSSE is 2.293.

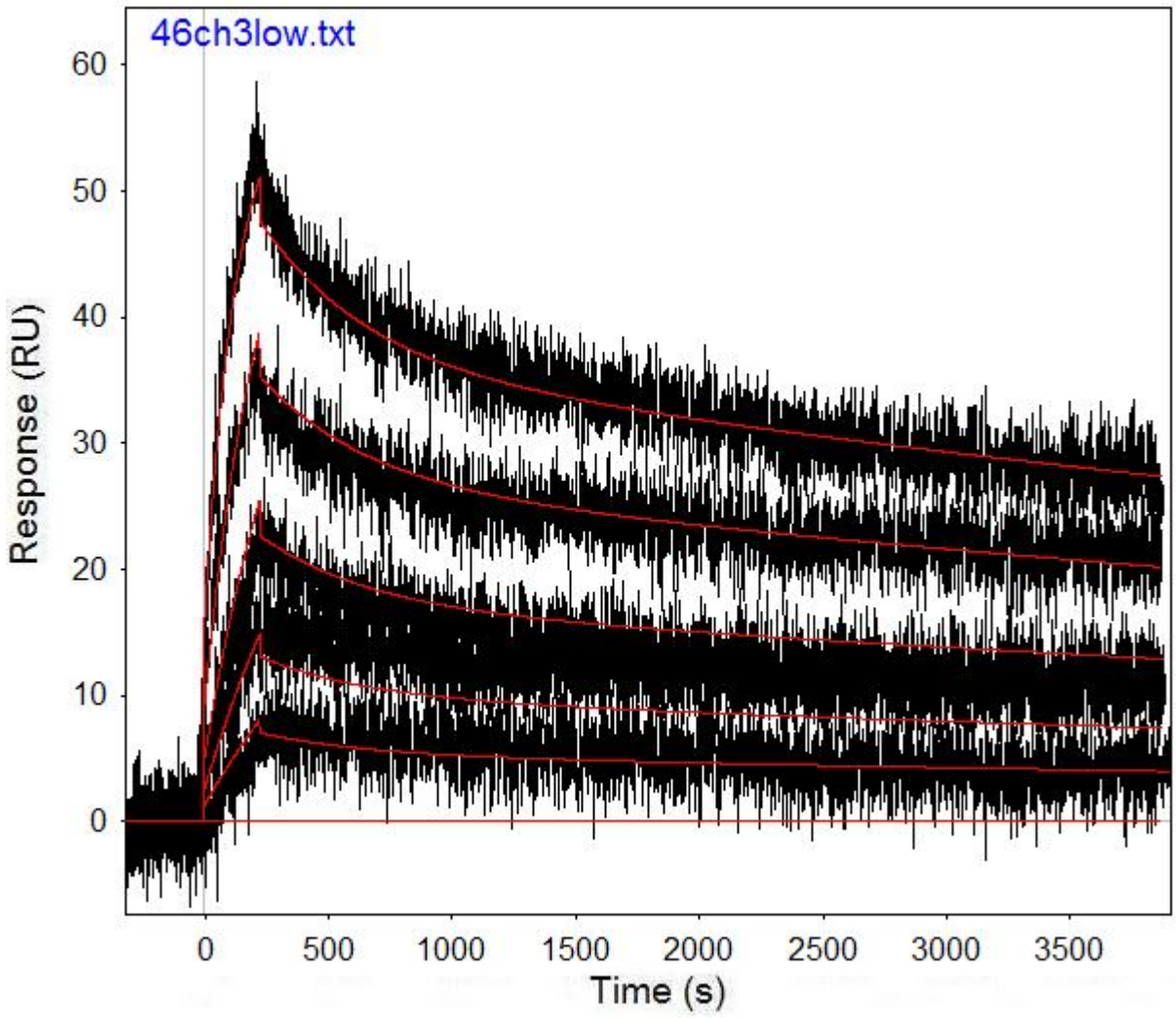

Figure B.5: Run 46 channel 3 model and data graph.

Table B.5: Run 46 channel 3 model parameters.

	kfwd1	krev1	kfwd2	krev2	kfwd3	krev3	ProA (RU)
Value	20613	0.00236	49198	7.86E-05	61160000	27.72	20.83
Error (abs)	329.2	8.544E-05	363	1.96E-06	3.44E+08	155.7	0.07252
Error (%)	1.59705	3.620339	0.737835	2.493001	561.9686	561.6883	0.348151704

Run 53, channel 3: Performed at pH 7.4 in PBST, at an IgG concentration of 0.267 µm. RSSE is 4.228.

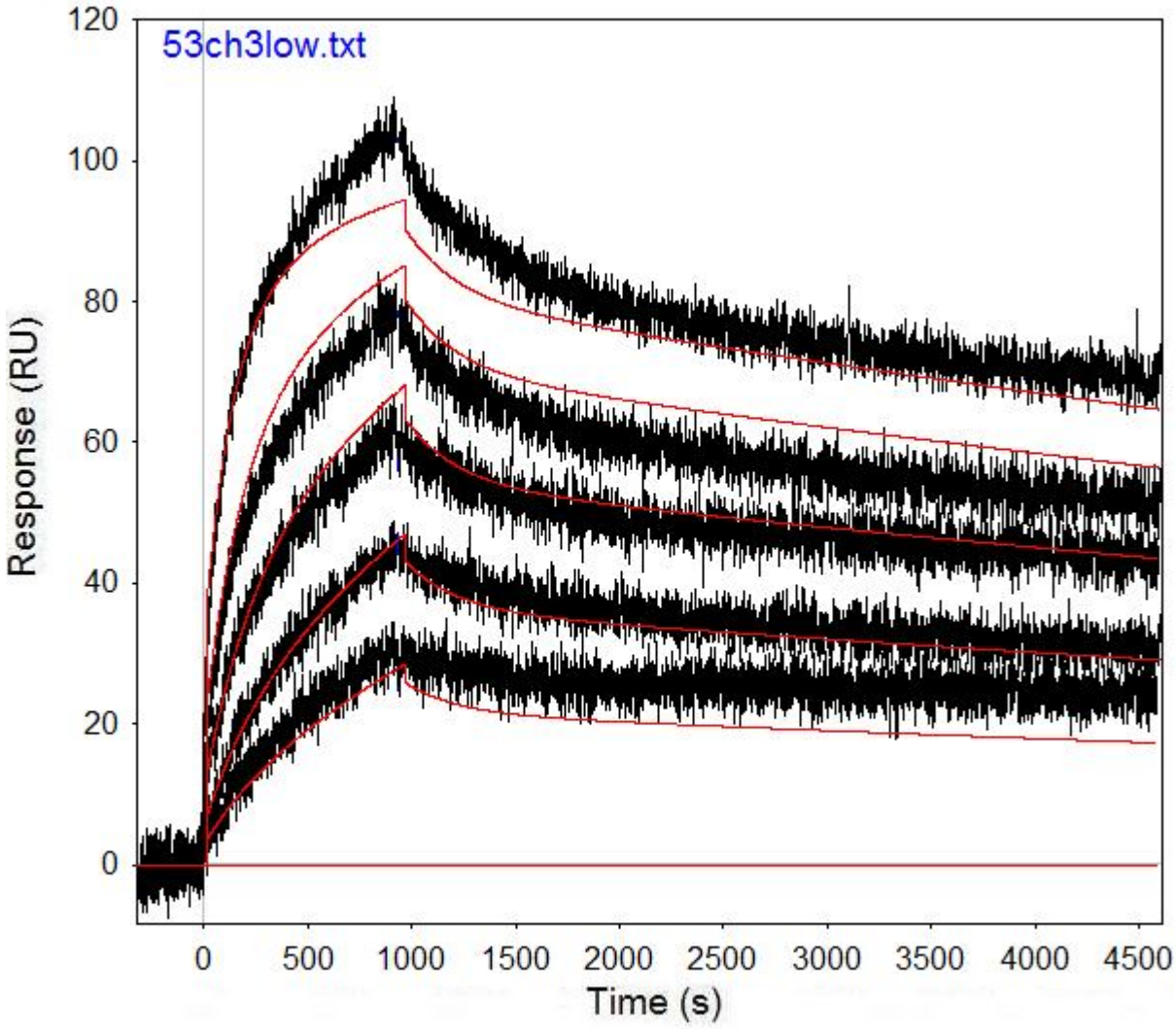

Figure B.6: Run 53, channel 3 model and data graph.

Table B.6: Run 46, channel 3 model parameters.

	kfwd1	krev1	kfwd2	krev2	kfwd3	krev3	ProA (RU)
Value	14154	0.004101	16689	6.05E-05	1.36E+08	64.9	33.88
Error (abs)	446	0.0001222	62.57	8.14E-07	1.57E+09	745.9	0.04519
Error (%)	3.151053	2.979761	0.374918	1.344953	1149.56	1149.307	0.133382527

Run 60, channel 3: Performed at pH 7.4 in PBST, at an IgG concentration of 0.267 µm. RSSE is 2.845.

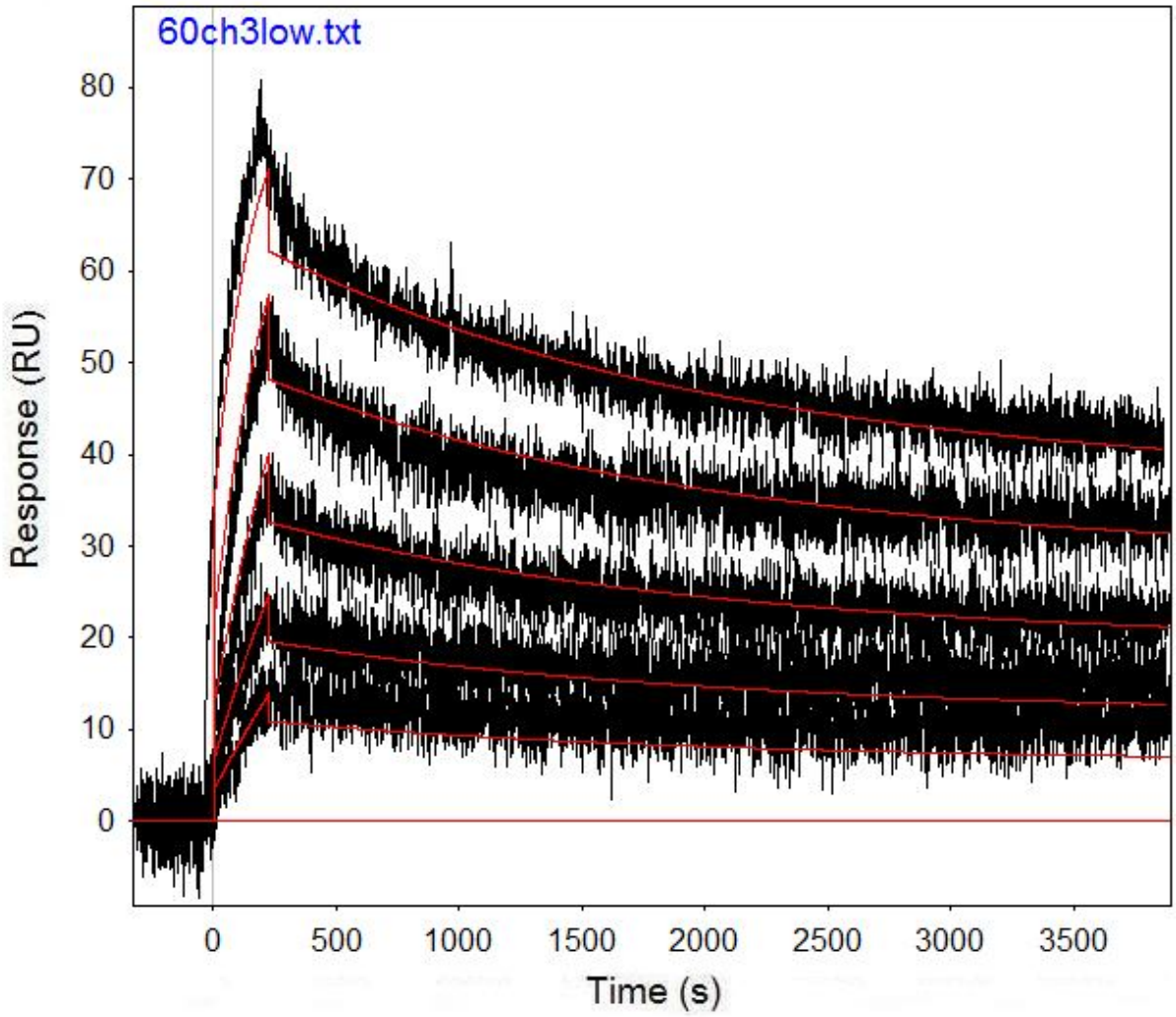

Figure B.7: Run 60, channel 3 model and data graph.

Table B.7: Run 60, channel 3 model parameters.

	kfwd1	krev1	kfwd2	krev2	kfwd3	krev3	ProA (RU)
Value	16766	0.0005403	23061	0	1.33E+08	50.97	28.03
Error (abs)	2448	0.0000697	2514	1.93E-05	1.91E+08	73.38	0.07415
Error (%)	14.60098	12.900241	10.90152		143.9759	143.967	0.264537995

Run 67, channel 3: Performed at pH 7.4 in PBST, at an IgG concentration of 0.267 µm. RSSE is 2.512.

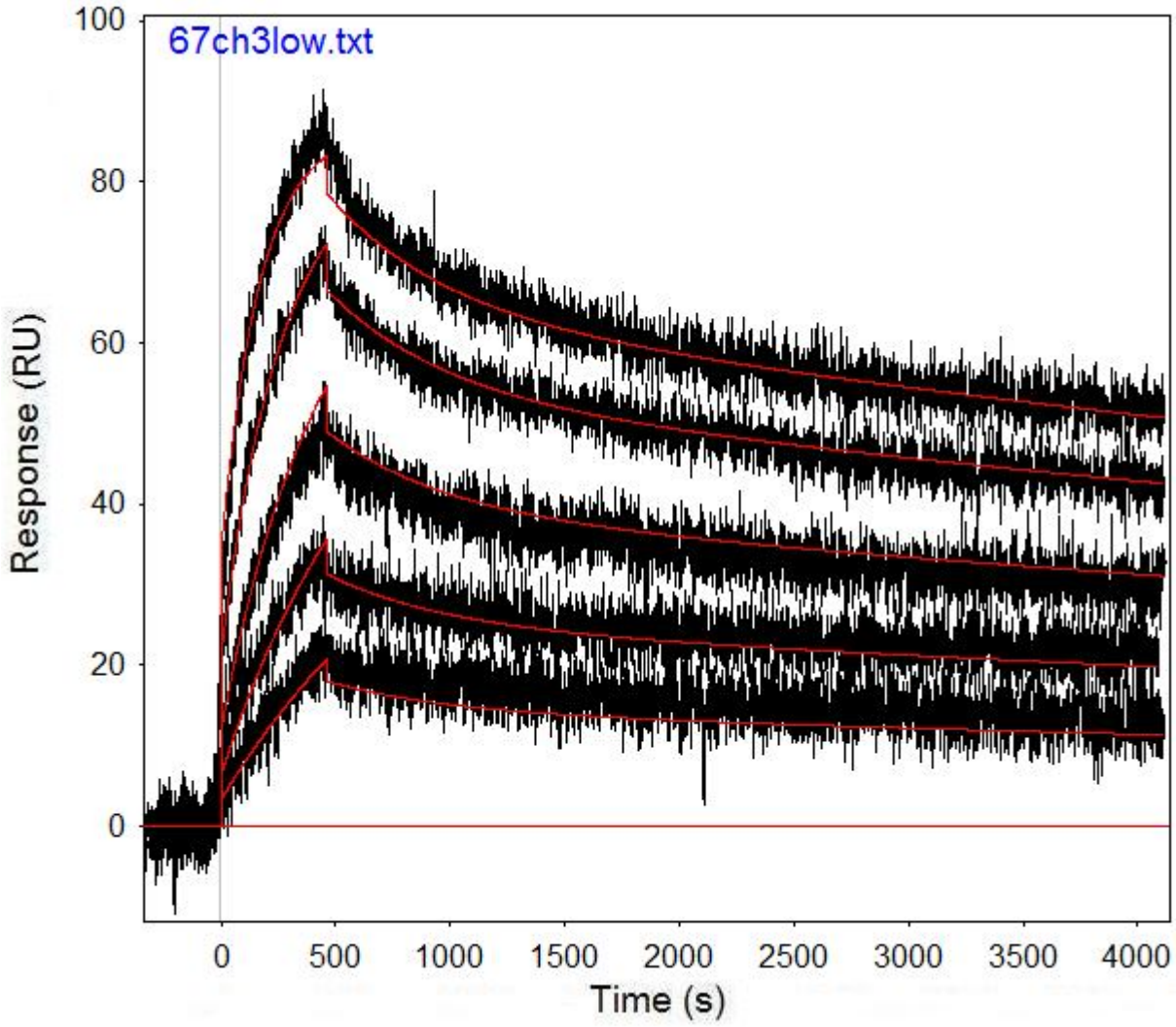

Figure B.8: Run 67, channel 3 model and data graph.

Table B.8: Run 67, channel 3 model parameters.

	kfwd1	krev1	kfwd2	krev2	kfwd3	krev3	ProA (RU)
Value	9706	0.001973	24332	6.33E-05	1.17E+08	50.04	30.27
Error (abs)	102.5	5.144E-05	106.6	1.26E-06	7.39E+08	316.4	0.0393
Error (%)	1.056048	2.6071972	0.438106	1.98137	632.6199	632.2942	0.129831516

Run 74, channel 3: Performed at pH 7.4 in PBST, at an IgG concentration of 0.533 µm. RSSE is 3.948.

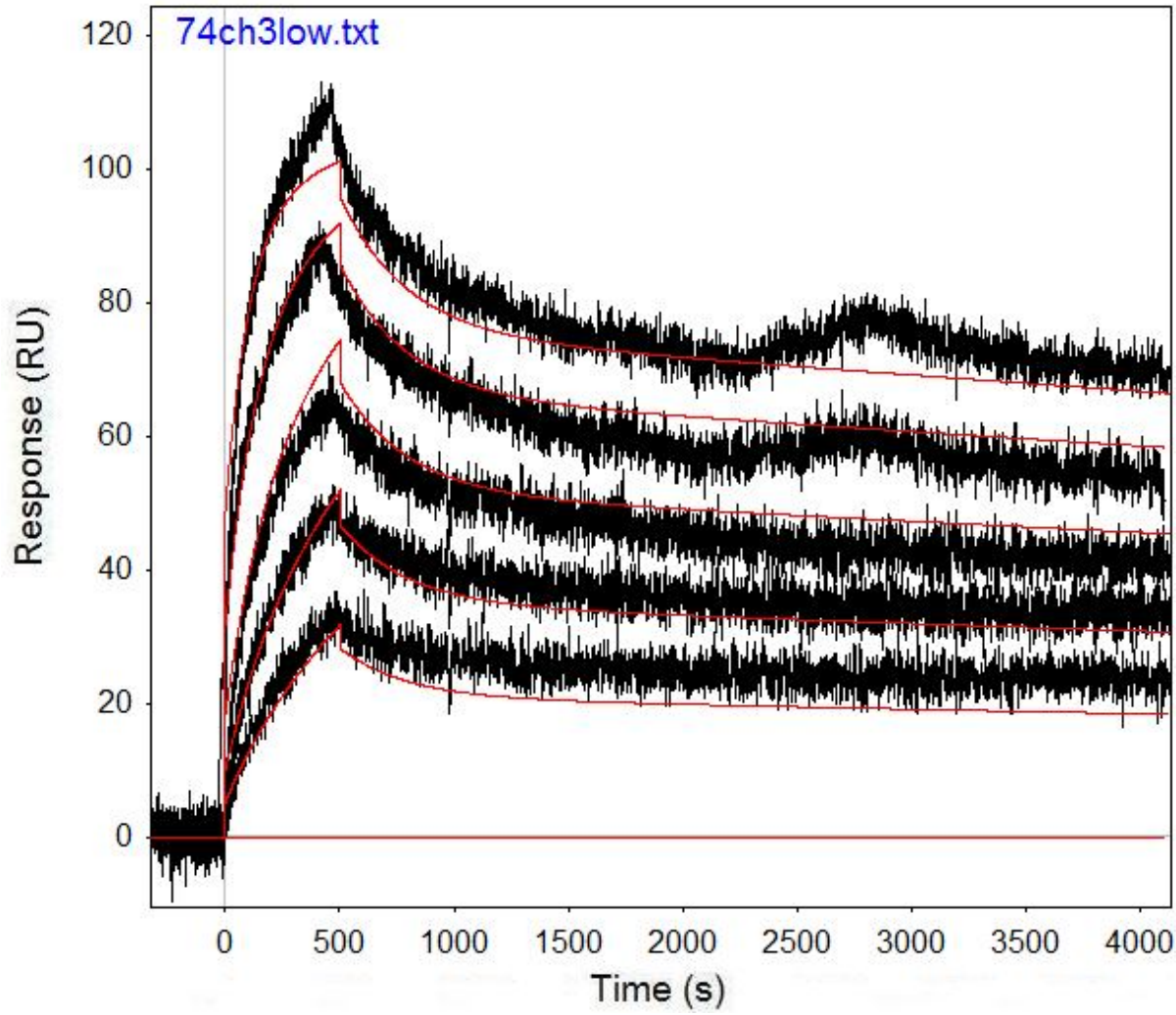

Figure B.9: Run 74, channel 3 model and data graph.

Table B.9: Run 74, channel 3 model parameters.

	kfwd1	krev1	kfwd2	krev2	kfwd3	krev3	ProA (RU)
Value	10838	0.00351	14167	3.59E-05	67420000	46.75	36.15
Error (abs)	171.6	6.952E-05	52.6	8.87E-07	2.34E+08	161.9	0.05076
Error (%)	1.583318	1.9806268	0.371285	2.469359	346.3364	346.3102	0.140414938

Run 82, channel 3: Performed at pH 7.4 in PBST, at an IgG concentration of 0.8 µm. RSSE is 4.589.

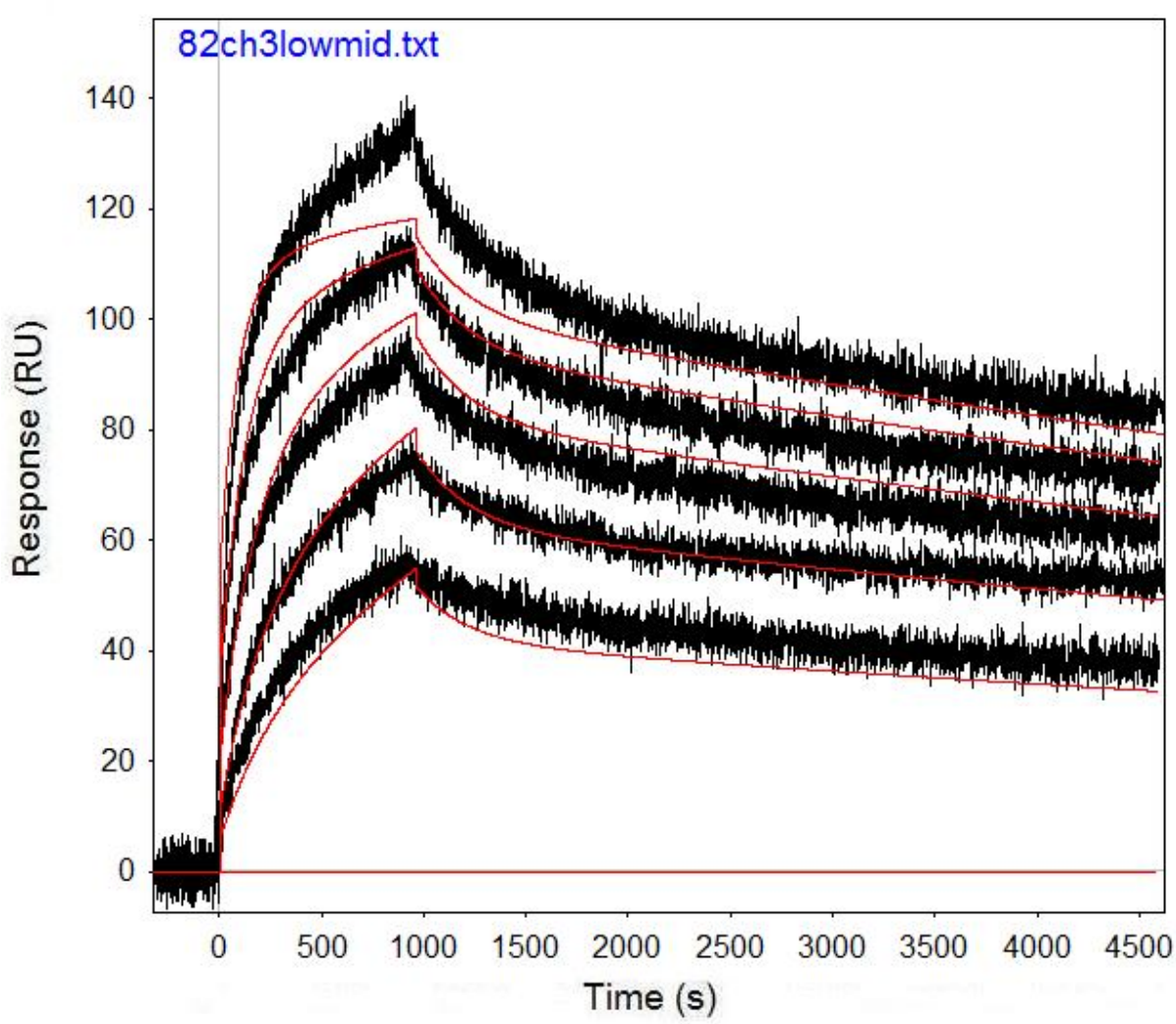

Figure B.11: Run 82, channel 3 model and data graph.

Table B.11: Run 82, channel 3 model parameters.

	kfwd1	krev1	kfwd2	krev2	kfwd3	krev3	ProA (RU)
Value	10879	0.004013	10407	6.66E-05	70480000	70.39	40.77
Error (abs)	202.8	7.265E-05	30.95	6.34E-07	2.81E+08	280.7	0.03606
Error (%)	1.864142	1.8103663	0.297396	0.951966	398.6947	398.7782	0.088447388

Run 89, channel 3: Performed at pH 7.4 in PBST, at an IgG concentration of 1.067 µm. RSSE is 5.527.

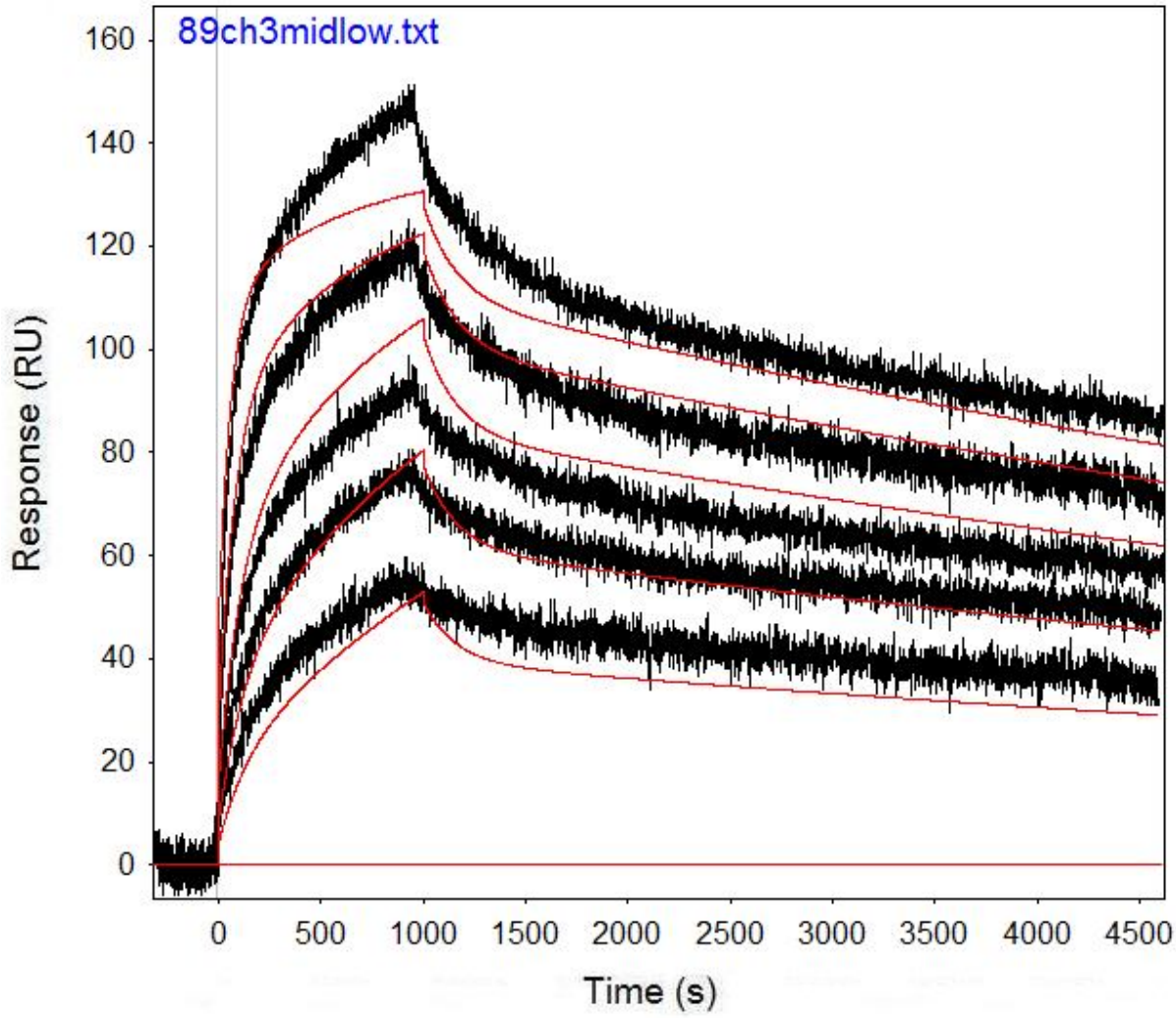

Figure B.12: Run 89, channel 3 model and data graph.

Table B.12: Run 89, channel 3 model parameters.

	kfwd1	krev1	kfwd2	krev2	kfwd3	krev3	ProA (RU)
Value	11794	0.006369	6026	8.41E-05	40330000	79.53	45.83
Error (abs)	256.8	0.0001198	19.9	6.5E-07	3.96E+08	781.9	0.04844
Error (%)	2.177378	1.880986	0.330236	0.773365	982.8911	983.151	0.10569496

Run 96, channel 3: Performed at pH 7.4 in PBST, at an IgG concentration of 1.067 µm. RSSE is 5.779.

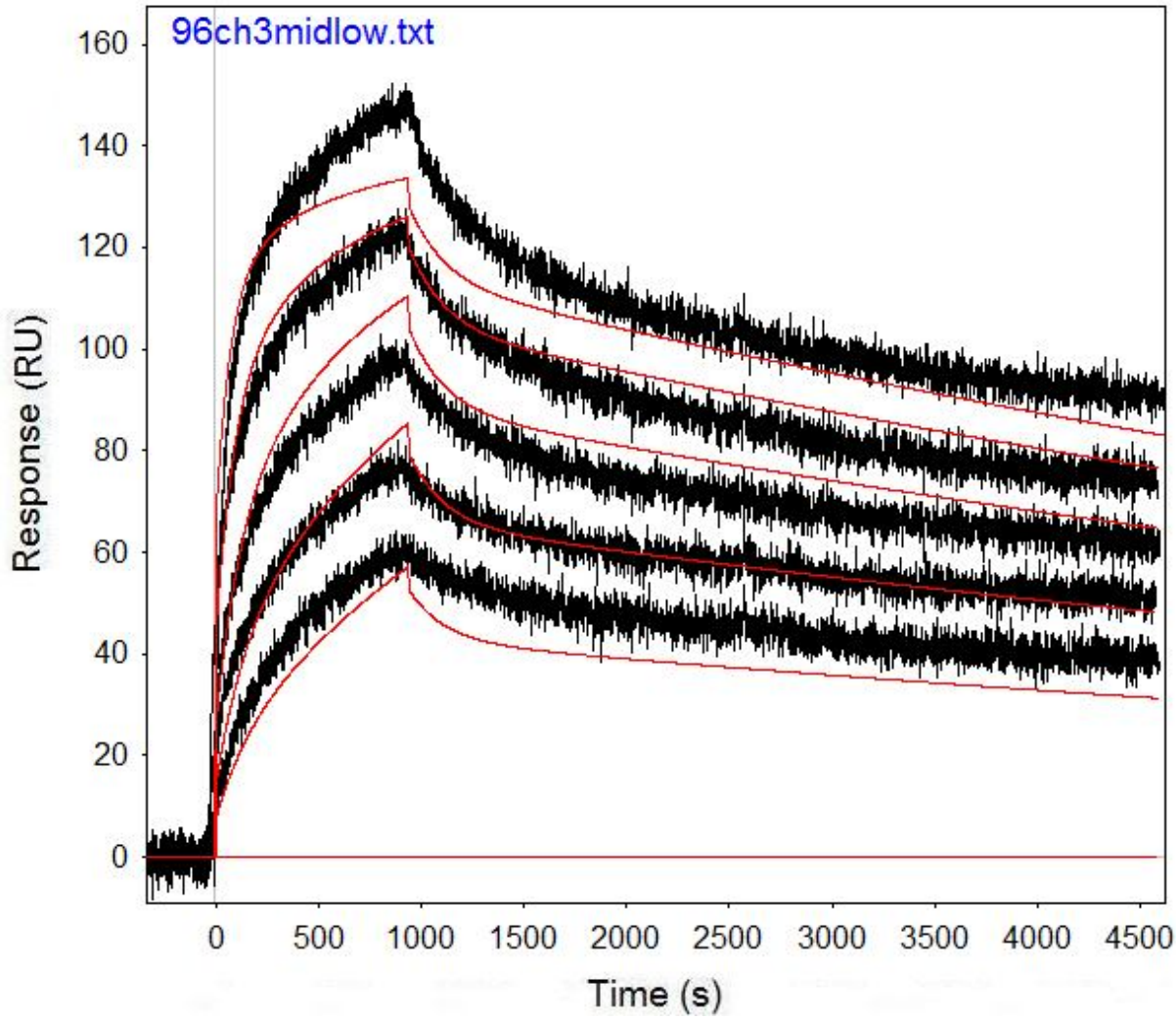

Figure B.13: Run 96, channel 3 model and data graph.

Table B.13: Run 96, channel 3 model parameters.

	kfwd1	krev1	kfwd2	krev2	kfwd3	krev3	ProA (RU)
Value	10137	0.005919	7029	8.53E-05	68090000	83.62	46.58
Error (abs)	277.7	0.0001378	22.91	6.57E-07	8.99E+08	1103	0.05013
Error (%)	2.739469	2.328096	0.325935	0.769898	1320.018	1319.062	0.107621297

Run 103, channel 3: Performed at pH 7.4 in PBST, at an IgG concentration of 1.067 µm. RSSE is 4.277.

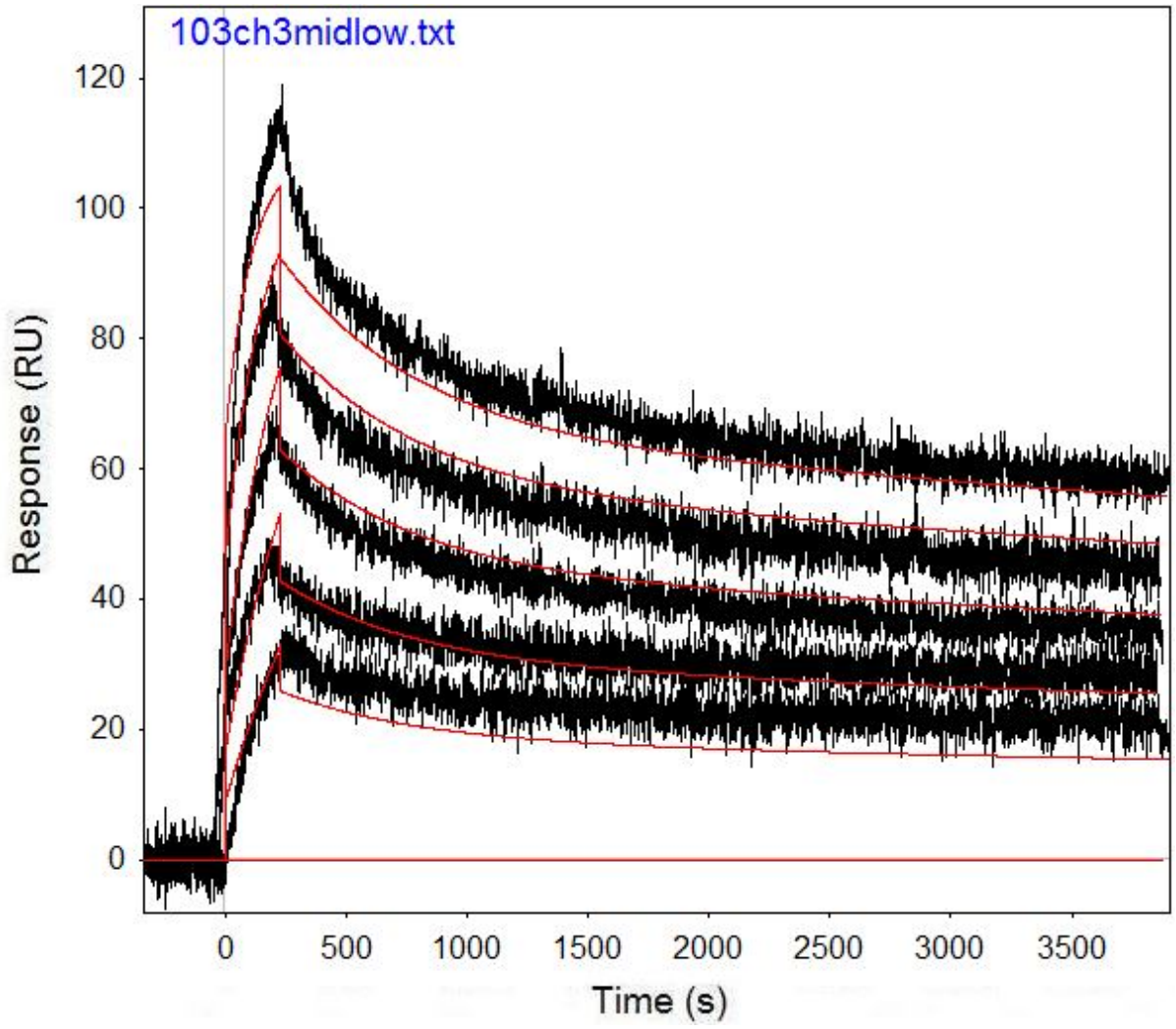

Figure B.14: Run 103, channel 3 model and data graph.

Table B.14: Run 103, channel 3 model parameters.

	kfwd1	krev1	kfwd2	krev2	kfwd3	krev3	ProA (RU)
Value	7059	0.001773	13576	4.48E-05	3604000	2.634	37.05
Error (abs)	85.21	0.0000515	103.9	2.26E-06	1377000	1.005	0.07634
Error (%)	1.207111	2.9046813	0.765321	5.050279	38.20755	38.1549	0.206045884

Run 110, channel 3: Performed at pH 7.4 in PBST, at an IgG concentration of 1.067 µm. RSSE is 4.656.

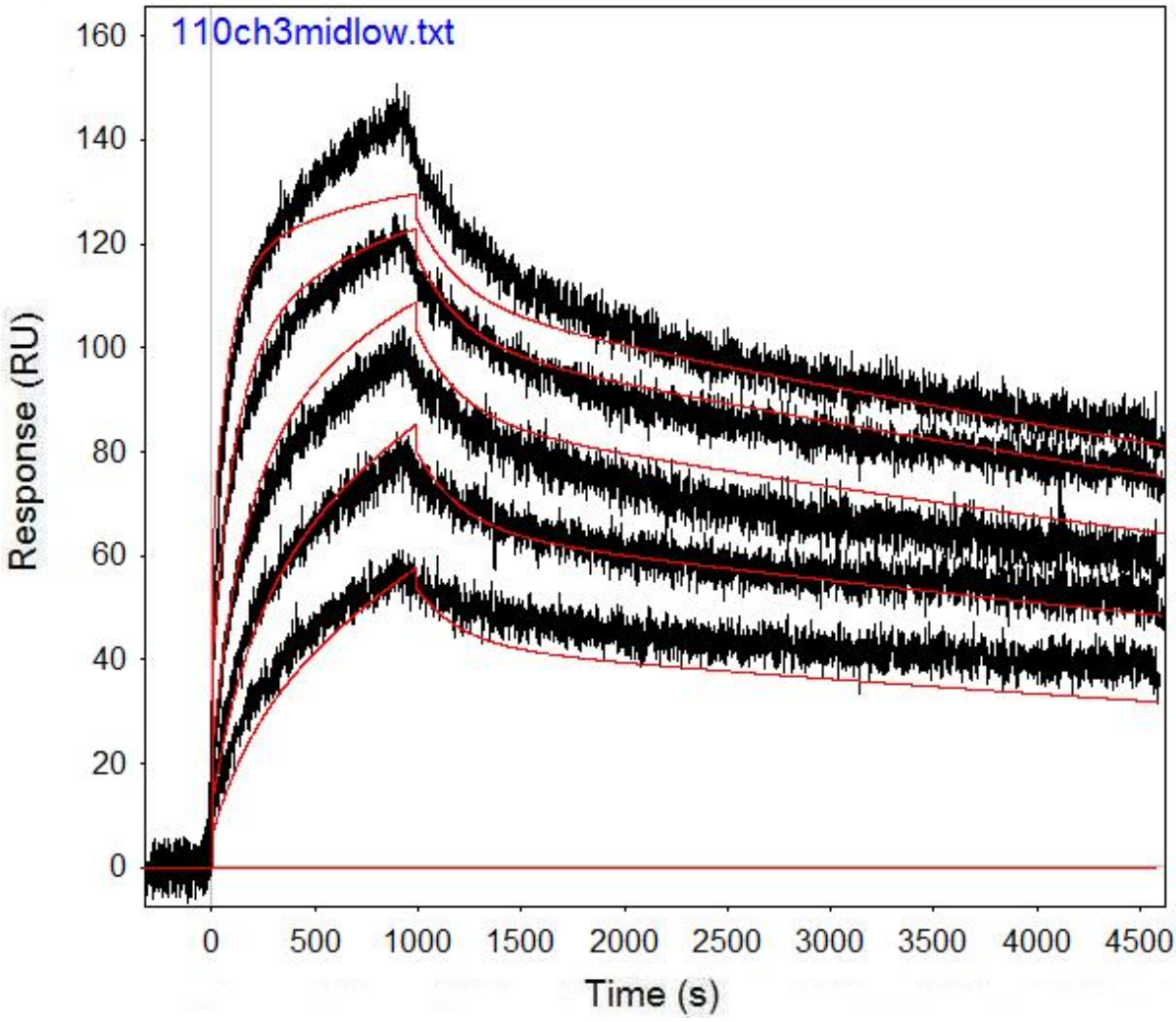

Figure B.15: Run 110, channel 3 model and data graph.

Table B.15: Run 110, channel 3 model parameters.

	kfwd1	krev1	kfwd2	krev2	kfwd3	krev3	ProA (RU)
Value	9182	0.004552	6989	8.08E-05	776600	1.032	44.99
Error (abs)	167.5	7.642E-05	20.02	6.06E-07	281400	0.3689	0.03892
Error (%)	1.824221	1.6788225	0.28645	0.749752	36.23487	35.74612	0.086508113

Run 313, channel 2: Performed at pH 7.4 in PBST, at an IgG concentration of 1.067 µm. RSSE is 7.731.

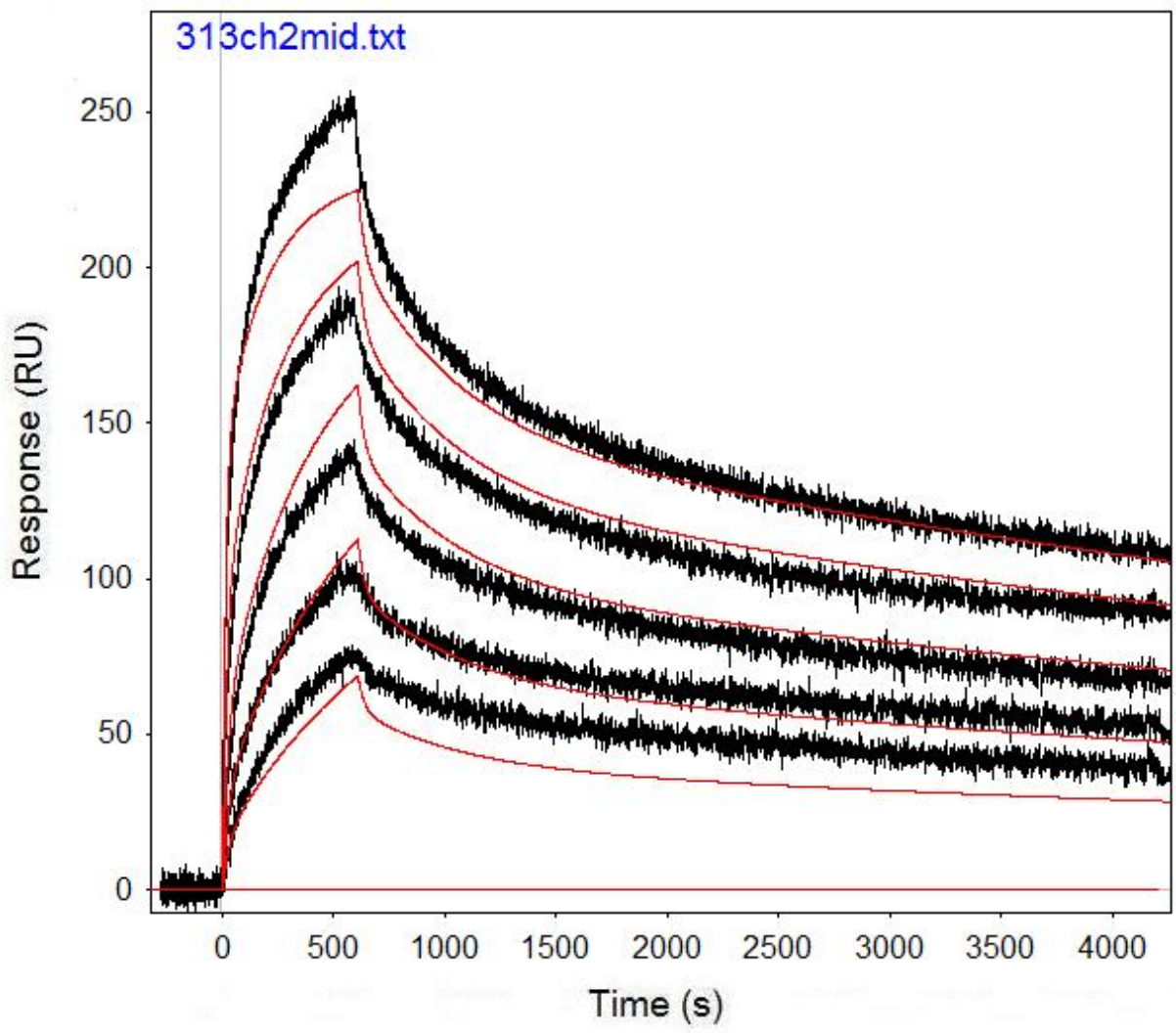

Figure B.16: Run 313, channel 2 model and data graph.

Table B.16: Run 313, channel 2 model parameters.

	kfwd1	krev1	kfwd2	krev2	kfwd3	krev3	ProA (RU)
Value	4180	0.002216	5028	9.21E-05	32905	0.03501	81.64
Error (abs)	65.62	5.22E-05	29.08	1.05E-06	1235	0.001465	0.1078
Error (%)	1.569856	2.356498	0.578361	1.135253	3.753229	4.184519	0.132043116

Run 320, channel 2: Performed at pH 7.4 in PBST, at an IgG concentration of 1.067 µm. RSSE is 3.766.

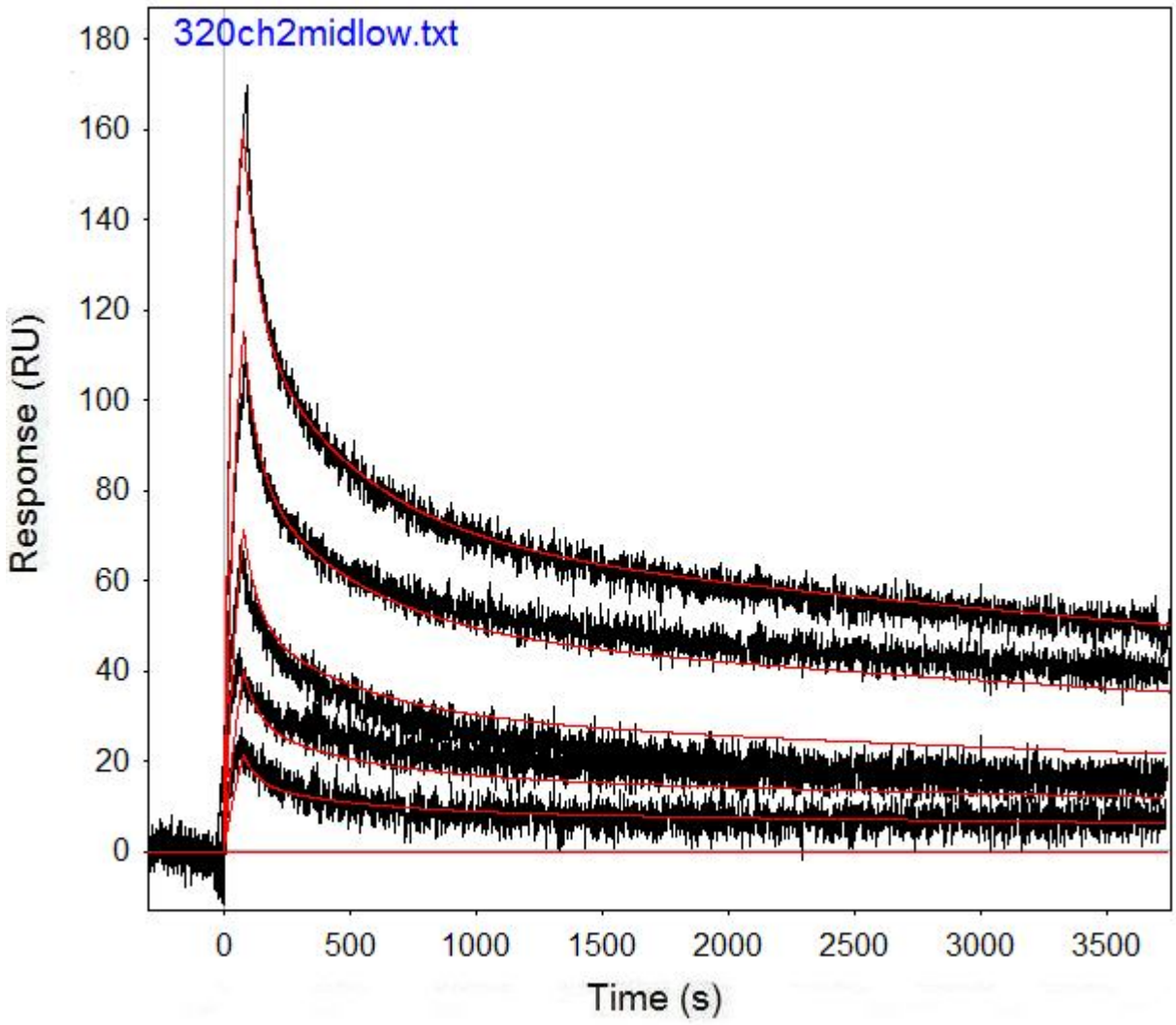

Figure B.17: Run 320, channel 2 model and data graph.

Table B.17: Run 320, channel 2 model parameters.

	kfwd1	krev1	kfwd2	krev2	kfwd3	krev3	ProA (RU)
Value	6672	0.00233	8883	9.24E-05	11398	0.01769	68.95
Error (abs)	118.6	6.73E-05	100.5	1.08E-06	203.2	0.000743	0.2877
Error (%)	1.777578	2.887983	1.131375	1.163672	1.782769	4.200113	0.417258883

Run 327, channel 3: Performed at pH 7.4 in PBST, at an IgG concentration of 1.067 µm. RSSE is 2.731.

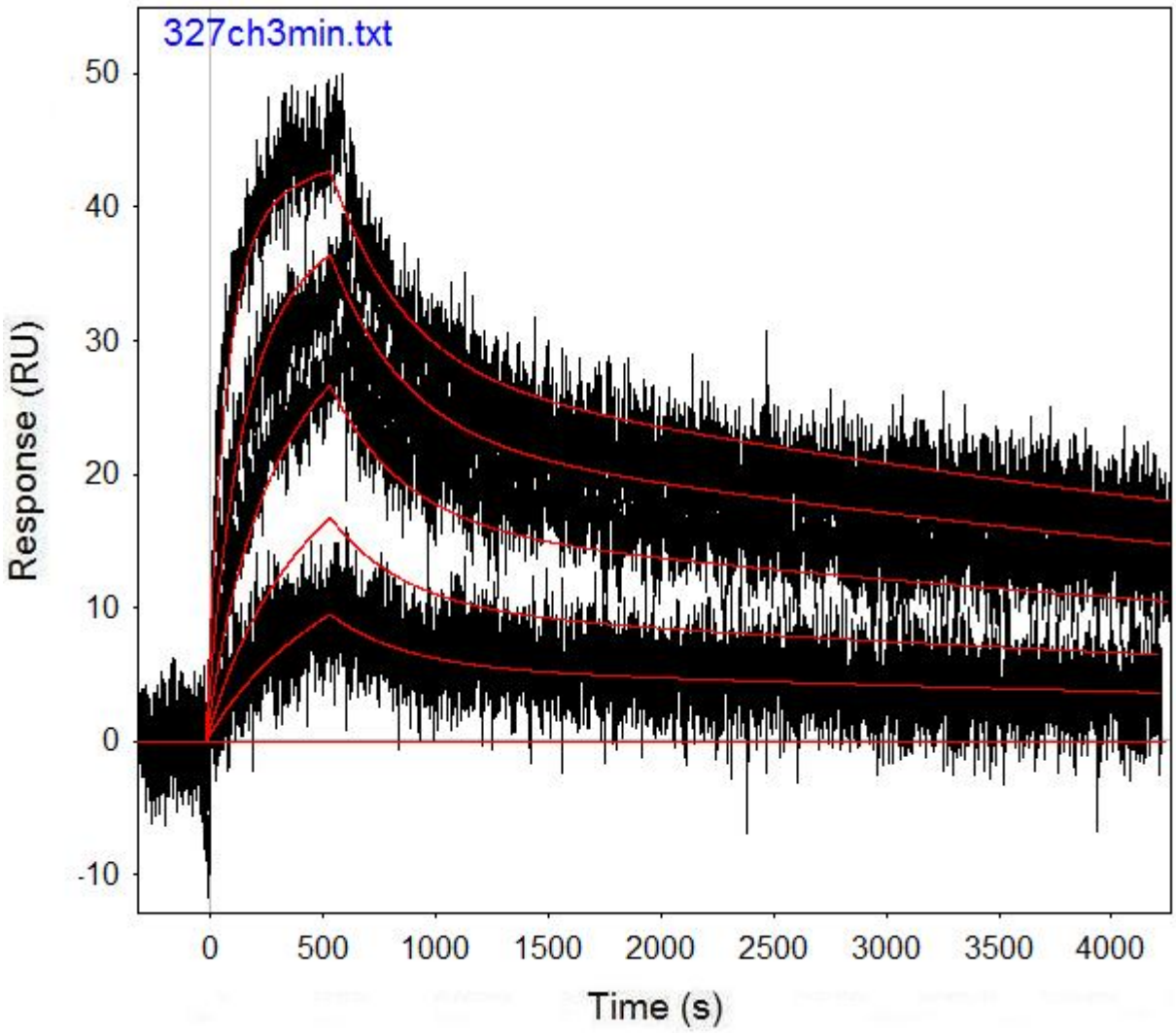

Figure B.18: Run 327, channel 3 model and data graph.

Table B.18: Run 327, channel 3 model parameters.

	kfwd1	krev1	kfwd2	krev2	kfwd3	krev3	ProA (RU)
Value	9456	0.004742	9516	0.000136			80.26
Error (abs)	82.67	5.37E-05	97.78	7.75E-07			0.317
Error (%)	0.87426	1.132855	1.027533	0.57			0.394966359

Run 334, channel 2: Performed at pH 7.4 in PBST, at an IgG concentration of 1.067 µm. RSSE is 4.242.

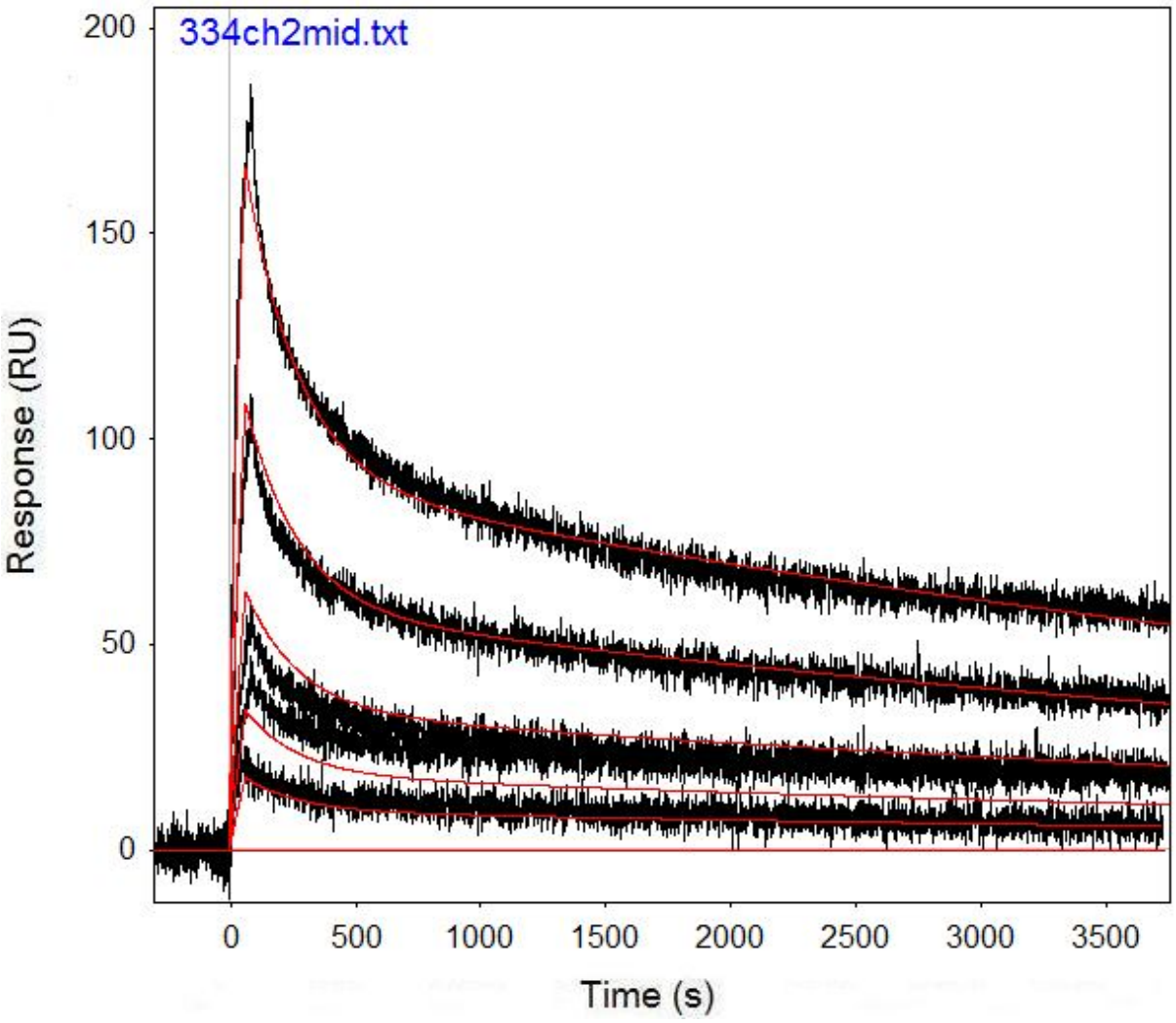

Figure B.19: Run 334, channel 2 model and data graph.

Table B.19: Run 334, channel 2 model parameters.

	kfwd1	krev1	kfwd2	krev2	kfwd3	krev3	ProA (RU)
Value	9456	0.004742	9516	0.000136			80.26
Error (abs)	82.67	5.37E-05	97.78	7.75E-07			0.317
Error (%)	0.87426	1.132855	1.027533	0.57			0.394966359

Run 341, channel 2: Performed at pH 7.4 in PBST, at an IgG concentration of 1.067 µm. RSSE is 4.938.

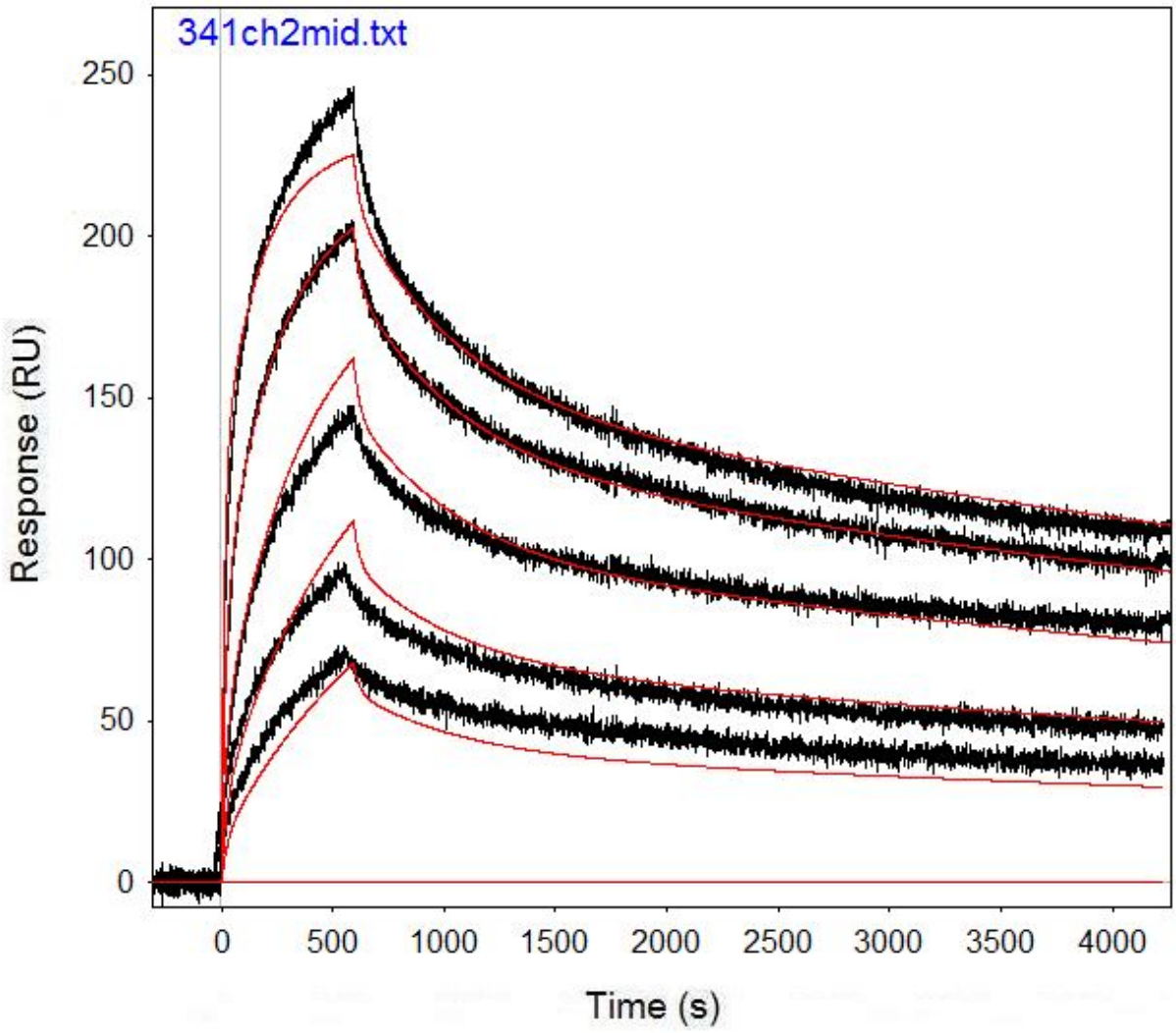

Figure B.20: Run 341, channel 2 model and data graph.

Table B.20: Run 341, channel 2 model parameters.

	kfwd1	krev1	kfwd2	krev2	kfwd3	krev3	ProA (RU)
Value	4335	0.00217	5197	8.52E-05	28754	0.03835	81.32
Error (abs)	36.31	3E-05	18.52	1.37E-05	805.8	0.001166	0.06834
Error (%)	0.838	1.381	0.356	16.117	2.802	3.040	0.084

Run 350, channel 2: Performed at pH 7.4 in PBST, at an IgG concentration of 1.067 µm. RSSE is 2.598.

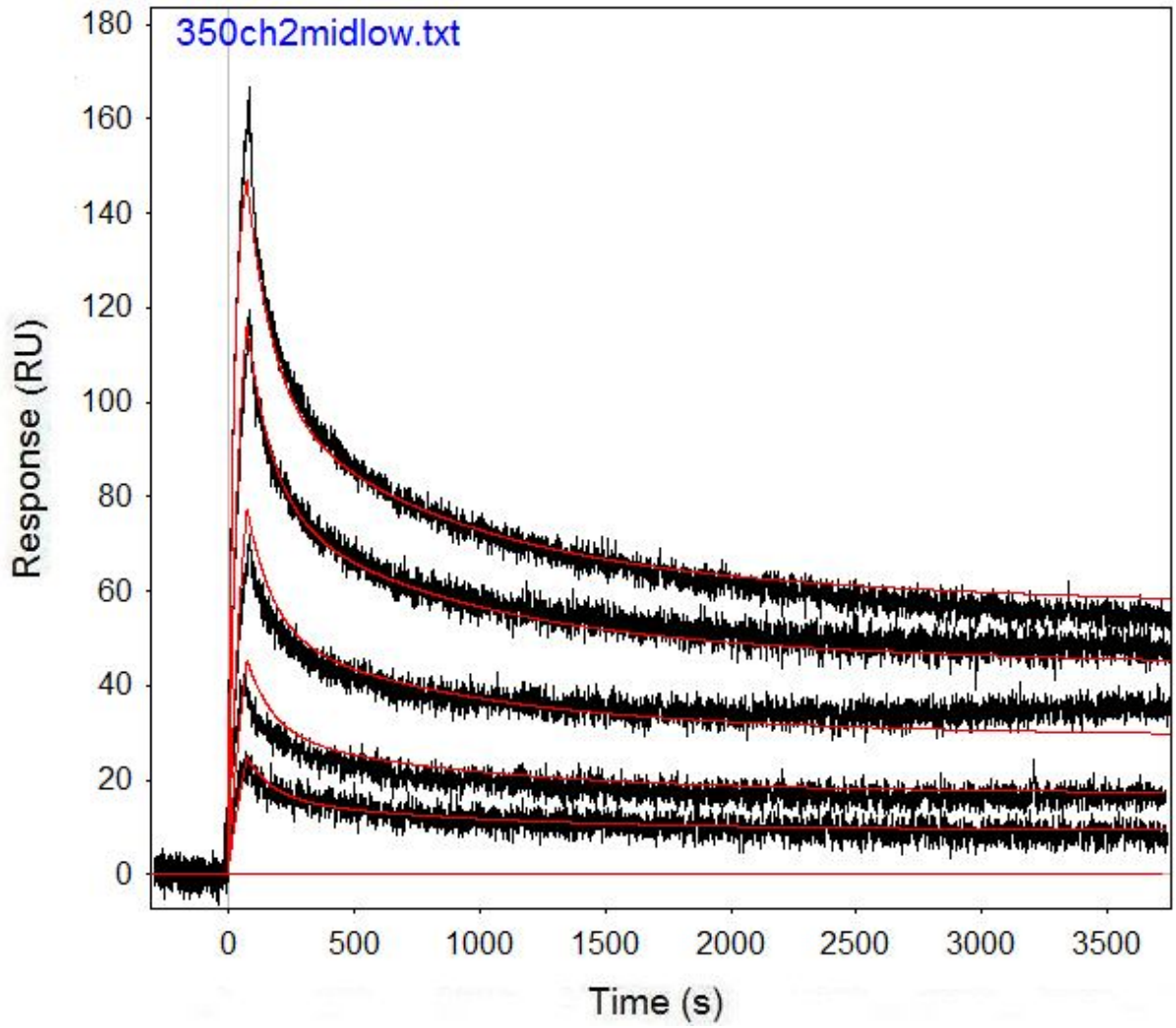

Figure B.21: Run 350, channel 2 model and data graph.

Table B.21: Run 350, channel 2 model parameters.

	kfwd1	krev1	kfwd2	krev2	kfwd3	krev3	ProA (RU)
Value	8551	0.001277	12710	1.79E-05	15335	0.009867	55.71
Error (abs)	106	4.98E-05	170.1	9.16E-07	131.4	0.000223	0.1214
Error (%)	1.240	3.896	1.338	5.120	0.857	2.257	0.218

Run 358, channel 2: Performed at pH 7.4 in PBST, at an IgG concentration of 1.067 µm. RSSE is 3.057.

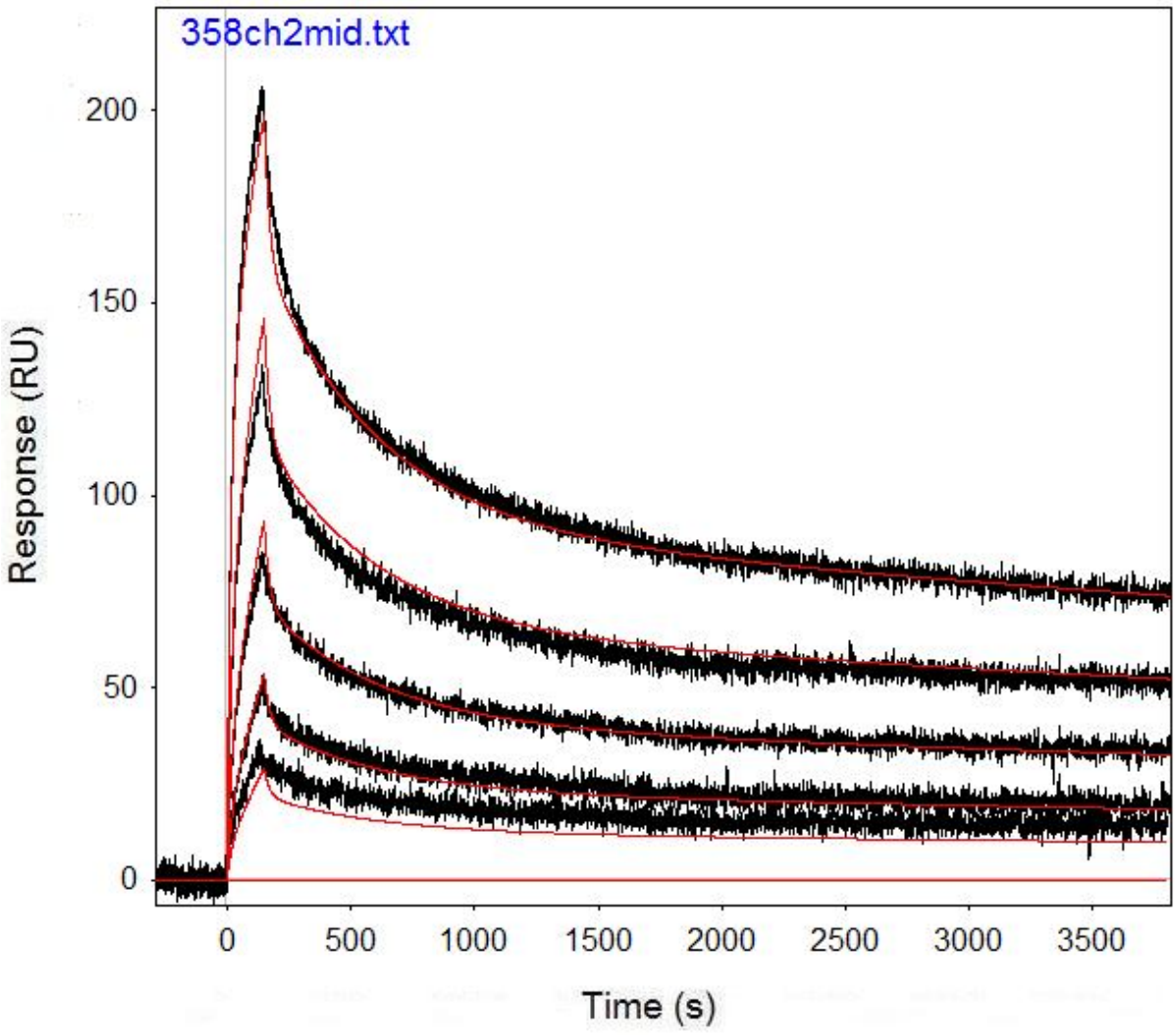

Figure B.22: Run 358, channel 2 model and data graph.

Table B.22: Run 358, channel 2 model parameters.

	kfwd1	krev1	kfwd2	krev2	kfwd3	krev3	ProA (RU)
Value	4373	0.002168	4860	6.05E-05	21145	0.04696	89.73
Error (abs)	27.25	2.34E-05	24.19	1.07E-06	469.7	0.001093	0.1703
Error (%)	0.623	1.078	0.498	1.767	2.221	2.328	0.190

Run 365, channel 2: Performed at pH 7.4 in PBST, at an IgG concentration of 1.067 µm. RSSE is 3.309.

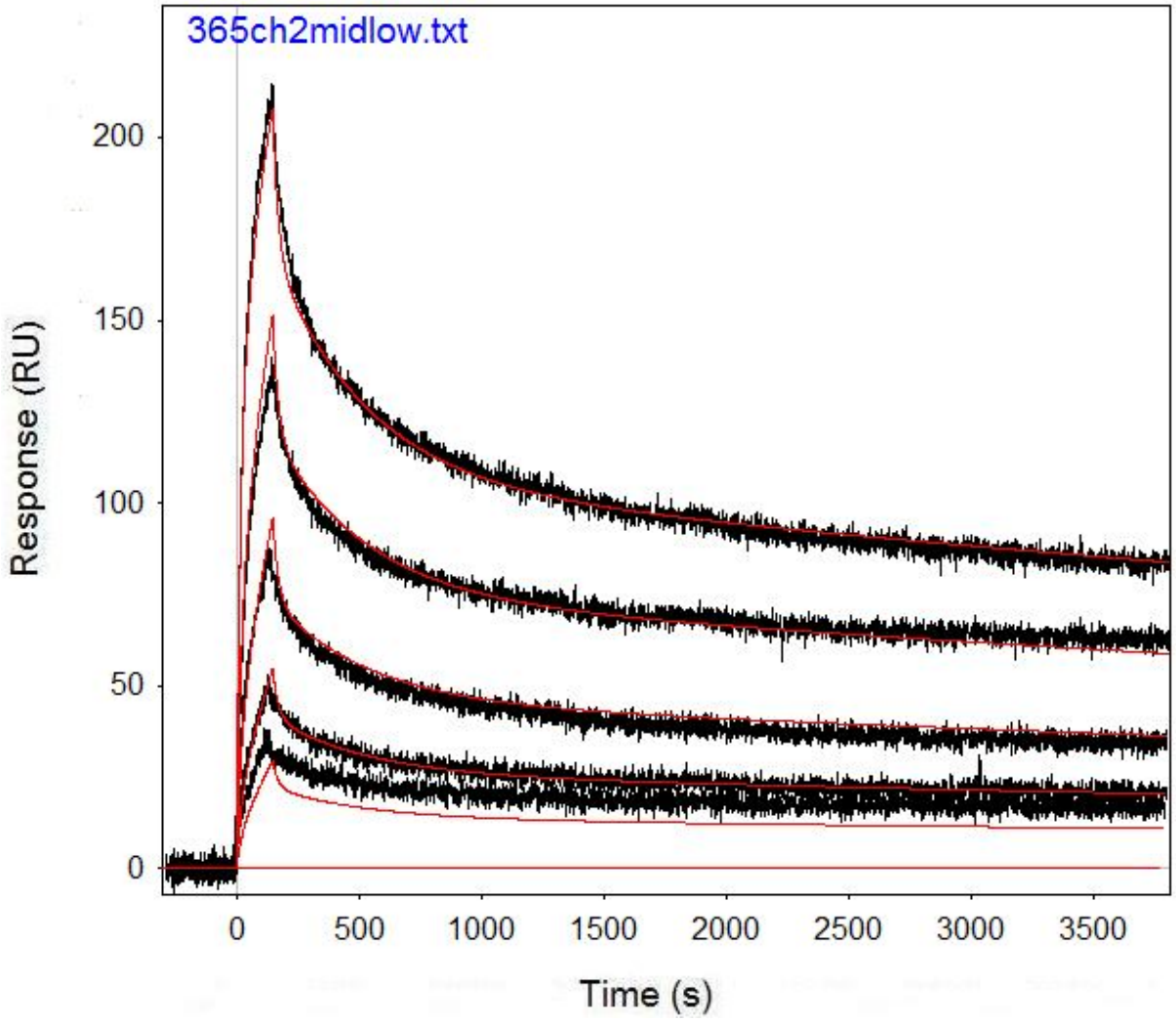

Figure B.23: Run 365, channel 2 model and data graph.

Table B.23: Run 365, channel 2 model parameters.

	kfwd1	krev1	kfwd2	krev2	kfwd3	krev3	ProA (RU)
Value	3816	0.002638	5235	6.49E-05	19164	0.0451	95.08
Error (abs)	31.7	3.3E-05	23.54	7.6E-07	434.5	0.001114	0.1883
Error (%)	0.831	1.252	0.450	1.173	2.267	2.470	0.198

Run 372, channel 2: Performed at pH 7.4 in PBST, at an IgG concentration of 1.067 µm. RSSE is 3.835.

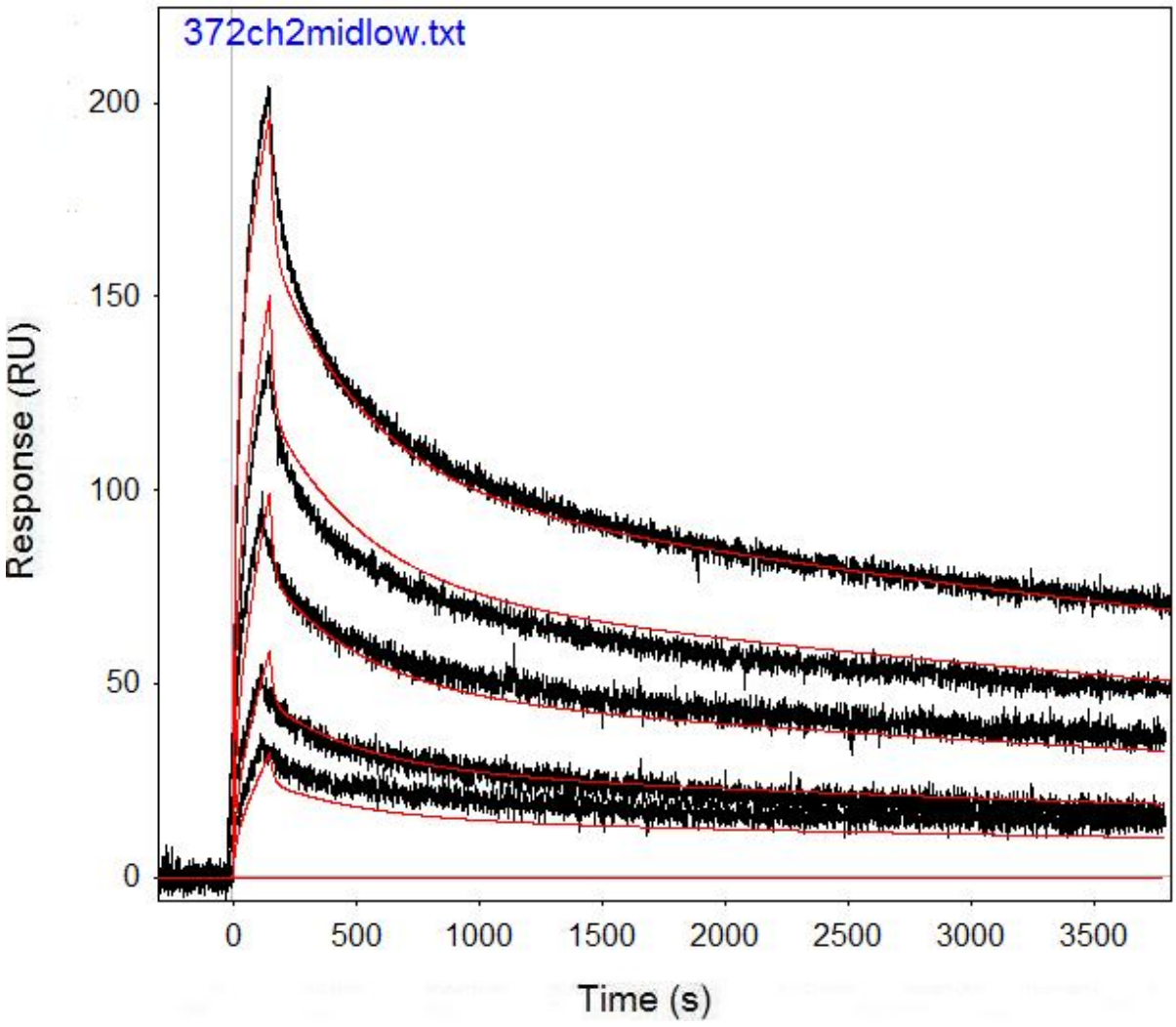

Figure B.24: Run 372, channel 2 model and data graph.

Table B.24: Run 372, channel 2 model parameters.

	kfwd1	krev1	kfwd2	krev2	kfwd3	krev3	ProA (RU)
Value	4806	0.002565	6412	0.000105	35315	0.06722	84.25
Error (abs)	39.33	3.52E-05	33.56	8.94E-07	1100	0.002134	0.1777
Error (%)	0.818	1.371	0.523	0.850	3.115	3.175	0.211

Run 387, channel 2: Performed at pH 7.0 in PBST, at an IgG concentration of 1.067 µm. RSSE is 3.214.

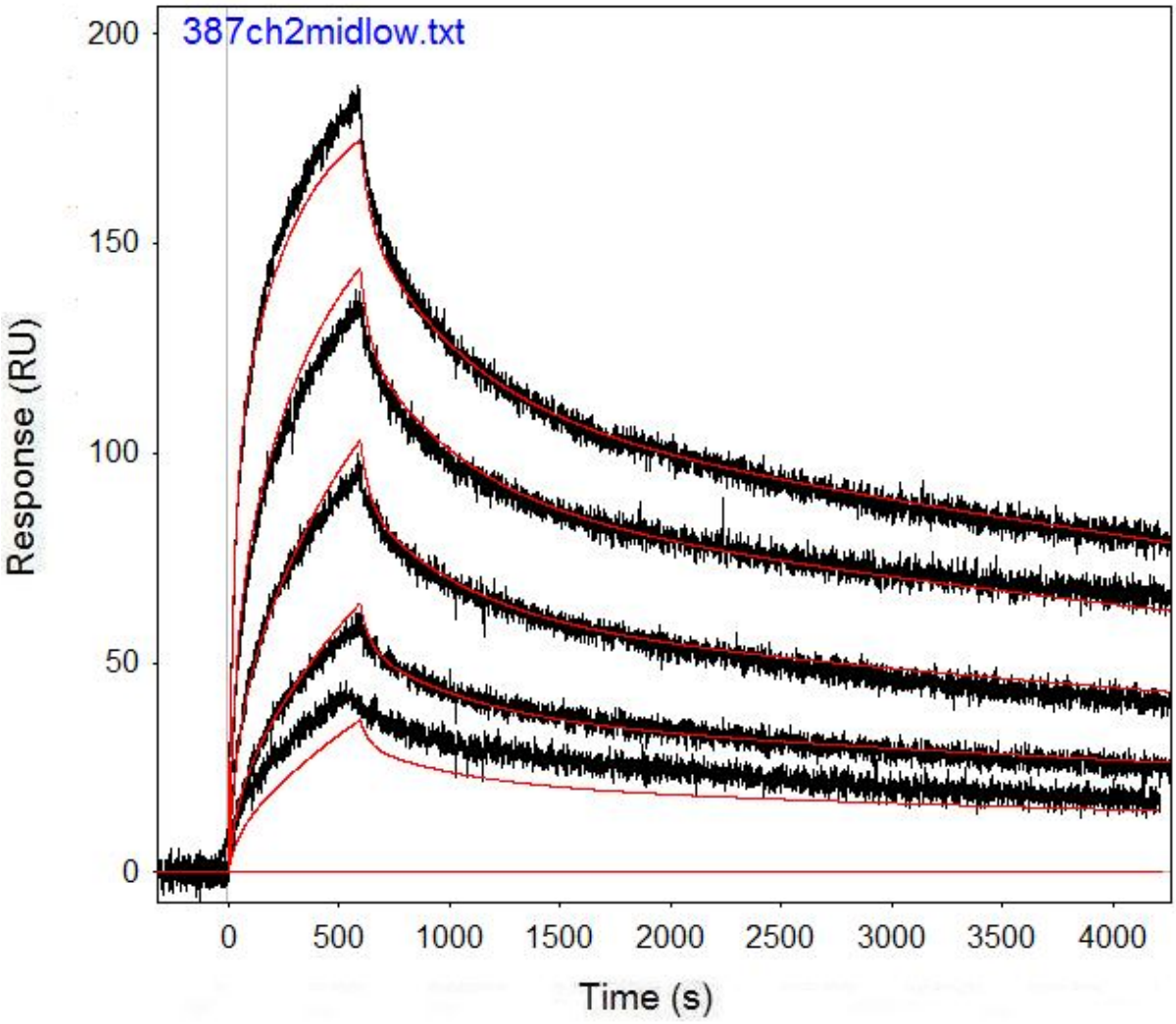

Figure B.25: Run 387, channel 2 model and data graph.

Table B.25: Run 387, channel 2 model parameters.

	kfwd1	krev1	kfwd2	krev2	kfwd3	krev3	ProA (RU)
Value	2387	0.002149	2938	9.51E-05	13070	0.0245	68.41
Error (abs)	26.8	3.42E-05	11.23	5.97E-07	279.8	0.000626	0.06673
Error (%)	1.123	1.593	0.382	0.628	2.141	2.555	0.098

Run 394, channel 2: Performed at pH 7.0 in PBST, at an IgG concentration of 1.067 µm. RSSE is 4.073.

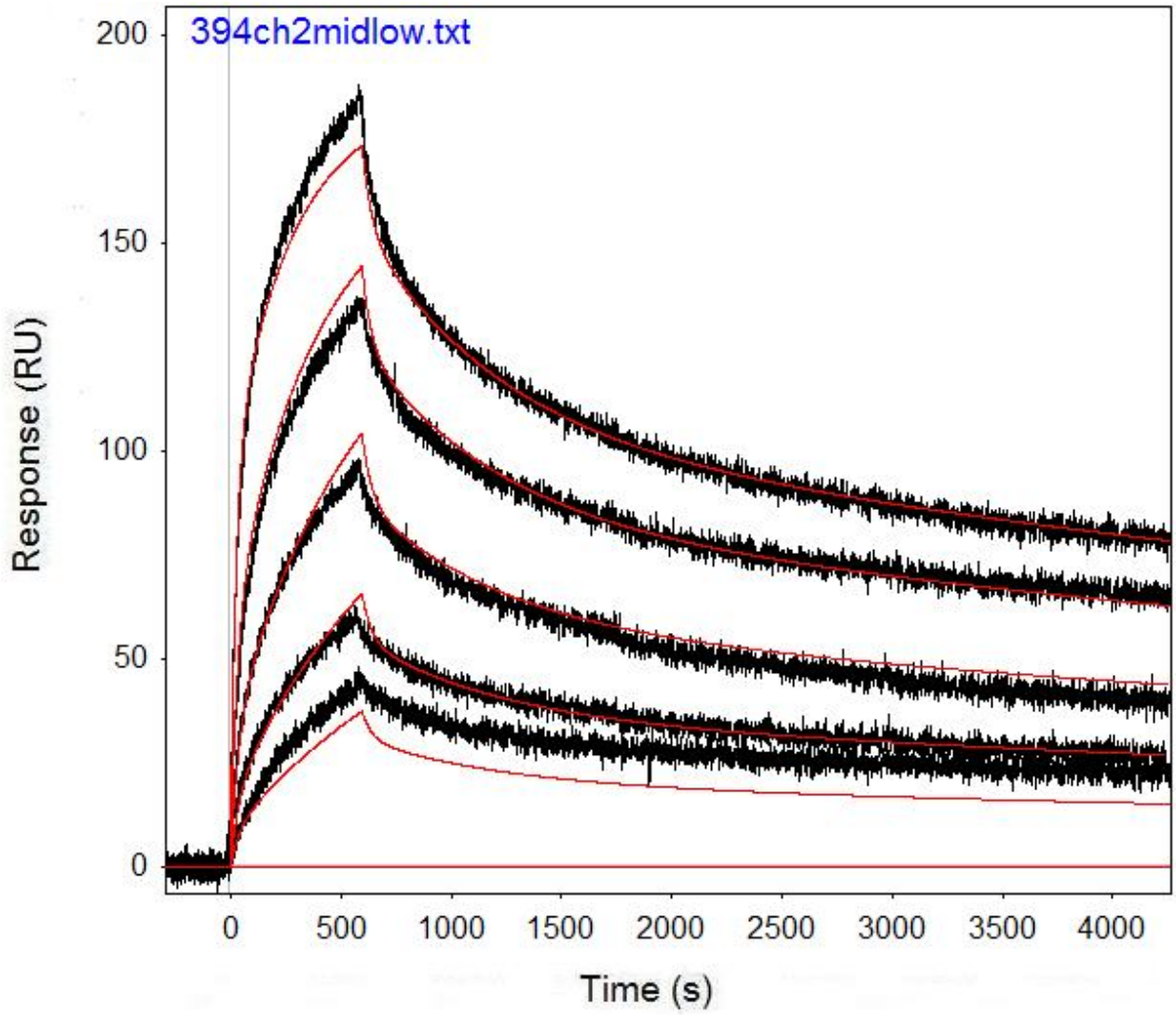

Figure B.26: Run 394, channel 2 model and data graph.

Table B.26: Run 394, channel 2 model parameters.

	kfwd1	krev1	kfwd2	krev2	kfwd3	krev3	ProA (RU)
Value	2394	0.001624	2889	7.8E-05	14220	0.02344	67.09
Error (abs)	22.93	3.5E-05	21.01	1.15E-06	357.7	0.000675	0.08101
Error (%)	0.958	2.156	0.727	1.470	2.515	2.879	0.121

Run 410, channel 2: Performed at pH 7.0 in PBST, at an IgG concentration of 1.067 µm. RSSE is 4.777.

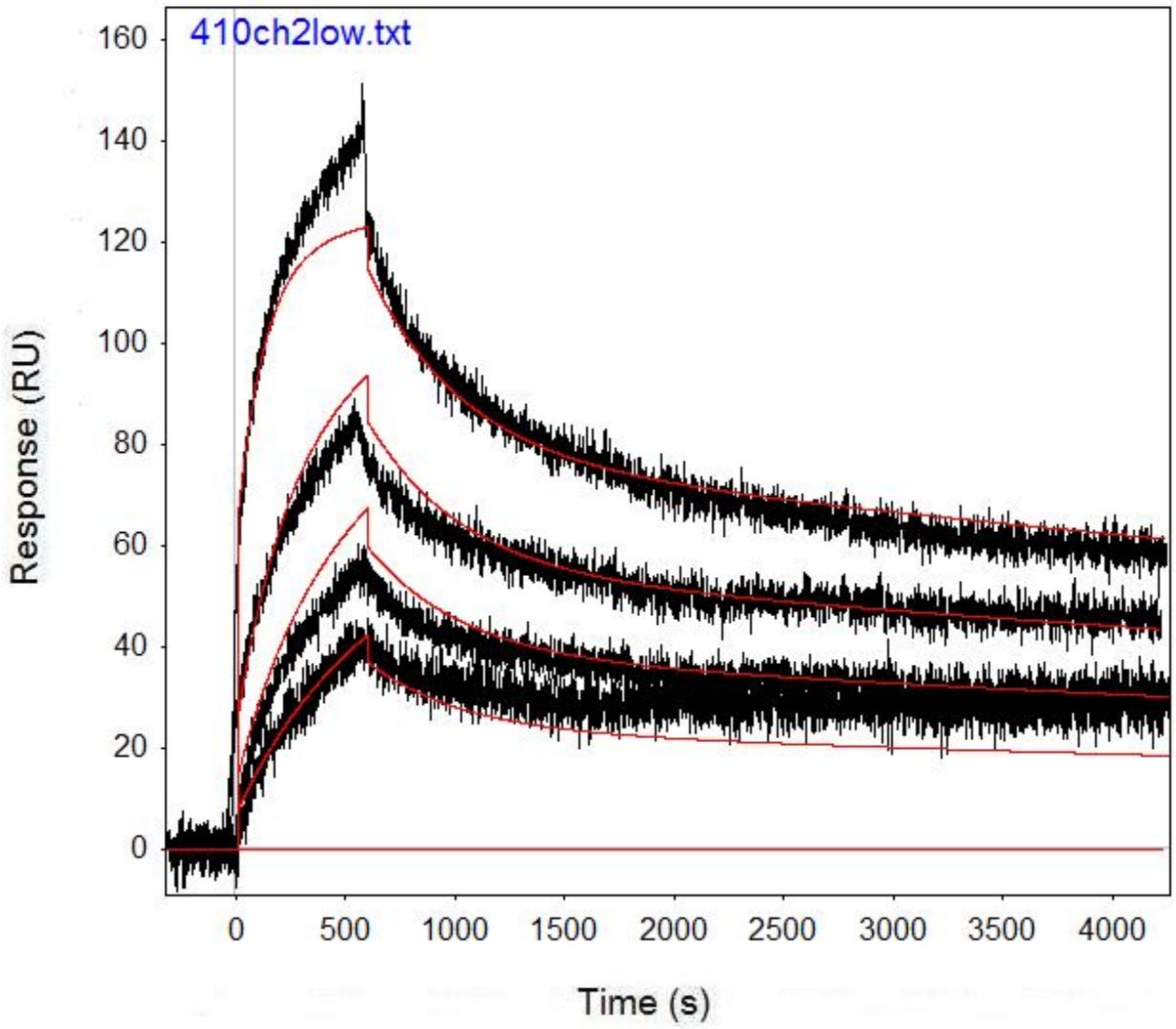

Figure B.27: Run 410, channel 2 model and data graph.

Table B.27: Run 410, channel 2 model parameters.

	kfwd1	krev1	kfwd2	krev2	kfwd3	krev3	ProA (RU)
Value	6313	0.002376	5799	6.59E-05	1.23E+08	132.8	43.87
Error (abs)	67.66	4.45E-05	35.77	7.46E-07	2.61E+08	282.1	0.0664
Error (%)	1.072	1.871	0.617	1.131	212.296	212.425	0.151

Run 417, channel 2: Performed at pH 7.0 in PBST, at an IgG concentration of 1.067 µm. RSSE is 3.449.

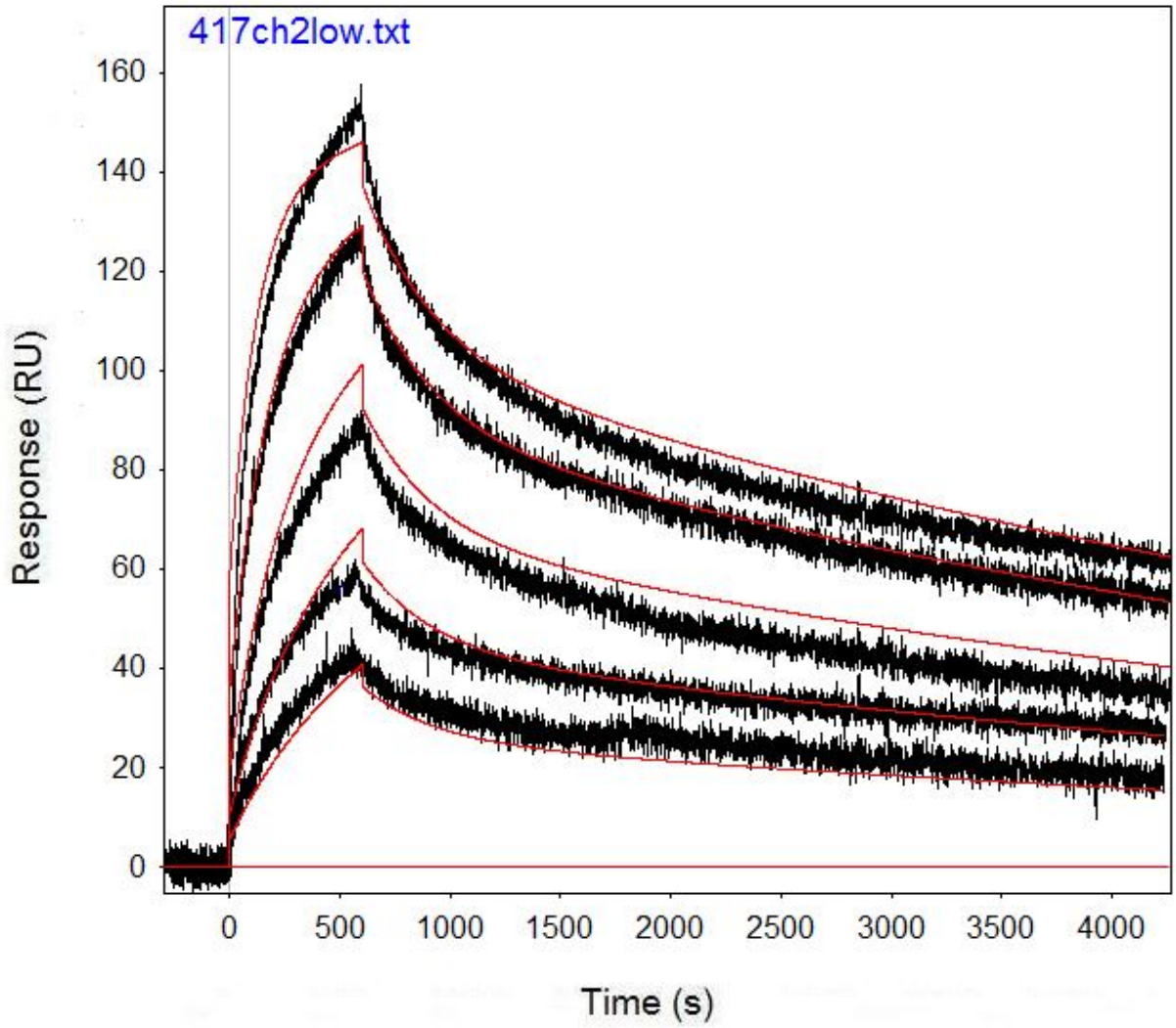

Figure B.28: Run 417, channel 2 model and data graph.

Table B.28: Run 417, channel 2 model parameters.

	kfwd1	krev1	kfwd2	krev2	kfwd3	krev3	ProA (RU)
Value	5332	0.003284	4709	0.000138	84420000	221.6	51.89
Error (abs)	44.43	3.7E-05	16.39	8.11E-07	2.33E+09	6107	0.07284
Error (%)	0.833	1.127	0.348	0.588	2757.640	2755.866	0.140

Run 424, channel 2: Performed at pH 7.0 in PBST, at an IgG concentration of 1.067 µm. RSSE is 4.466.

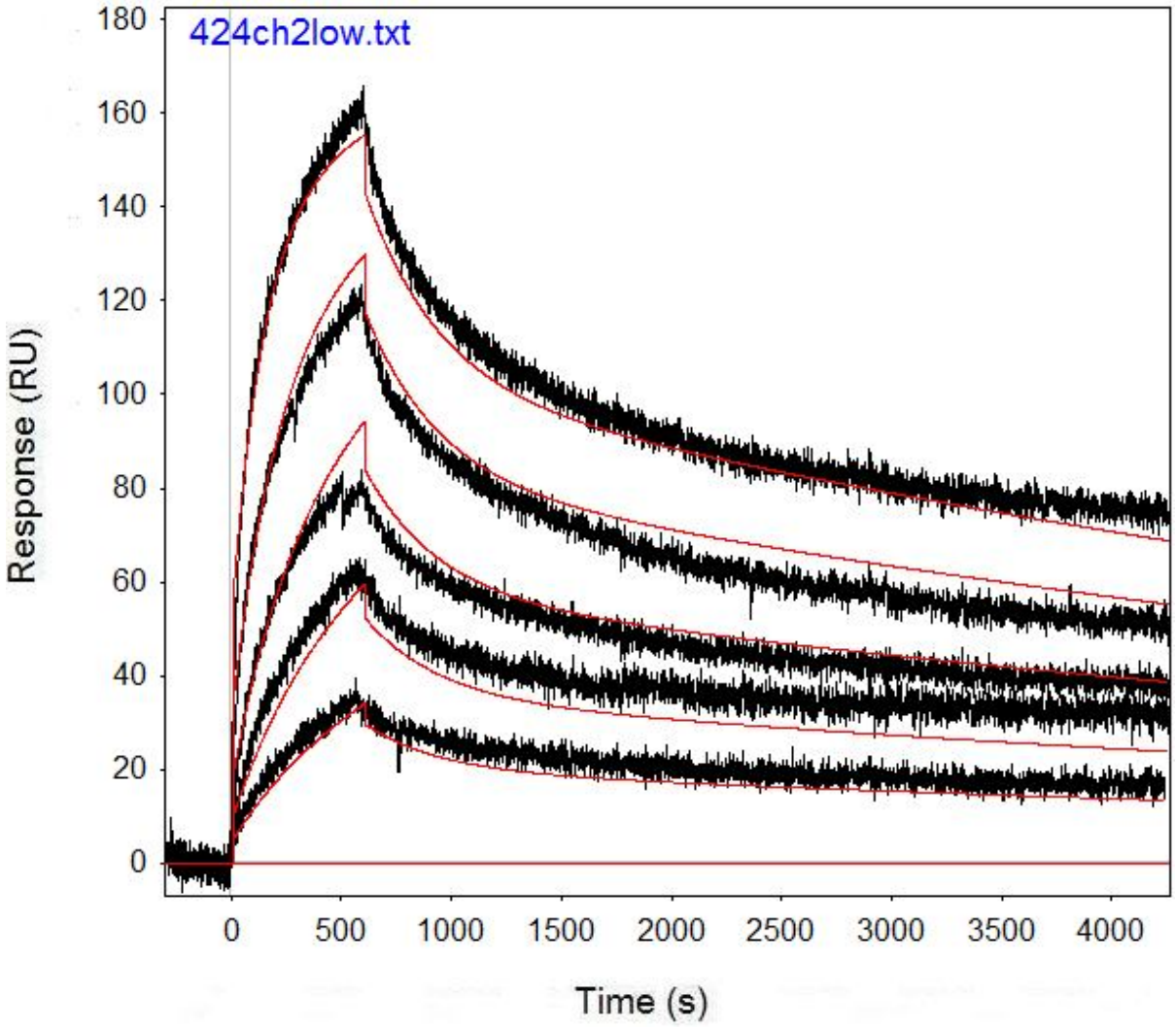

Figure B.29: Run 424, channel 2 model and data graph.

Table B.29: Run 424, channel 2 model parameters.

	kfwd1	krev1	kfwd2	krev2	kfwd3	krev3	ProA (RU)
Value	3436	0.003064	3273	0.000109	90350000	202.9	60.2
Error (abs)	39.76	4.32E-05	13.84	1.11E-06	1.39E+09	3114	0.1002
Error (%)	1.157	1.410	0.423	1.015	1536.248	1534.746	0.166

Run 431, channel 2: Performed at pH 7.0 in PBST, at an IgG concentration of 1.067 µm. RSSE is 4.822.

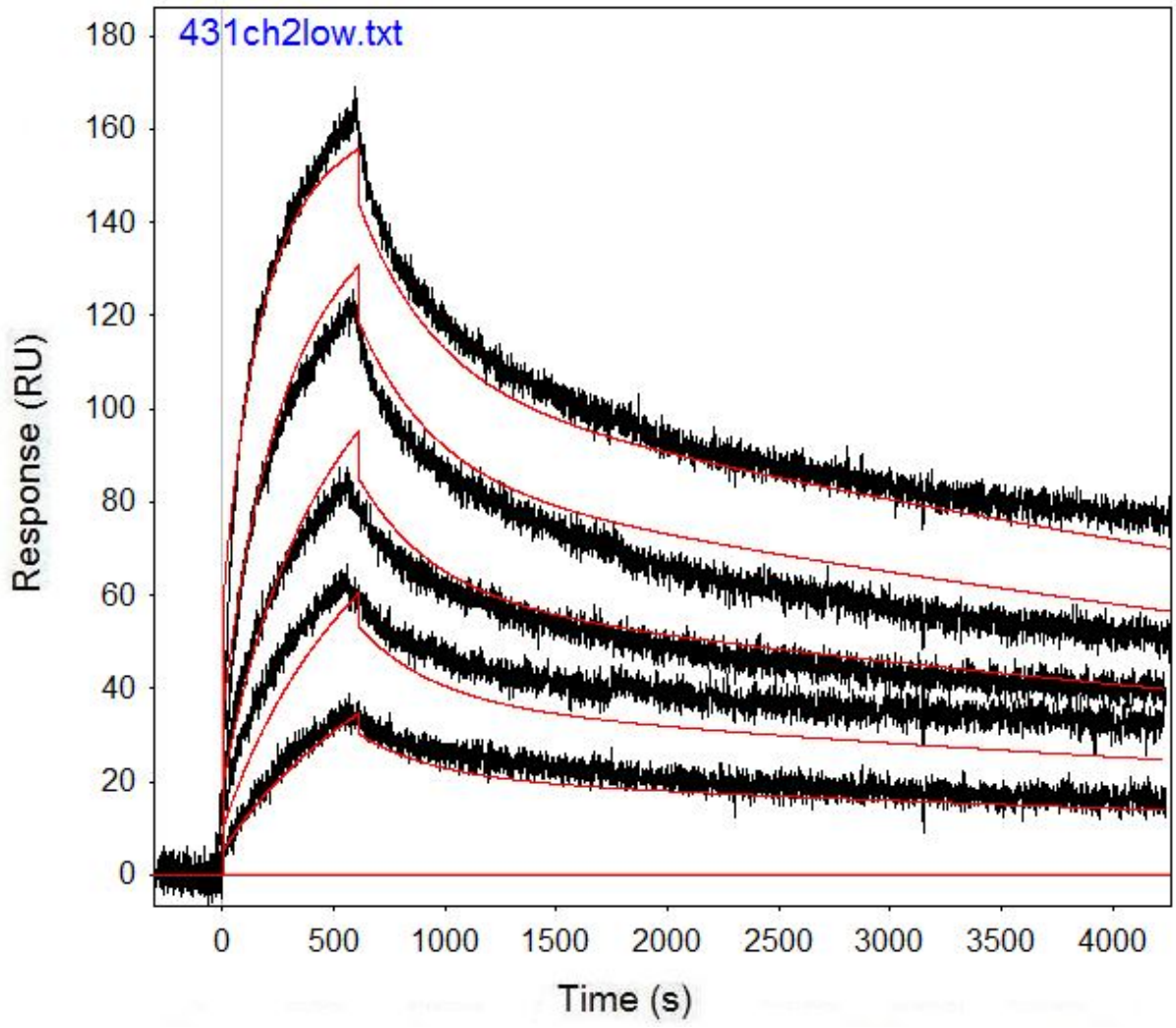

Figure B.30: Run 431, channel 2 model and data graph.

Table B.30: Run 431, channel 2 model parameters.

	kfwd1	krev1	kfwd2	krev2	kfwd3	krev3	ProA (RU)
Value	3240	0.00296	3352	0.000111	93500000	197.3	60.08
Error (abs)	37.96	5.27E-05	17.63	5.73E-06	6E+08	1265	0.09547
Error (%)	1.172	1.779	0.526	5.185	641.283	641.156	0.159

Run 438, channel 2: Performed at pH 7.0 in PBST, at an IgG concentration of 0.5 µm. RSSE is 2.663.

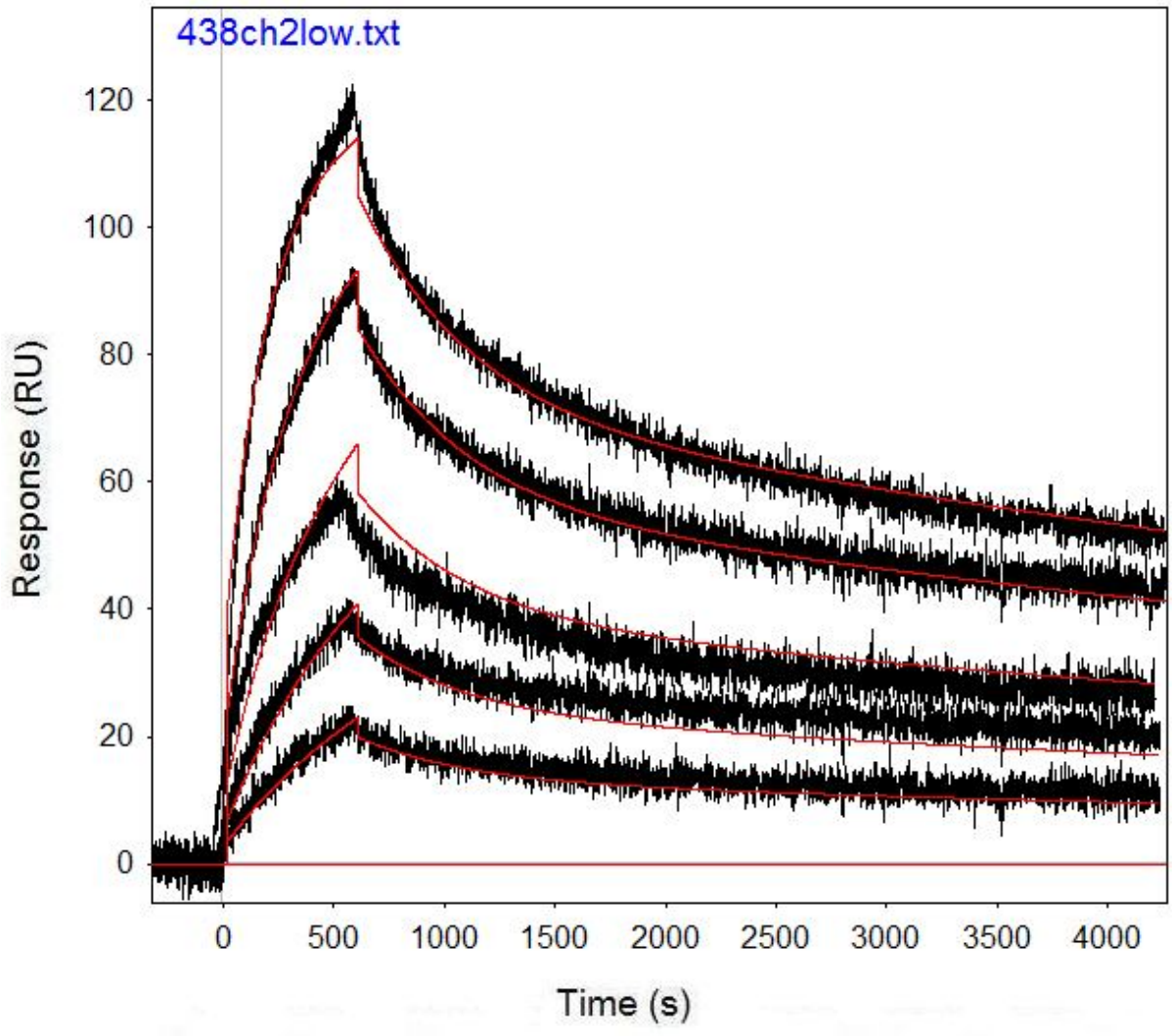

Figure B.31: Run 438, channel 2 model and data graph.

Table B.31: Run 438, channel 2 model parameters.

	kfwd1	krev1	kfwd2	krev2	kfwd3	krev3	ProA (RU)
Value	5490	0.002082	6144	8.85E-05	1574000000	1777	44.56
Error (abs)	33.75	2.66E-05	27.03	0.001548	1.881E+11	212400	0.05449
Error (%)	0.615	1.276	0.440	1749.746	11950.445	11952.729	0.122

Run 445, channel 2: Performed at pH 7.0 in PBST, at an IgG concentration of 0.5 µm. RSSE is 2.741.

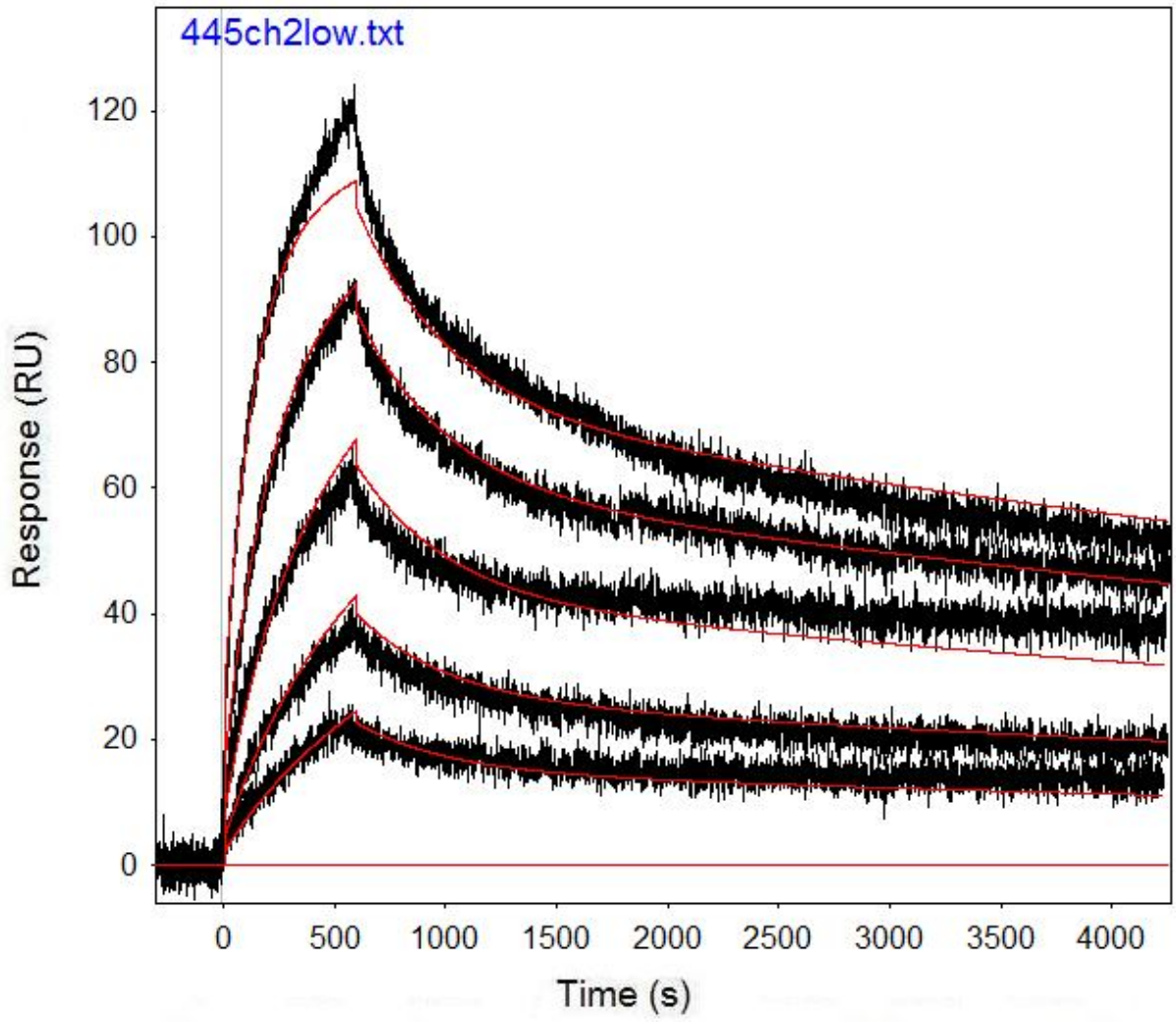

Figure B.32: Run 445, channel 2 model and data graph.

Table B.32: Run 445, channel 2 model parameters.

	kfwd1	krev1	kfwd2	krev2	kfwd3	krev3	ProA (RU)
Value	7495	0.00245	7636	8.05E-05	1392000000	2205	40.96
Error (abs)	49.11	3.3E-05	32.42	0.000371	2.368E+10	37506	0.05074
Error (%)	0.655	1.347	0.425	460.907	1701.149	1700.952	0.124

Run 462, channel 3: Performed at pH 7.4 in PBST, at an IgG concentration of 5.733 µm. RSSE is 3.056.

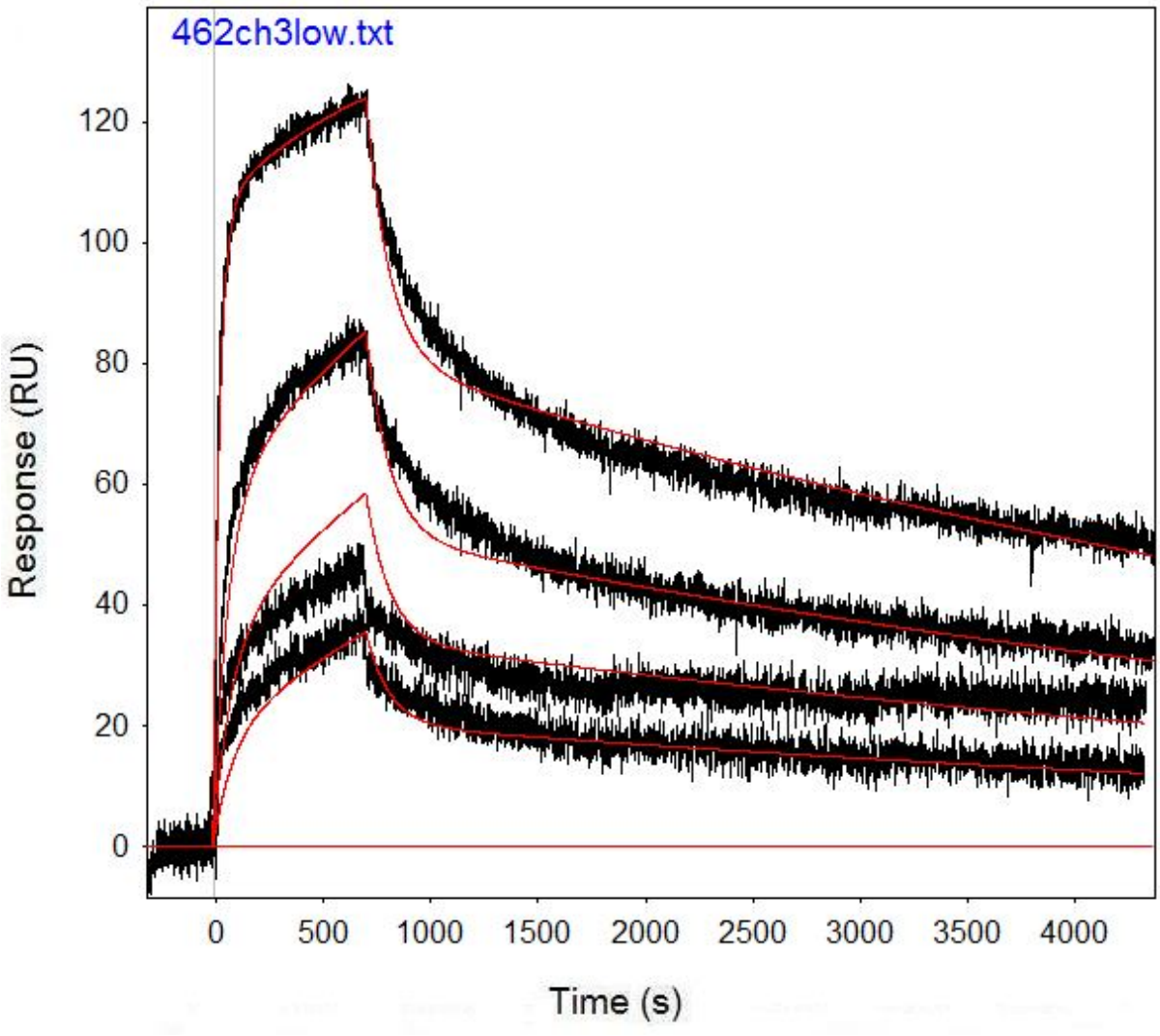

Figure B.33: Run 462, channel 3 model and data graph.

Table B.33: Run 462, channel 3 model parameters.

	kfwd1	krev1	kfwd2	krev2	kfwd3	krev3	ProA (RU)
Value	7022	0.009264	1377	0.0001418			46.96
Error (abs)	65.38	9.11E-05	4.11	1.403			0.05018
Error (%)	0.931	0.984	0.298	989421.721			0.107

Run 469, channel 3: Performed at pH 7.4 in PBST, at an IgG concentration of 5.733 µm. RSSE is 2.916.

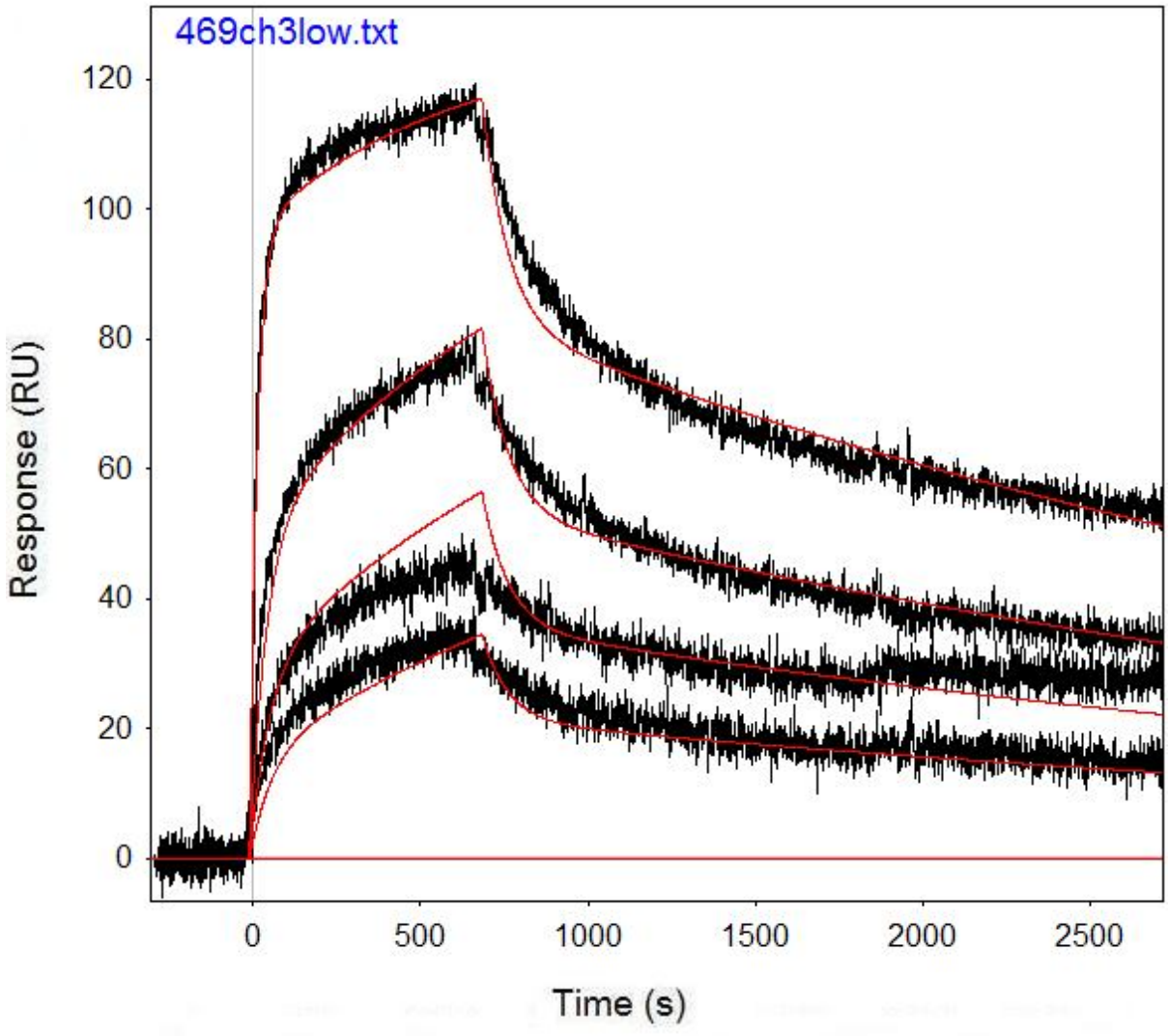

Figure B.34: Run 469, channel 3 model and data graph.

Table B.34: Run 469, channel 3 model parameters.

	kfwd1	krev1	kfwd2	krev2	kfwd3	krev3	ProA (RU)
Value	9247	0.01303	1658	0.0002344			43.95
Error (abs)	110.1	0.000165	6.041	1.403			0.0506
Error (%)	1.191	1.263	0.364	598549.488			0.115

Run 485, channel 2: Performed at pH 6.5 in PBST, at an IgG concentration of 1.067 µm. RSSE is 10.91.

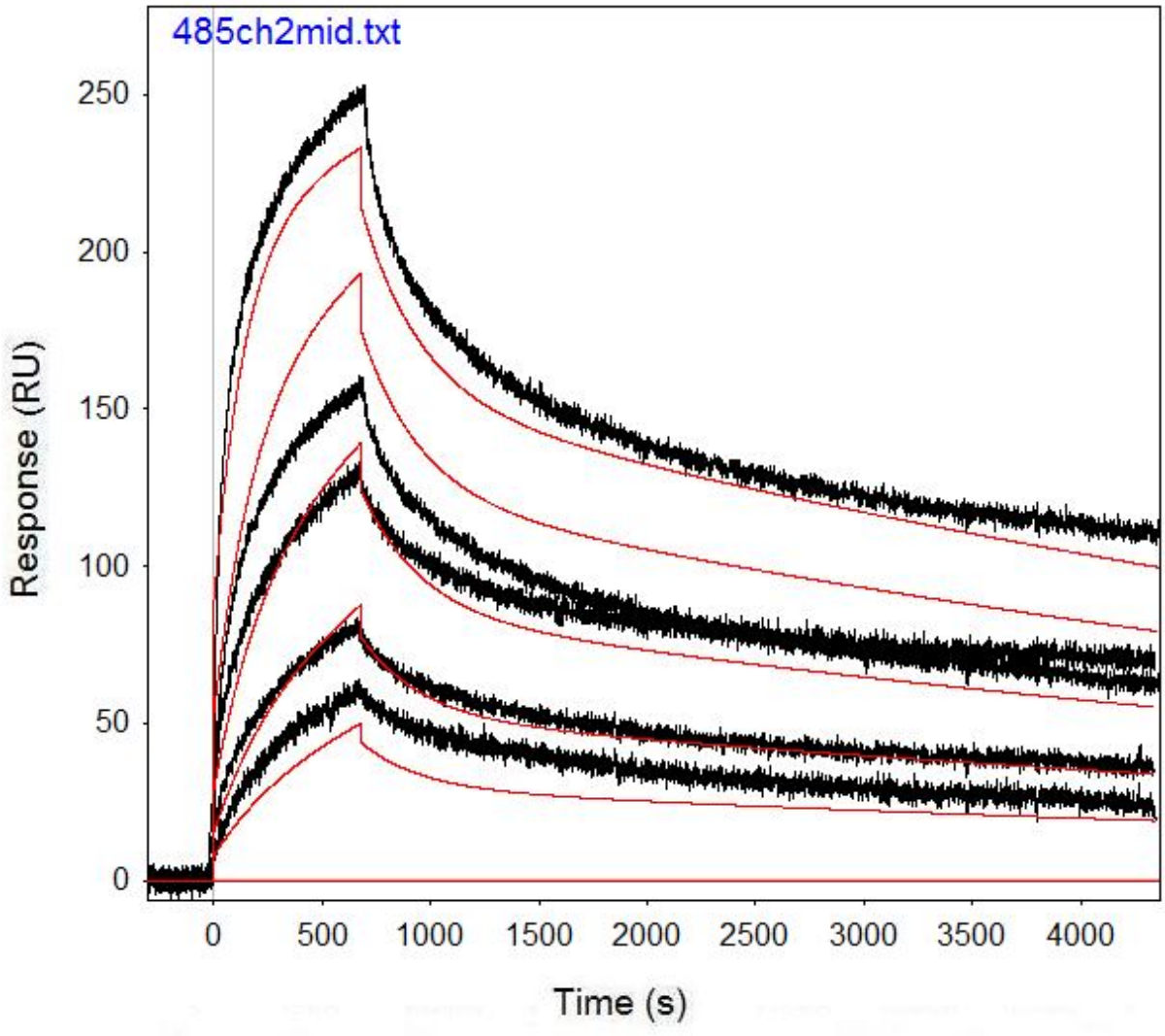

Figure B.35: Run 485, channel 2 model and data graph.

Table B.35: Run 485, channel 2 model parameters.

	kfwd1	krev1	kfwd2	krev2	kfwd3	krev3	ProA (RU)
Value	2755	0.000119	3700	0.003712	8961000	21.67	92.22
Error (abs)	16.75	1.51E-06	72.11	1.403	54990000	133	0.2124
Error (%)	0.608	1.268	1.949	37796.336	613.659	613.752	0.230

Run 492, channel 3: Performed at pH 6.5 in PBST, at an IgG concentration of 1.067 µm. RSSE is 1.941.

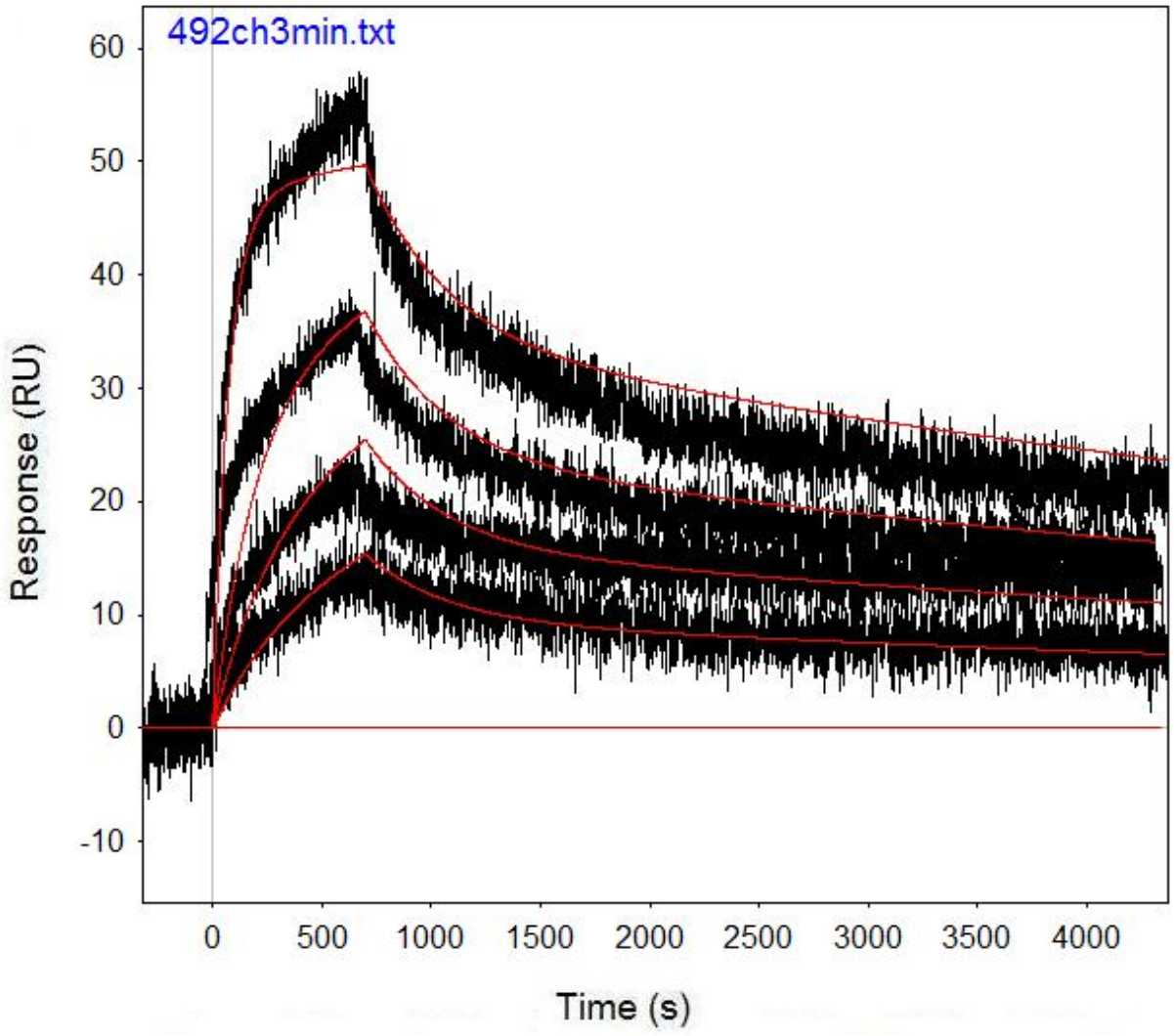

Figure B.36: Run 492, channel 3 model and data graph.

Table B.36: Run 492, channel 3 model parameters.

	kfwd1	krev1	kfwd2	krev2	kfwd3	krev3	ProA (RU)
Value	4819	0.000104	6677	0.002799	26880000	36.07	17.9
Error (abs)	28.35	1.69E-06	82.5	1.403	346600000	464.9	0.02742
Error (%)	0.588	1.619	1.236	50125.045	1289.435	1288.883	0.153

Run 499, channel 2: Performed at pH 6.5 in PBST, at an IgG concentration of 1.067 µm. RSSE is 4.586.

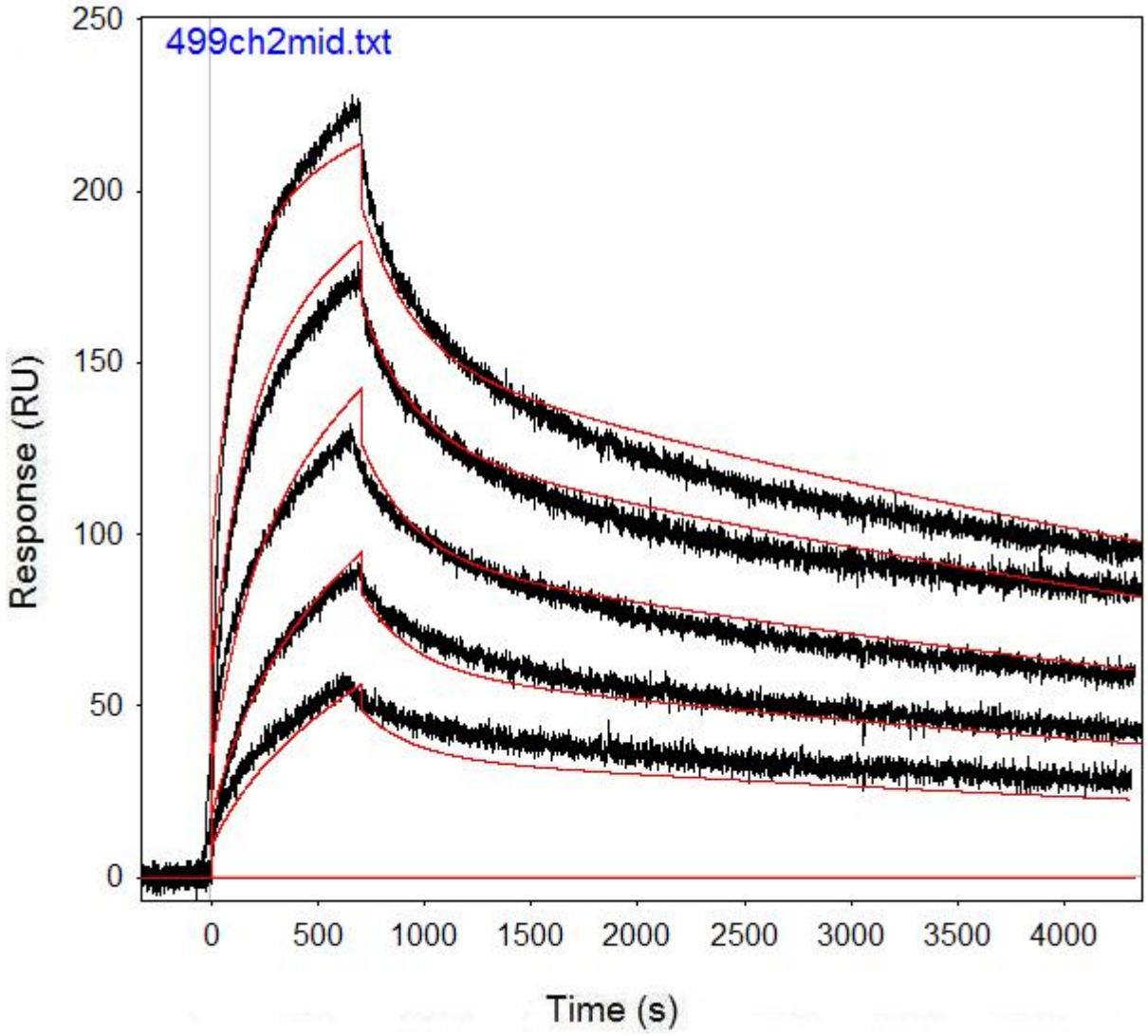

Figure B.37: Run 499, channel 2 model and data graph.

Table B.37: Run 499, channel 2 model parameters.

	kfwd1	krev1	kfwd2	krev2	kfwd3	krev3	ProA (RU)
Value	3853	0.000116	4908	0.003761	1452000000	2434	78.81
Error (abs)	12.67	6.46E-07	52.89	1.403	7.928E+10	132900	0.1453
Error (%)	0.329	0.557	1.078	37303.909	5460.055	5460.148	0.184

Run 499, channel 3: Performed at pH 6.5 in PBST, at an IgG concentration of 1.067 µm. RSSE is 2.444.

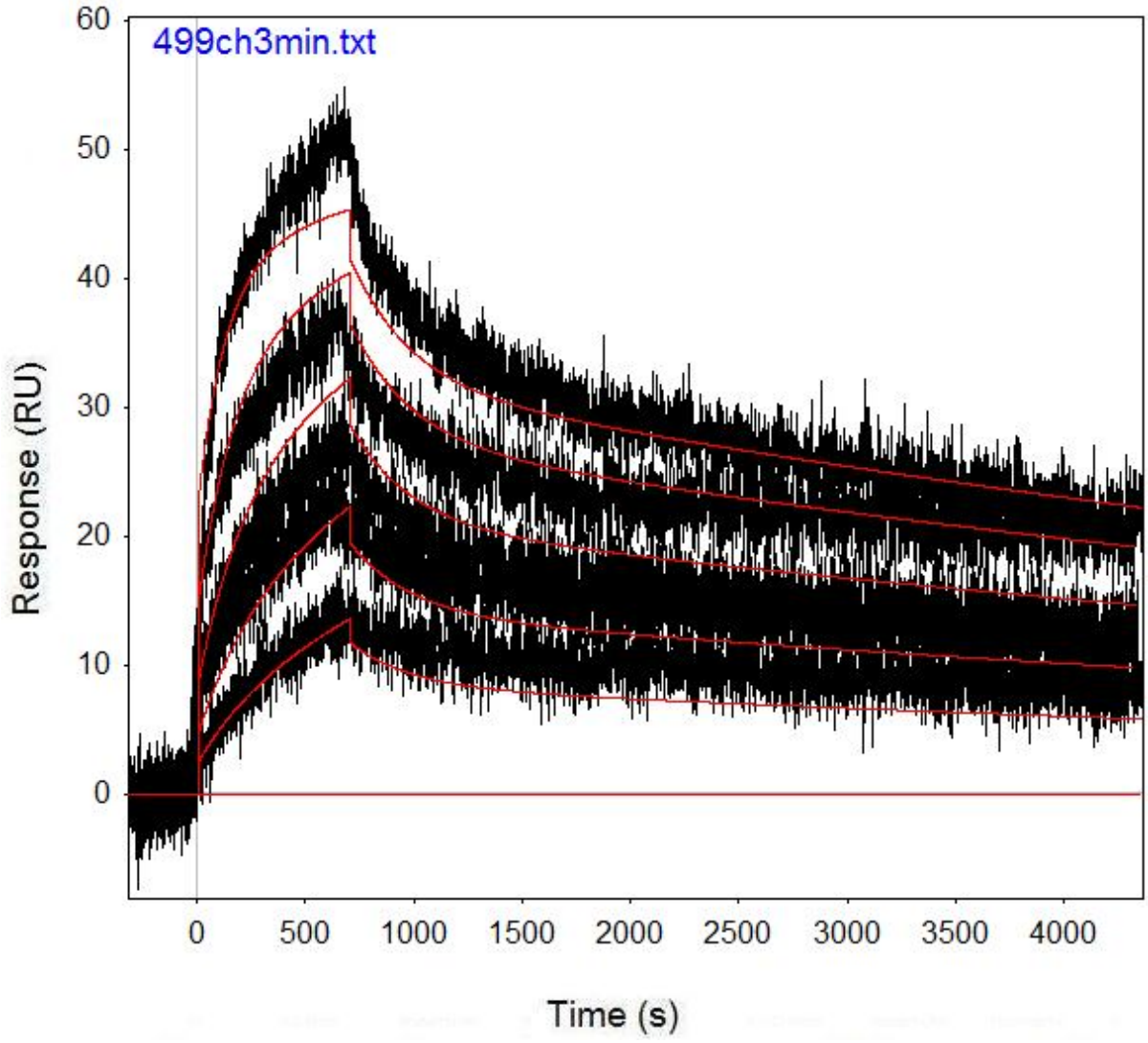

Figure B.38: Run 499, channel 3 model and data graph.

Table B.38: Run 499, channel 3 model parameters.

	kfwd1	krev1	kfwd2	krev2	kfwd3	krev3	ProA (RU)
Value	4536	9.88E-05	5129	0.003657	1599000000	2035	16.65
Error (abs)	27.81	1.49E-06	145.1	1.403	4.504E+11	573300	0.06062
Error (%)	0.613	1.508	2.829	38364.780	28167.605	28171.990	0.364

Run 506, channel 2: Performed at pH 6.5 in PBST, at an IgG concentration of 1.067 µm. RSSE is 3.735.

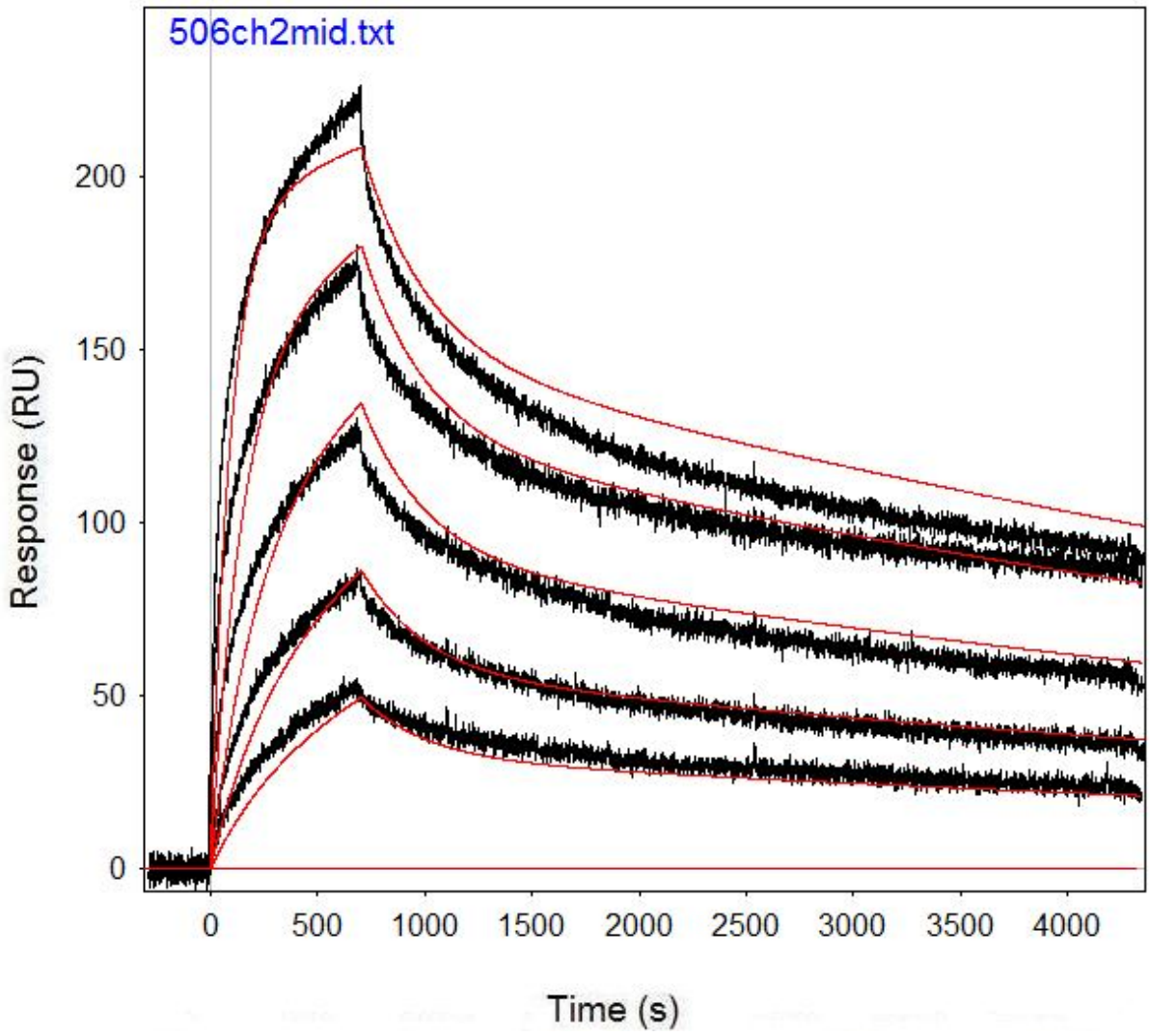

Figure B.39: Run 506, channel 2 model and data graph.

Table B.39: Run 506, channel 2 model parameters.

	kfwd1	krev1	kfwd2	krev2	kfwd3	krev3	ProA (RU)
Value	3466	0.000115	4813	0.003389	214100000	612.6	78.64
Error (abs)	9.007	5.82E-07	30.84	1.403	8454000000	24183	0.09663
Error (%)	0.260	0.508	0.641	41398.643	3948.622	3947.600	0.123

Run 506, channel 3: Performed at pH 6.5 in PBST, at an IgG concentration of 1.067 µm. RSSE is 2.589.

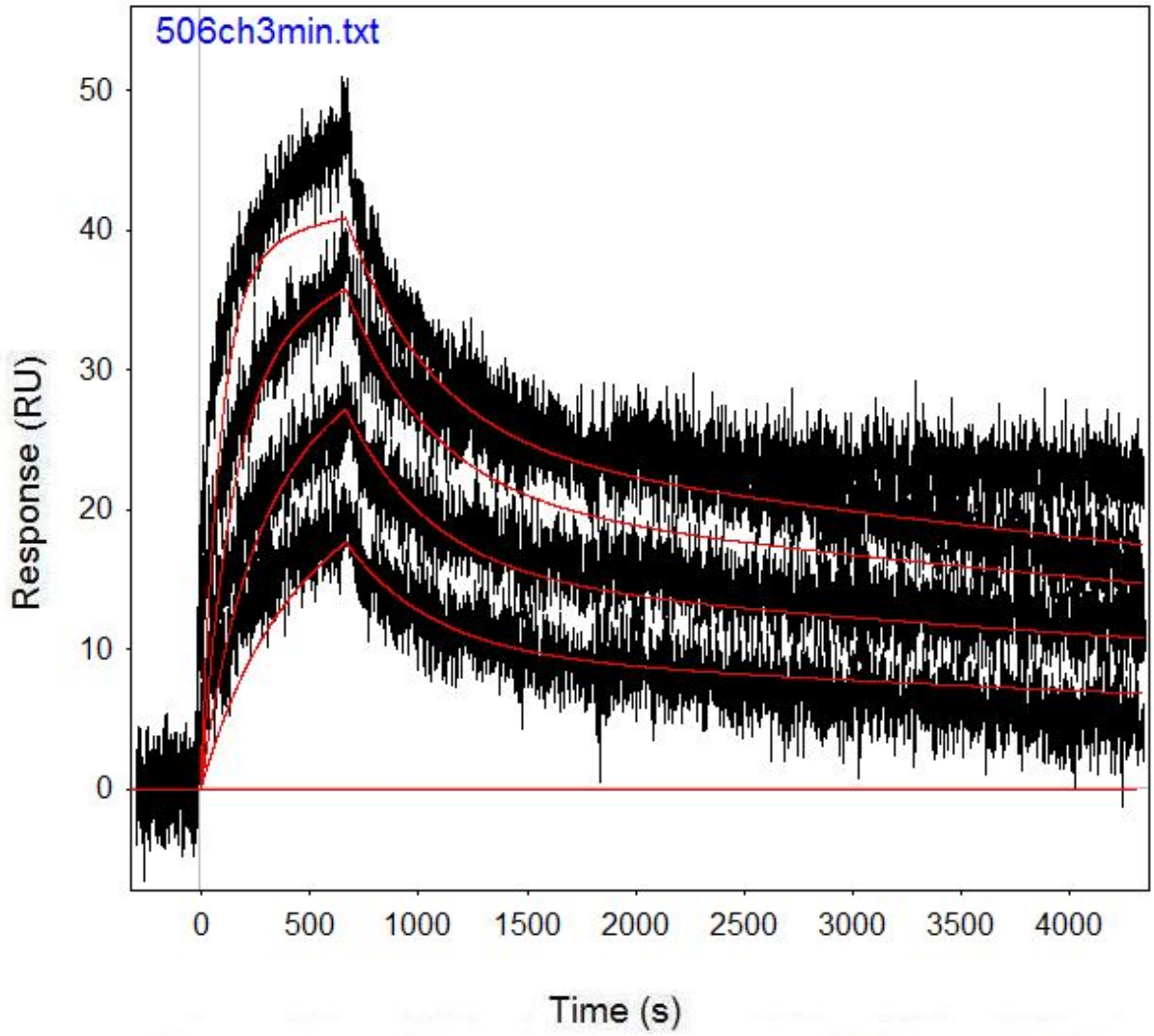

Figure B.40: Run 506, channel 3 model and data graph.

Table B.40: Run 506, channel 3 model parameters.

	kfwd1	krev1	kfwd2	krev2	kfwd3	krev3	ProA (RU)
Value	3442	9.99E-05	4194	0.00273	243600000	425.7	16.86
Error (abs)	34.25	2.37E-06	92.91	1.403	2.497E+10	43633	0.08578
Error (%)	0.995	2.372	2.215	51391.941	10250.411	10249.706	0.509

Run 513, channel 2: Performed at pH 6.5 in PBST, at an IgG concentration of 1.5 µm. RSSE is 7.921.

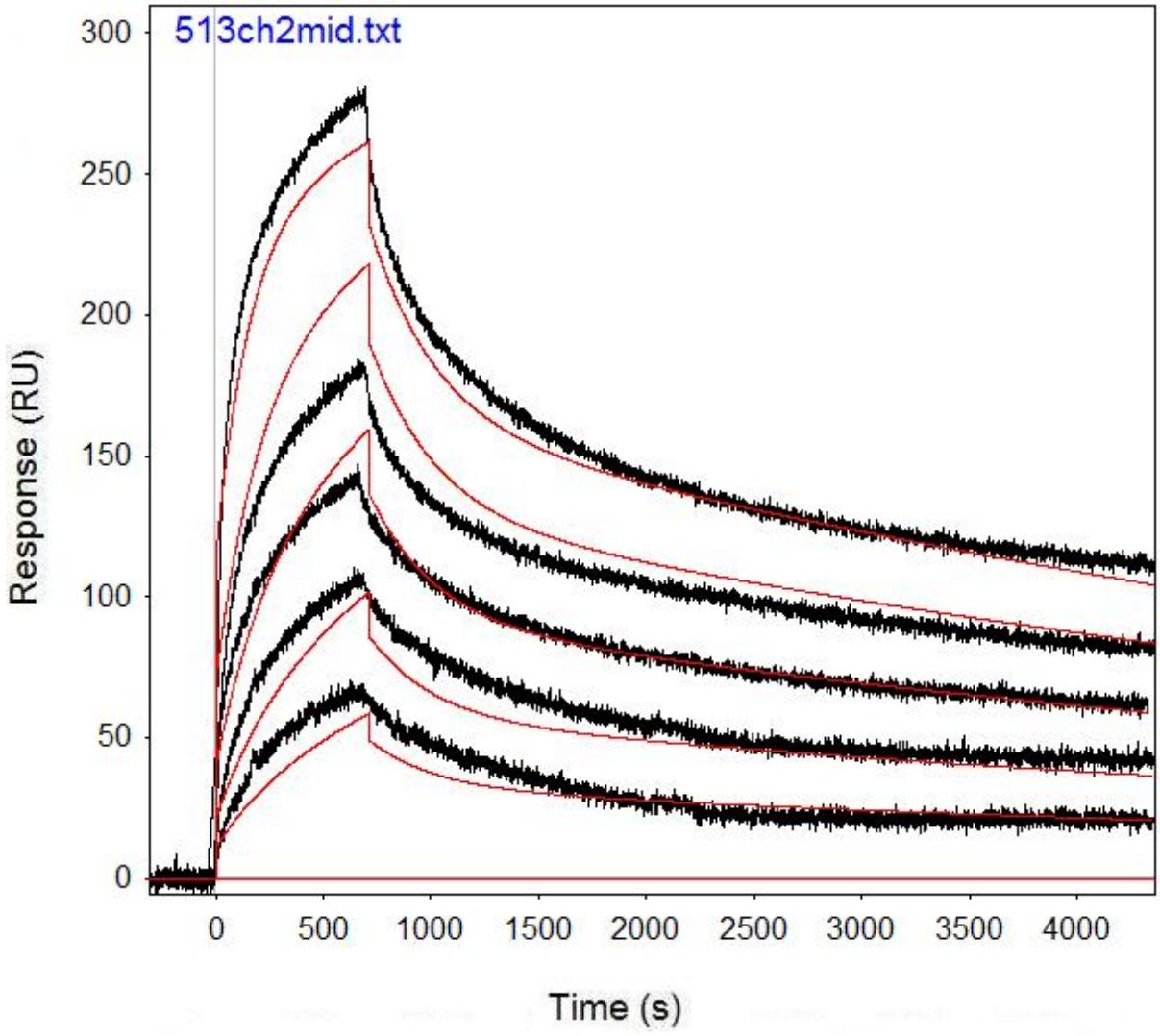

Figure B.41: Run 513, channel 2 model and data graph.

Table B.41: Run 513, channel 2 model parameters.

	kfwd1	krev1	kfwd2	krev2	kfwd3	krev3	ProA (RU)
Value	1867	0.000122	2530	0.003343	201900000	500	103.2
Error (abs)	9.829	1.15E-06	32.59	1.403	8574000000	21233	0.1606
Error (%)	0.526	0.939	1.288	41968.292	4246.657	4246.600	0.156

Run 520, channel 2: Performed at pH 6.5 in PBST, at an IgG concentration of 1.5 µm. RSSE is 9.985.

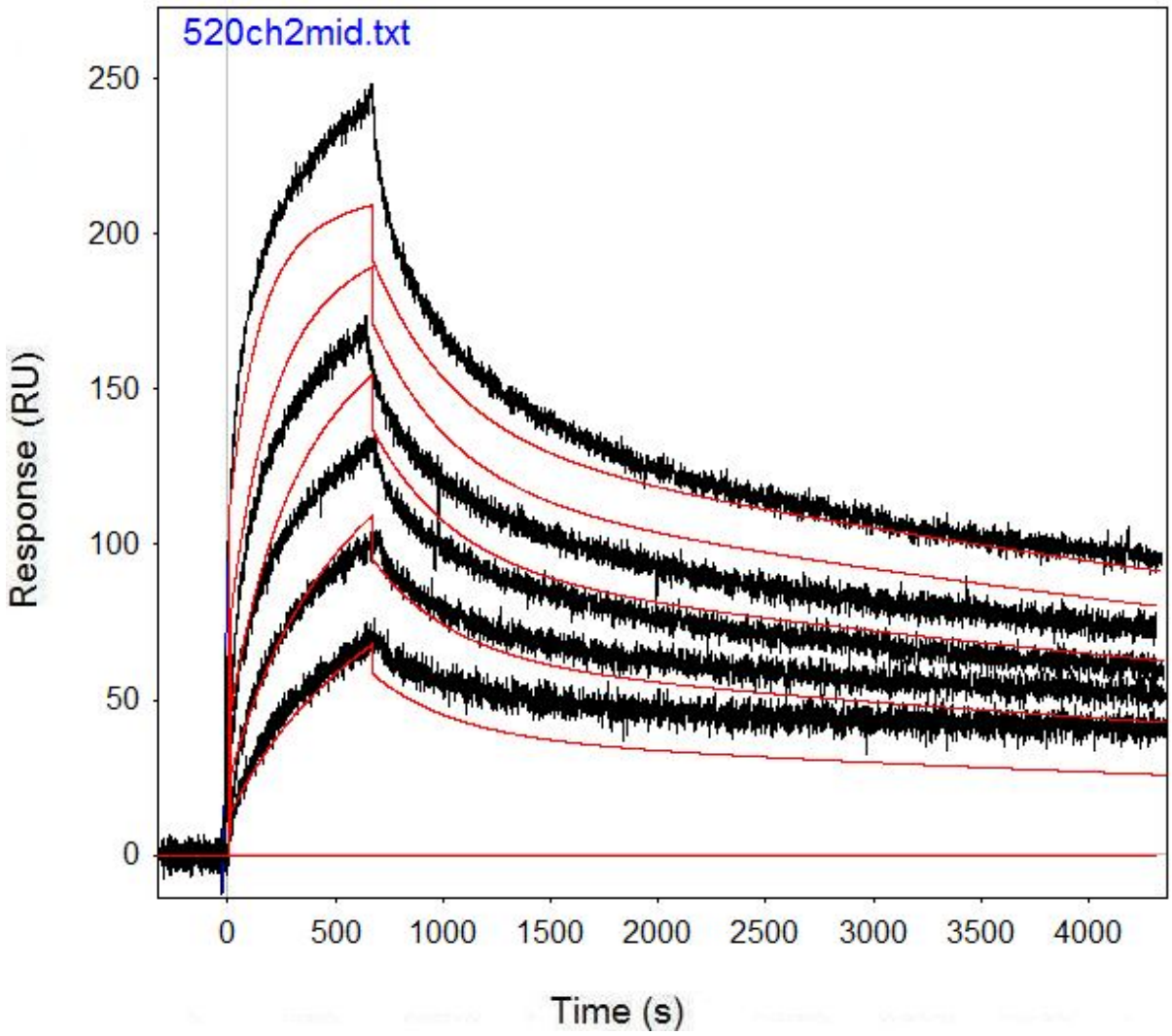

Figure B.42: Run 520, channel 2 model and data graph.

Table B.42: Run 520, channel 2 model parameters.

	kfwd1	krev1	kfwd2	krev2	kfwd3	krev3	ProA (RU)
Value	3477	0.000105	3958	0.002679	273800000	418.4	75.87
Error (abs)	22.66	1.79E-06	56.46	1.403	5910000000	9030	0.1298
Error (%)	0.652	1.705	1.426	52370.287	2158.510	2158.222	0.171

Run 527, channel 2: Performed at pH 6.5 in PBST, at an IgG concentration of 0.5 µm. RSSE is 5.65.

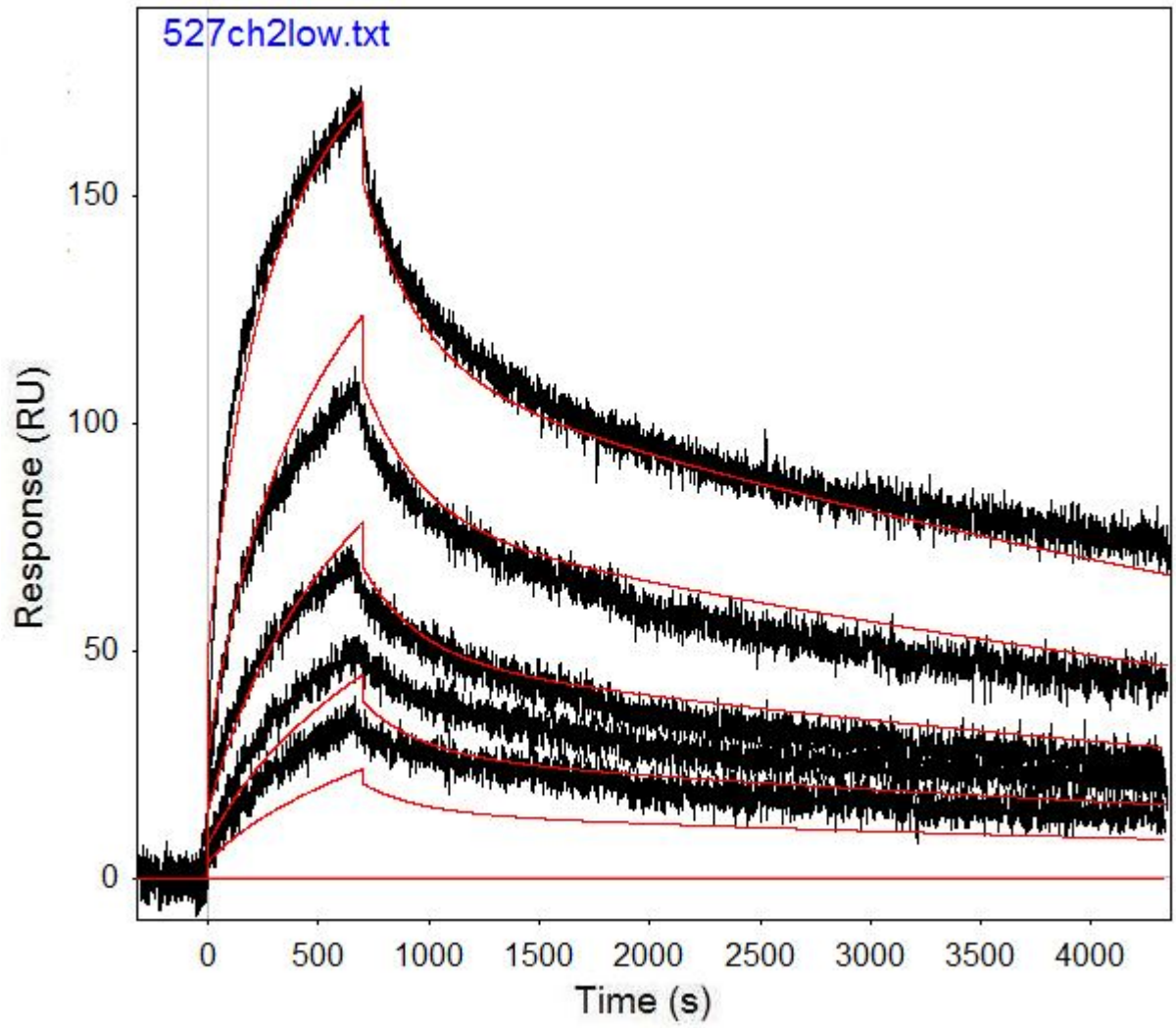

Figure B.43: Run 527, channel 2 model and data graph.

Table B.43: Run 527, channel 2 model parameters.

	kfwd1	krev1	kfwd2	krev2	kfwd3	krev3	ProA (RU)
Value	3038	0.000141	3763	0.003885	100100000	202.9	80.81
Error (abs)	16.64	1.23E-06	68.73	1.403	396100000	802.8	0.2159
Error (%)	0.548	0.873	1.826	36113.256	395.704	395.663	0.267

Run 536, channel 2: Performed at pH 6.5 in PBST, at an IgG concentration of 0.5 µm. RSSE is 6.389.

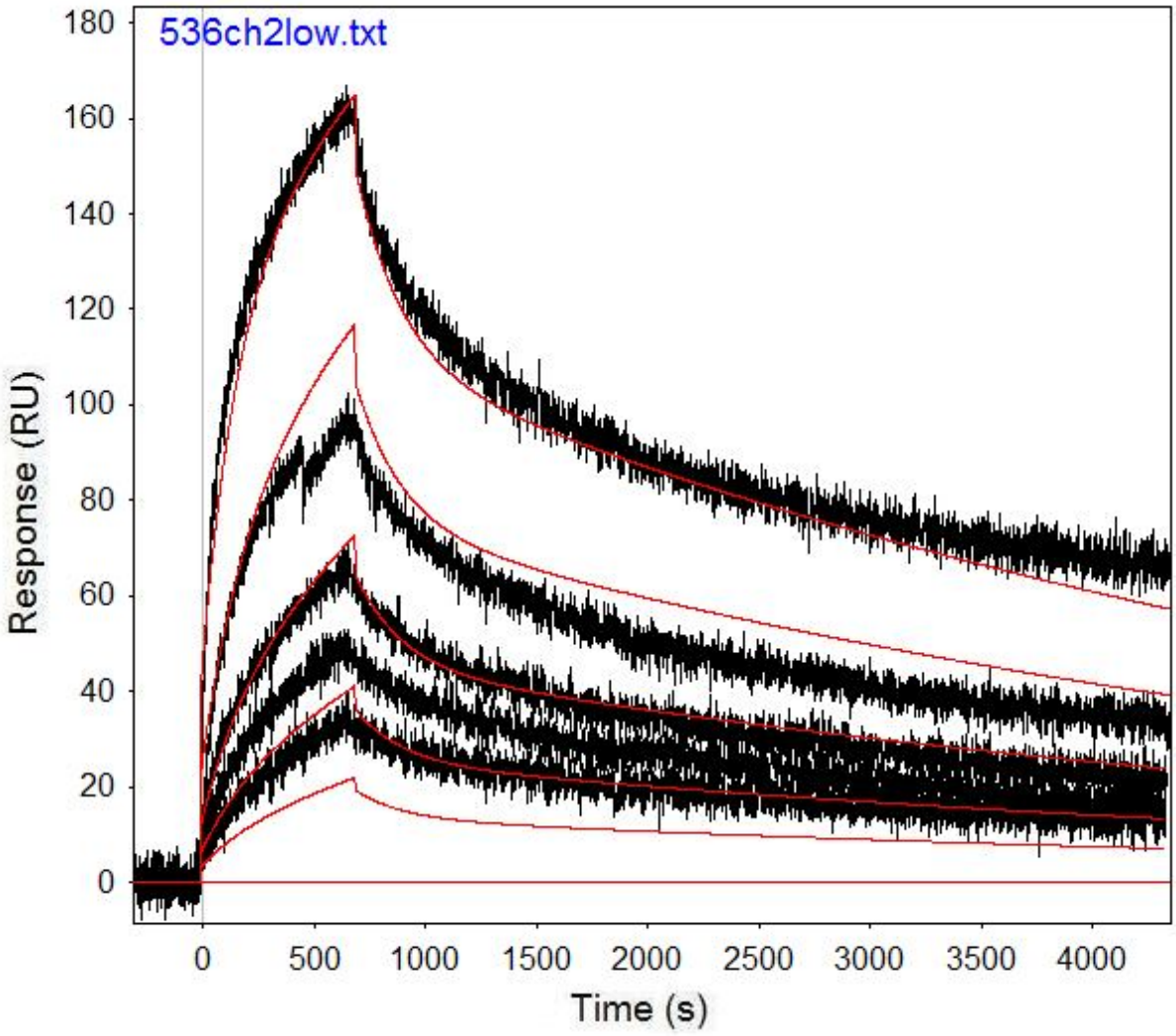

Figure B.44: Run 536, channel 2 model and data graph.

Table B.44: Run 536, channel 2 model parameters.

	kfwd1	krev1	kfwd2	krev2	kfwd3	krev3	ProA (RU)
Value	2828	0.000178	4208	0.004911	107700000	286.5	81.99
Error (abs)	19.57	1.37E-06	113.4	1.403	4180000000	11119	0.3085
Error (%)	0.692	0.771	2.695	28568.520	3881.151	3880.977	0.376

Run 552, channel 3: Performed at pH 6.0 in PBST, at an IgG concentration of 1.067 µm. RSSE is 2.402.

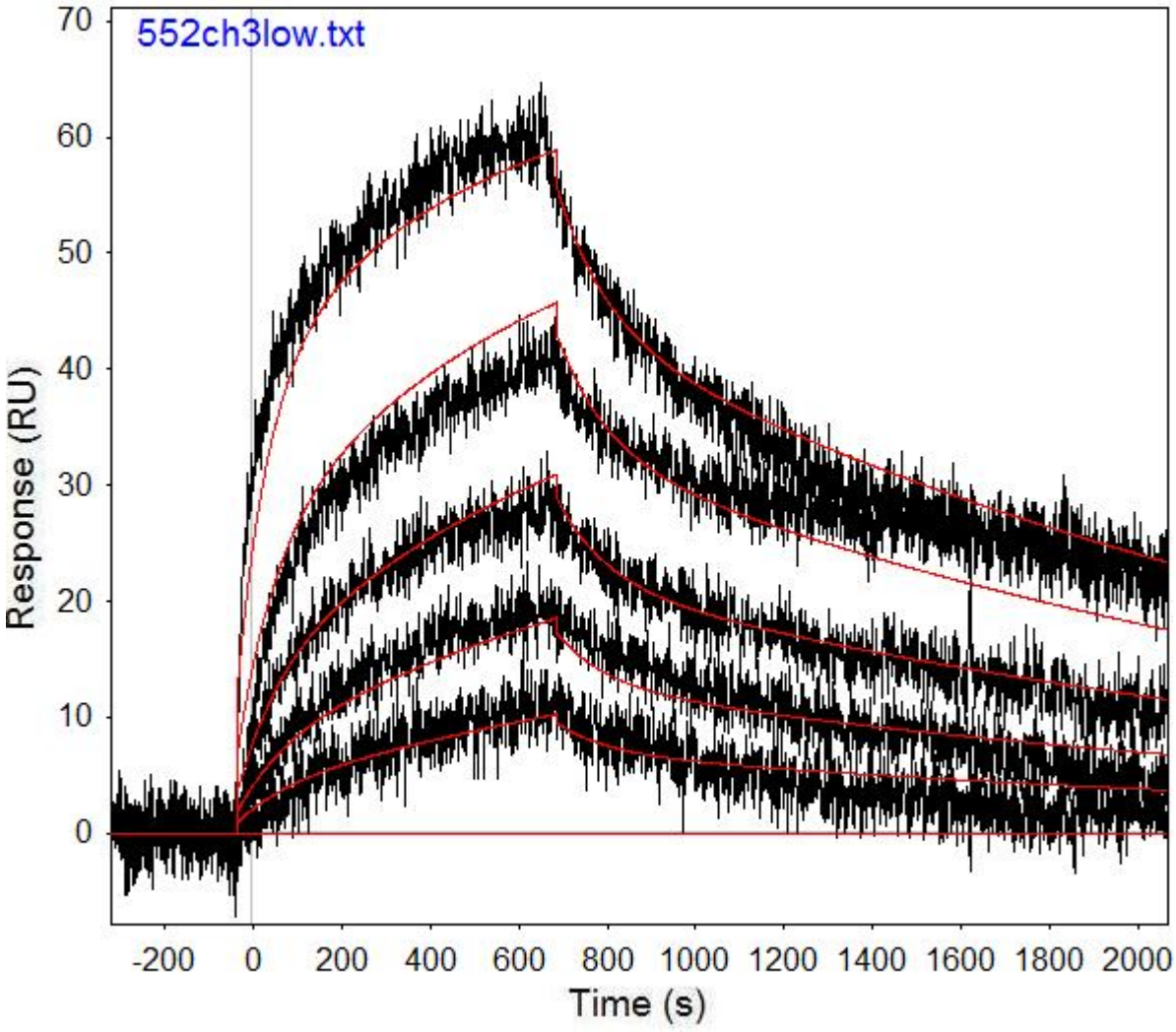

Figure B.45: Run 552, channel 3 model and data graph.

Table B.45: Run 552, channel 3 model parameters.

	kfwd1	krev1	kfwd2	krev2	kfwd3	krev3	ProA (RU)
Value	2445	0.000458	5057	0.009021	105200000	596.4	25.54
Error (abs)	26.76	5.98E-06	179.5	1.403	7818000000	44261	0.1182
Error (%)	1.094	1.305	3.550	15552.599	7431.559	7421.362	0.463

Run 566, channel 3: Performed at pH 6.0 in PBST, at an IgG concentration of 1.067 µm. RSSE is 2.064.

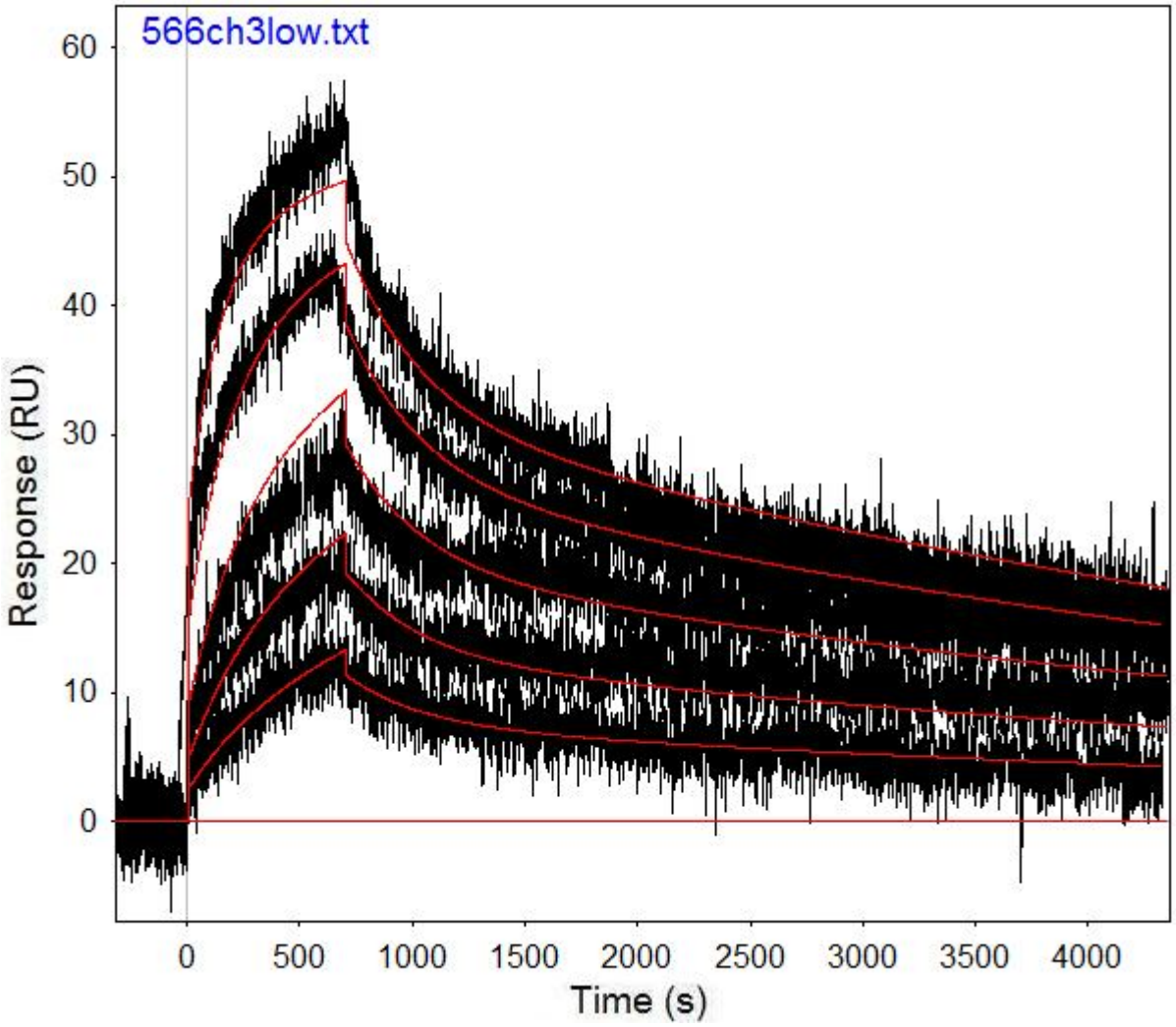

Figure B.46: Run 566, channel 3 model and data graph.

Table B.46: Run 566, channel 3 model parameters.

	kfwd1	krev1	kfwd2	krev2	kfwd3	krev3	ProA (RU)
Value	3577	0.000155	4356	0.003034	130300000	186.7	18.7
Error (abs)	22.23	1.69E-06	67.82	1.403	3471000000	4972	0.03498
Error (%)	0.621	1.092	1.557	46242.584	2663.853	2663.096	0.187

Run 566, channel 5: Performed at pH 6.0 in PBST, at an IgG concentration of 1.067 µm. RSSE is 9.70.

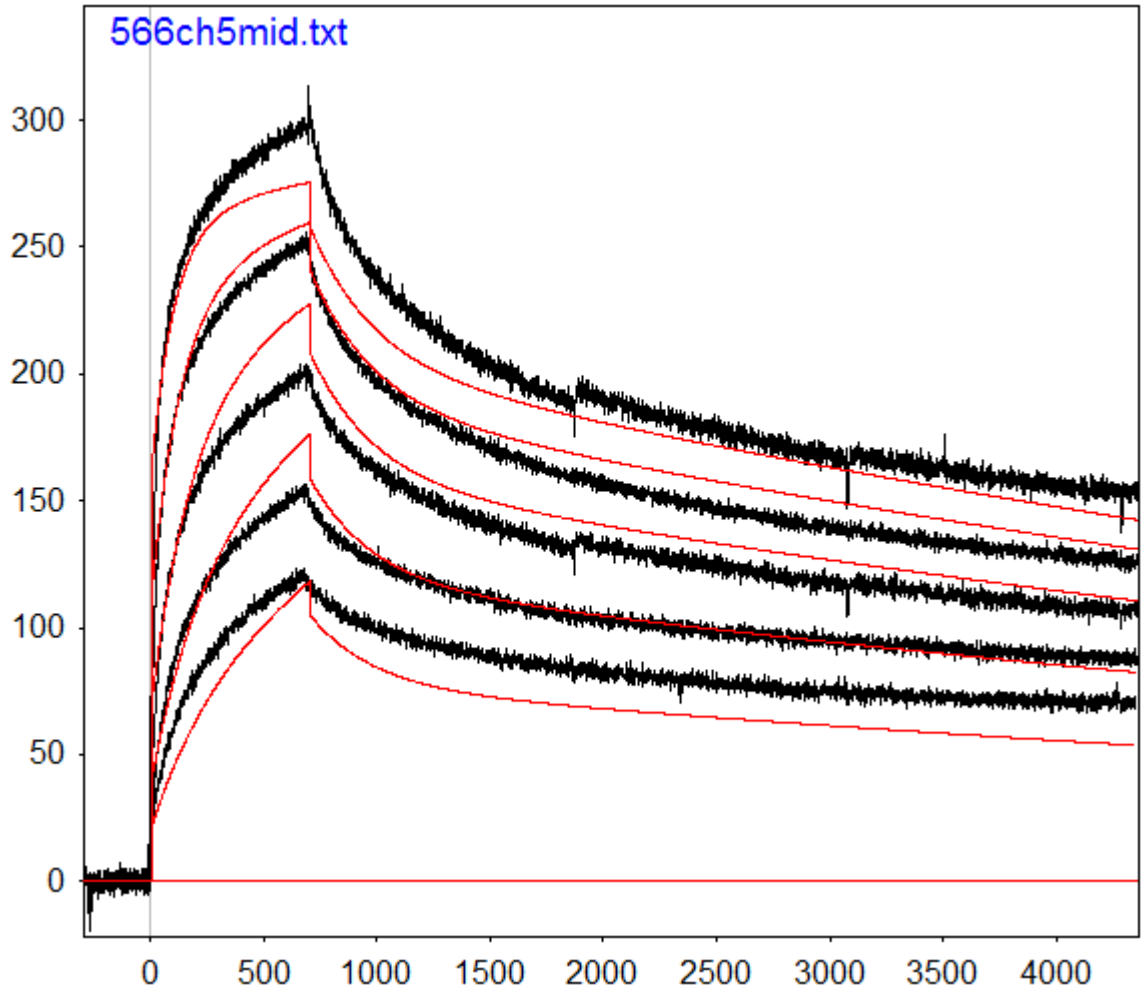

Figure B.47: Run 566, channel 5 model and data graph.

Table B.47: Run 566, channel 5 model parameters.

	kfwd1	krev1	kfwd2	krev2	kfwd3	krev3	ProA (RU)
Value	8209	0.0001	8528	0.003672	202700000	166.5	96.48
Error (abs)	36.48	8.21E-07	142.2	1.403	1897000000	1558	0.09867
Error (%)	0.444	0.820	1.667	38208.061	935.866	935.736	0.102

Run 573, channel 5: Performed at pH 6.0 in PBST, at an IgG concentration of 1.067 µm. RSSE is 9.056.

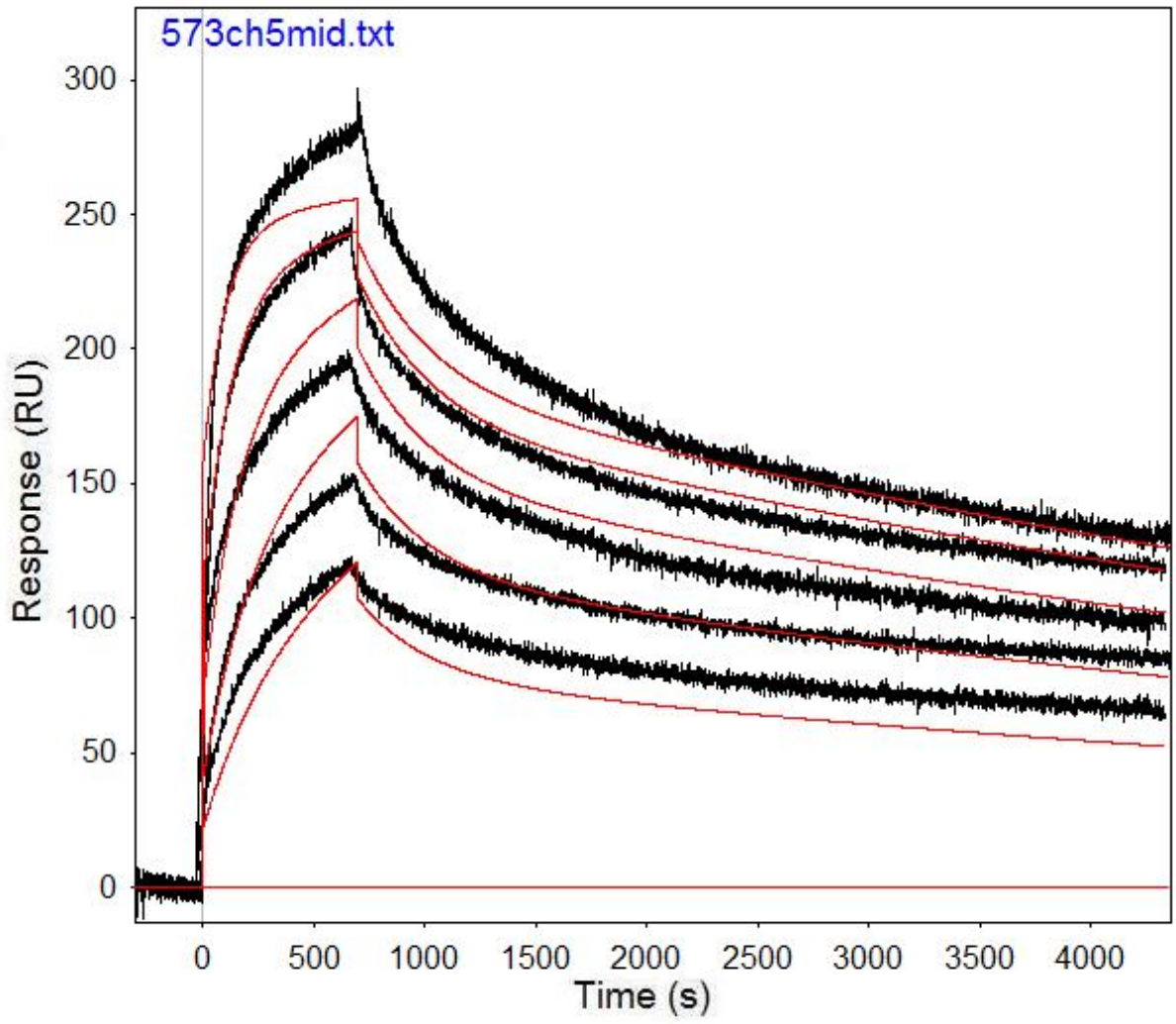

Figure B.48: Run 573, channel 5 model and data graph.

Table B.48: Run 573, channel 5 model parameters.

	kfwd1	krev1	kfwd2	krev2	kfwd3	krev3	ProA (RU)
Value	9545	0.000109	9359	0.003171	131700000	97.85	88.78
Error (abs)	35.01	9.15E-07	121.9	1.403	1161000000	862.7	0.08539
Error (%)	0.367	0.837	1.302	44244.718	881.549	881.656	0.096

Run 581, channel 2: Performed at pH 6.0 in PBST, at an IgG concentration of 1.067 µm. RSSE is 8.364.

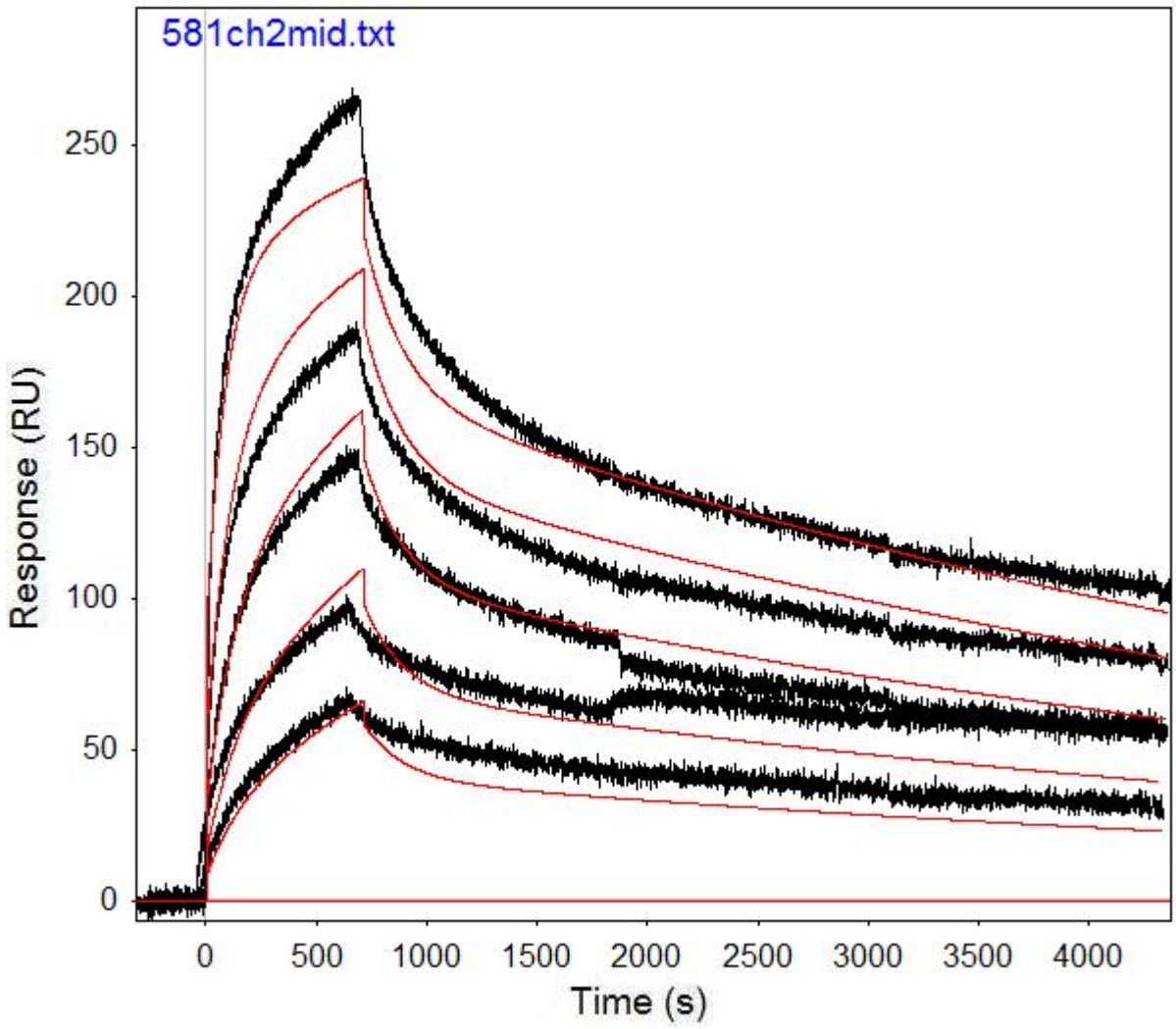

Figure B.49: Run 581, channel 2 model and data graph.

Table B.49: Run 581, channel 2 model parameters.

	kfwd1	krev1	kfwd2	krev2	kfwd3	krev3	ProA (RU)
Value	4047	0.000155	7455	0.005712	1193000000	2253	90.02
Error (abs)	16.75	8.96E-07	139.2	1.403	9.209E+10	173900	0.1512
Error (%)	0.414	0.578	1.867	24562.325	7719.195	7718.597	0.168

Run 581, channel 3: Performed at pH 6.0 in PBST, at an IgG concentration of 1.067 µm. RSSE is 3.668.

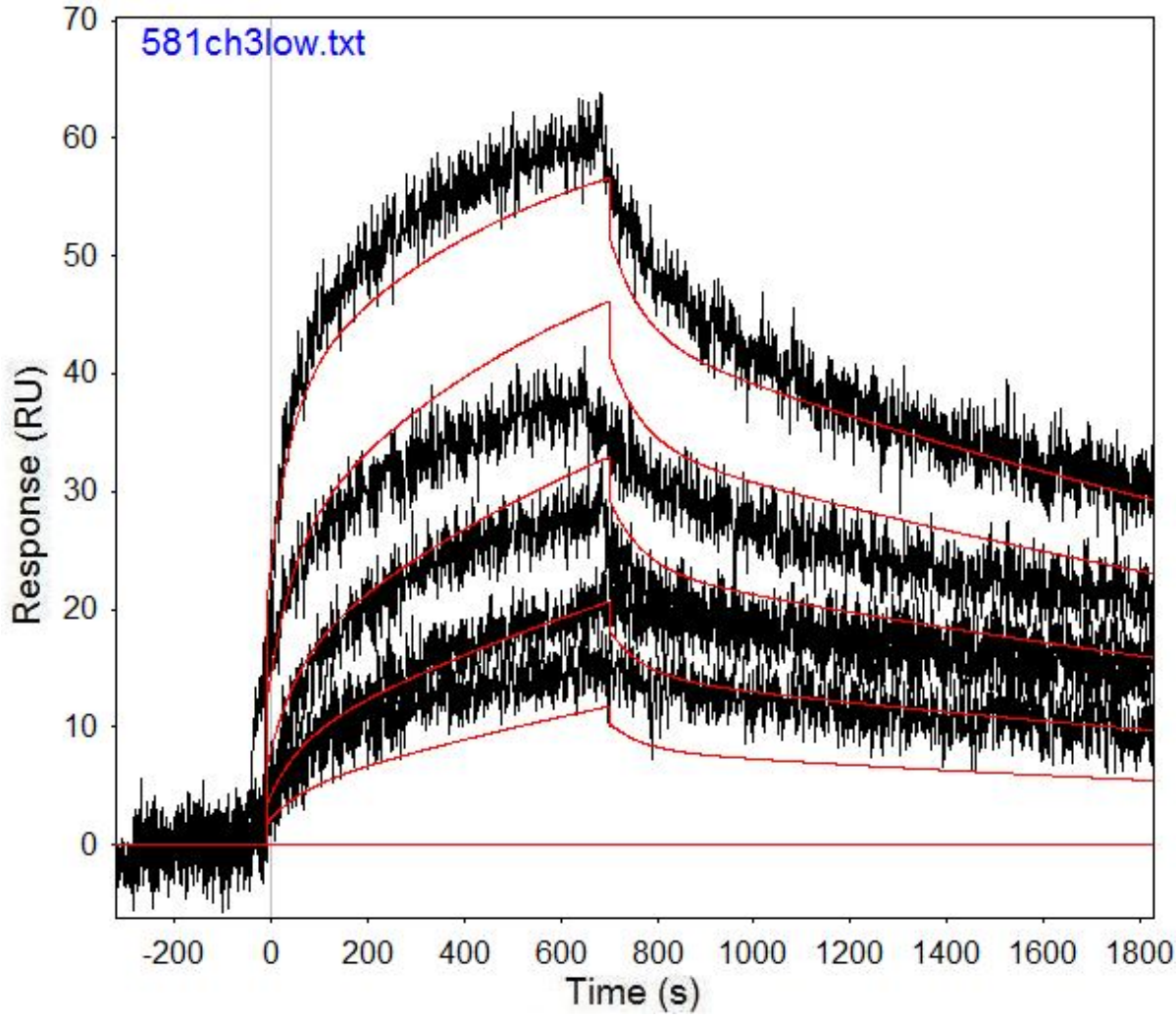

Figure B.50: Run 581, channel 3 model and data graph.

Table B.50: Run 581, channel 3 model parameters.

	kfwd1	krev1	kfwd2	krev2	kfwd3	krev3	ProA (RU)
Value	3149	0.000347	8654	0.01506	1045000000	2664	23.01
Error (abs)	42.46	8.48E-06	790.8	1.403	1.564E+12	3987000	0.1192
Error (%)	1.348	2.445	9.138	9316.069	149665.072	149662.162	0.518

Run 597, channel 5: Performed at pH 6.0 in PBST, at an IgG concentration of 1.067 µm. RSSE is 8.55.

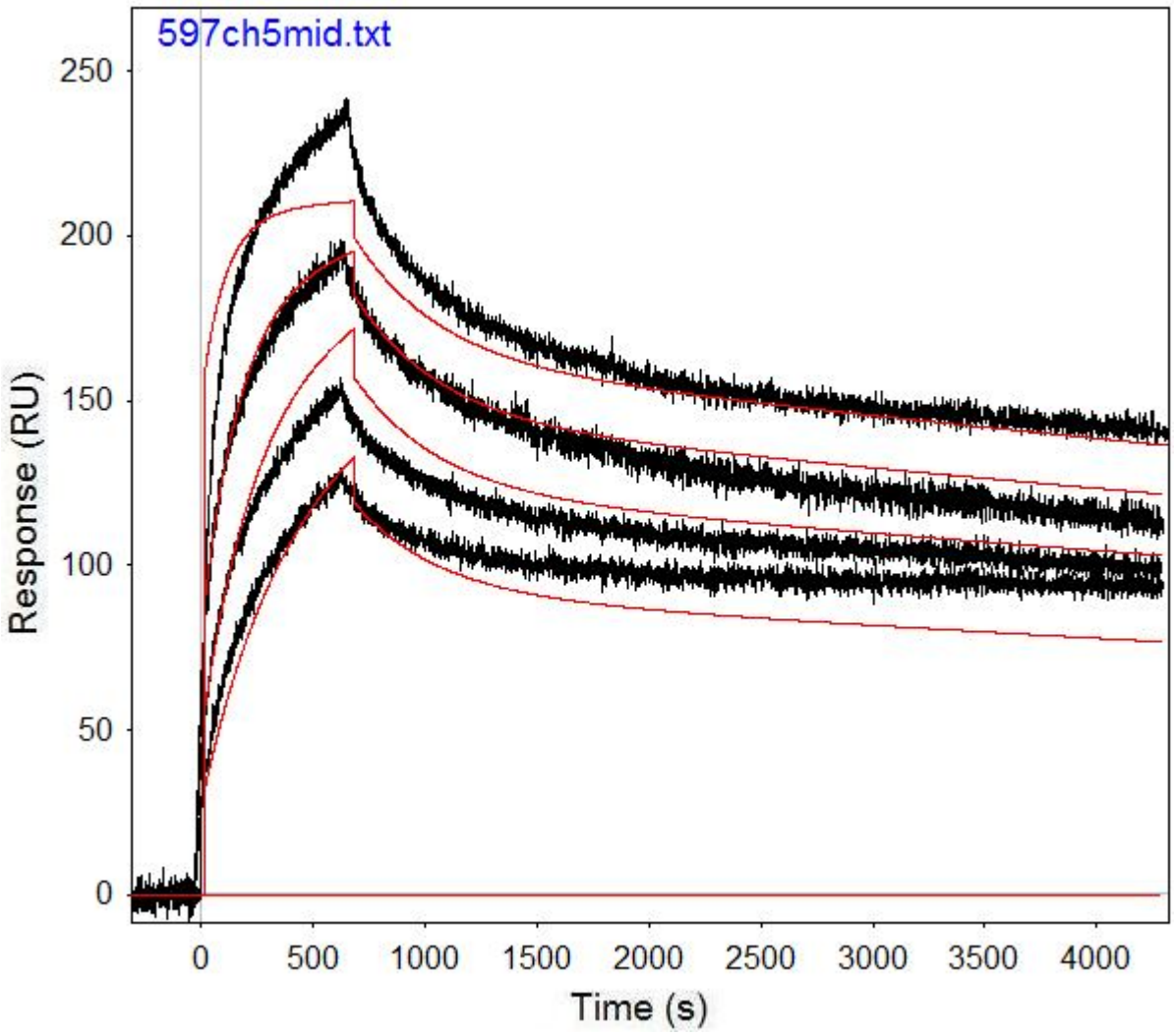

Figure B.51: Run 597, channel 5 model and data graph.

Table B.51: Run 597, channel 5 model parameters.

	kfwd1	krev1	kfwd2	krev2	kfwd3	krev3	ProA (RU)
Value	17379	4.88E-05	12451	0.0027	1208000000	482.1	71.54
Error (abs)	104.5	1.09E-06	234.8	1.403	1.165E+11	46507	0.09143
Error (%)	0.601	2.224	1.886	51962.963	9644.040	9646.754	0.128

Run 604, channel 2: Performed at pH 6.0 in PBST, at an IgG concentration of 1.067 µm. RSSE is 5.641.

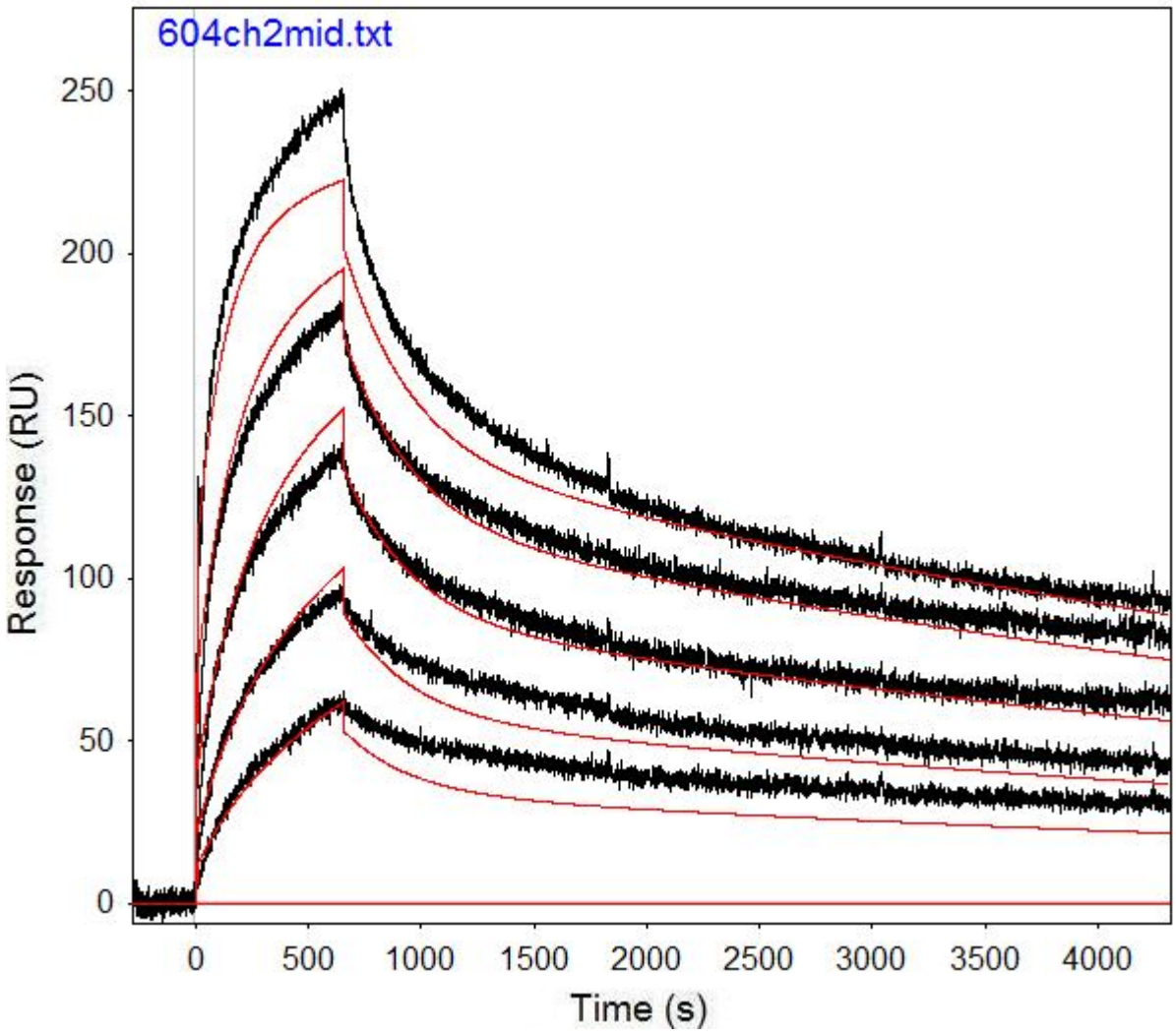

Figure B.52: Run 604, channel 2 model and data graph.

Table B.52: Run 604, channel 2 model parameters.

	kfwd1	krev1	kfwd2	krev2	kfwd3	krev3	ProA (RU)
Value	4271	0.000122	5028	0.002961	589700000	820.3	83.22
Error (abs)	17.13	9.41E-07	43.79	1.403	2.577E+10	35840	0.1104
Error (%)	0.401	0.772	0.871	47382.641	4370.019	4369.133	0.133

Run 604, channel 3: Performed at pH 6.0 in PBST, at an IgG concentration of 1.067 µm. RSSE is 2.48.

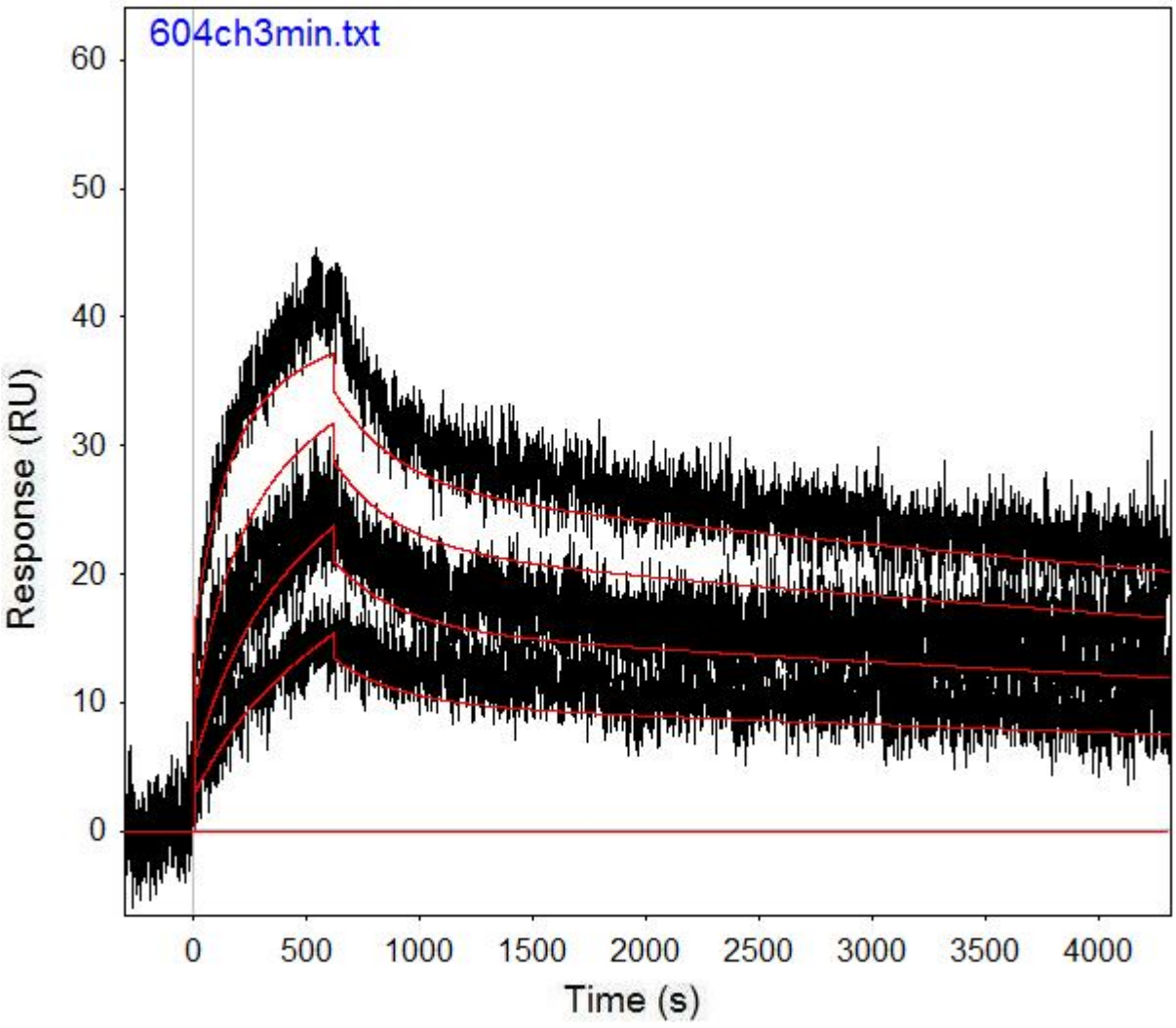

Figure B.53: Run 604, channel 3 model and data graph.

Table B.53: Run 604, channel 3 model parameters.

	kfwd1	krev1	kfwd2	krev2	kfwd3	krev3	ProA (RU)
Value	7927	7.52E-05	6818	0.003422	817600000	770.1	14.1
Error (abs)	90.23	1.82E-06	232.9	1.403	1.744E+11	164200	0.04588
Error (%)	1.138	2.425	3.416	40999.416	21330.724	21321.906	0.325

Run 611, channel 3: Performed at pH 6.0 in PBST, at an IgG concentration of 1.5 µm. RSSE is 2.364.

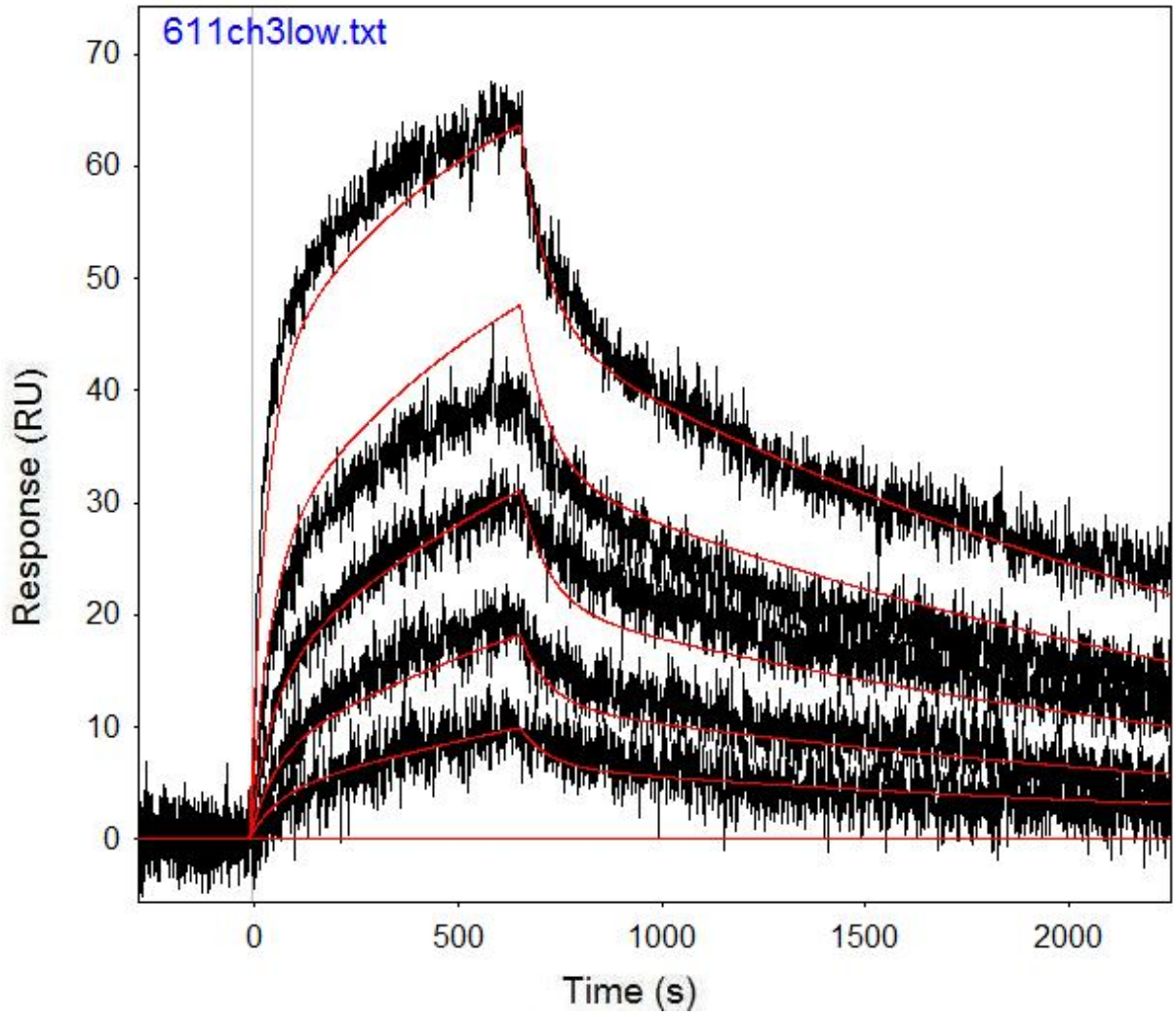

Figure B.54: Run 611, channel 3 model and data graph.

Table B.54: Run 611, channel 3 model parameters.

	kfwd1	krev1	kfwd2	krev2	kfwd3	krev3	ProA (RU)
Value	1481	0.000458	6832	0.01467			29.45
Error (abs)	11.57	3.72E-06	142.8	1.403			0.09733
Error (%)	0.781	0.812	2.090	9563.736			0.330

Run 611, channel 5: Performed at pH 6.0 in PBST, at an IgG concentration of 1.5 µm. RSSE is 9.692.

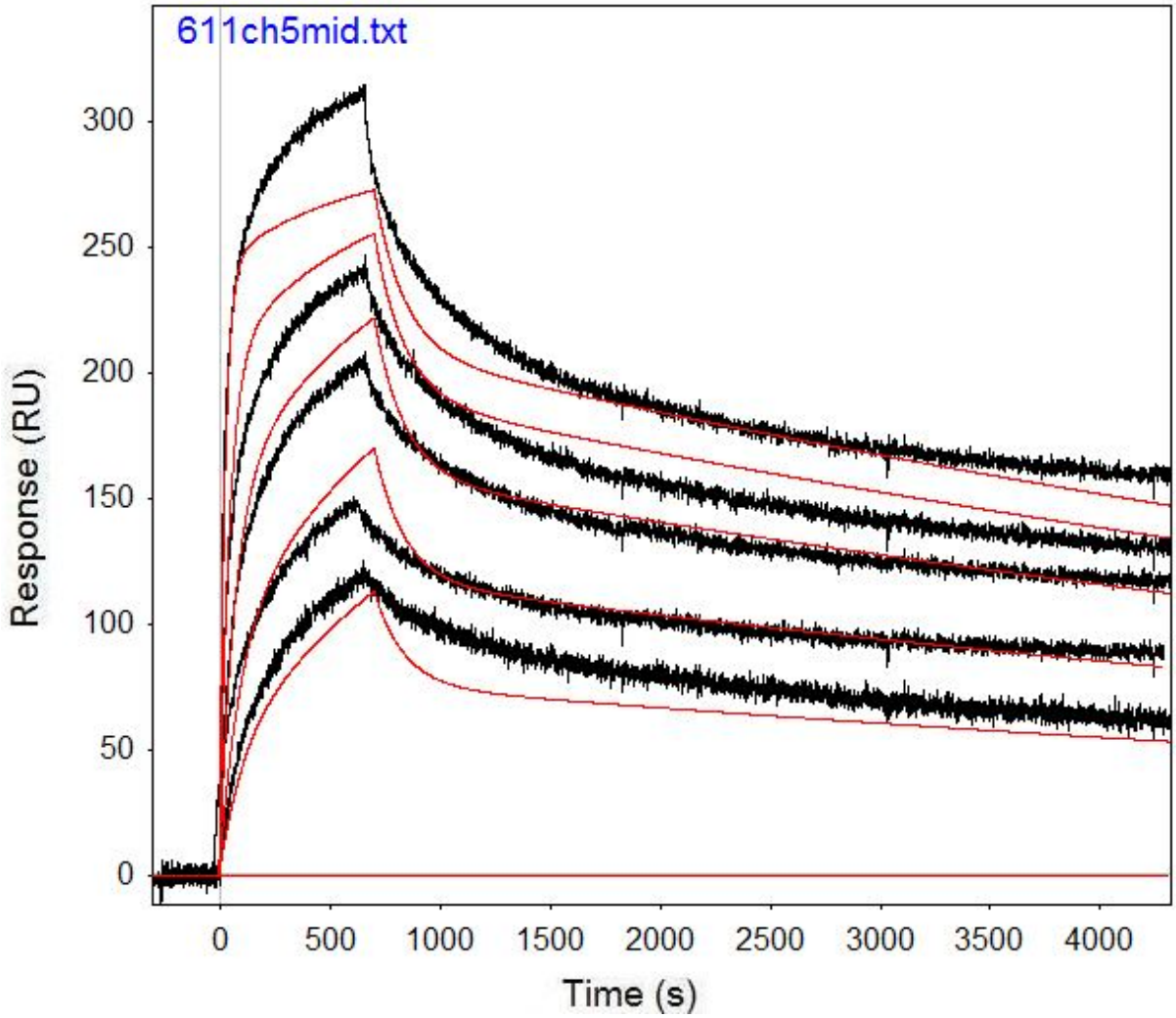

Figure B.55: Run 611, channel 5 model and data graph.

Table B.55: Run 611, channel 5 model parameters.

	kfwd1	krev1	kfwd2	krev2	kfwd3	krev3	ProA (RU)
Value	5612	9.68E-05	15998	0.007418			96.18
Error (abs)	18.81	6.06E-07	187.5	1.403			0.09853
Error (%)	0.335	0.626	1.172	18913.454			0.102

Run 633, channel 2: Performed at pH 6.0 in PBST, at an IgG concentration of 0.5 µm. RSSE is 5.076.

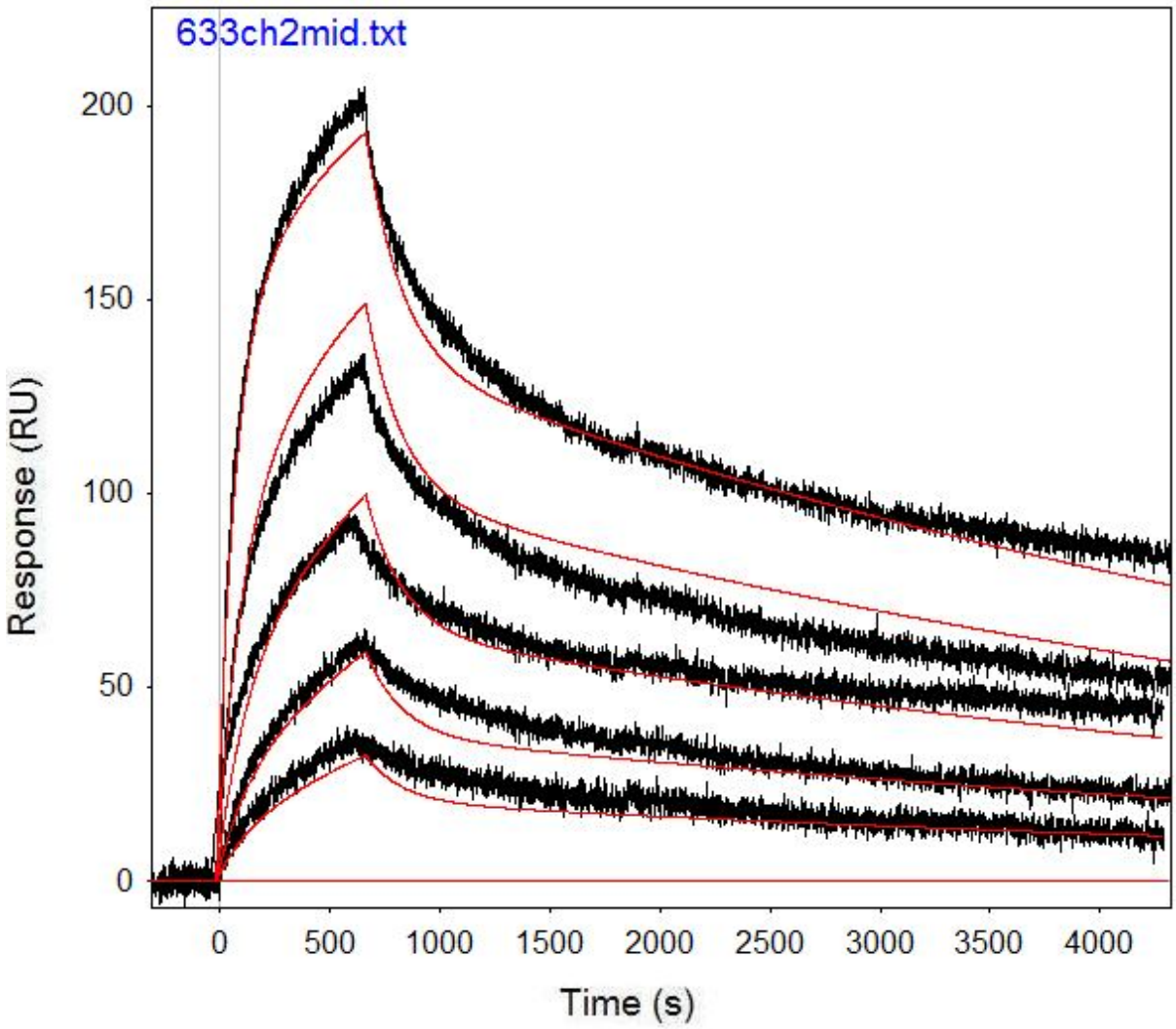

Figure B.56: Run 633, channel 2 model and data graph.

Table B.56: Run 633, channel 2 model parameters.

	kfwd1	krev1	kfwd2	krev2	kfwd3	krev3	ProA (RU)
Value	4439	0.000155	10734	0.006111			83.08
Error (abs)	17.02	7.29E-07	102.8	1.403			0.1398
Error (%)	0.383	0.469	0.958	22958.599			0.168

Run 640, channel 2: Performed at pH 6.0 in PBST, at an IgG concentration of 0.5 µm. RSSE is 6.002.

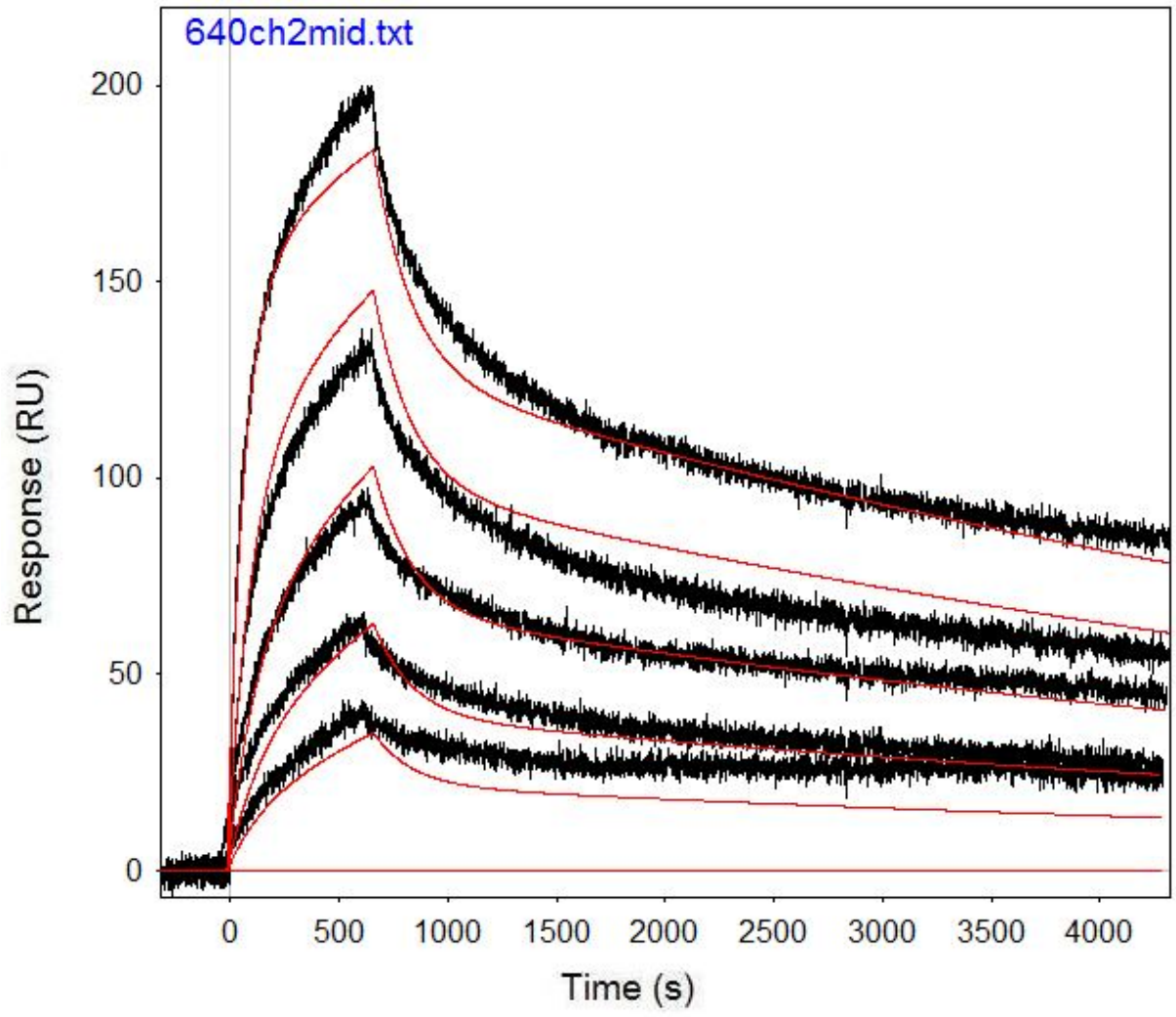

Figure B.57: Run 640, channel 2 model and data graph.

Table B.57: Run 640, channel 2 model parameters.

	kfwd1	krev1	kfwd2	krev2	kfwd3	krev3	ProA (RU)
Value	5318	0.000132	12785	0.005704			75.08
Error (abs)	23.48	8.64E-07	139.8	1.403			0.1345
Error (%)	0.442	0.655	1.093	24596.774			0.179

Run 7, channel 5: Performed at pH 6.0 in Sodium Acetate, at an IgG concentration of 1.067 µm. RSSE is 6.577.

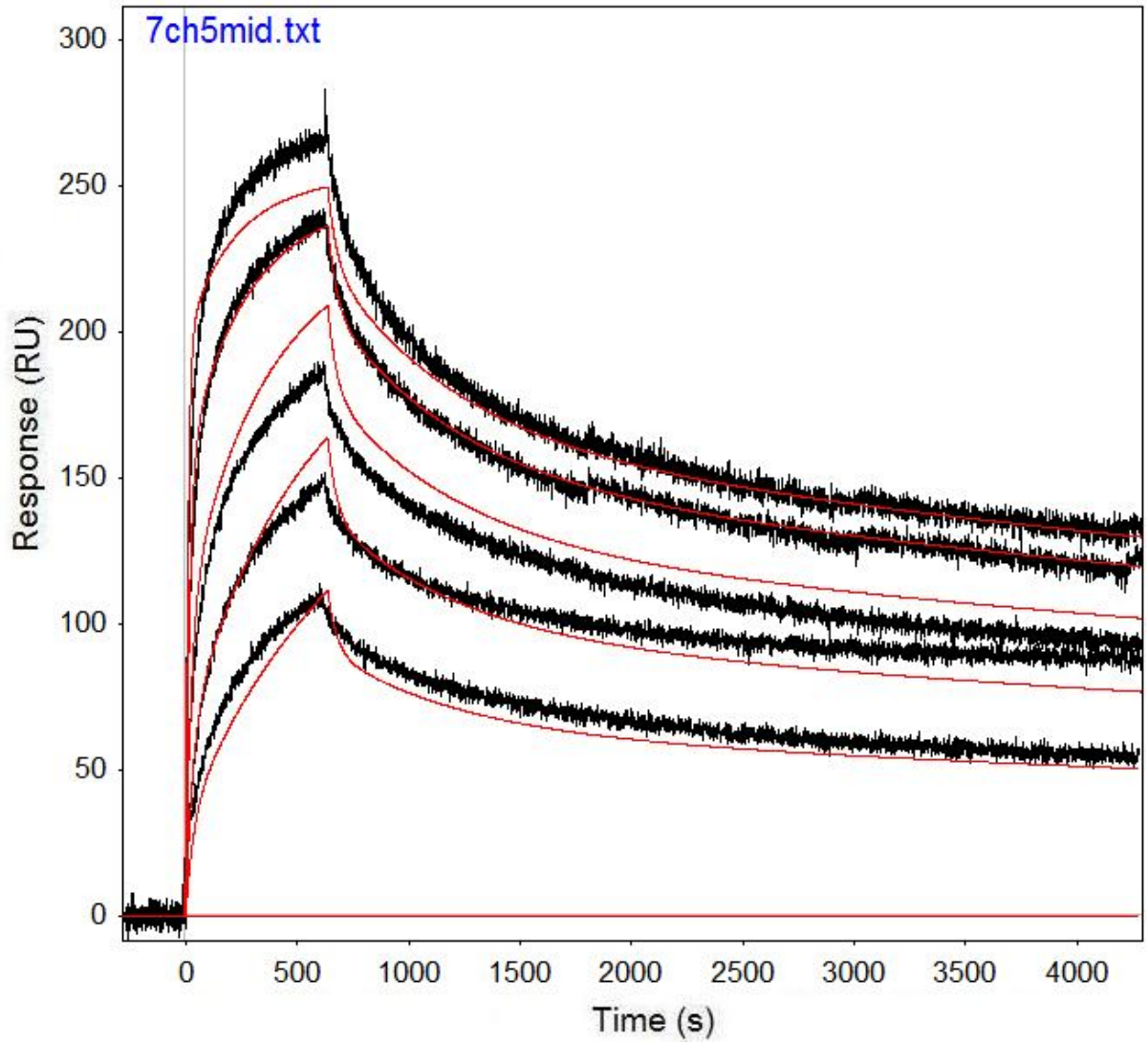

Figure B.58: Run 7, channel 5 model and data graph.

Table B.58: Run 7, channel 5 model parameters.

	kfwd1	krev1	kfwd2	krev2	kfwd3	krev3	ProA (RU)
Value	6114	0.001705	8133	5.99E-05	50407	0.02506	87
Error (abs)	63.77	3.507E-05	44.67	1.51E-06	1000	0.000582	0.06757
Error (%)	1.043	2.057	0.549	2.516	1.984	2.322	0.078

Run 16, channel 2: Performed at pH 6.0 in Sodium Acetate, at an IgG concentration of 1.067 µm. RSSE is 7.487.

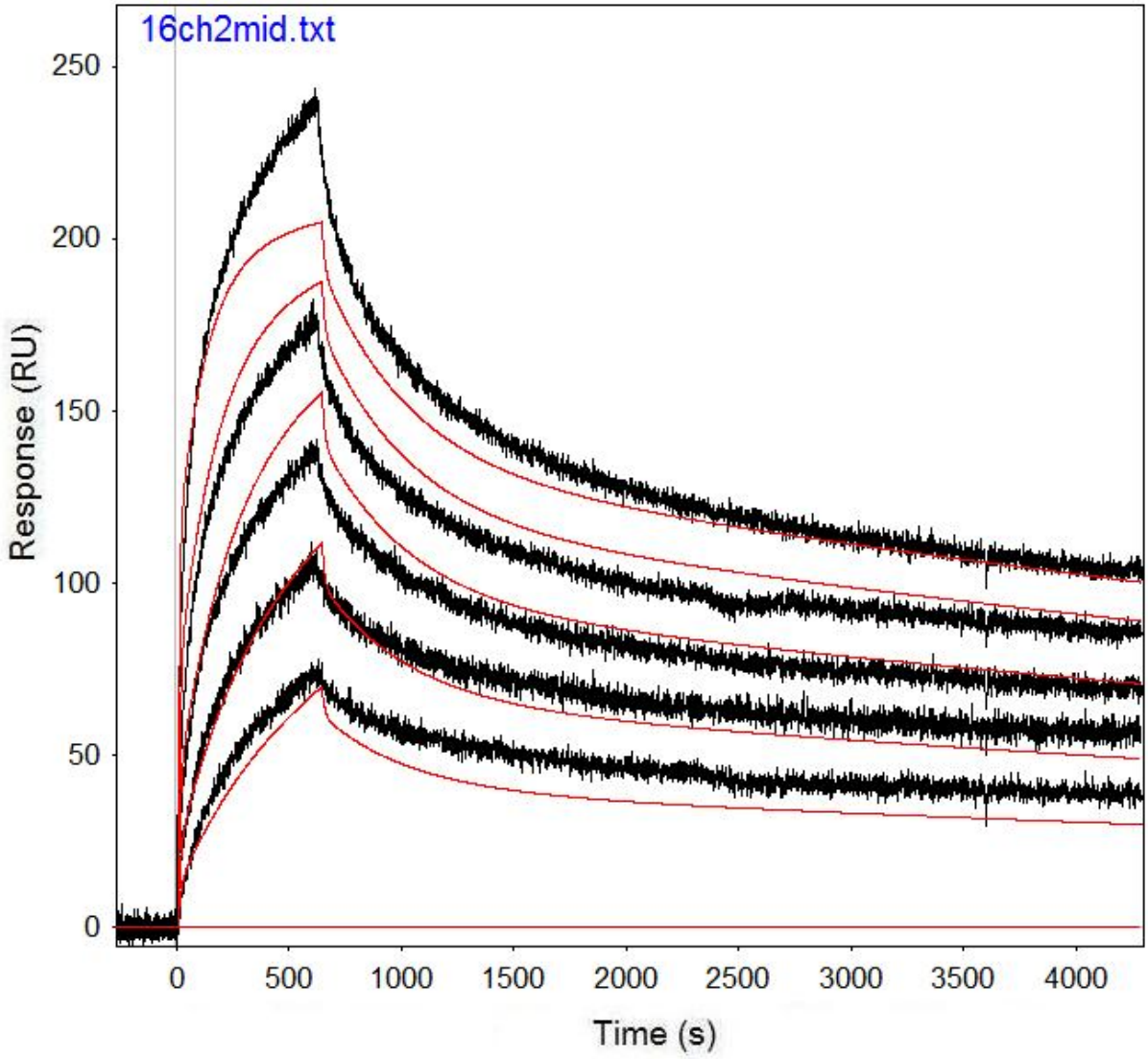

Figure B.59: Run 16, channel 2 model and data graph.

Table B.59: Run 16, channel 2 model parameters.

	kfwd1	krev1	kfwd2	krev2	kfwd3	krev3	ProA (RU)
Value	6172	0.002596	5540	8.01E-05	73823	0.08835	73.35
Error (abs)	72.91	4.317E-05	26.93	1.32E-06	4452	0.005486	0.09246
Error (%)	1.181	1.663	0.486	1.648	6.031	6.209	0.126

Run 16, channel 3: Performed at pH 6.0 in Sodium Acetate, at an IgG concentration of 1.067 µm. RSSE is 1.917.

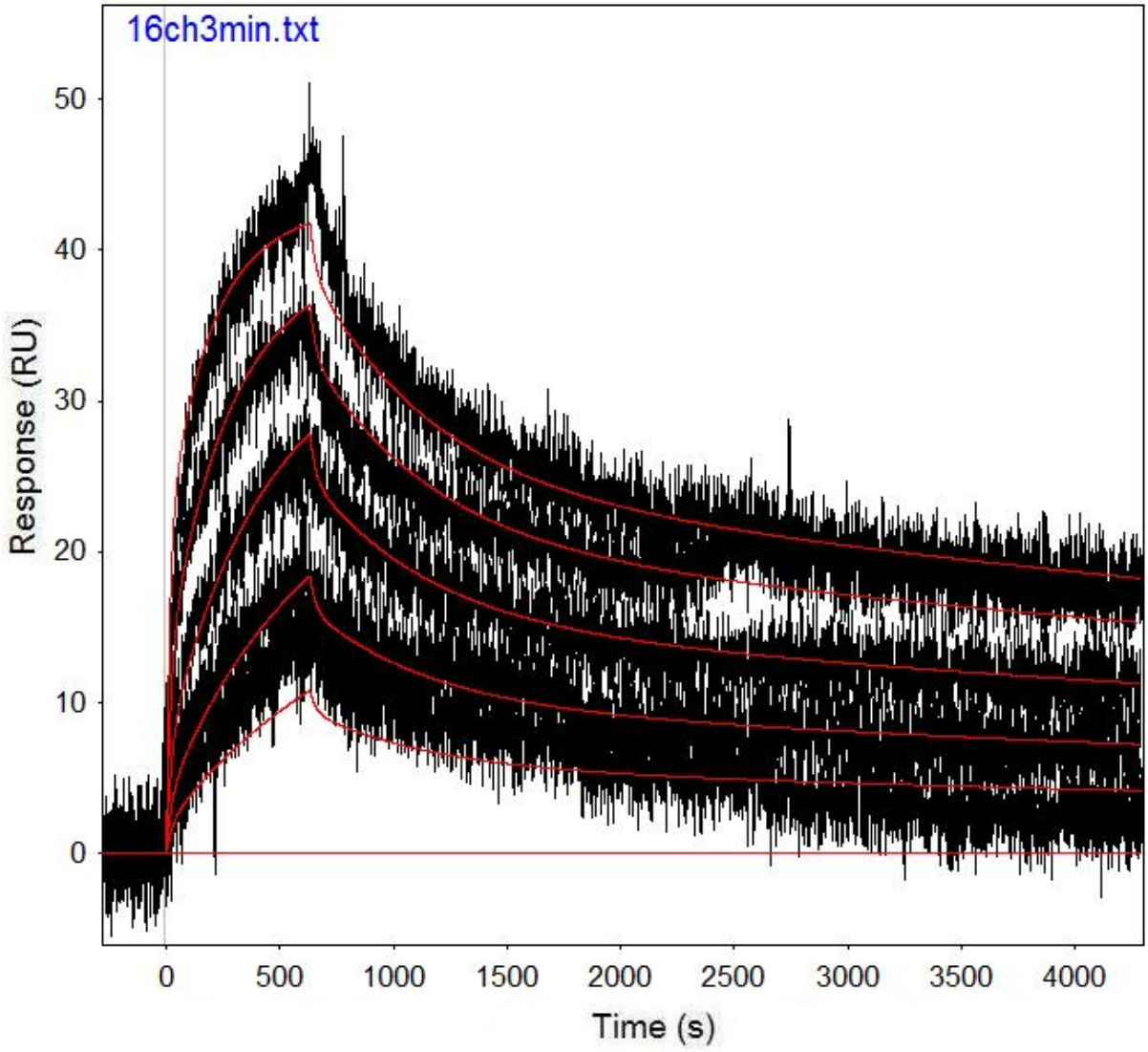

Figure B.60: Run 16, channel 3 model and data graph.

Table B.60: Run 16, channel 3 model parameters.

	kfwd1	krev1	kfwd2	krev2	kfwd3	krev3	ProA (RU)
Value	4004	0.001911	3459	8.18E-05	23315	0.04064	15.52
Error (abs)	51.27	4.782E-05	34.64	2.87E-06	1533	0.00281	0.03086
Error (%)	1.280	2.502	1.001	3.509	6.575	6.914	0.199

Run 38, channel 2: Performed at pH 6.0 in sodium acetate, at an IgG concentration of 1.067 µm. RSSE is 4.995.

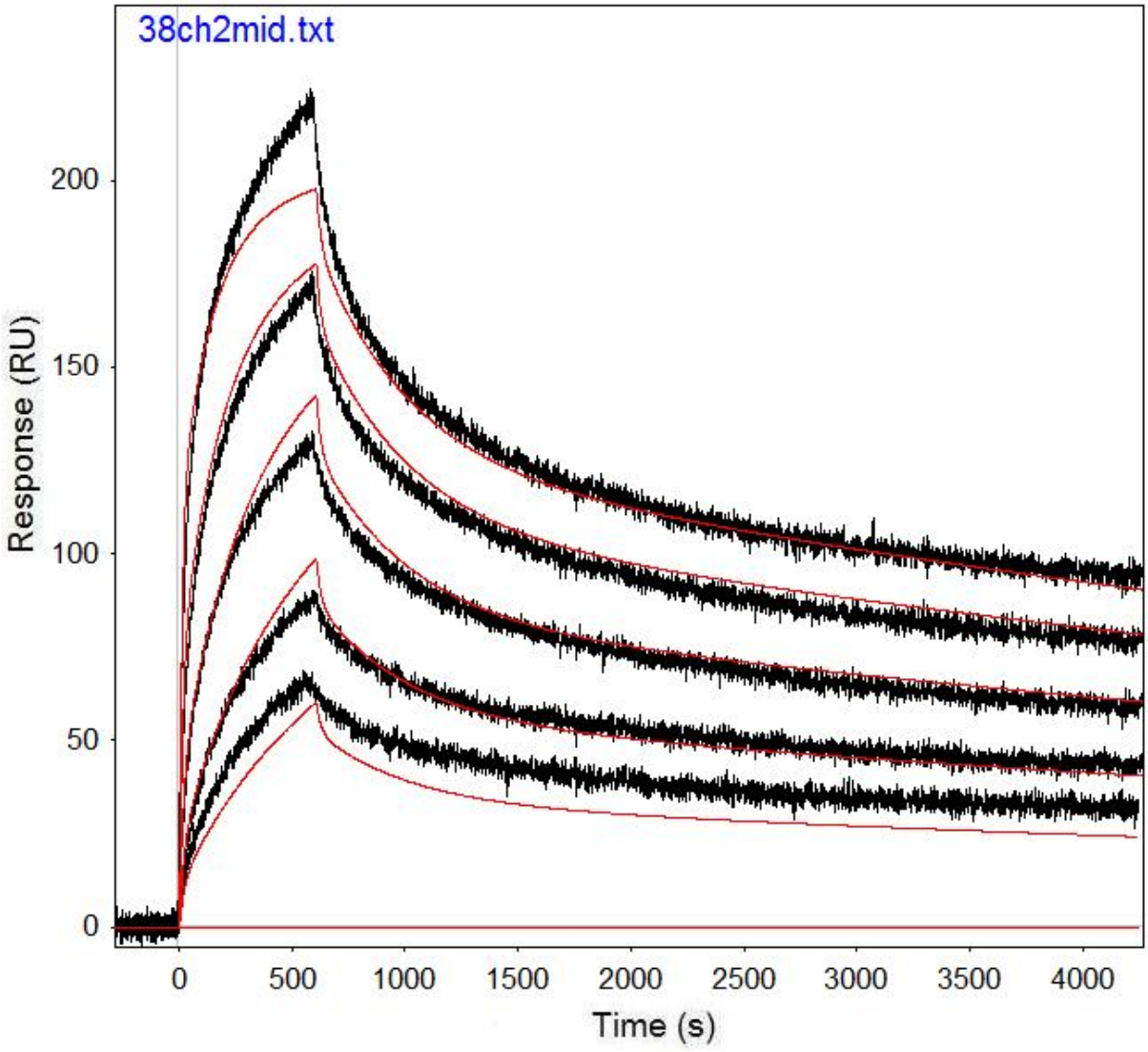

Figure B.61: Run 38, channel 2 model and data graph.

Table B.61: Run 38, channel 2 model parameters.

	kfwd1	krev1	kfwd2	krev2	kfwd3	krev3	ProA (RU)
Value	5313	0.002493	4815	8.88E-05	37727	0.04947	71.93
Error (abs)	49.14	3.213E-05	18.31	1.06E-06	1305	0.001829	0.07035
Error (%)	0.925	1.289	0.380	1.191	3.459	3.697	0.098

Run 38, channel 3: Performed at pH 6.0 in sodium acetate, at an IgG concentration of 1.067 µm. RSSE is 2.004.

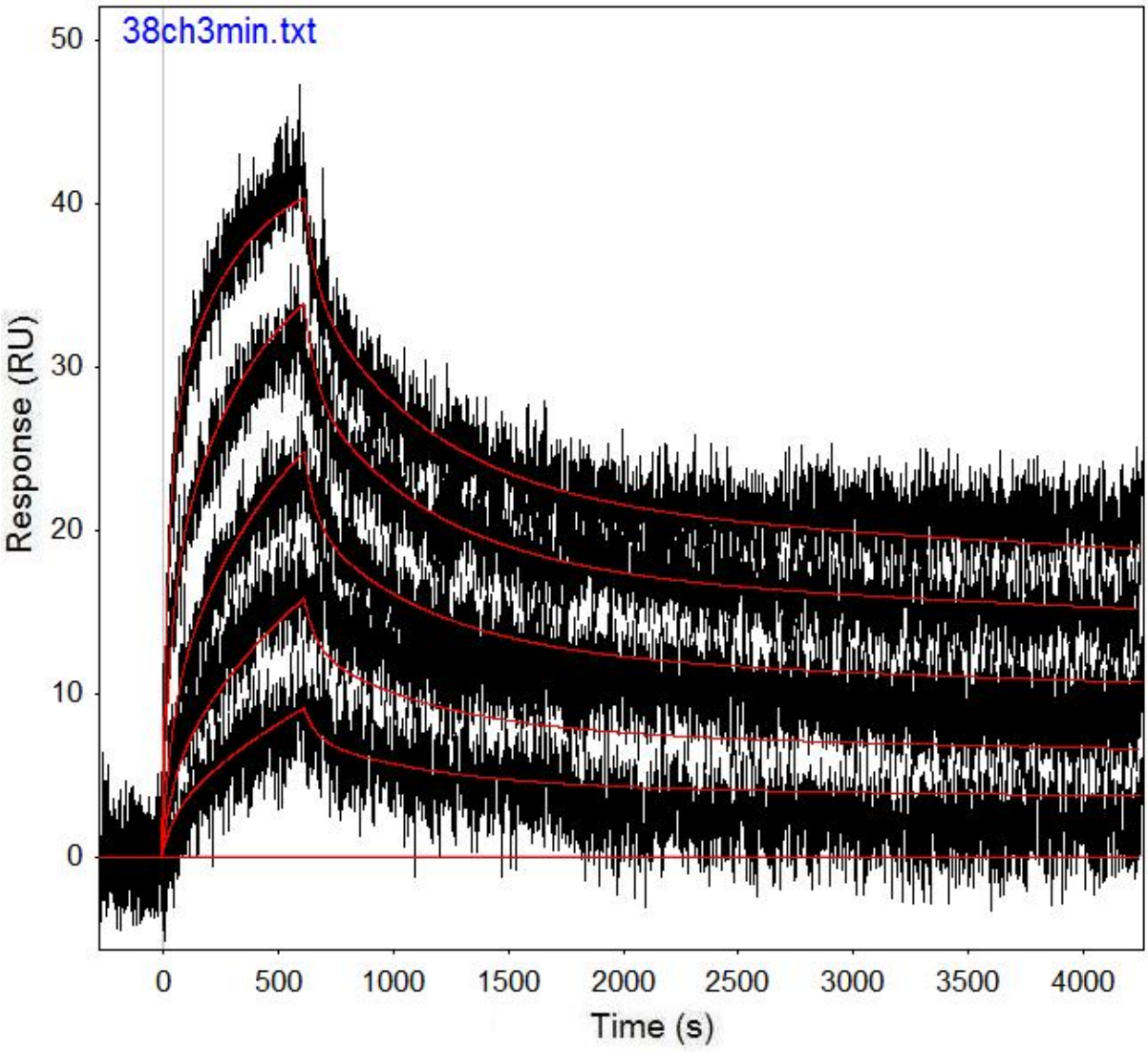

Figure B.62: Run 38, channel 3 model and data graph.

Table B.62: Run 38, channel 3 model parameters.

	kfwd1	krev1	kfwd2	krev2	kfwd3	krev3	ProA (RU)
Value	3011	0.00185	2552	3.84E-05	13609	0.01941	15.7
Error (abs)	74.11	6.878E-05	33.21	3.59E-06	616	0.001102	0.03879
Error (%)	2.461	3.718	1.301	9.331	4.526	5.677	0.247

Run 43, channel 2: Performed at pH 6.0 in sodium acetate, at an IgG concentration of 1.067 µm. RSSE is 2.962.

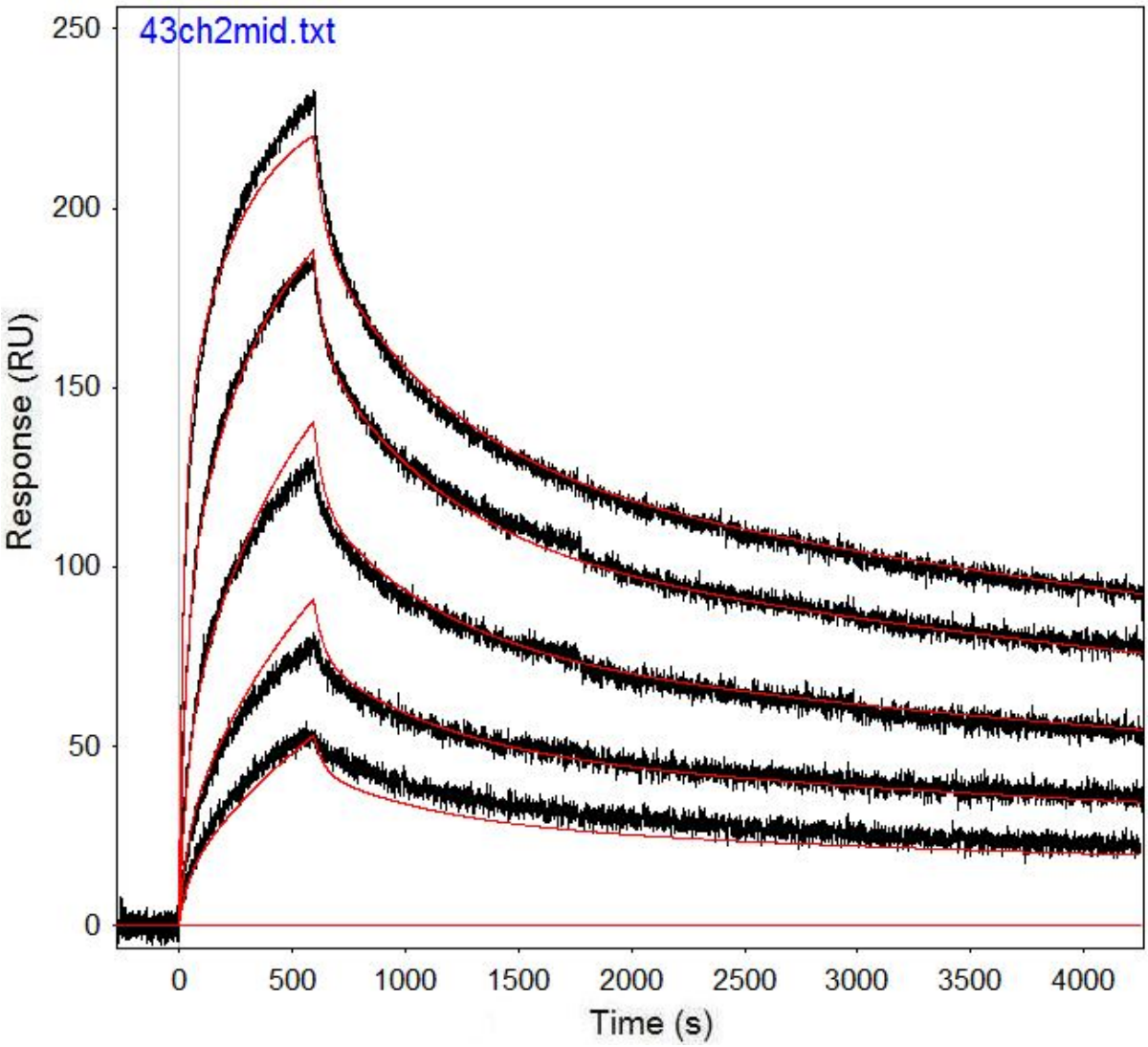

Figure B.63: Run 43, channel 2 model and data graph.

Table B.63: Run 43, channel 2 model parameters.

	kfwd1	krev1	kfwd2	krev2	kfwd3	krev3	ProA (RU)
Value	3032	0.001805	3256	9.07E-05	17174	0.02331	83.76
Error (abs)	17.79	1.964E-05	11.84	1.01E-06	224.3	0.000359	0.05358
Error (%)	0.587	1.088	0.364	1.117	1.306	1.541	0.064

Run 43, channel 3: Performed at pH 6.0 in sodium acetate, at an IgG concentration of 1.067 µm. RSSE is 1.916.

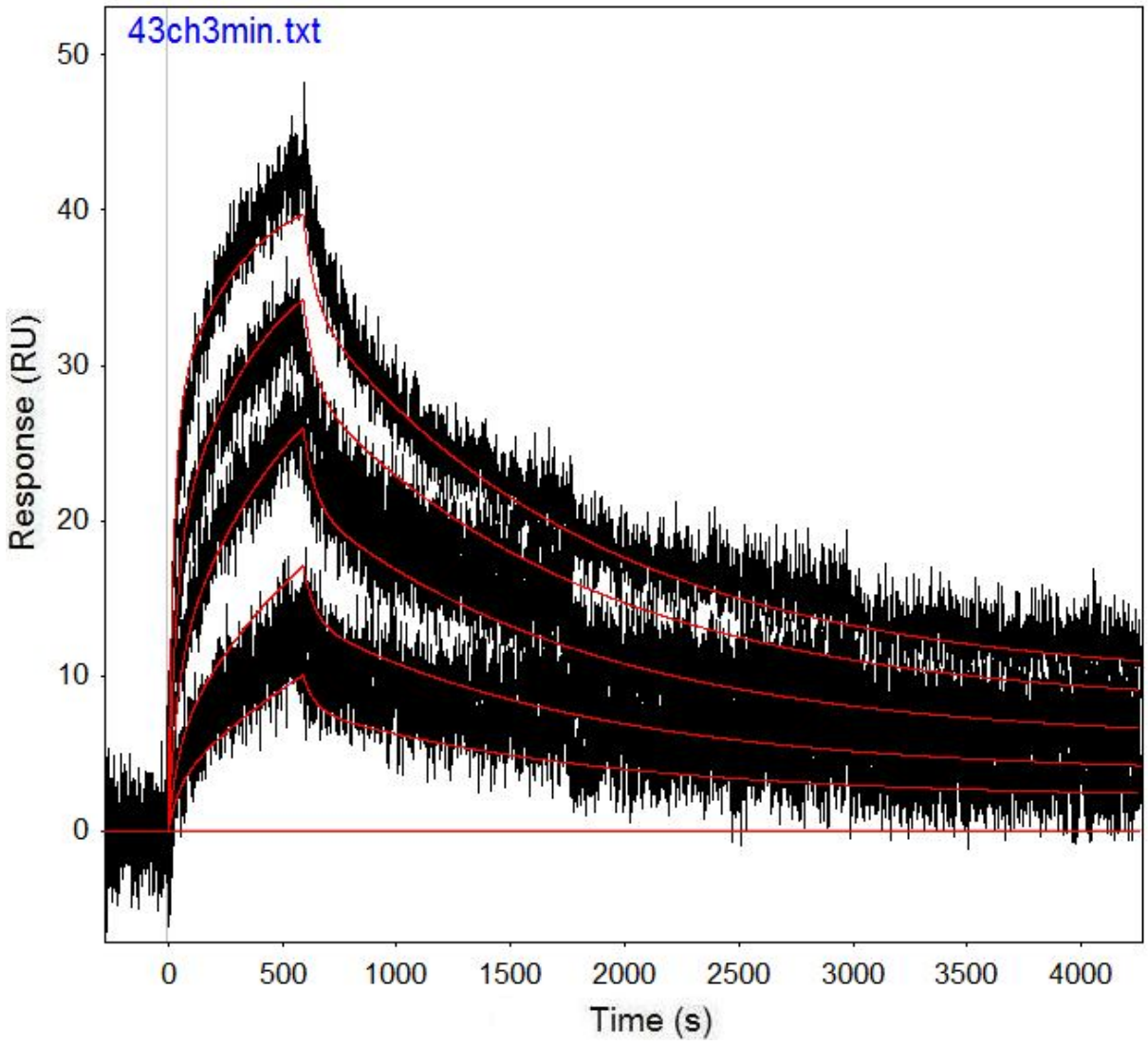

Figure B.64: Run 43, channel 3 model and data graph.

Table B.64: Run 43, channel 3 model parameters.

	kfwd1	krev1	kfwd2	krev2	kfwd3	krev3	ProA (RU)
Value	4750	0.0007959	1404	0	18471	0.01984	15
Error (abs)	137.6	3.747E-05	170.5	2.54E-05	709.6	0.00084	0.0352
Error (%)	2.897	4.708	12.144		3.842	4.233	0.235

Run 48, channel 2: Performed at pH 6.0 in sodium acetate, at an IgG concentration of 1.5 µm. RSSE is 8.123.

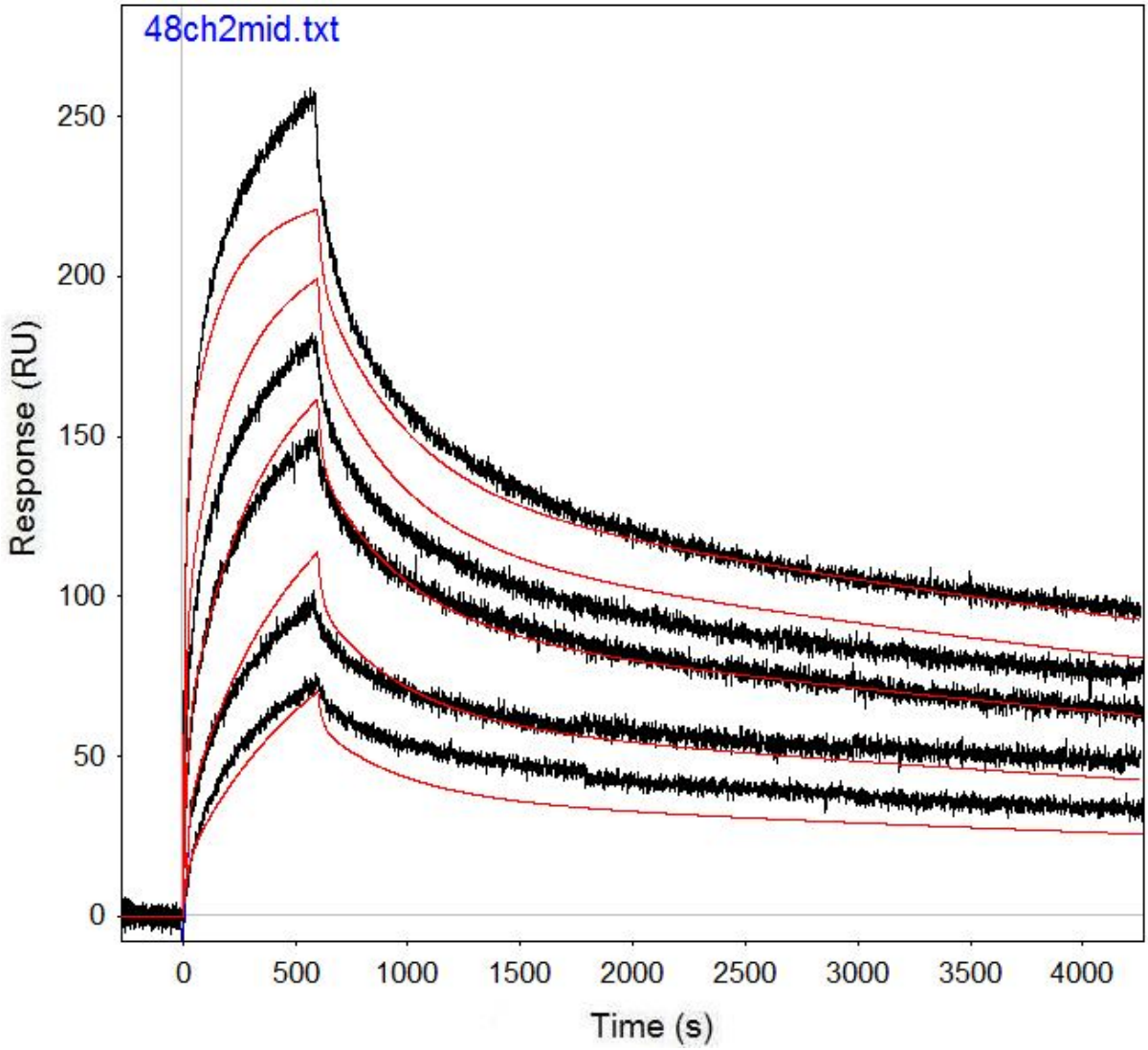

Figure B.65: Run 48, channel 2 model and data graph.

Table B.65: Run 48, channel 2 model parameters.

	kfwd1	krev1	kfwd2	krev2	kfwd3	krev3	ProA (RU)
Value	4217	0.002677	3513	0.000101	35956	0.05294	80.46
Error (abs)	61.49	4.916E-05	19.43	1.54E-06	1716	0.0027	0.1149
Error (%)	1.458	1.836	0.553	1.521	4.772	5.100	0.143

Run 59, channel 2: Performed at pH 6.0 in sodium acetate, at an IgG concentration of 0.5 µm. RSSE is 4.38.

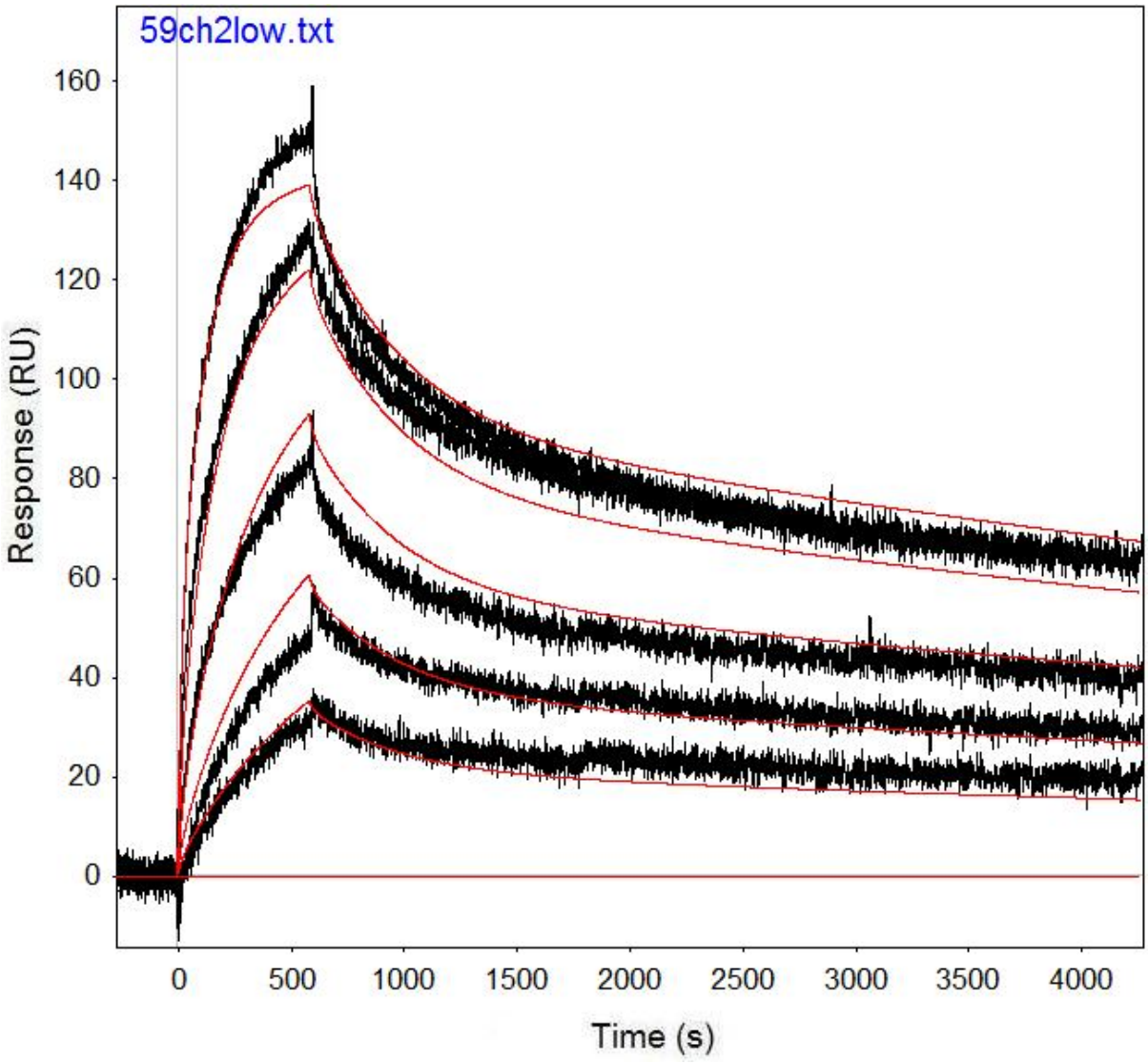

Figure B.66: Run 59, channel 2 model and data graph.

Table B.66: Run 59, channel 2 model parameters.

	kfwd1	krev1	kfwd2	krev2	kfwd3	krev3	ProA (RU)
Value	10208	0.002524	8941	8.51E-05	21348	0.04545	51.19
Error (abs)	100.9	0.0000389	41.77	1.25E-06	2190	0.004621	0.07234
Error (%)	0.988	1.541	0.467	1.472	10.259	10.167	0.141

Run 64, channel 2: Performed at pH 6.0 in sodium acetate, at an IgG concentration of 0.5 µm. RSSE is 4.476.

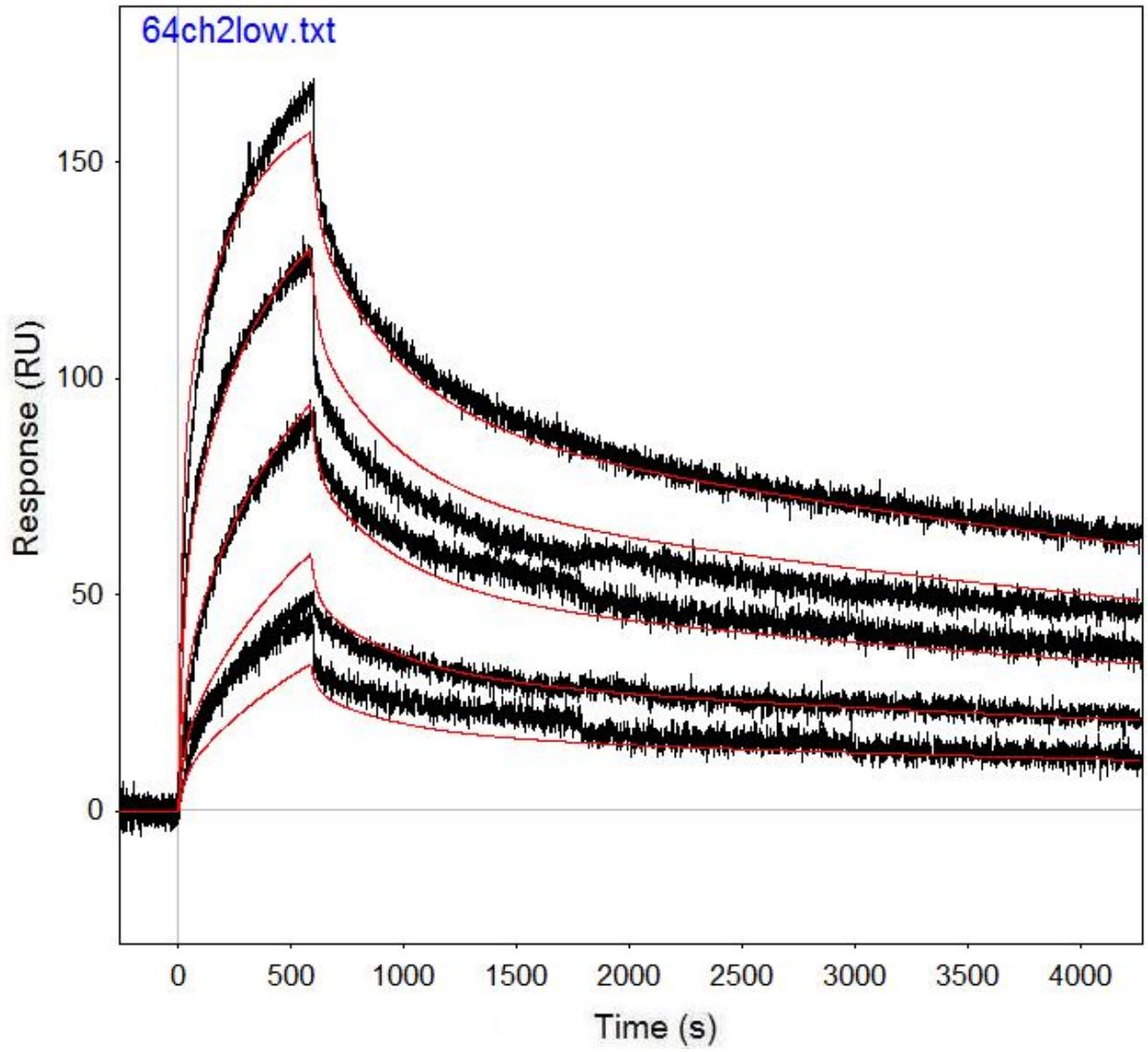

Figure B.67: Run 64, channel 2 model and data graph.

Table B.67: Run 64, channel 2 model parameters.

	kfwd1	krev1	kfwd2	krev2	kfwd3	krev3	ProA (RU)
Value	6784	0.002606	6020	0.000108	46668	0.0356	61.98
Error (abs)	105.5	4.833E-05	31.75	1.45E-06	1580	0.001374	0.09543
Error (%)	1.555	1.855	0.527	1.344	3.386	3.860	0.154

Run 75, channel 5: Performed at pH 5.5 in sodium acetate, at an IgG concentration of 1.067 µm. RSSE is 9.746.

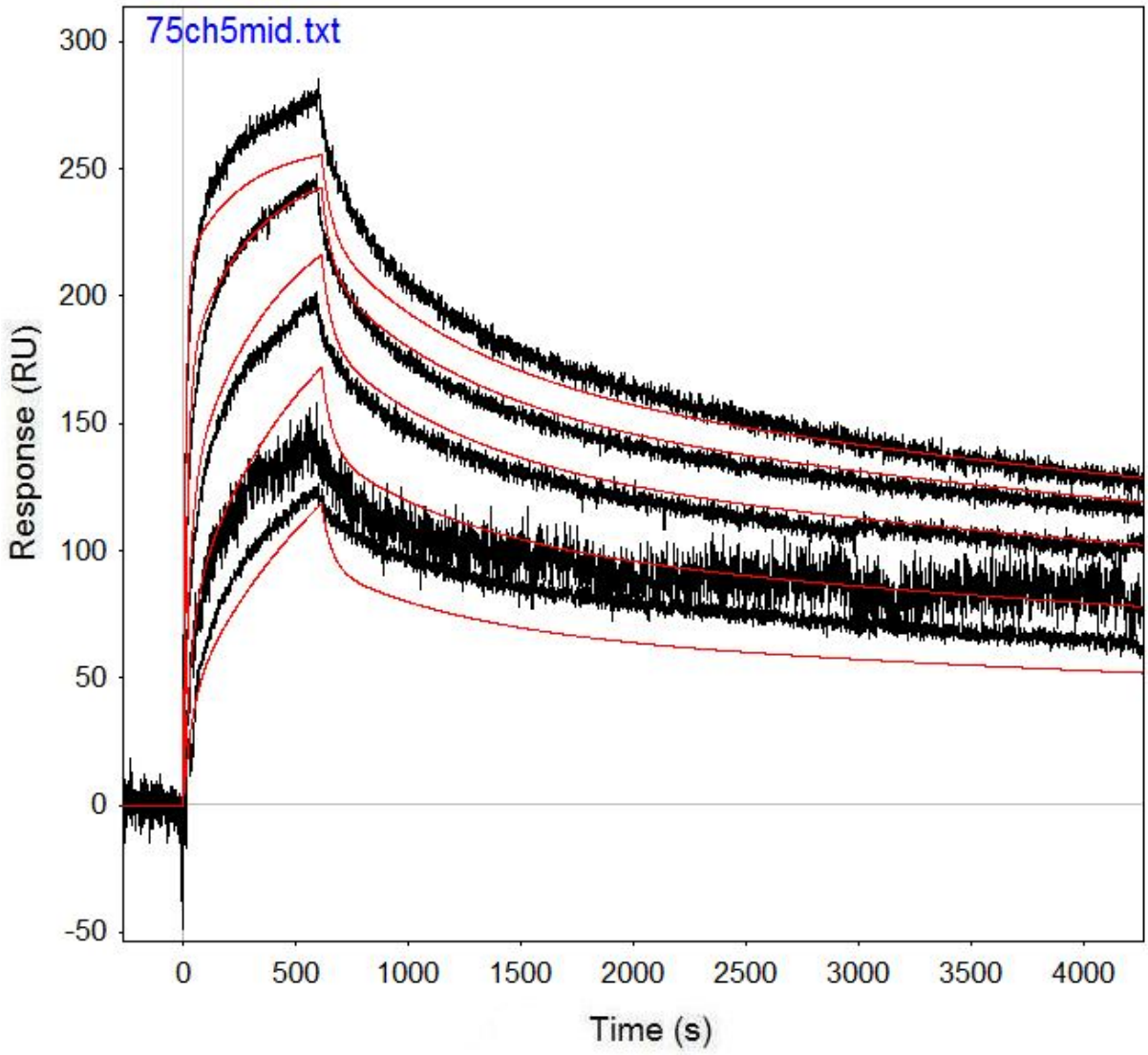

Figure B.68: Run 75, channel 5 model and data graph.

Table B.68: Run 75, channel 5 model parameters.

	kfwd1	krev1	kfwd2	krev2	kfwd3	krev3	ProA (RU)
Value	5668	0.001527	9045	6.94E-05	54179	0.0221	88.85
Error (abs)	89.99	5.882E-05	90.81	2.7E-06	1361	0.000661	0.0994
Error (%)	1.588	3.852	1.004	3.884	2.512	2.990	0.112

Run 80, channel 2: Performed at pH 5.5 in sodium acetate, at an IgG concentration of 1.067 µm. RSSE is 10.69.

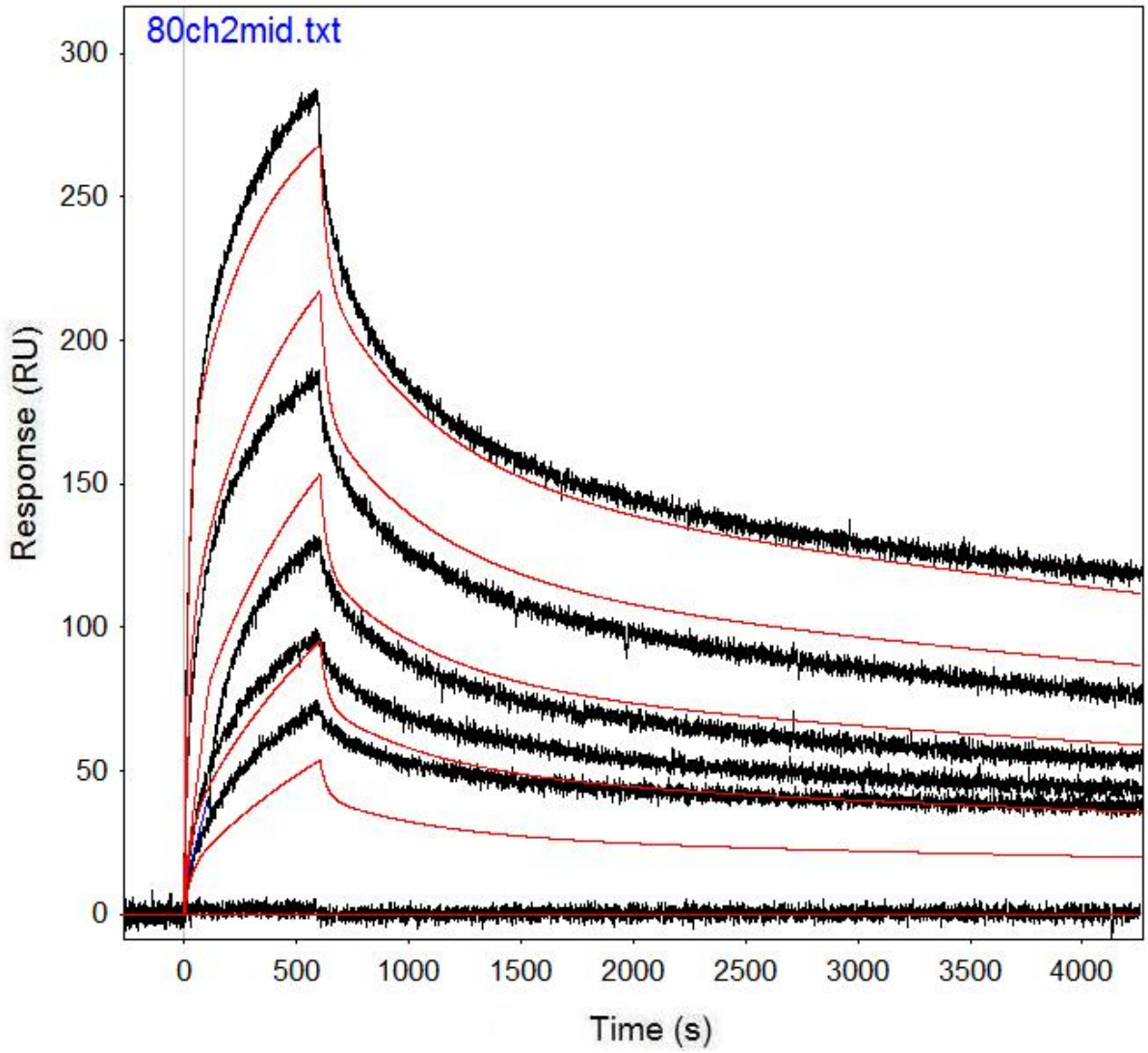

Figure B.69: Run 80, channel 2 model and data graph.

Table B.69: Run 80, channel 2 model parameters.

	kfwd1	krev1	kfwd2	krev2	kfwd3	krev3	ProA (RU)
Value	2100	0.001994	2336	8.21E-05	23780	0.03395	109
Error (abs)	42.22	6.661E-05	23.12	2.75E-06	999.5	0.001574	0.2494
Error (%)	2.010	3.341	0.990	3.354	4.203	4.636	0.229

Run 85, channel 2: Performed at pH 5.5 in sodium acetate, at an IgG concentration of 1.067 µm. RSSE is 7.782.

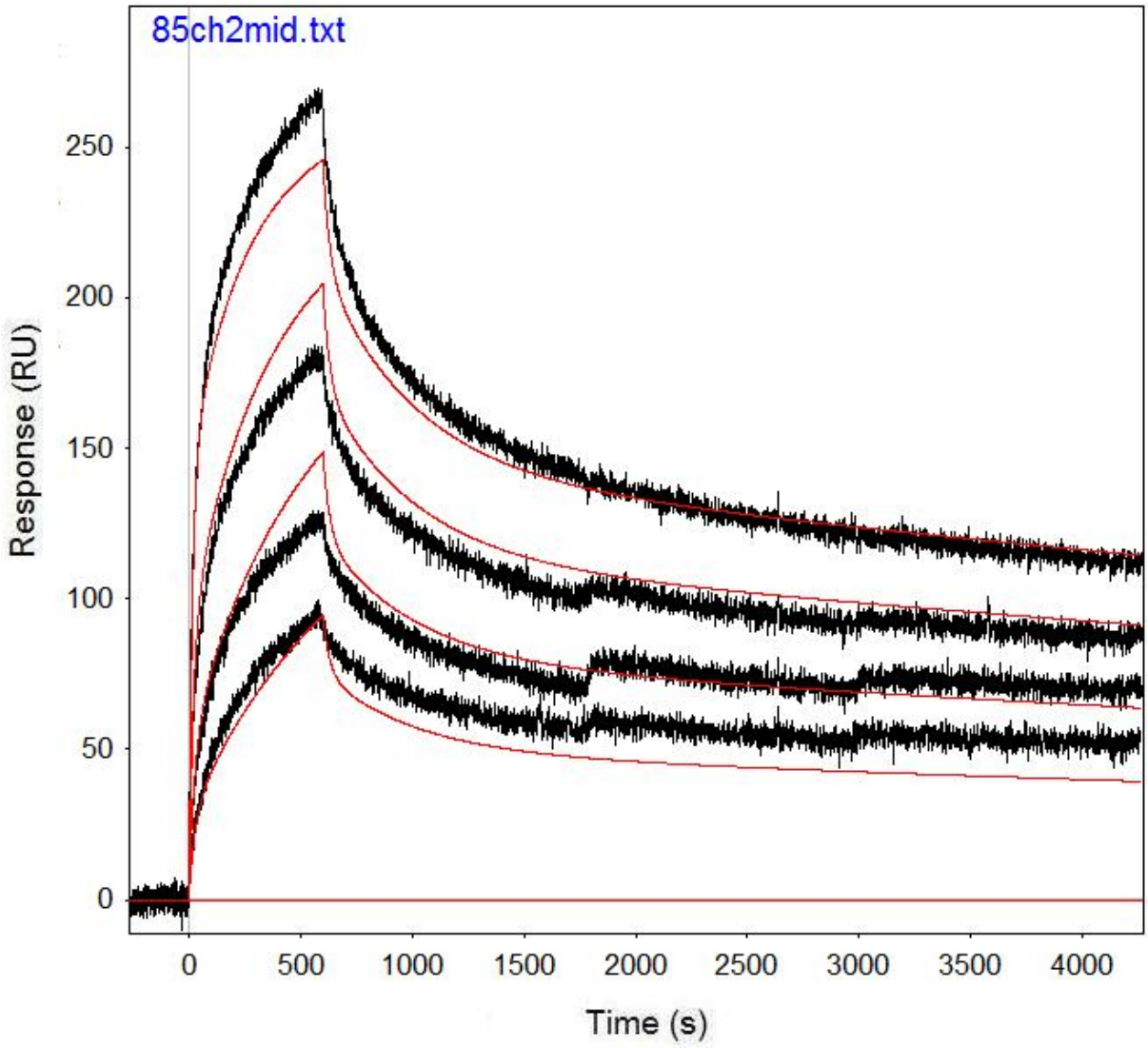

Figure B.70: Run 85, channel 2 model and data graph.

Table B.70: Run 85, channel 2 model parameters.

	kfwd1	krev1	kfwd2	krev2	kfwd3	krev3	ProA (RU)
Value	2854	0.002459	2768	6.07E-05	23694	0.0326	96.85
Error (abs)	54.83	5.582E-05	16.12	1.54E-06	769.7	0.00123	0.1626
Error (%)	1.921	2.270	0.582	2.539	3.249	3.773	0.168

Run 96, channel 2: Performed at pH 5.5 in sodium acetate, at an IgG concentration of 1.067 µm. RSSE is 6.284.

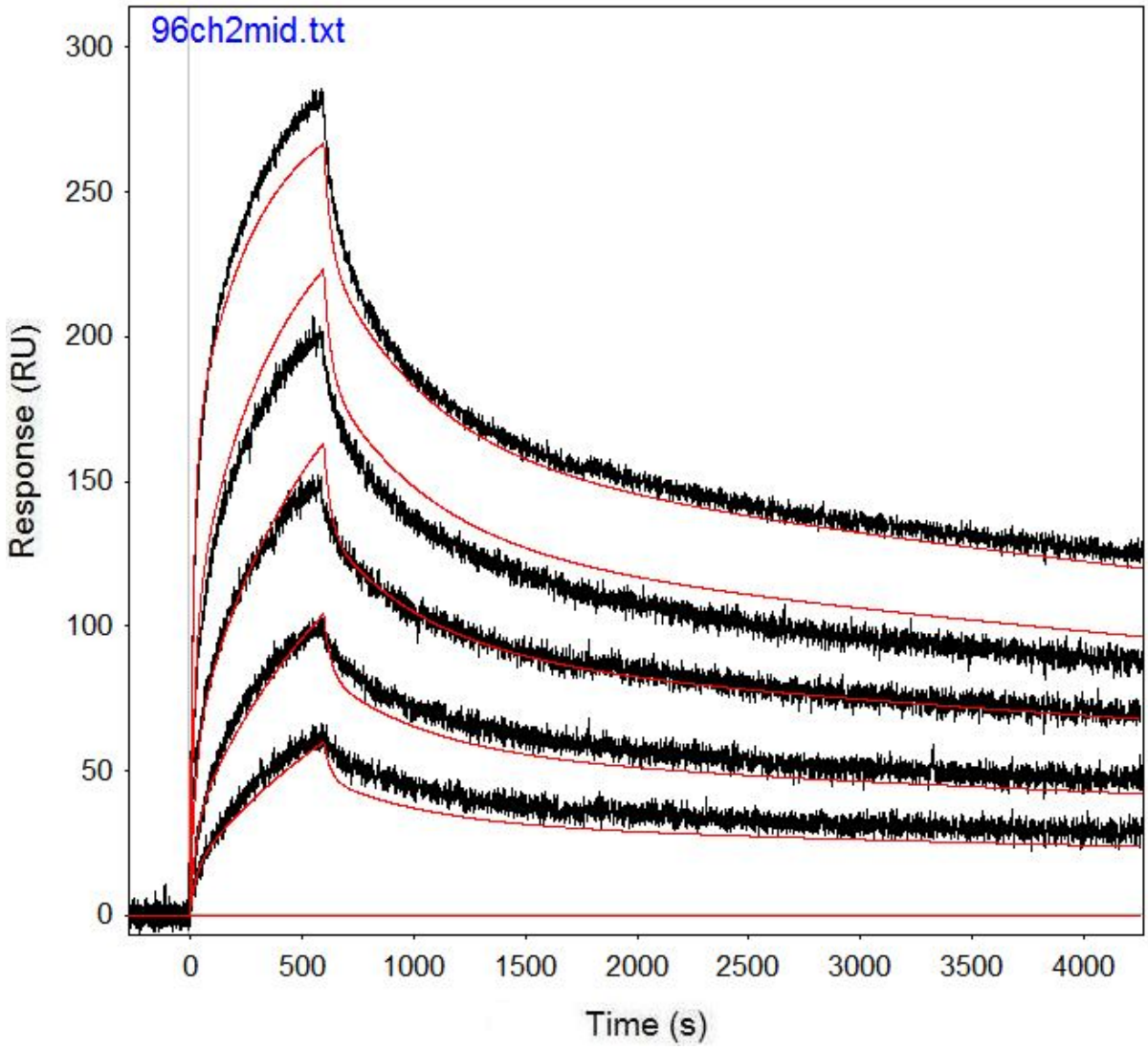

Figure B.71: Run 96, channel 2 model and data graph.

Table B.71: Run 96, channel 2 model parameters.

	kfwd1	krev1	kfwd2	krev2	kfwd3	krev3	ProA (RU)
Value	2652	0.002143	2927	7.49E-05	24556	0.0327	104.1
Error (abs)	32.44	3.856E-05	14.16	1.34E-06	595.9	0.000896	0.1237
Error (%)	1.223	1.799	0.484	1.791	2.427	2.739	0.119

Run 96, channel 3: Performed at pH 5.5 in sodium acetate, at an IgG concentration of 1.067 µm. RSSE is 2.808.

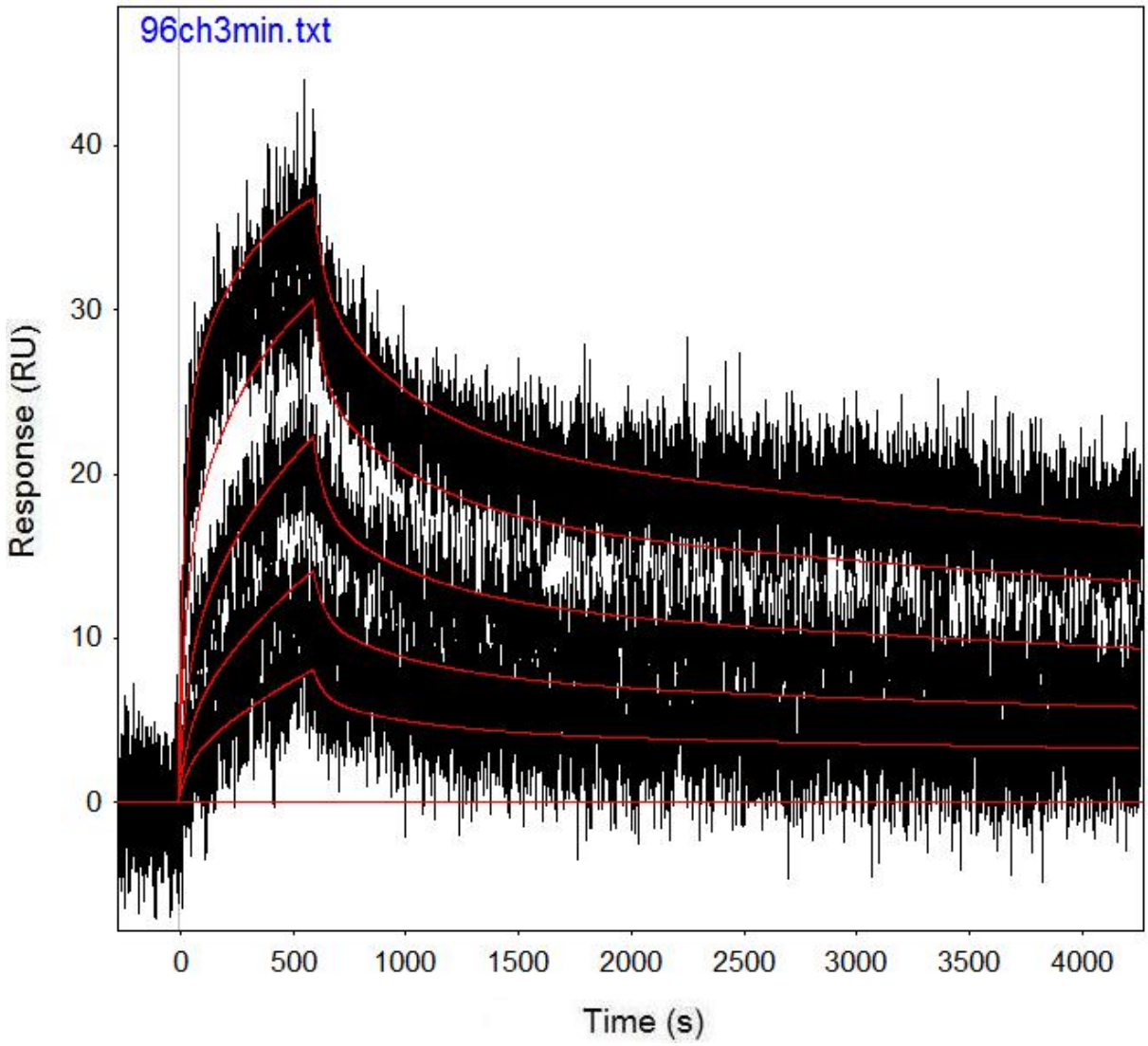

Figure B.72: Run 96, channel 3 model and data graph.

Table B.72: Run 96, channel 3 model parameters.

	kfwd1	krev1	kfwd2	krev2	kfwd3	krev3	ProA (RU)
Value	2469	0.002142	2829	7.09E-05	15219	0.0204	14.46
Error (abs)	140.5	0.0001531	46.66	4.52E-06	1009	0.001751	0.05666
Error (%)	5.691	7.148	1.649	6.380	6.630	8.583	0.392

Run 107, channel 5: Performed at pH 5.5 in sodium acetate, at an IgG concentration of 1.5 µm. RSSE is 5.697.

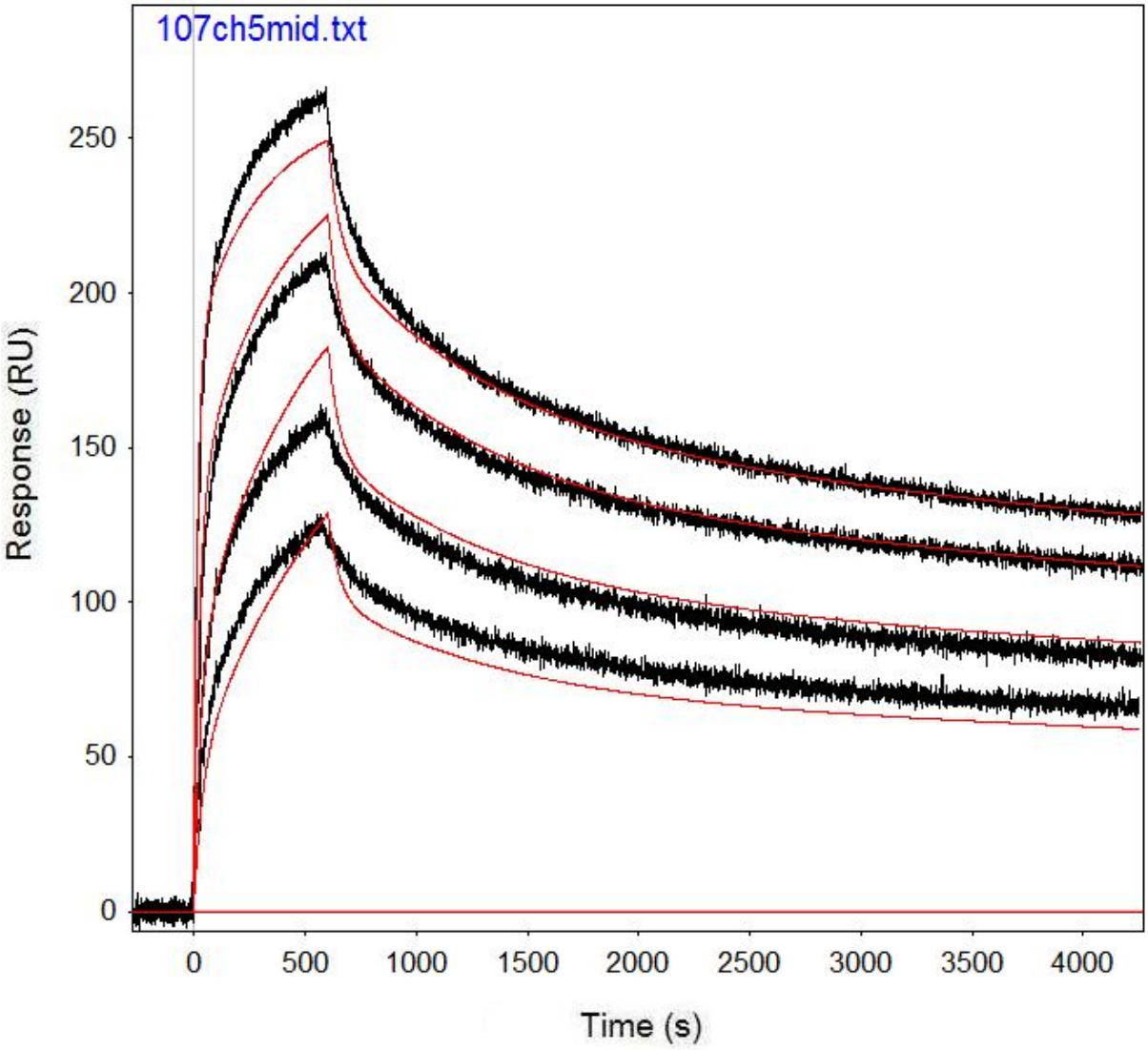

Figure B.73: Run 107, channel 5 model and data graph.

Table B.73: Run 107, channel 5 model parameters.

	kfwd1	krev1	kfwd2	krev2	kfwd3	krev3	ProA (RU)
Value	2332	0.001332	3449	4.67E-05	20634	0.02081	90.26
Error (abs)	21.86	3.579E-05	29.99	2.23E-06	345.6	0.000406	0.07953
Error (%)	0.937	2.687	0.870	4.773	1.675	1.952	0.088

Run 117, channel 2: Performed at pH 5.5 in sodium acetate, at an IgG concentration of 0.5 µm. RSSE is 4.442.

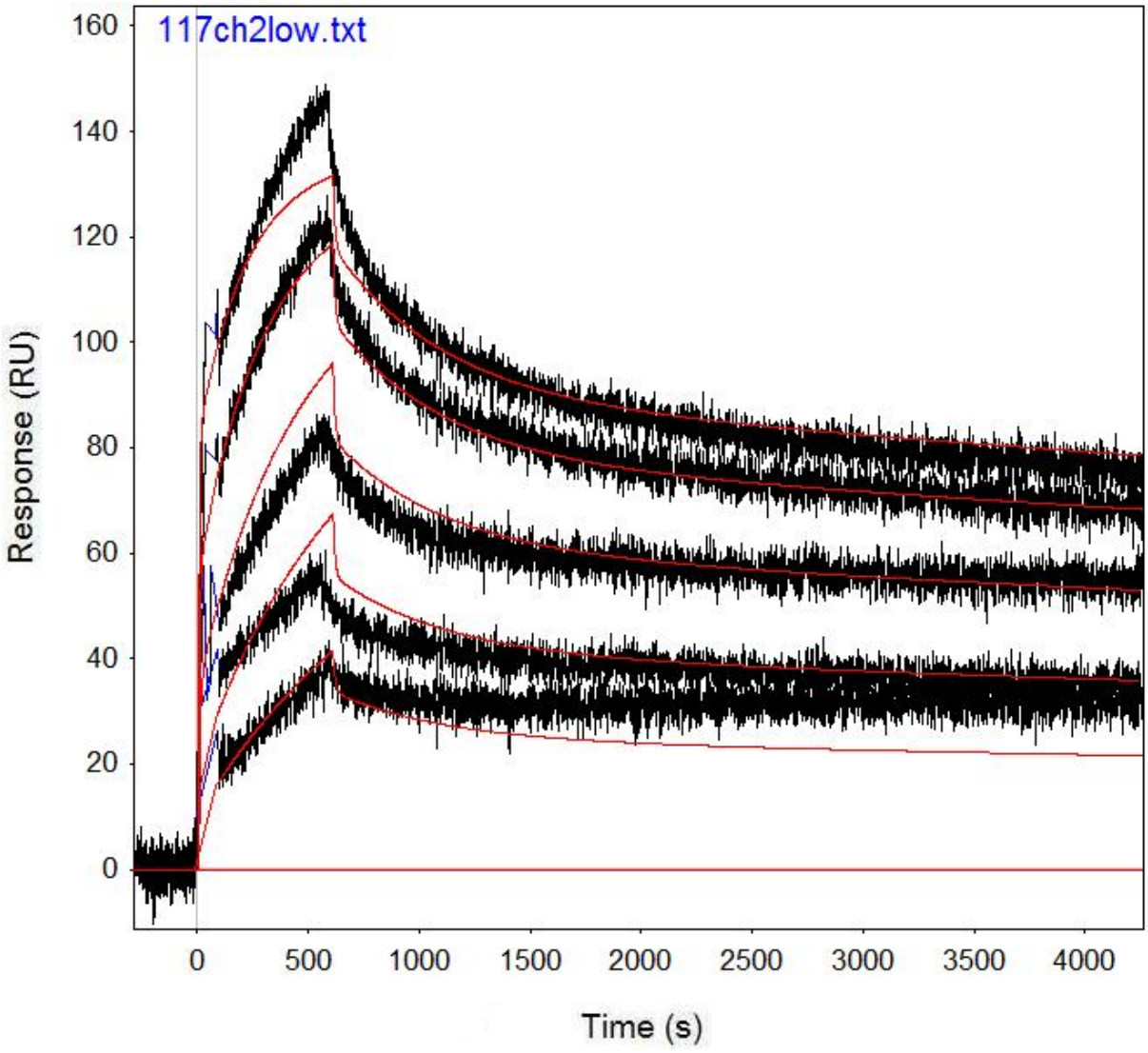

Figure B.74: Run 117, channel 2 model and data graph.

Table B.74: Run 117, channel 2 model parameters.

	kfwd1	krev1	kfwd2	krev2	kfwd3	krev3	ProA (RU)
Value	7441	0.00203	11421	3.66E-05	270200	0.109	47.5
Error (abs)	105.5	5.043E-05	58.8	1.42E-06	14231	0.006018	0.05859
Error (%)	1.418	2.484	0.515	3.878	5.267	5.521	0.123

Run 128, channel 2: Performed at pH 5.5 in sodium acetate, at an IgG concentration of 1.5 µm. RSSE is 6.90.

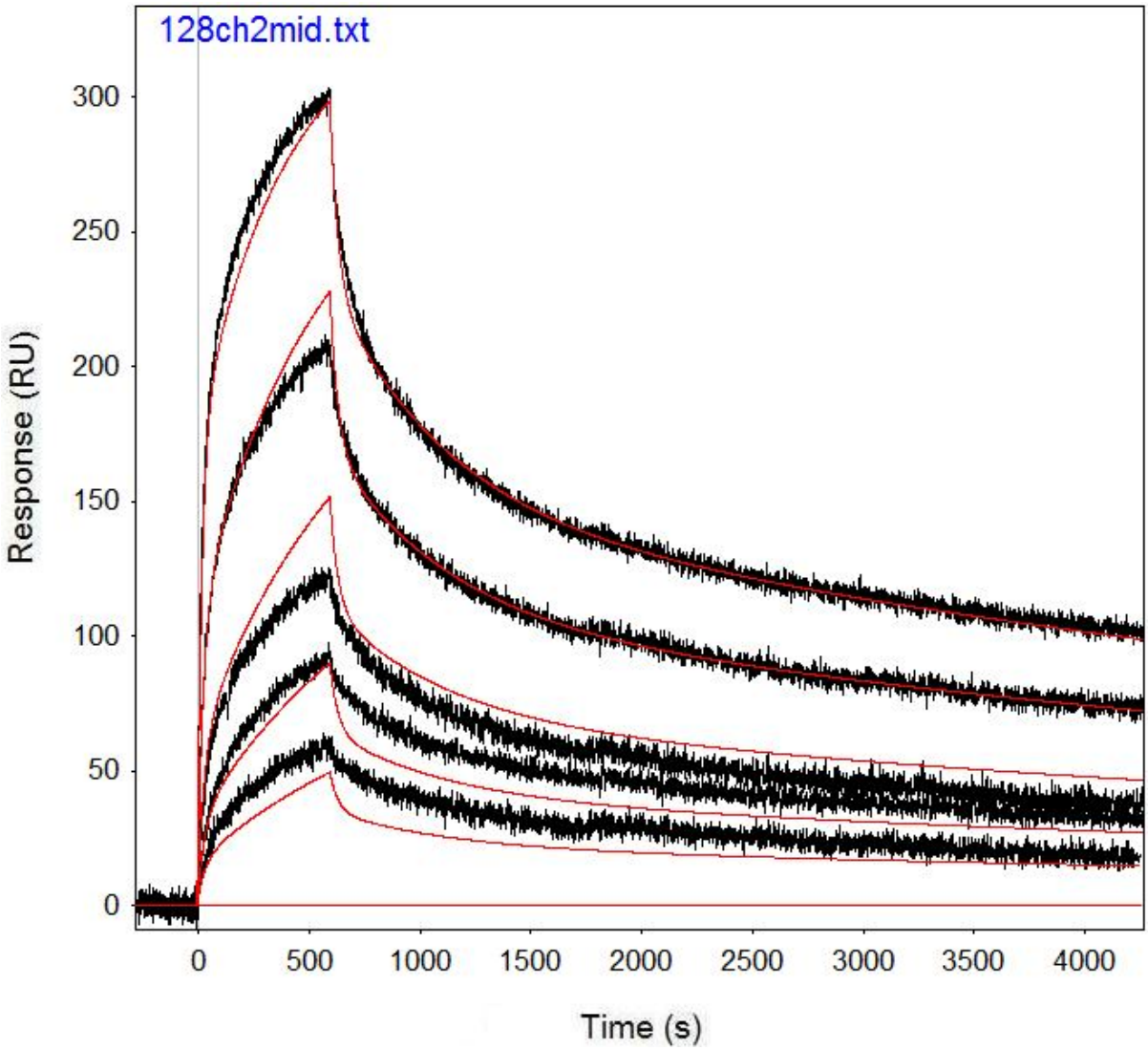

Figure B.75: Run 128, channel 2 model and data graph.

Table B.75: Run 128, channel 2 model parameters.

	kfwd1	krev1	kfwd2	krev2	kfwd3	krev3	ProA (RU)
Value	1103	0.001927	1090	0.000108	12139	0.02793	133.6
Error (abs)	14.2	0.0000427	8.595	2.2E-06	241.4	0.000648	0.2328
Error (%)	1.287	2.216	0.789	2.031	1.989	2.321	0.174

Run 134, channel 2: Performed at pH 5.5 in sodium acetate, at an IgG concentration of 0.5 µm. RSSE is 3.462.

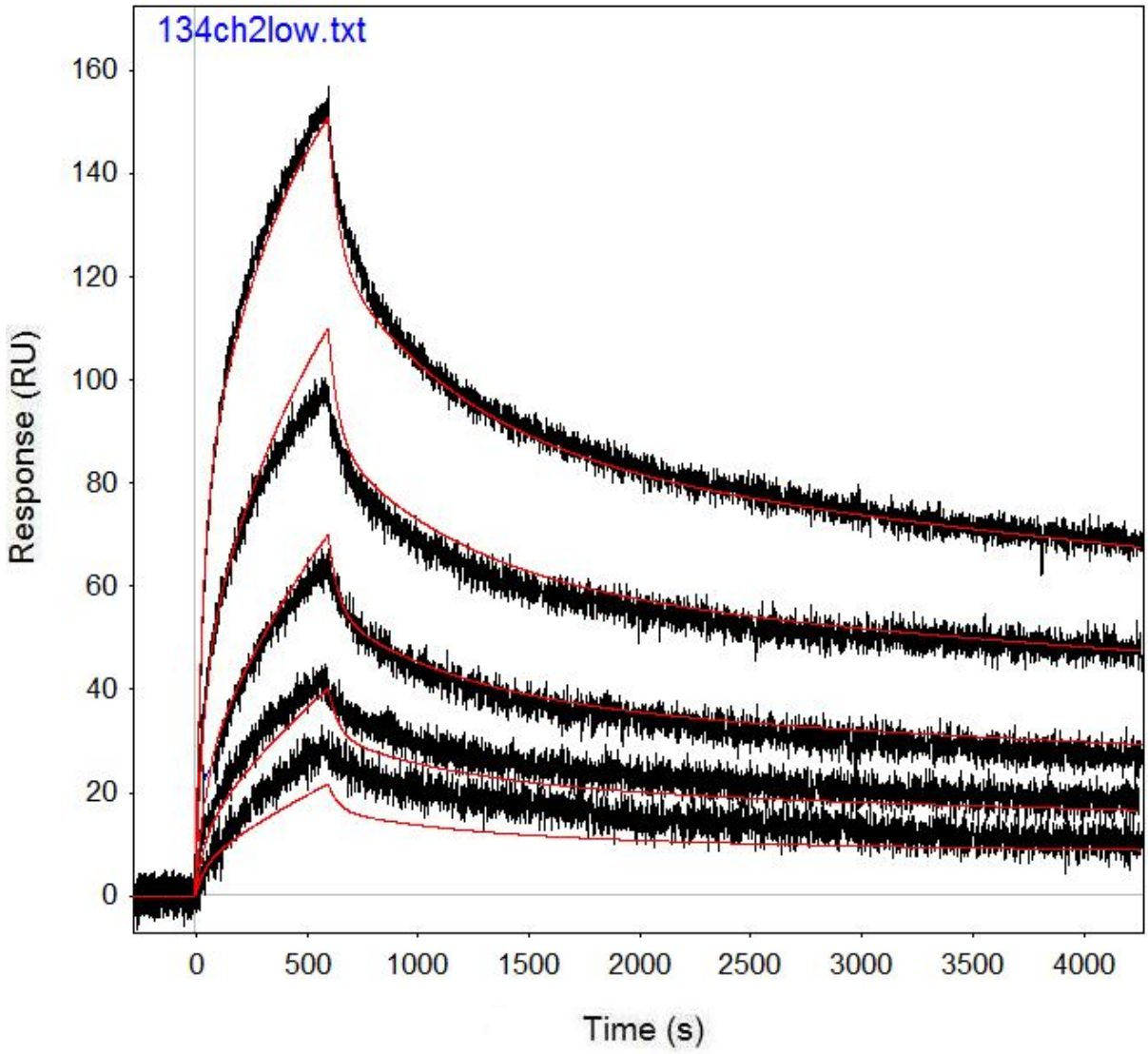

Figure B.76: Run 134, channel 2 model and data graph.

Table B.76: Run 134, channel 2 model parameters.

	kfwd1	krev1	kfwd2	krev2	kfwd3	krev3	ProA (RU)
Value	2365	0.001627	3063	6.28E-05	18731	0.02224	70.22
Error (abs)	29.88	4.418E-05	25.65	2.21E-06	447.3	0.000625	0.1327
Error (%)	1.263	2.715	0.837	3.517	2.388	2.810	0.189

Run 143, channel 2: Performed at pH 5.0 in sodium acetate, at an IgG concentration of 1.067 µm. RSSE is 7.557.

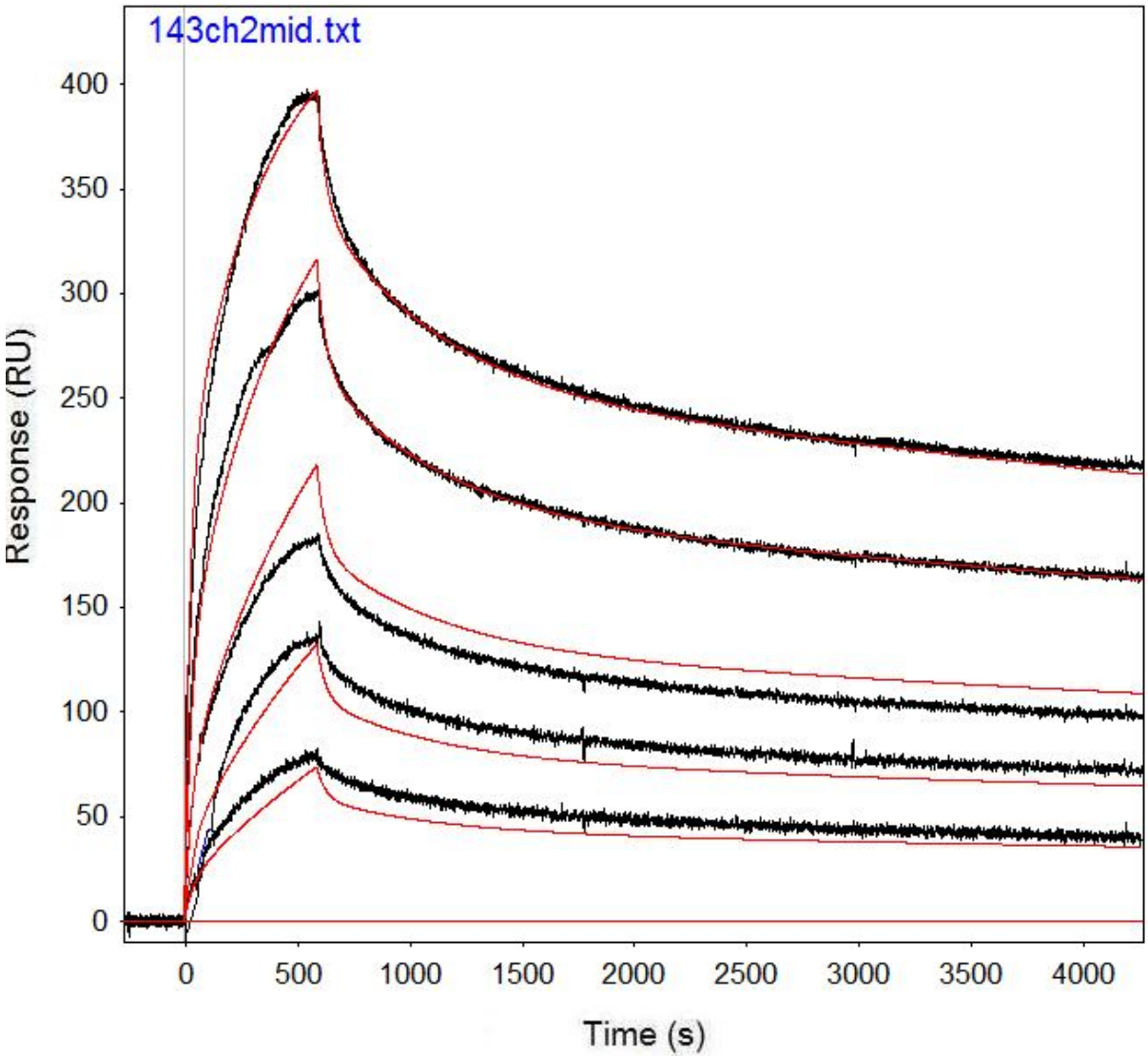

Figure B.77: Run 143, channel 2 model and data graph.

Table B.77: Run 143, channel 2 model parameters.

	kfwd1	krev1	kfwd2	krev2	kfwd3	krev3	ProA (RU)
Value	1590	0.00192	2510	4.93E-05	14211	0.02616	161.6
Error (abs)	19.59	3.893E-05	10.48	1.11E-06	294.8	0.000625	0.1774
Error (%)	1.232	2.028	0.418	2.254	2.074	2.390	0.110

Run 148, channel 2: Performed at pH 5.0 in sodium acetate, at an IgG concentration of 1.067 µm. RSSE is 13.95.

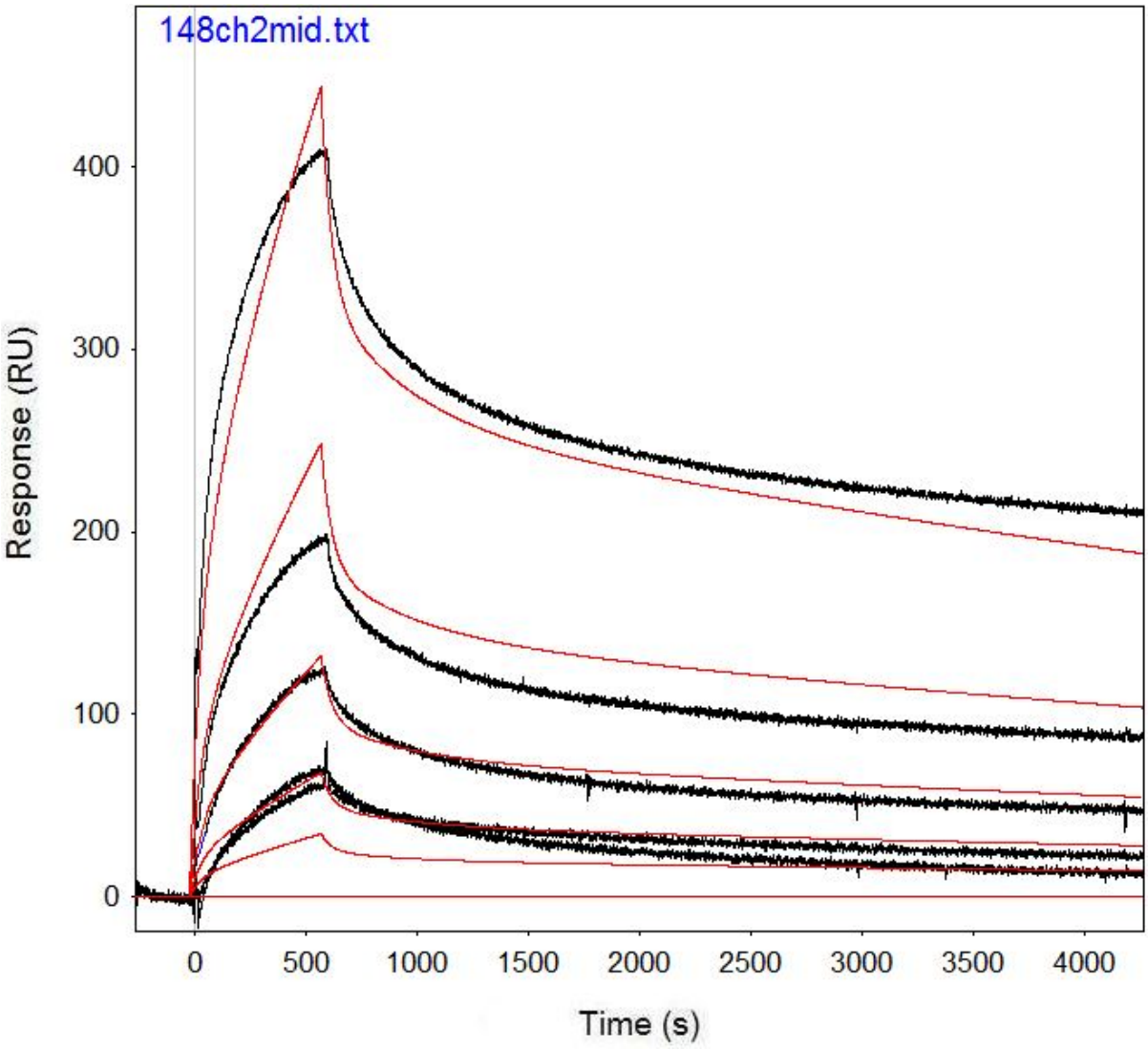

Figure B.78: Run 148, channel 2 model and data graph.

Table B.78: Run 148, channel 2 model parameters.

	kfwd1	krev1	kfwd2	krev2	kfwd3	krev3	ProA (RU)
Value	161.1	0.002568	321.2	0.00009	1889	0.02134	544.1
Error (abs)	11.18	0.0001747	5.045	1.99E-06	69.16	0.001043	6.582
Error (%)	6.940	6.803	1.571	2.214	3.661	4.888	1.210

Run 153, channel 5: Performed at pH 5.0 in sodium acetate, at an IgG concentration of 1.067 µm. RSSE is 20.77.

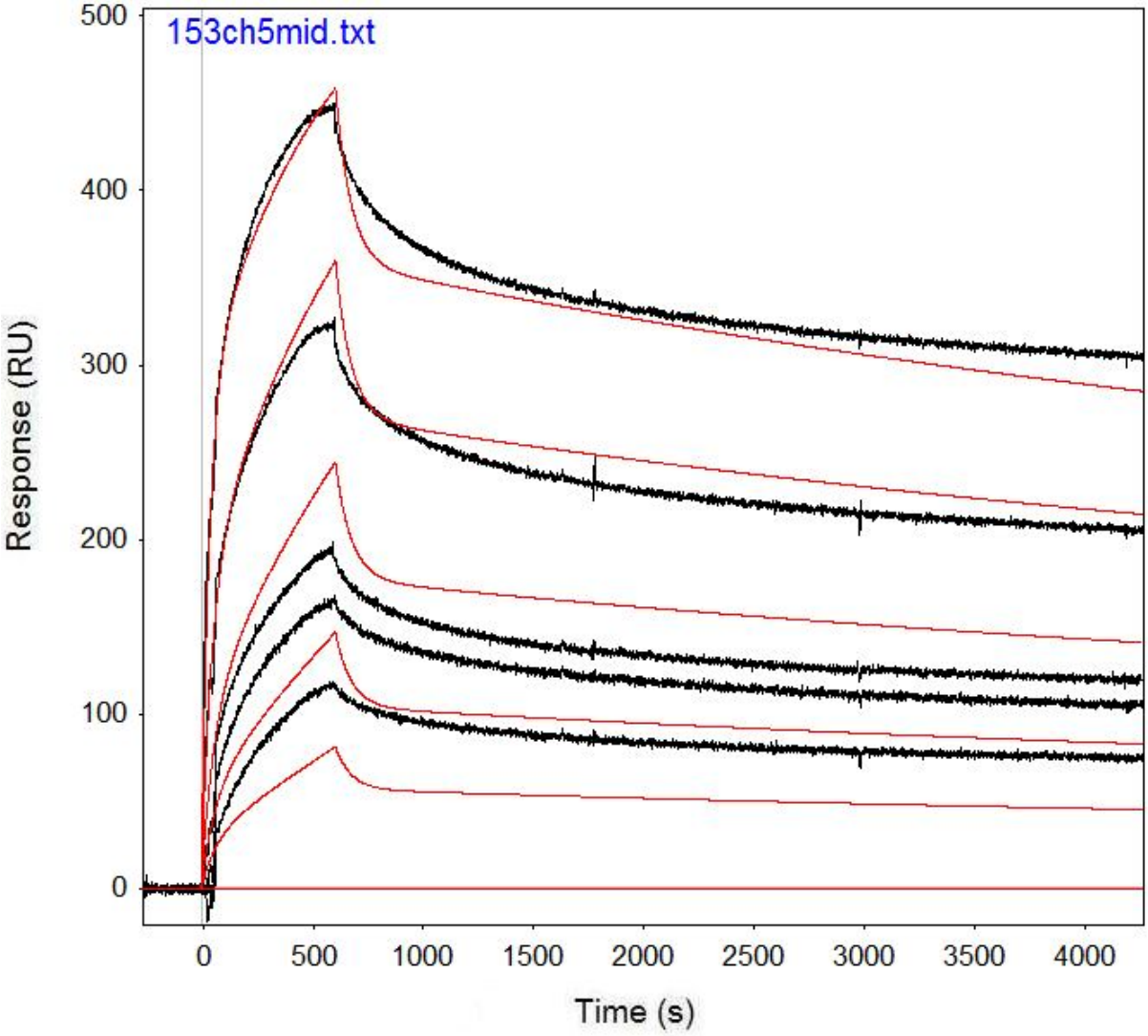

Figure B.79: Run 153, channel 5 model and data graph.

Table B.79: Run 153, channel 5 model parameters.

	kfwd1	krev1	kfwd2	krev2	kfwd3	krev3	ProA (RU)
Value	1366	0.0001516	1393	0	10403	0.01425	191.2
Error (abs)	9330	0.0006219	9350	0.000434	295.4	0.000464	0.4909
Error (%)	683.016	410.224	671.213		2.840	3.259	0.257

Run 158, channel 2: Performed at pH 5.0 in sodium acetate, at an IgG concentration of 1.067 µm. RSSE is 7.403.

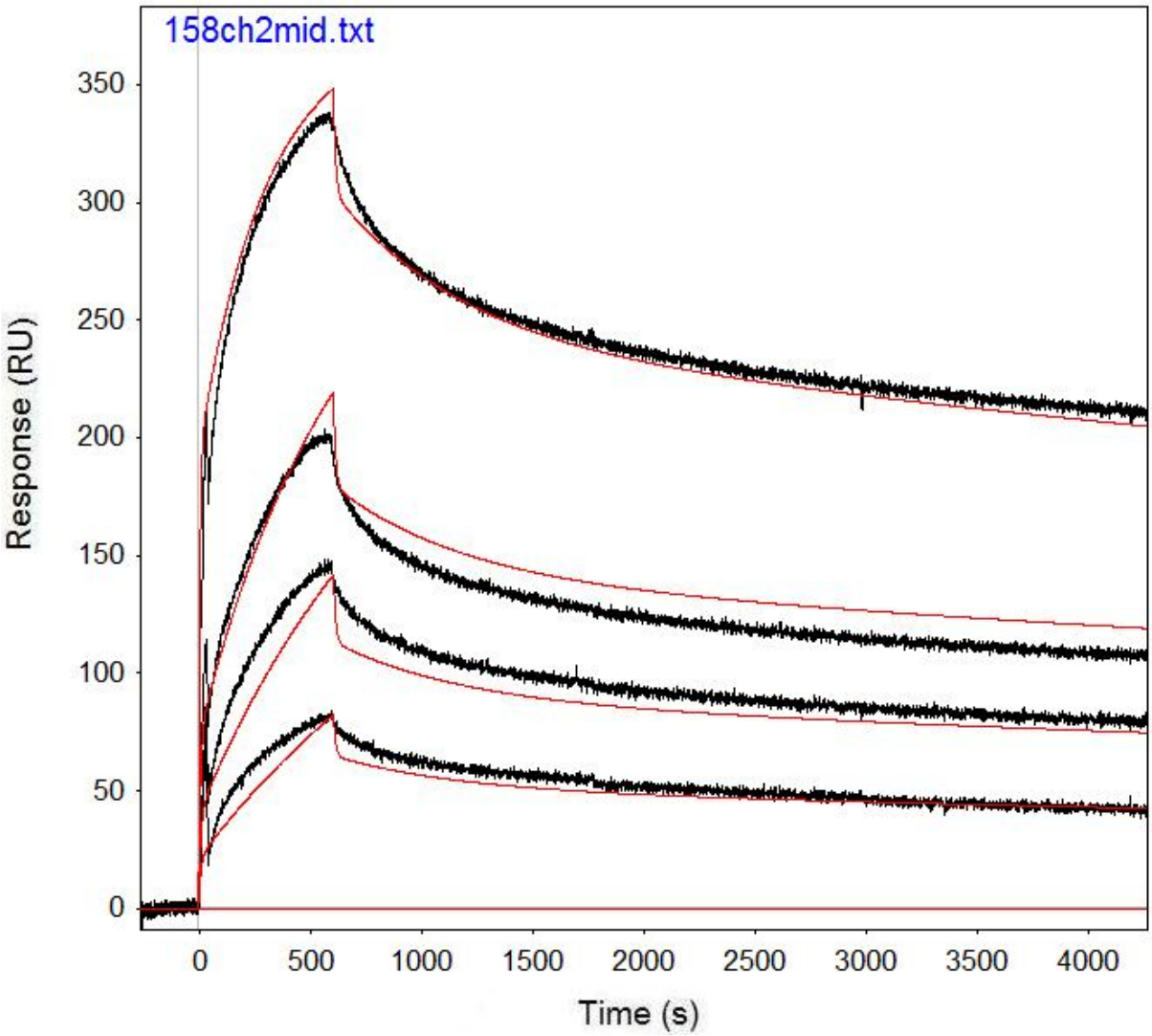

Figure B.80: Run 158, channel 2 model and data graph.

Table B.80: Run 158, channel 2 model parameters.

	kfwd1	krev1	kfwd2	krev2	kfwd3	krev3	ProA (RU)
Value	1725	0.001747	3671	4.53E-05	83825	0.1006	132.4
Error (abs)	19.58	4.661E-05	17.88	1.37E-06	3446	0.004207	0.1358
Error (%)	1.135	2.668	0.487	3.020	4.111	4.182	0.103

Run 171, channel 2: Performed at pH 5.0 in sodium acetate, at an IgG concentration of 1.5 µm. RSSE is 6.622.

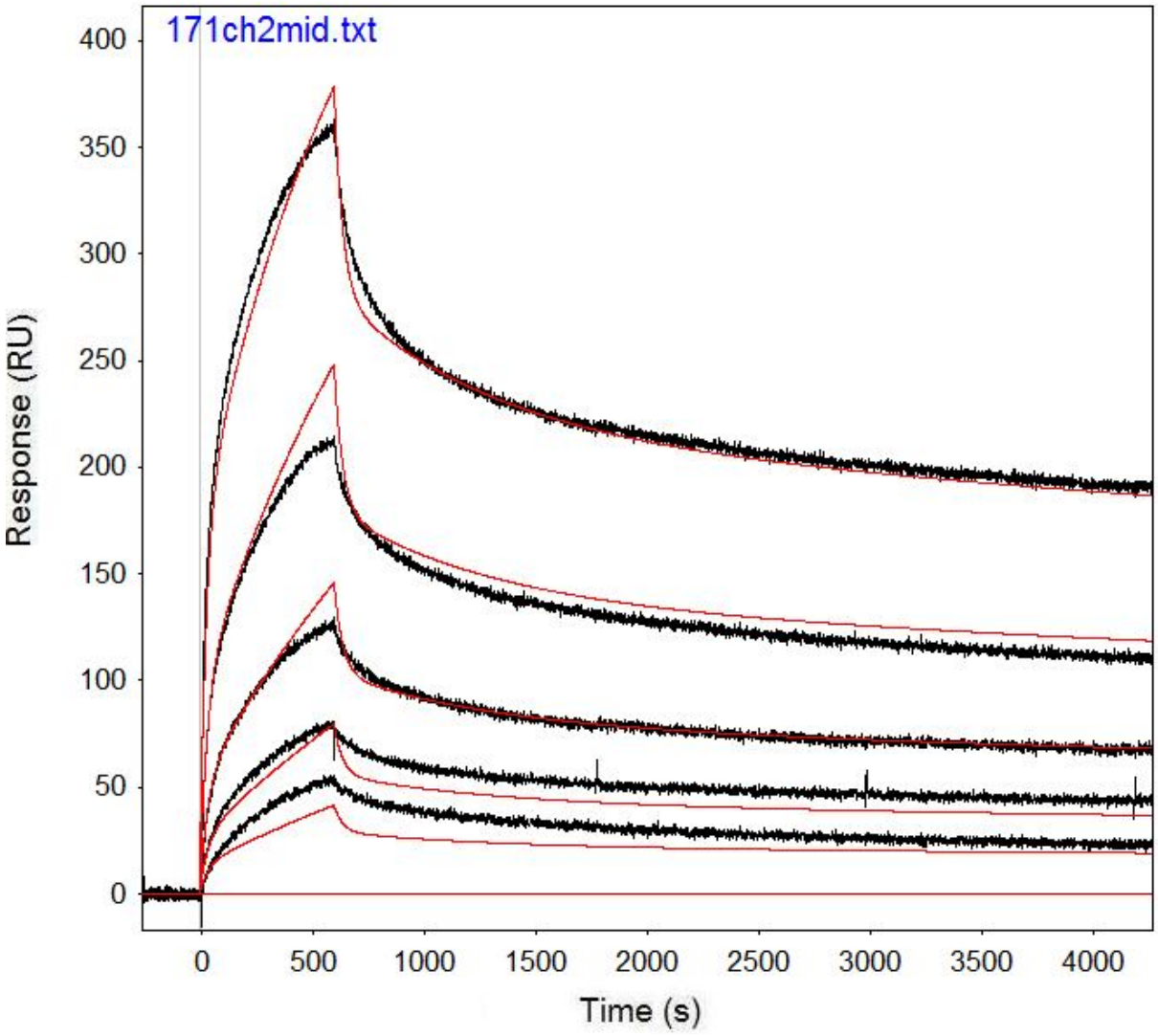

Figure B.81: Run 171, channel 2 model and data graph.

Table B.81: Run 171, channel 2 model parameters.

	kfwd1	krev1	kfwd2	krev2	kfwd3	krev3	ProA (RU)
Value	294.1	0.001421	605.5	3.78E-05	5556	0.02649	225.6
Error (abs)	3.649	4.868E-05	4.833	1.98E-06	91.72	0.000499	0.494
Error (%)	1.241	3.426	0.798	5.241	1.651	1.882	0.219

Run 176, channel 2: Performed at pH 5.0 in sodium acetate, at an IgG concentration of 0.5 µm. RSSE is 6.466.

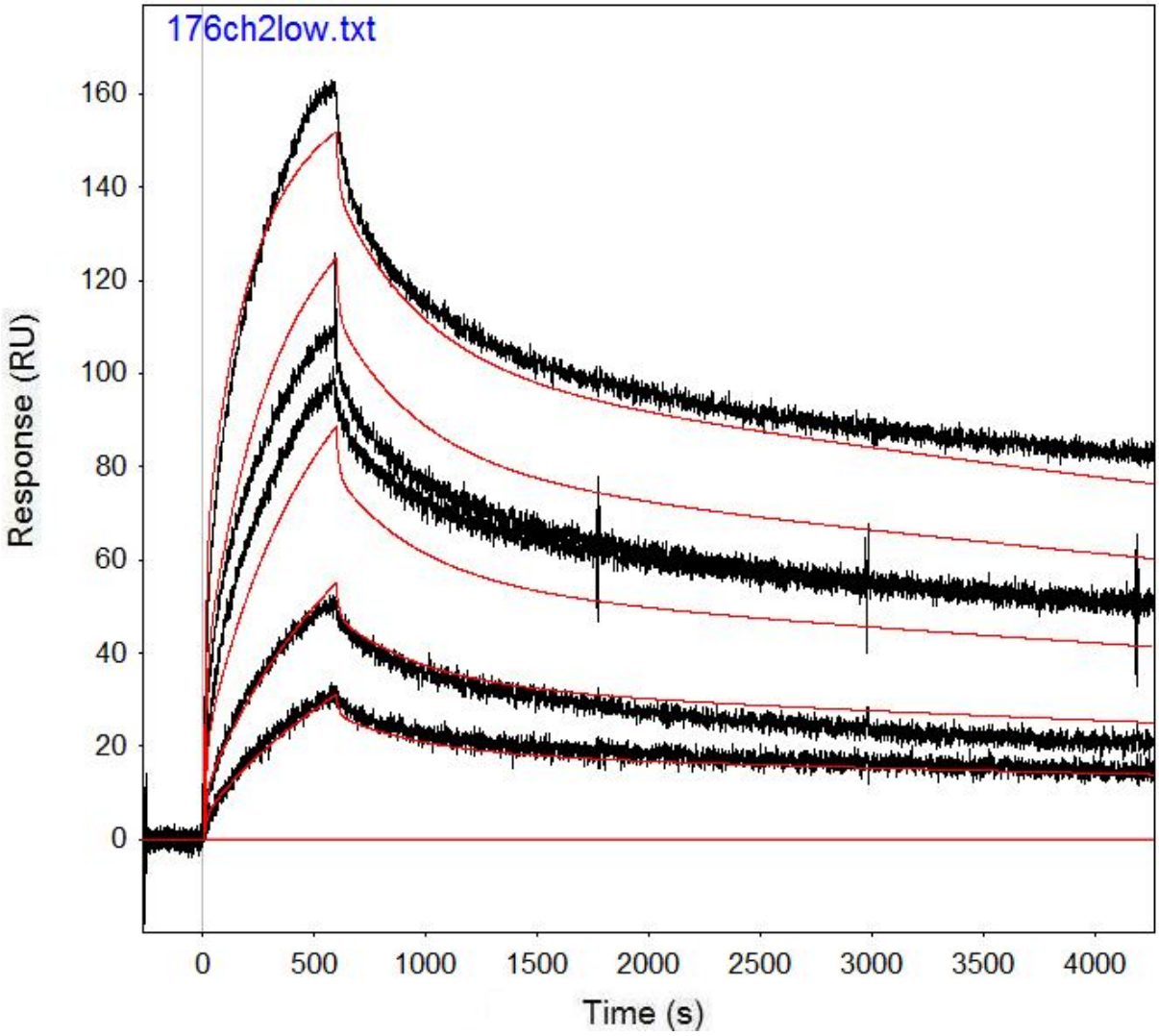

Figure B.82: Run 176, channel 2 model and data graph.

Table B.82: Run 176, channel 2 model parameters.

	kfwd1	krev1	kfwd2	krev2	kfwd3	krev3	ProA (RU)
Value	5629	0.002585	6437	7.63E-05	70902	0.07616	59.46
Error (abs)	104.6	0.0000681	42.01	1.71E-06	5937	0.006559	0.1321
Error (%)	1.858	2.634	0.653	2.241	8.374	8.612	0.222

Run 176, channel 3: Performed at pH 5.0 in sodium acetate, at an IgG concentration of 0.5 µm. RSSE is 1.781.

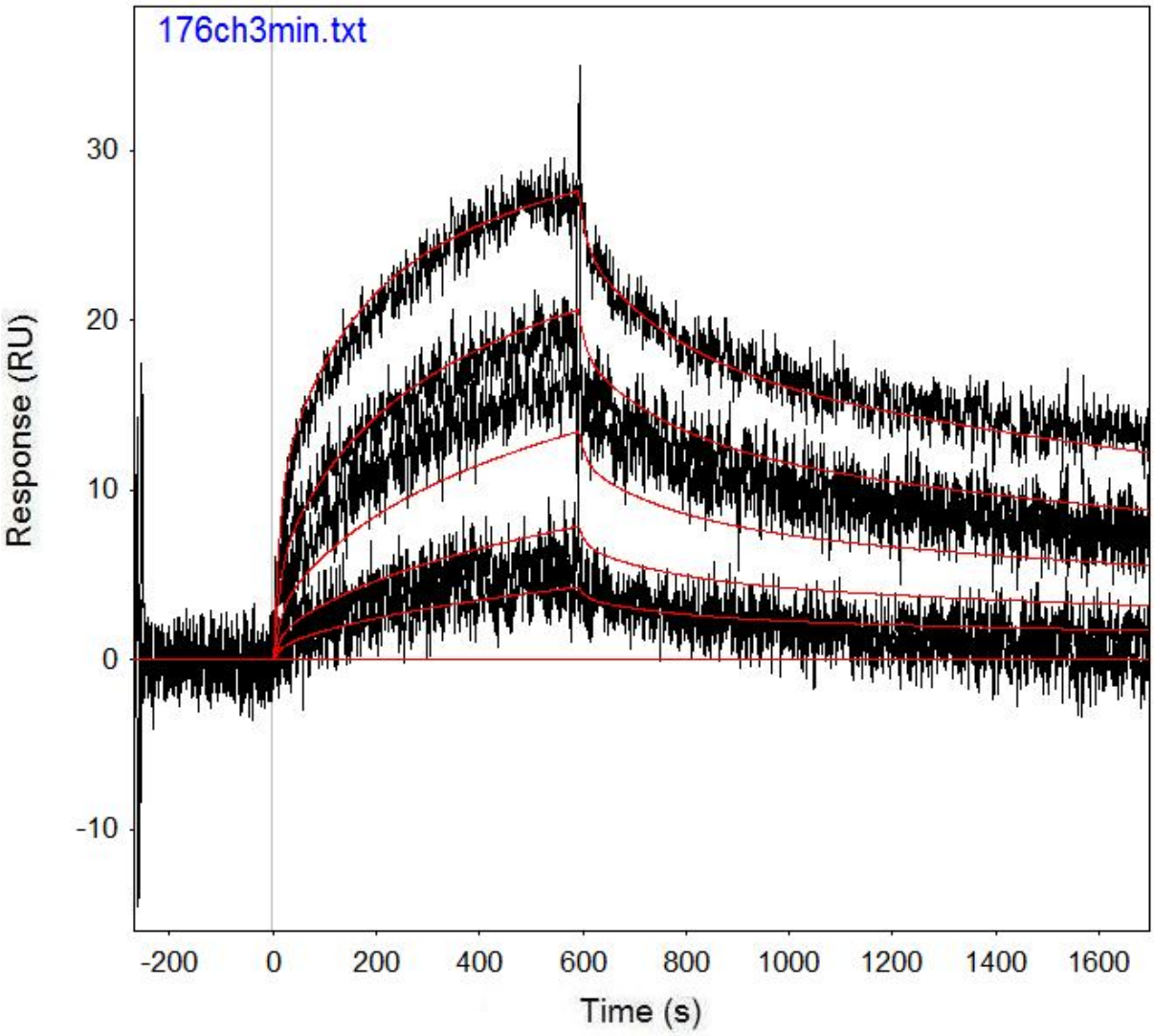

Figure B.83: Run 176, channel 3 model and data graph.

Table B.83: Run 176, channel 3 model parameters.

	kfwd1	krev1	kfwd2	krev2	kfwd3	krev3	ProA (RU)
Value	6301	0.005535	4147	0.000326	41682	0.06999	12.74
Error (abs)	522.4	0.0006209	163.5	3.13E-05	6302	0.01288	0.08052
Error (%)	8.291	11.218	3.943	9.586	15.119	18.403	0.632

Run 181, channel 2: Performed at pH 5.0 in sodium acetate, at an IgG concentration of 0.5 µm. RSSE is 6.028.

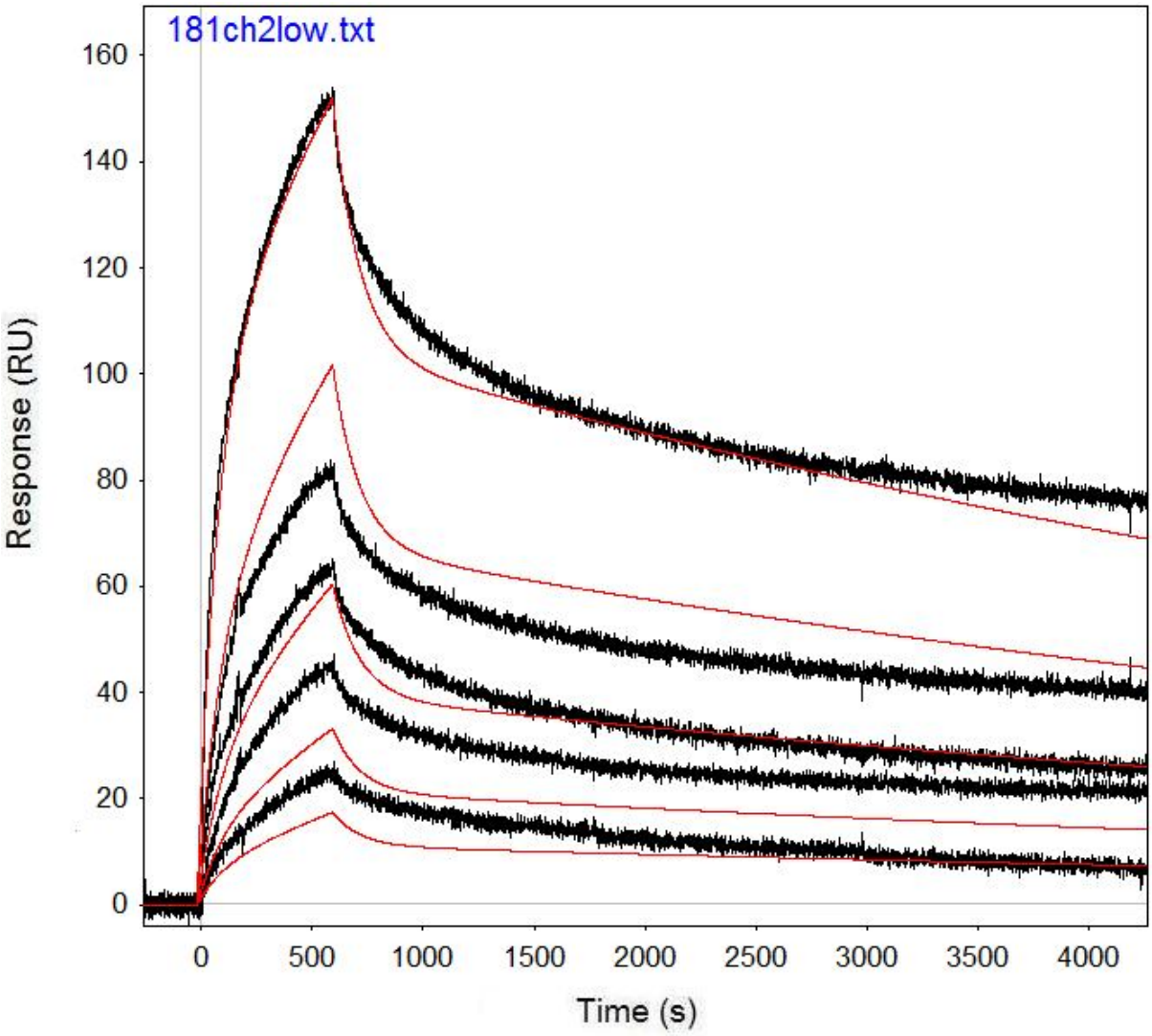

Figure B.84: Run 181, channel 2 model and data graph.

Table B.84: Run 181, channel 2 model parameters.

	kfwd1	krev1	kfwd2	krev2	kfwd3	krev3	ProA (RU)
Value	2483	0.0001124	7044	0.008284			84.63
Error (abs)	18.8	1.017E-06	125.9	0.000164			0.3791
Error (%)	0.757	0.905	1.787	1.976			0.448

Run 181, channel 5: Performed at pH 5.0 in sodium acetate, at an IgG concentration of 0.5 µm. RSSE is 9.984.

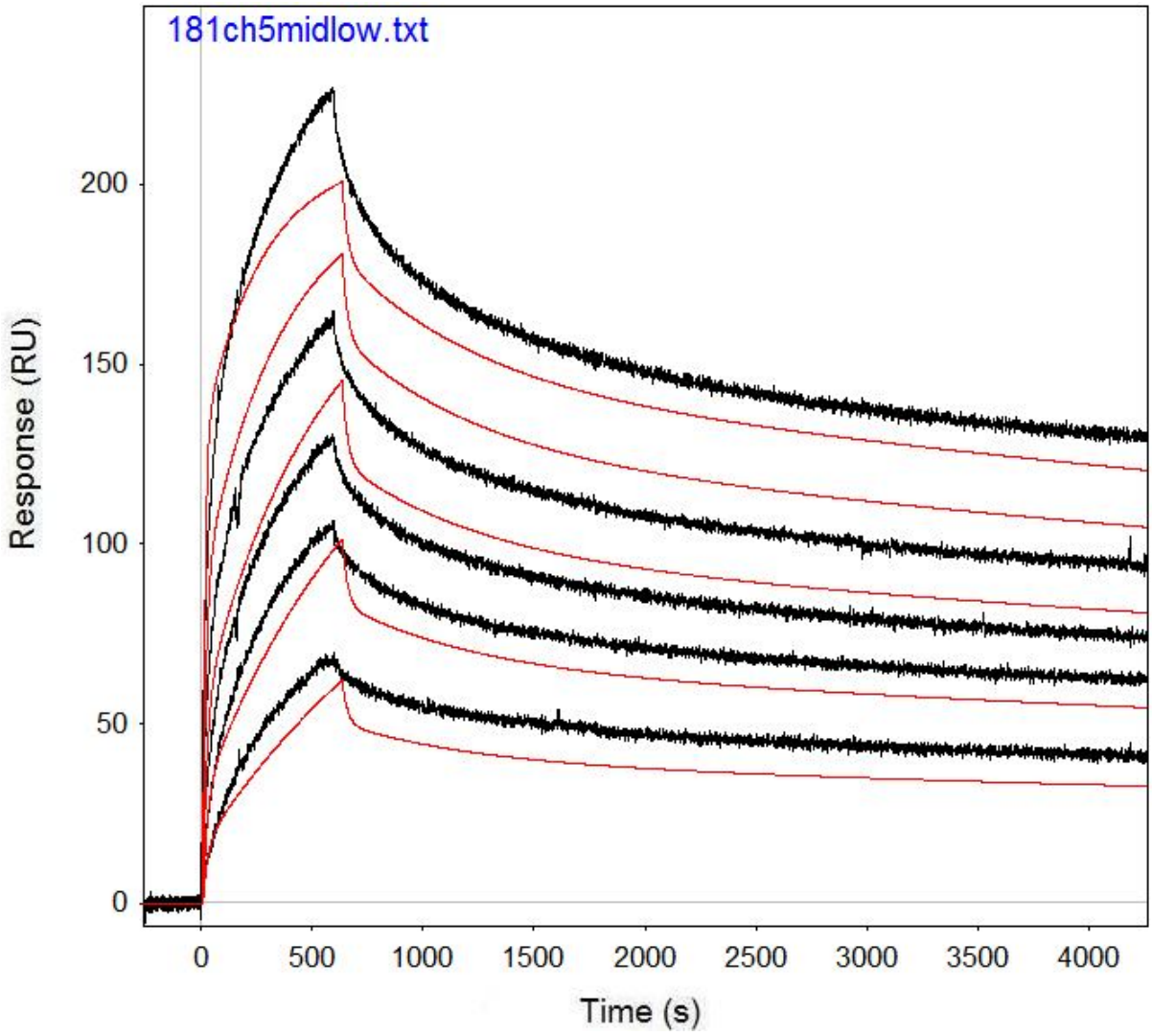

Figure B.85: Run 181, channel 5 model and data graph.

Table B.85: Run 181, channel 5 model parameters.

	kfwd1	krev1	kfwd2	krev2	kfwd3	krev3	ProA (RU)
Value	11428	4.899E-05	5245	0.001639	106600	0.0428	72.32
Error (abs)	116.7	2.799E-06	119.6	9.07E-05	5360	0.002294	0.1291
Error (%)	1.021	5.713	2.280	5.536	5.028	5.360	0.179

Run 187, channel 2: Performed at pH 5.0 in sodium acetate, at an IgG concentration of 1.067 µm. RSSE is 3.70.

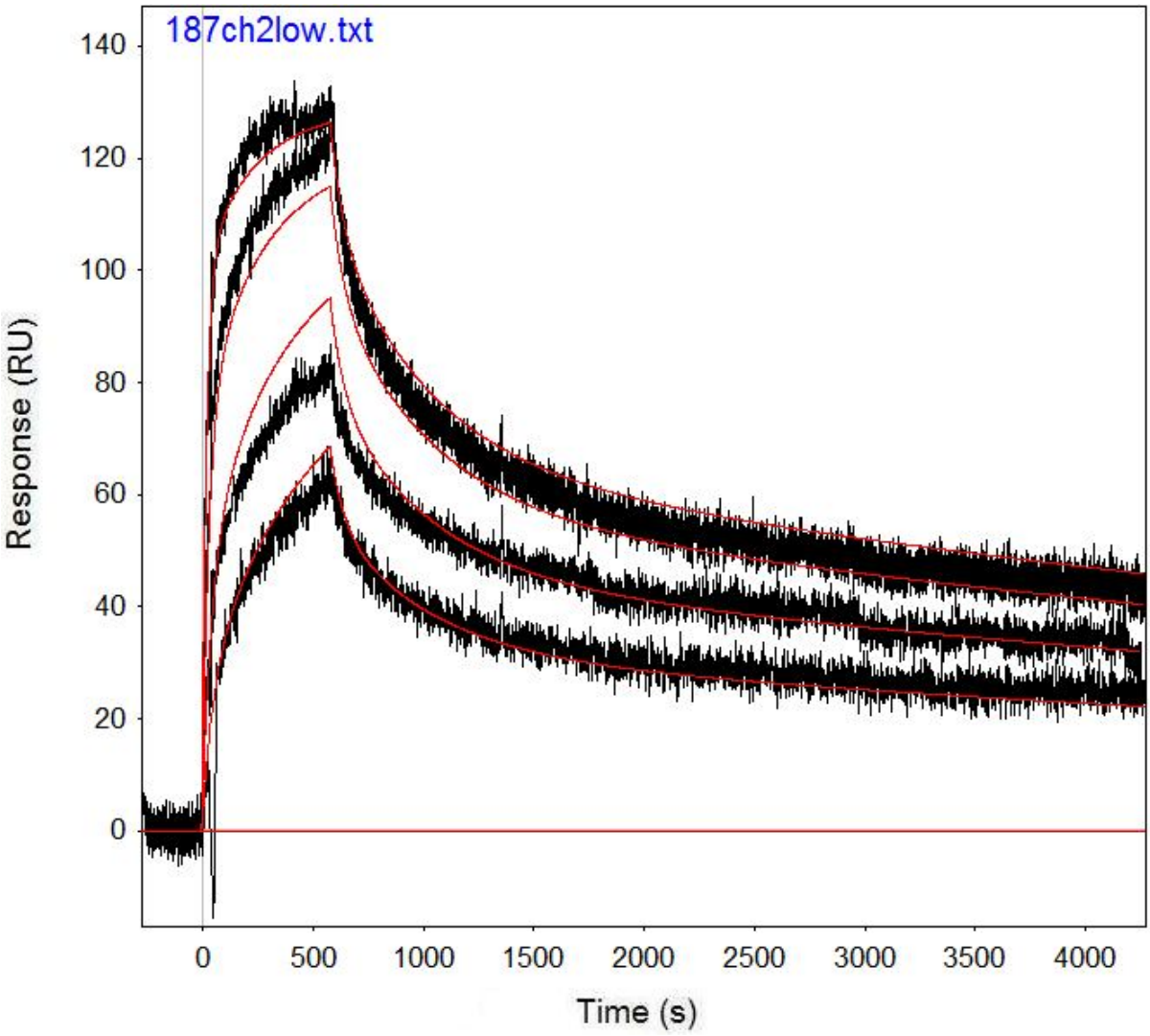

Figure B.86: Run 187, channel 2 model and data graph.

Table B.86: Run 187, channel 2 model parameters.

	kfwd1	krev1	kfwd2	krev2	kfwd3	krev3	ProA (RU)
Value	3395	9.795E-05	4708	0.002282	16106	0.01672	45.91
Error (abs)	22.38	1.833E-06	92.25	4.67E-05	360.2	0.000539	0.05488
Error (%)	0.659	1.871	1.959	2.047	2.236	3.226	0.120

Run 187, channel 5: Performed at pH 5.0 in sodium acetate, at an IgG concentration of 1.067 µm. RSSE is 9.193.

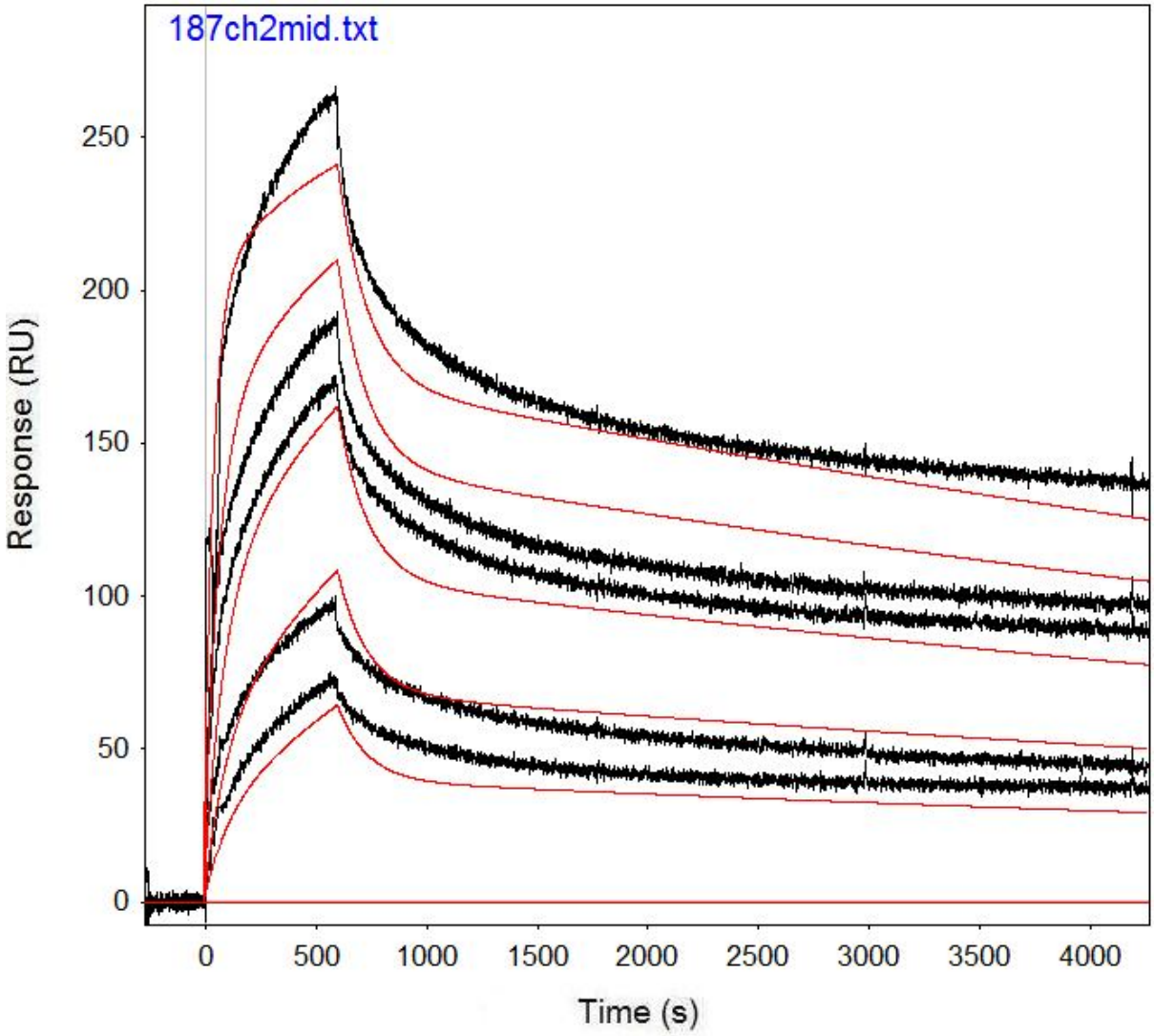

Figure B.87: Run 187, channel 5 model and data graph.

Table B.87: Run 187, channel 5 model parameters.

	kfwd1	krev1	kfwd2	krev2	kfwd3	krev3	ProA (RU)
Value	1553	0.0000842	4602	0.007504			90.93
Error (abs)	6.574	7.582E-07	59.36	0.000103			0.1425
Error (%)	0.423	0.900	1.290	1.377			0.157

Run 192, channel 2: Performed at pH 5.0 in sodium acetate, at an IgG concentration of 3.0 µm. RSSE is 10.54.

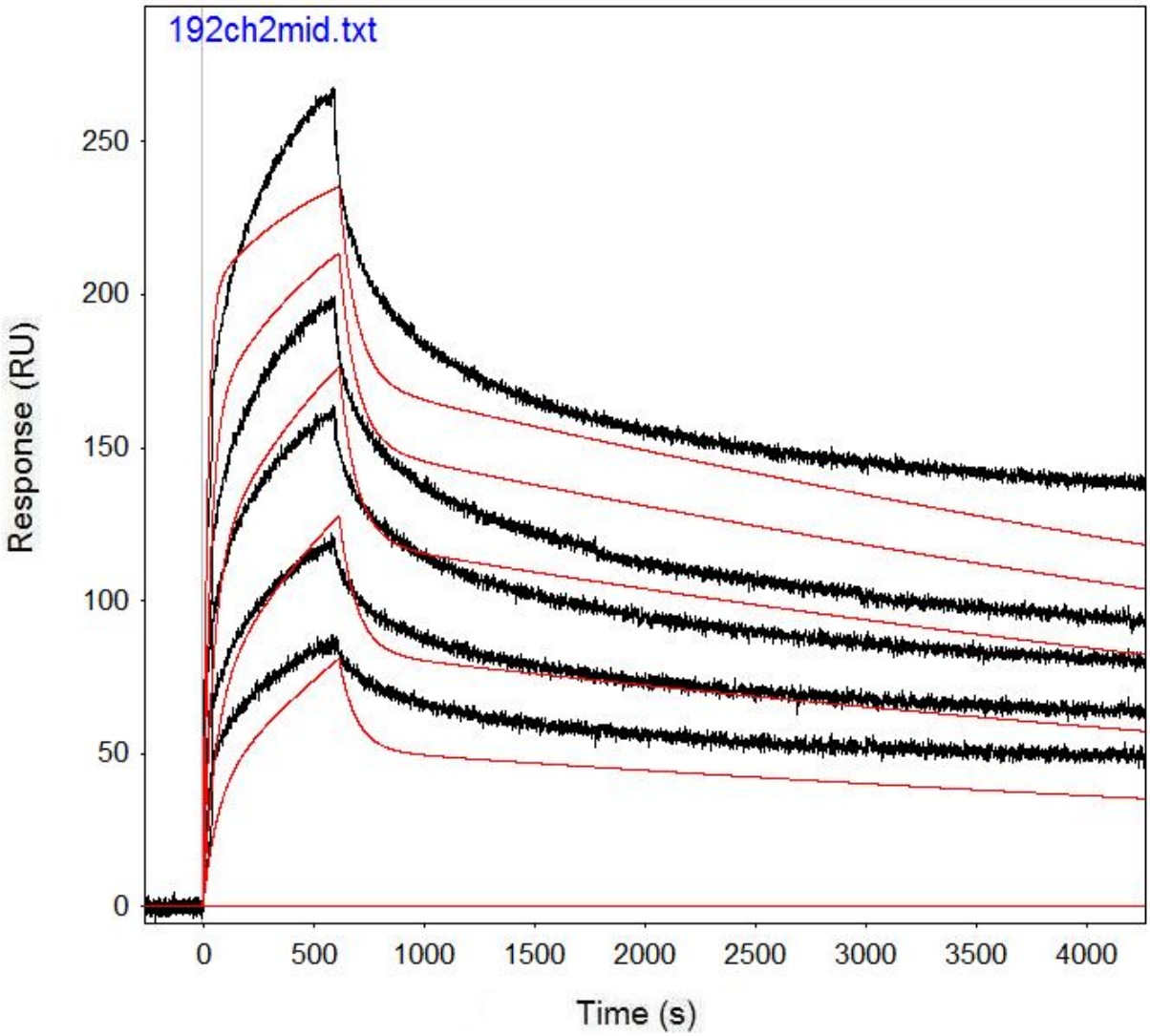

Figure B.88: Run 192, channel 2 model and data graph.

Table B.88: Run 192, channel 2 model parameters.

	kfwd1	krev1	kfwd2	krev2	kfwd3	krev3	ProA (RU)
Value	2305	0.0001025	11447	0.01303			85.48
Error (abs)	10.1	7.682E-07	201.4	0.00023			0.1337
Error (%)	0.438	0.749	1.759	1.764			0.156

Run 198, channel 2: Performed at pH 5.0 in sodium acetate, at an IgG concentration of 0.5 µm. RSSE is 4.977.

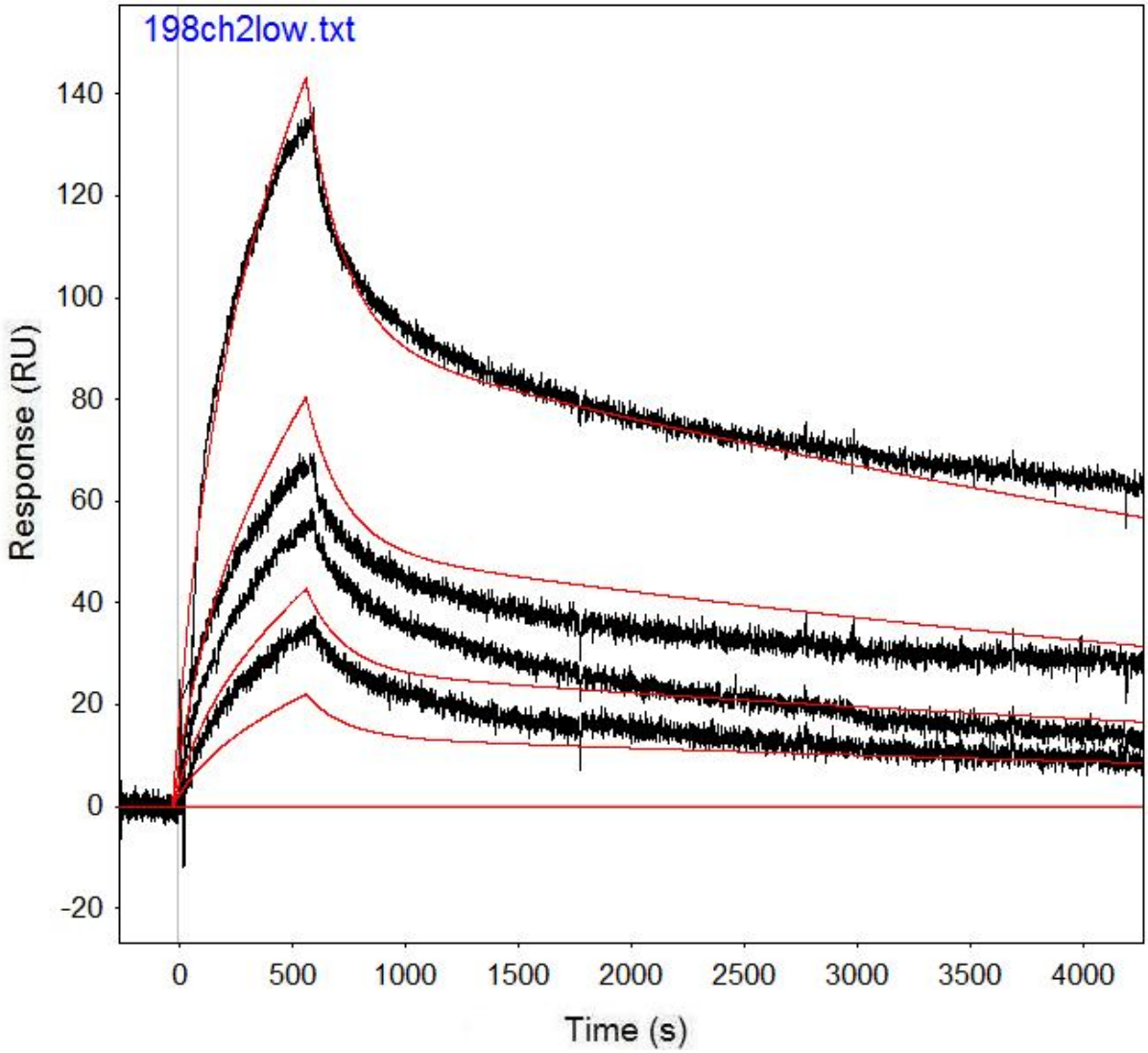

Figure B.89: Run 198, channel 2 model and data graph.

Table B.89: Run 198, channel 2 model parameters.

	kfwd1	krev1	kfwd2	krev2	kfwd3	krev3	ProA (RU)
Value	826.5	0.0001301	1798	0.006192			161.5
Error (abs)	13	1.15E-06	33.87	0.000112			2.063
Error (%)	1.573	0.884	1.884	1.814			1.277

B.2: Data from IgG in PBST Experiments

Run 189, channel 4: Performed at pH 4.5 in sodium acetate, at an IgG concentration of 1.067 µm. RSSE is 2.723.

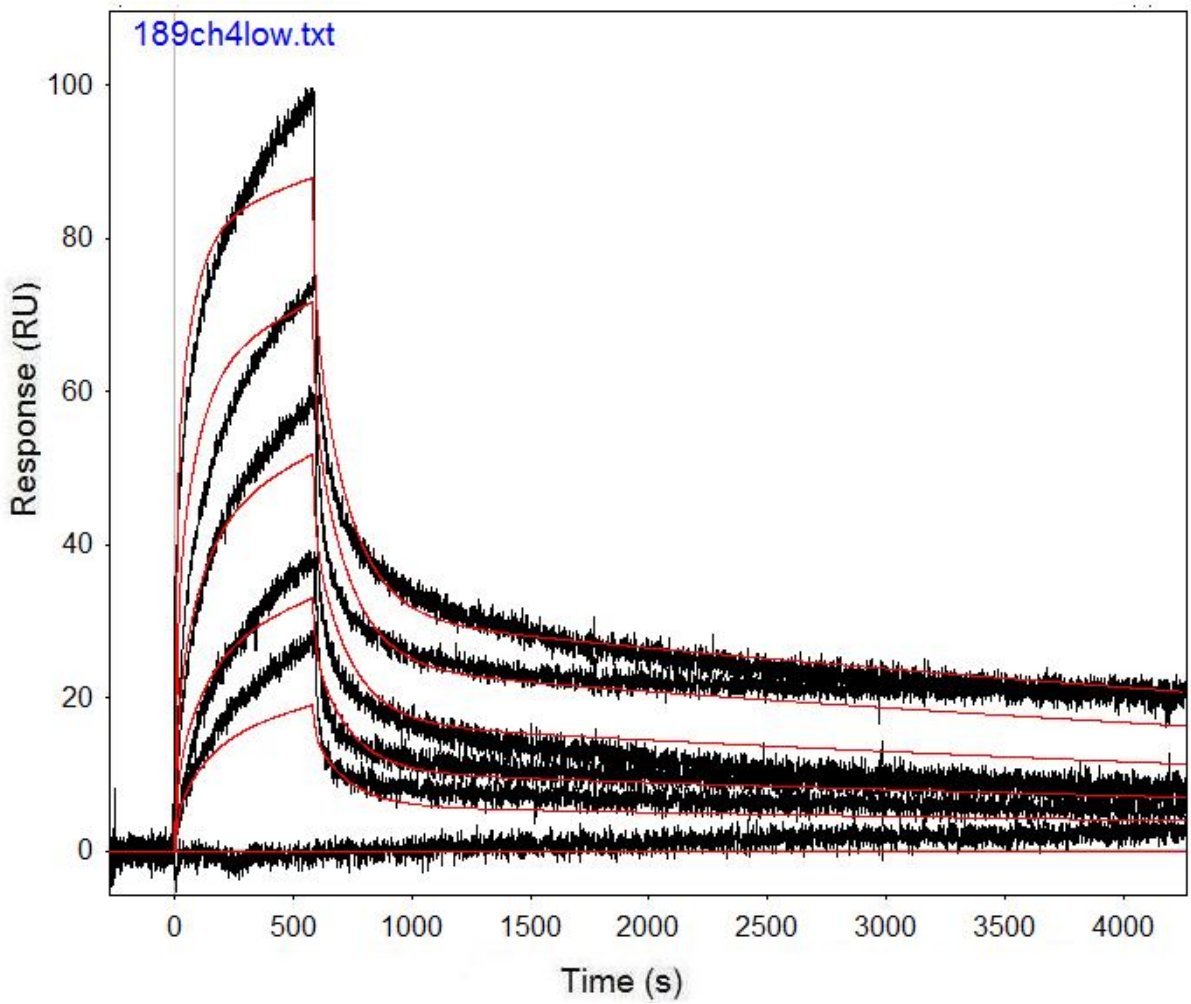

Figure B.90: Run 189, channel 4 model and data graph.

Table B.90: Run 189, channel 4 model parameters.

	kfwd1	krev1	kfwd2	krev2	kfwd3	krev3	ProA (RU)
Value	46210	0.0763	1630	0.000108	10538	0.006885	37.22
Error (abs)	2339	0.004519	9.192	1.47E-06	211.7	9.06E-05	0.07445
Error (%)	5.062	5.923	0.564	1.370	2.009	1.315	0.200

Run 220, channel 3: Performed at pH 4.5 in sodium acetate, at an IgG concentration of 3.0 µm. RSSE is 2.92.

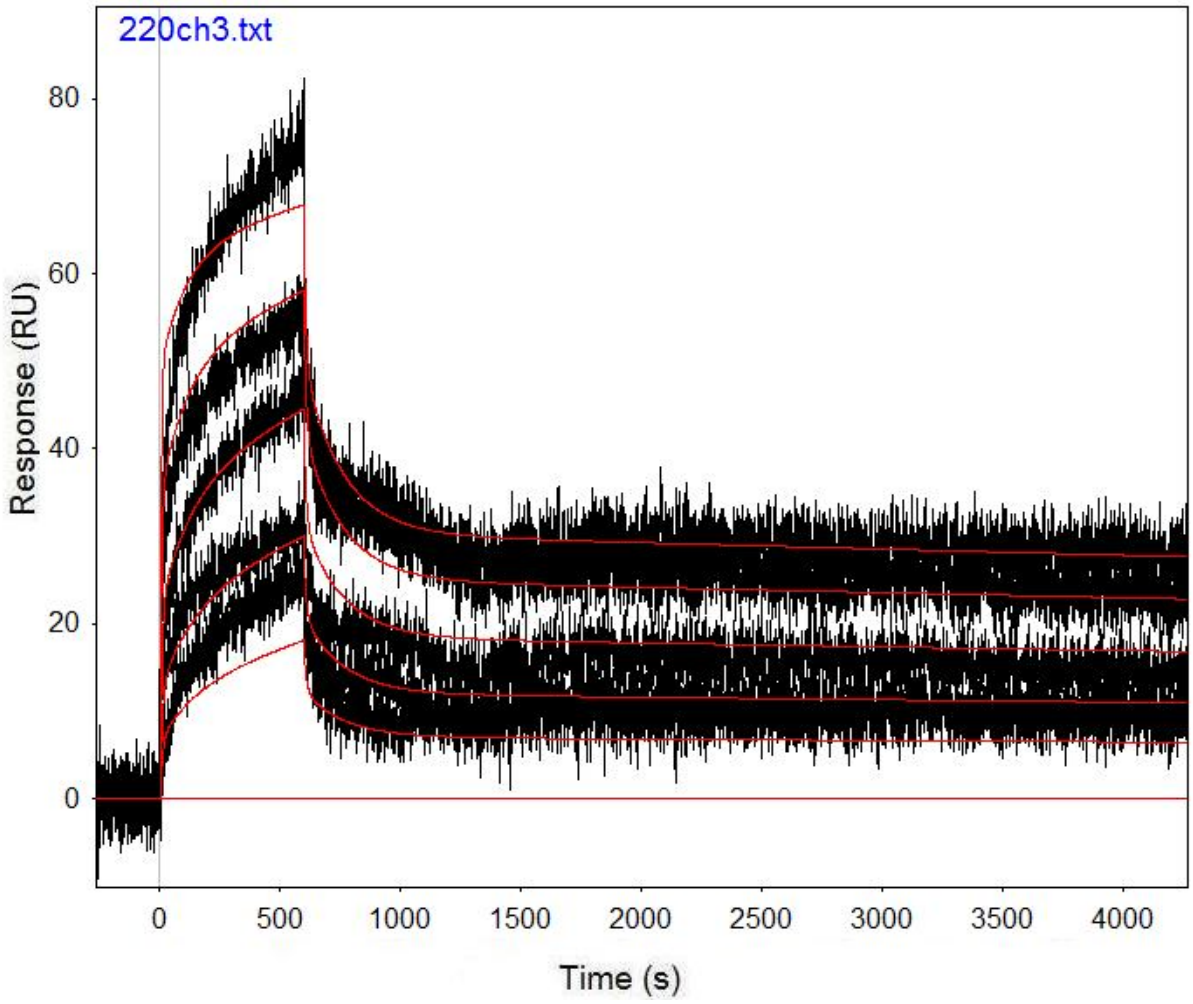

Figure B.91: Run 220, channel 3 model and data graph.

Table B.91: Run 220, channel 3 model parameters.

	kfwd1	krev1	kfwd2	krev2	kfwd3	krev3	ProA (RU)
Value	48197	0.1	959.6	2.52E-05	2840	0.006171	26.79
Error (abs)	2333	0.00553	5.682	1.34E-06	107.6	0.000159	0.05545
Error (%)	4.841	5.530	0.592	5.316	3.789	2.573	0.207

Run 220, channel 4: Performed at pH 4.5 in sodium acetate, at an IgG concentration of 3.0 µm. RSSE is 5.088.

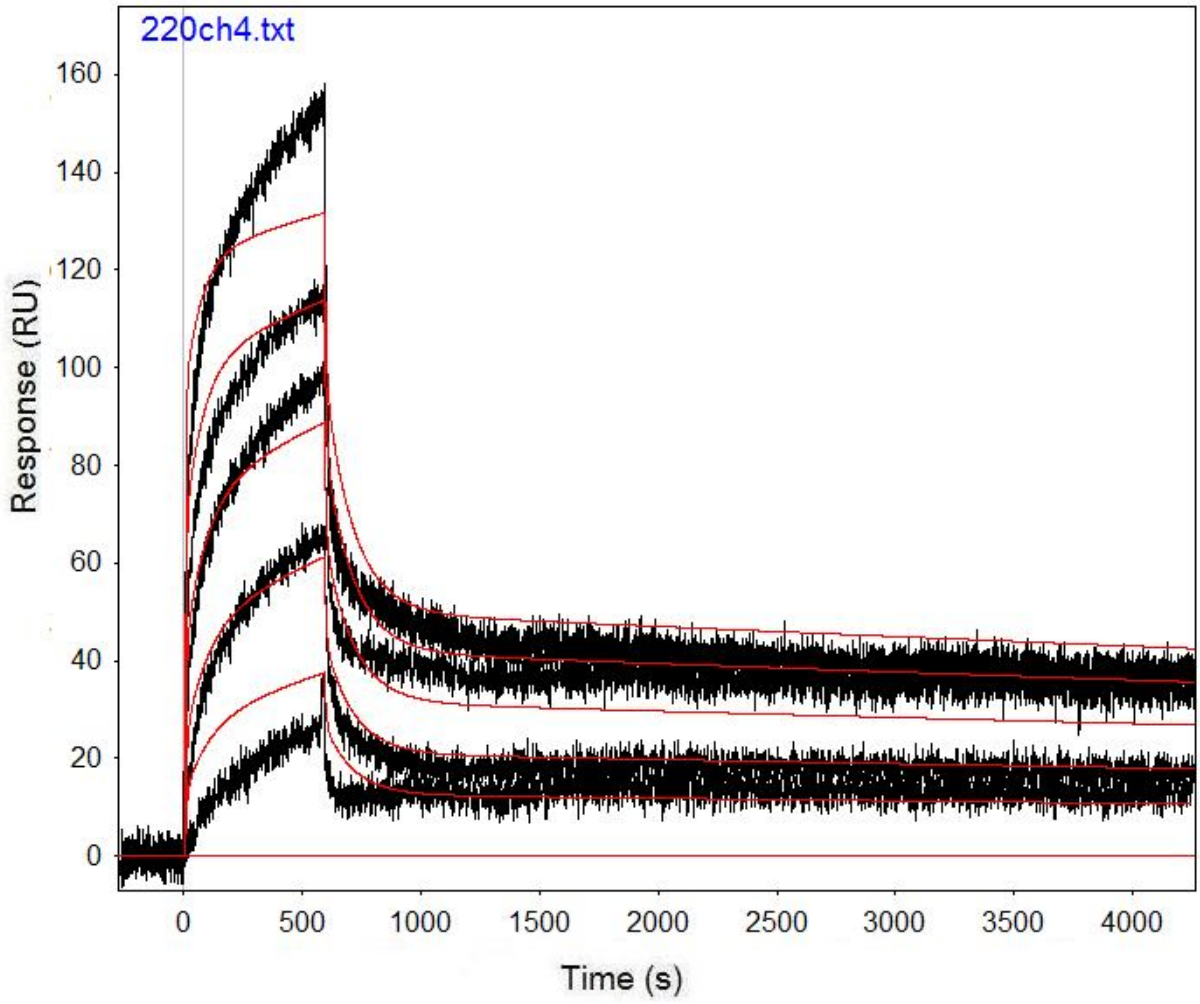

Figure B.92: Run 220, channel 4 model and data graph.

Table B.92: Run 220, channel 4 model parameters.

	kfwd1	krev1	kfwd2	krev2	kfwd3	krev3	ProA (RU)
Value	70223	0.1479	929.7	4.47E-05	5518	0.008435	51.58
Error (abs)	4147	0.009674	5.258	1.32E-06	159.1	0.000159	0.09631
Error (%)	5.905	6.541	0.566	2.948	2.883	1.883	0.187

Run 237, channel 4: Performed at pH 4.0 in sodium acetate, at an IgG concentration of 0.5 µm. RSSE is 3.922.

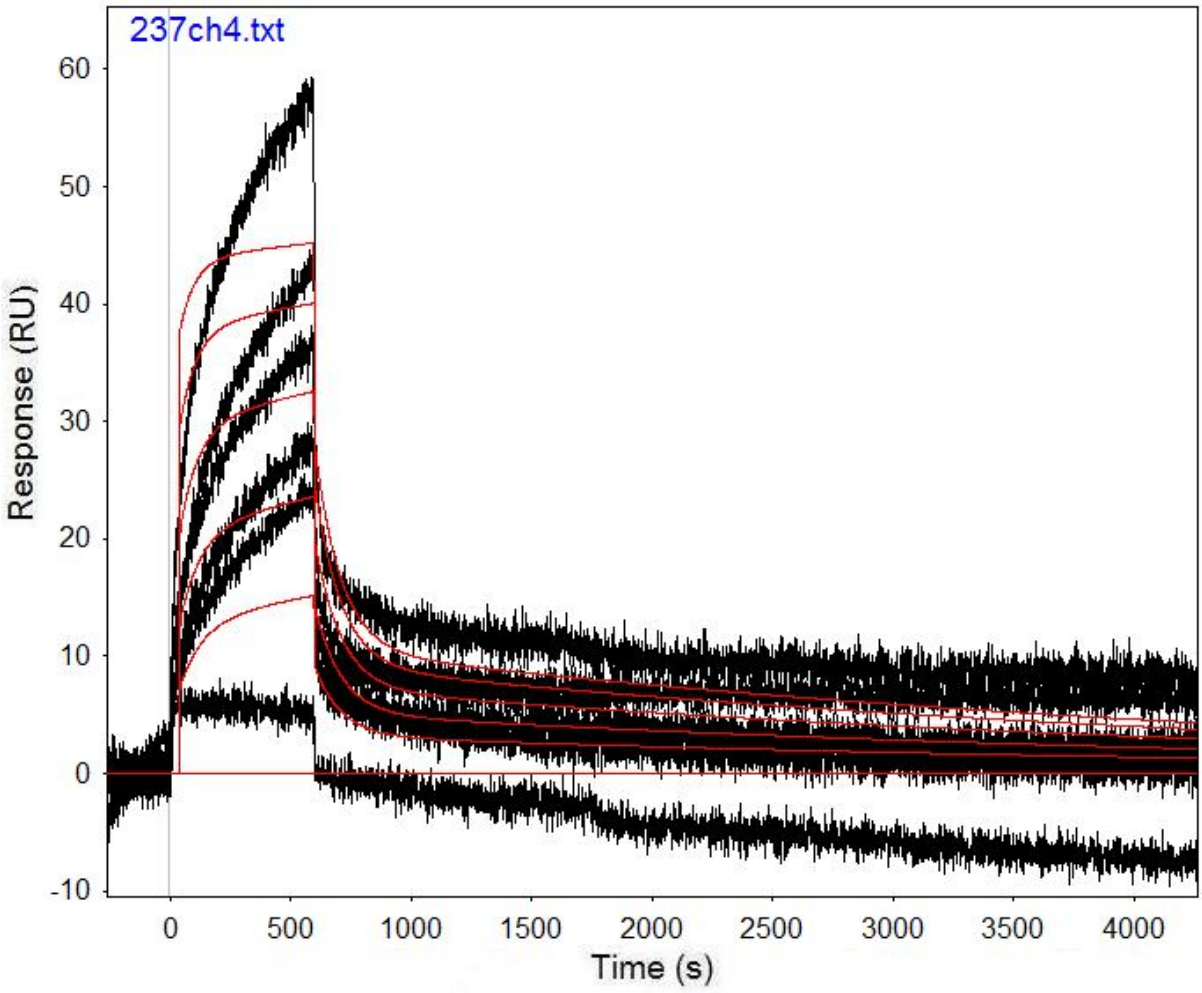

Figure B.93: Run 237, channel 4 model and data graph.

Table B.93: Run 237, channel 4 model parameters.

	kfwd1	krev1	kfwd2	krev2	kfwd3	krev3	ProA (RU)
Value	5164	0.000245	48901	0.00931	3014000	0.5878	17.24
Error (abs)	97.88	6.793E-06	2731	0.000364	633500	0.1262	0.07389
Error (%)	1.895	2.773	5.585	3.913	21.019	21.470	0.429

Run 248, channel 4: Performed at pH 4.0 in sodium acetate, at an IgG concentration of 1.067 µm. RSSE is 3.402.

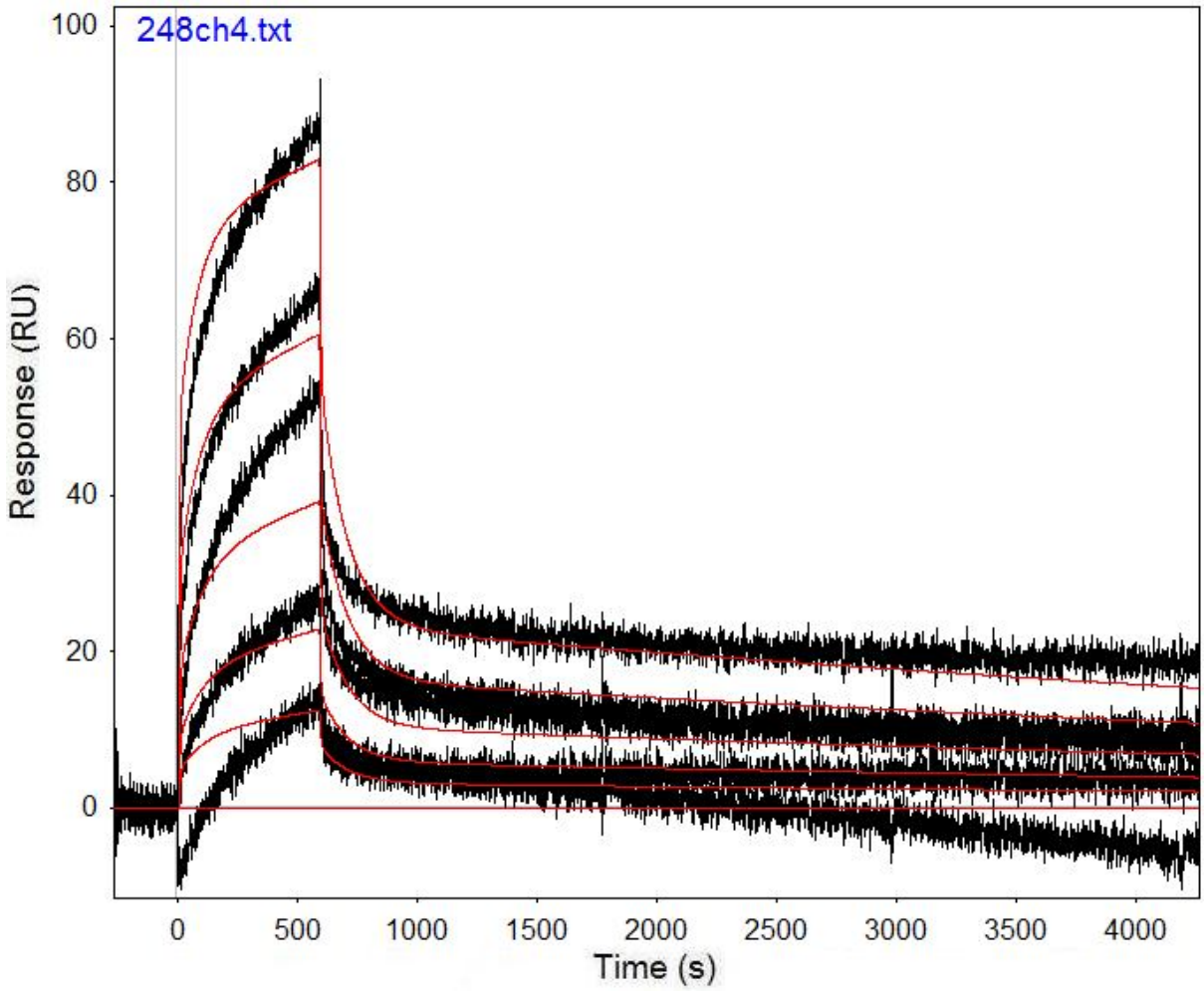

Figure B.94: Run 248, channel 4 model and data graph.

Table B.94: Run 248, channel 4 model parameters.

	kfwd1	krev1	kfwd2	krev2	kfwd3	krev3	ProA (RU)
Value	720.2	0.0001143	5660	0.008892	110900	0.198	42.92
Error (abs)	6.995	2.469E-06	189.5	0.000197	7951	0.01533	0.1831
Error (%)	0.971	2.160	3.348	2.215	7.170	7.742	0.427

Run 258, channel 4: Performed at pH 4.0 in sodium acetate, at an IgG concentration of 3.0 µm. RSSE is 3.582.

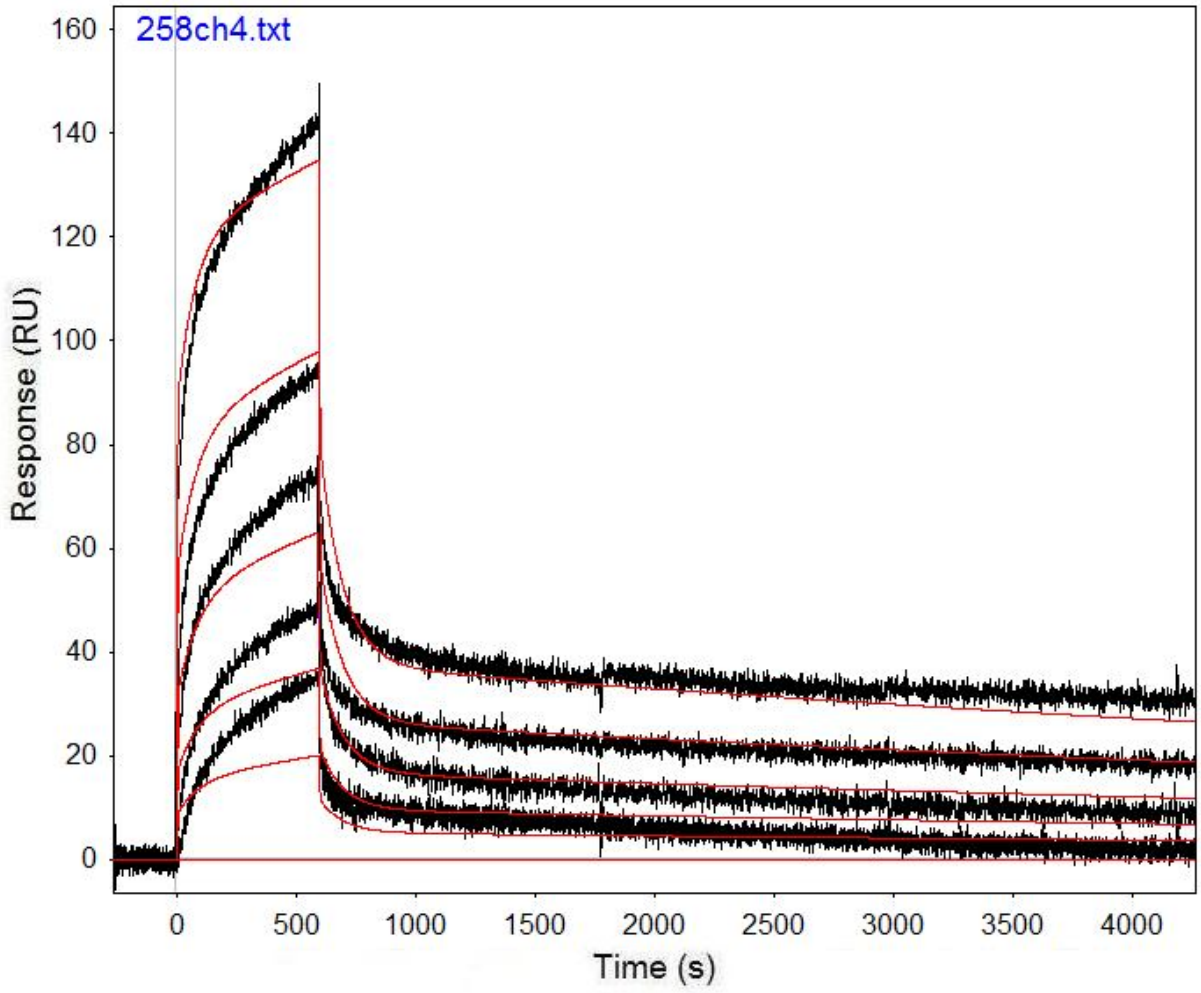

Figure B.95: Run 258, channel 4 model and data graph.

Table B.95: Run 258, channel 4 model parameters.

	kfwd1	krev1	kfwd2	krev2	kfwd3	krev3	ProA (RU)
Value	244.5	9.554E-05	1898	0.01025	74083	0.3248	70.69
Error (abs)	1.512	1.505E-06	48.77	0.000175	3483	0.01621	0.1965
Error (%)	0.618	1.575	2.570	1.704	4.701	4.991	0.278

Run 263, channel 4: Performed at pH 4.0 in sodium acetate, at an IgG concentration of 3.0 µm. RSSE is 4.363.

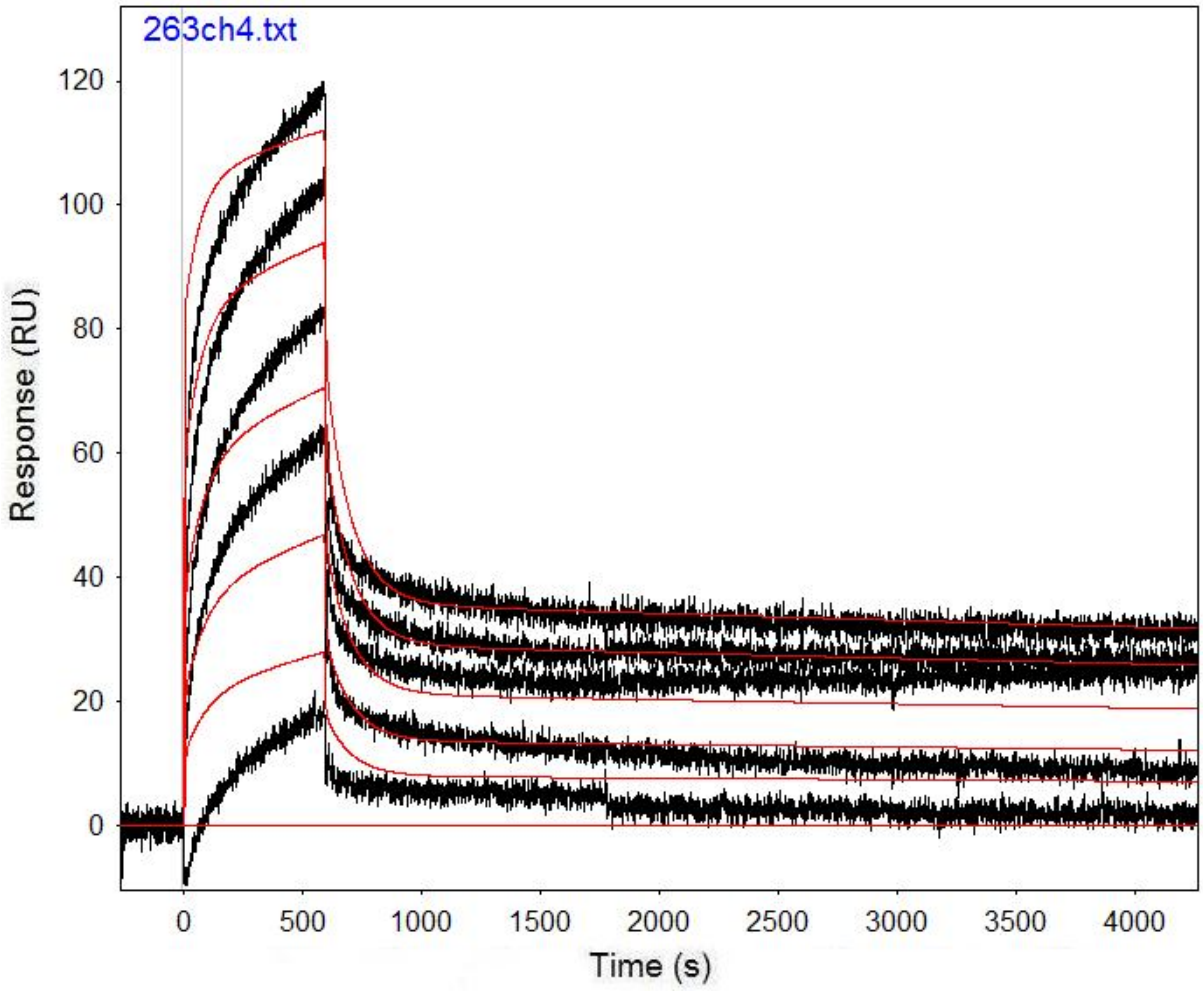

Figure B.96: Run 263, channel 4 model and data graph.

Table B.96: Run 263, channel 4 model parameters.

	kfwd1	krev1	kfwd2	krev2	kfwd3	krev3	ProA (RU)
Value	638.7	3.283E-05	4643	0.009398	119500	0.2519	45.85
Error (abs)	4.102	1.548E-06	143	0.000191	7938	0.01787	0.09948
Error (%)	0.642	4.715	3.080	2.032	6.643	7.094	0.217

Run 280, channel 4: Performed at pH 3.5 in sodium acetate, at an IgG concentration of 1.067 µm. RSSE is 7.355.

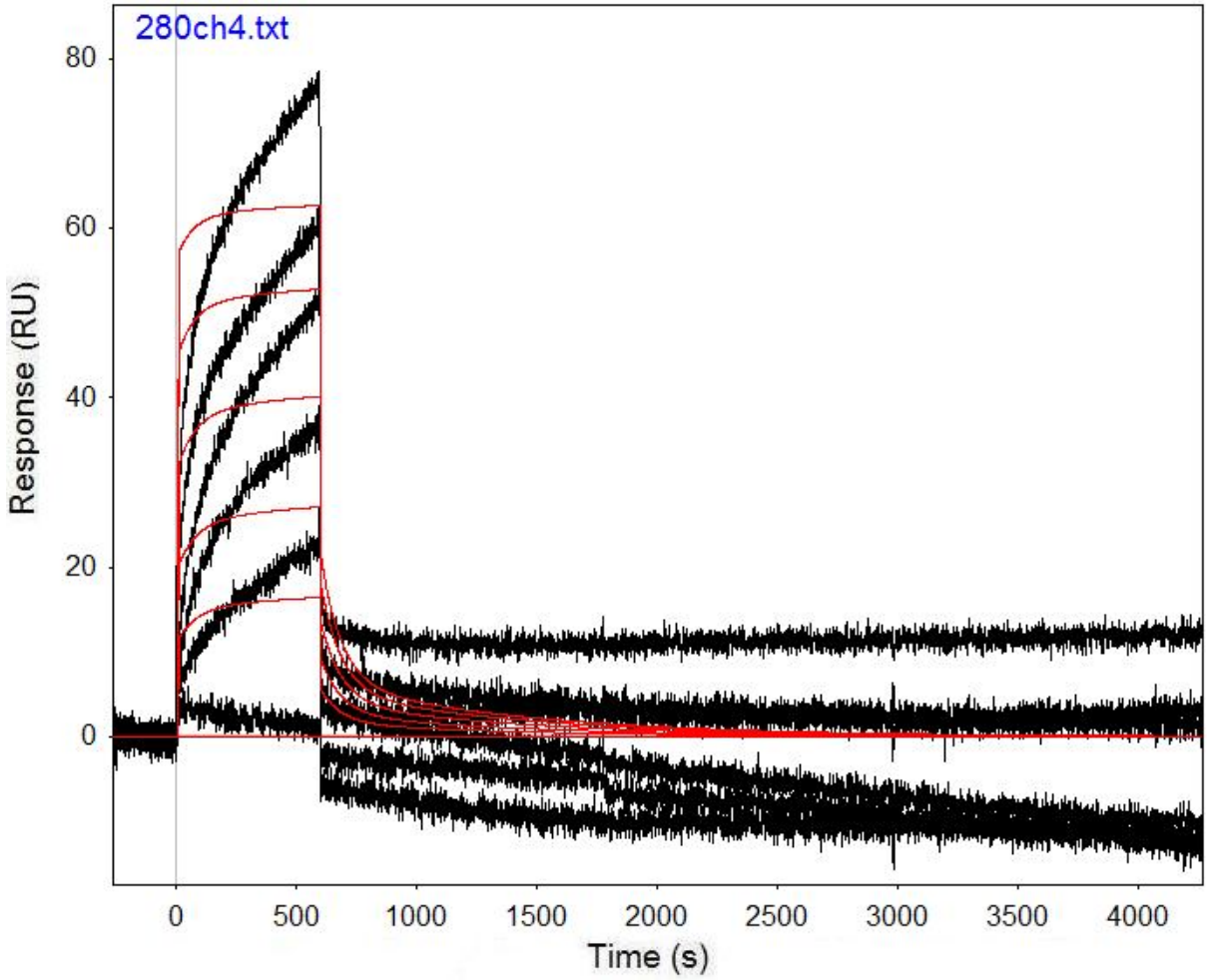

Figure B.97: Run 280, channel 4 model and data graph.

Table B.97: Run 280, channel 4 model parameters.

	kfwd1	krev1	kfwd2	krev2	kfwd3	krev3	ProA (RU)
Value	961.2	0.001209	11913	0.01187	7896000	2.974	25.66
Error (abs)	131.7	0.0001245	1793	0.001508	2801000	1.064	0.1805
Error (%)	13.702	10.298	15.051	12.704	35.474	35.777	0.703

Run 290, channel 4: Performed at pH 3.5 in sodium acetate, at an IgG concentration of 3.0 µm. RSSE is 10.65.

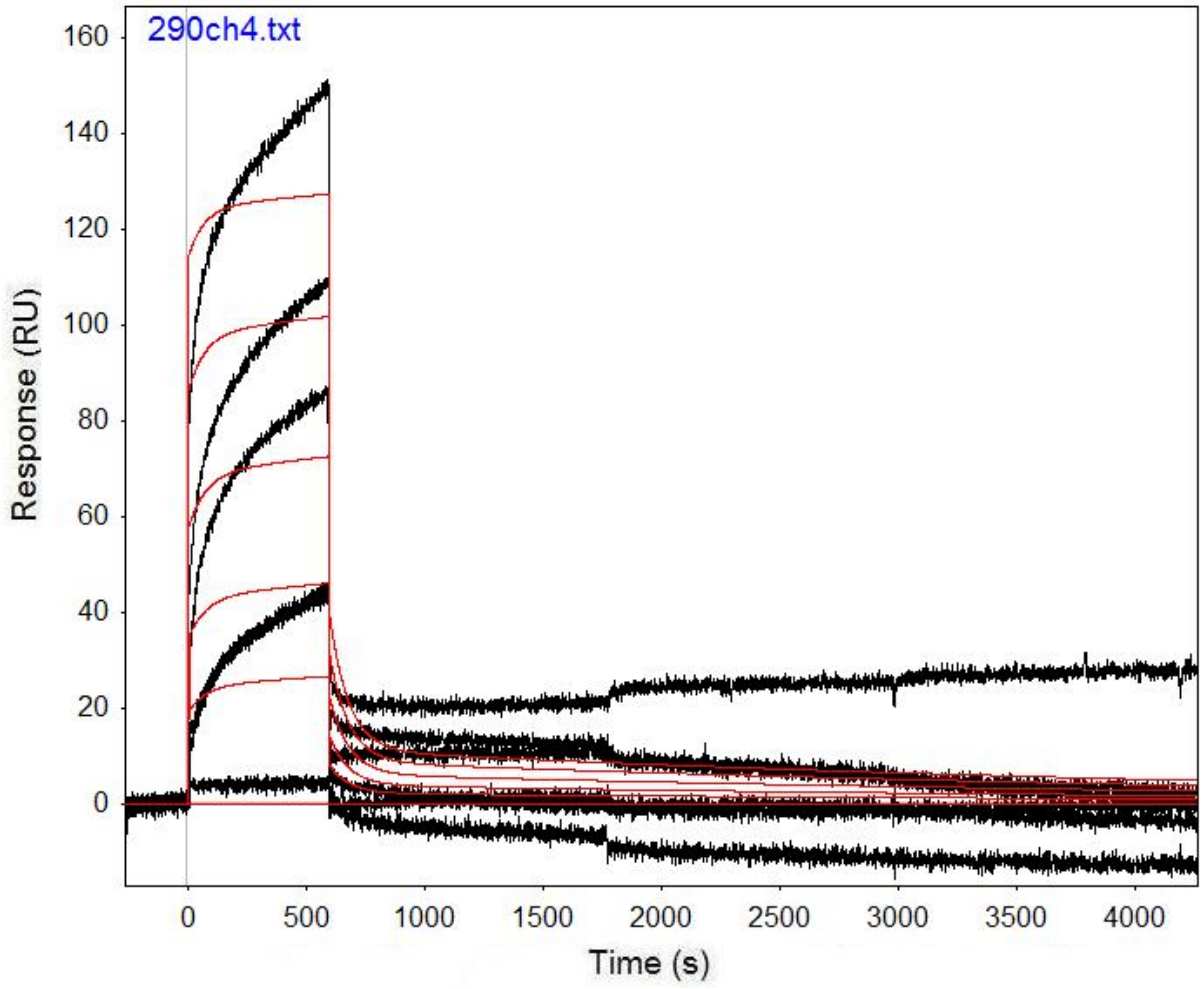

Figure B.98: Run 290, channel 4 model and data graph.

Table B.98: Run 290, channel 4 model parameters.

	kfwd1	krev1	kfwd2	krev2	kfwd3	krev3	ProA (RU)
Value	149.8	0.0002294	2782	0.01243	4255000	6.241	56.65
Error (abs)	5.876	1.754E-05	316.9	0.000985	3920000	5.754	0.3469
Error (%)	3.923	7.646	11.391	7.924	92.127	92.197	0.612

Run 350, channel 4: Performed at pH 3.0 in sodium acetate, at an IgG concentration of 3.0 µm. RSSE is 7.049.

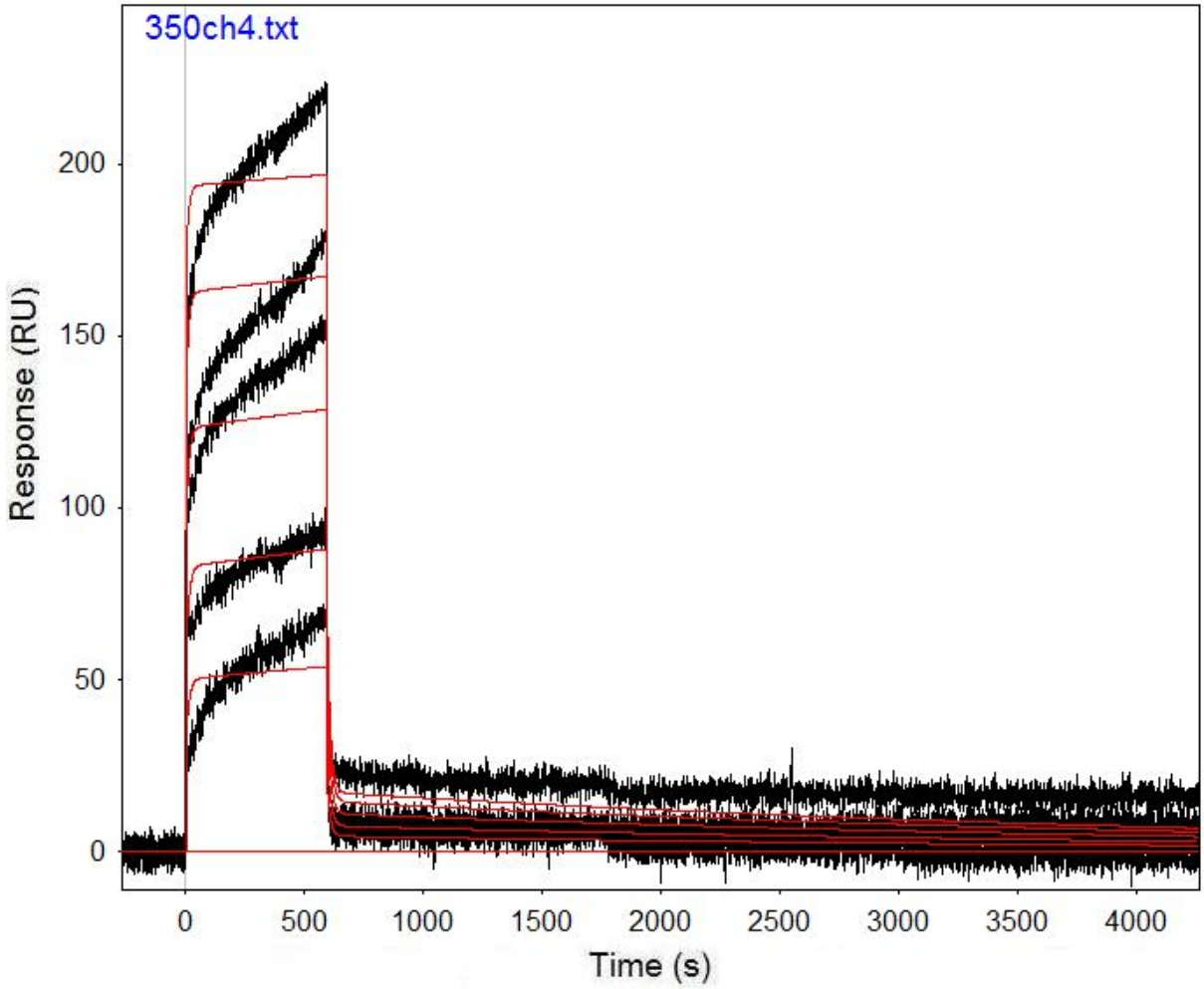

Figure B.99: Run 350, channel 4 model and data graph.

Table B.99: Run 350, channel 4 model parameters.

	kfwd1	krev1	kfwd2	krev2	kfwd3	krev3	ProA (RU)
Value	241.1	0.0002495	30610	0.07583	2.14E+08	210.4	79.65
Error (abs)	3.212	6.362E-06	3014	0.004758	8.23E+08	810.6	0.1613
Error (%)	1.332	2.550	9.846	6.275	384.759	385.266	0.203

Run 362, channel 4: Performed at pH 5.0 in sodium acetate, at an IgG concentration of 1.067 µm. RSSE is 3.296.

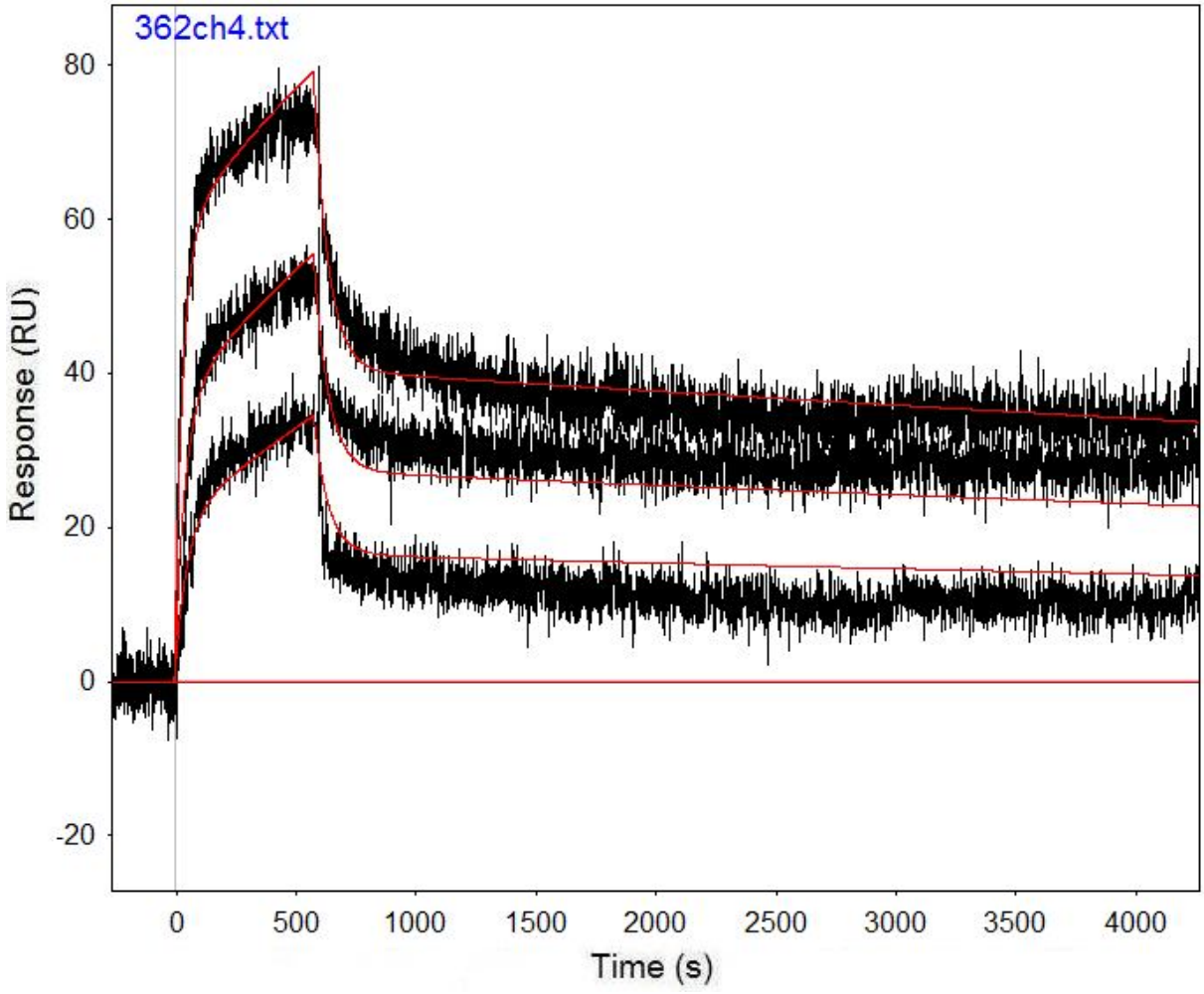

Figure B.100: Run 362, channel 4 model and data graph.

Table B.100: Run 362, channel 4 model parameters.

	kfwd1	krev1	kfwd2	krev2	kfwd3	krev3	ProA (RU)
Value	1056	4.942E-05	11593	0.01639	42.89	-8.858	571.5
Error (abs)	8.941	1.123E-06	196.2	0.000285	0.1991	0.4923	0.8206
Error (%)	0.847	2.272	1.692	1.736	0.464	-5.558	0.144

Run 372, channel 4: Performed at pH 5.0 in sodium acetate, at an IgG concentration of 1.067 µm. RSSE is 2.453.

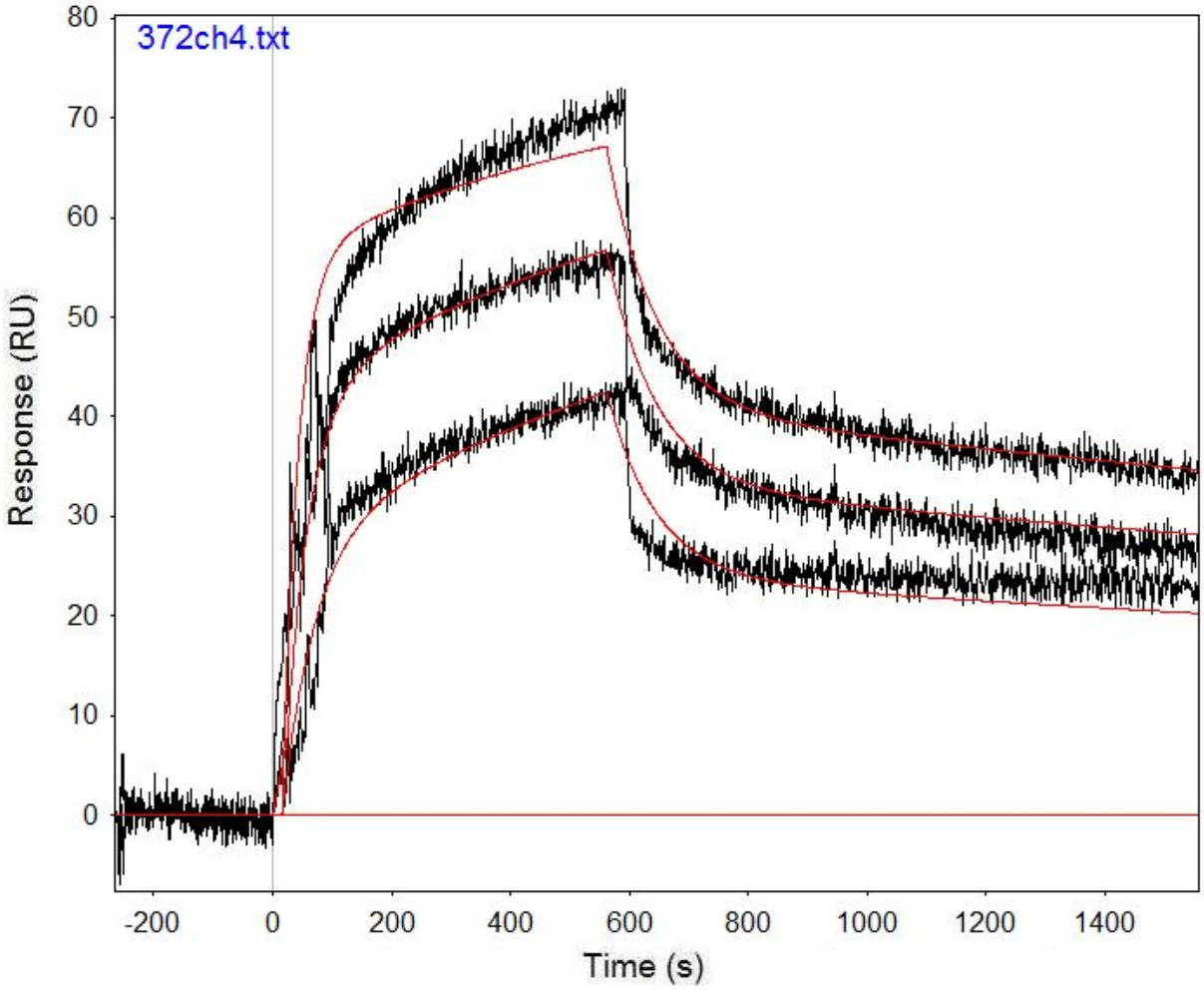

Figure B.101: Run 372, channel 4 model and data graph.

Table B.101: Run 372, channel 4 model parameters.

	kfwd1	krev1	kfwd2	krev2	kfwd3	krev3	ProA (RU)
Value	3671	0.0001645	21283	0.01195	26.59	16.05	561.5
Error (abs)	37.05	7.941E-06	321.2	0.000223	0.06972	0.3361	0.902
Error (%)	1.009	4.827	1.509	1.862	0.262	2.094	0.161

Run 400, channel 4: Performed at pH 7.4 in PBST, at an IgG concentration of 1.067 µm. RSSE is 2.806.

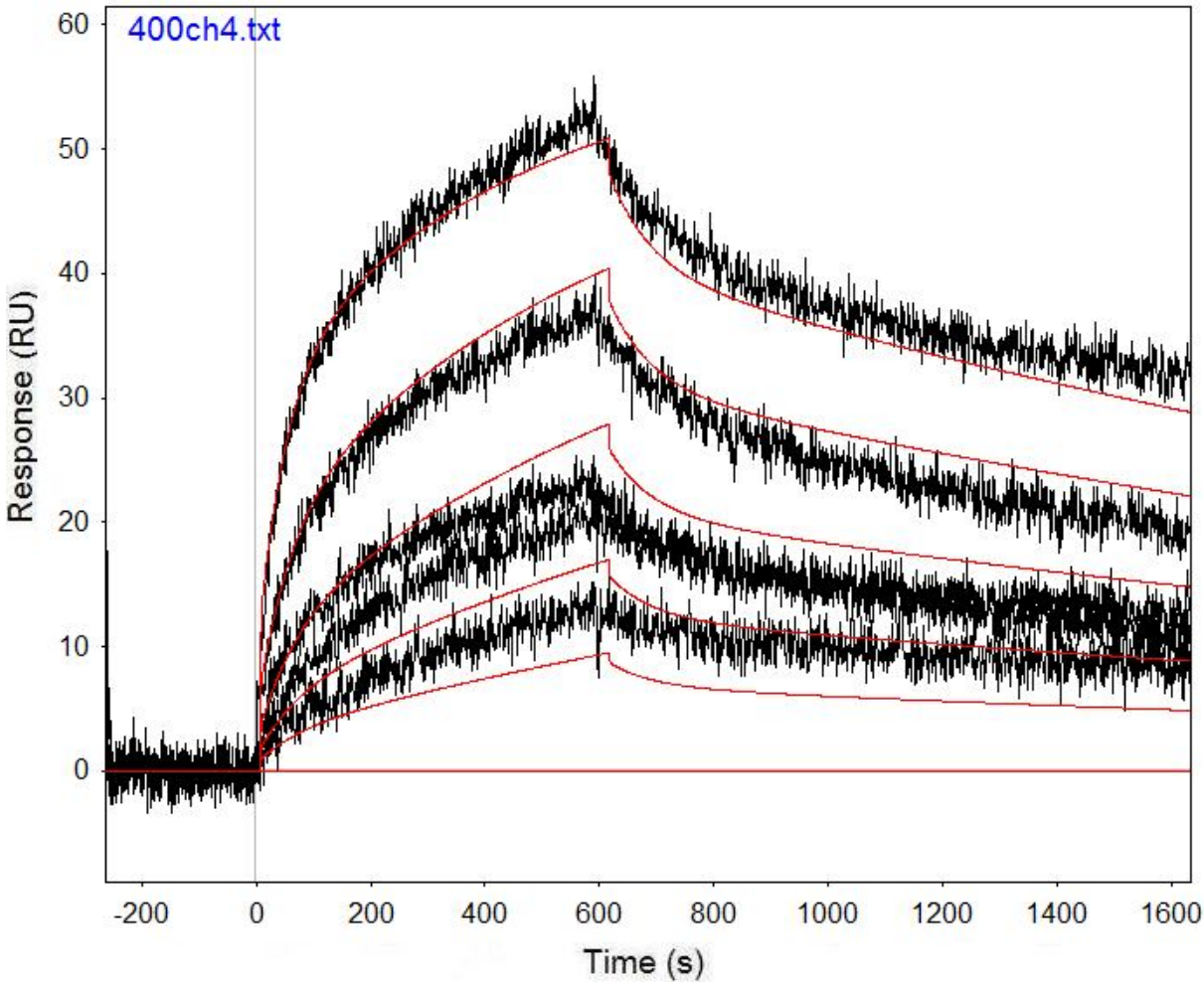

Figure B.102: Run 400, channel 4 model and data graph.

Table B.102: Run 400, channel 4 model parameters.

	kfwd1	krev1	kfwd2	krev2	kfwd3	krev3	ProA (RU)
Value	3268	0.0003312	156600	0.7298	7226	0.01363	21.02
Error (abs)	38.47	8.827E-06	81998	0.3873	511.9	0.000843	0.0845
Error (%)	1.177	2.665	52.361	53.069	7.084	6.185	0.402

Run 410, channel 4: Performed at pH 7.4 in PBST, at an IgG concentration of 1.067 µm. RSSE is 1.901.

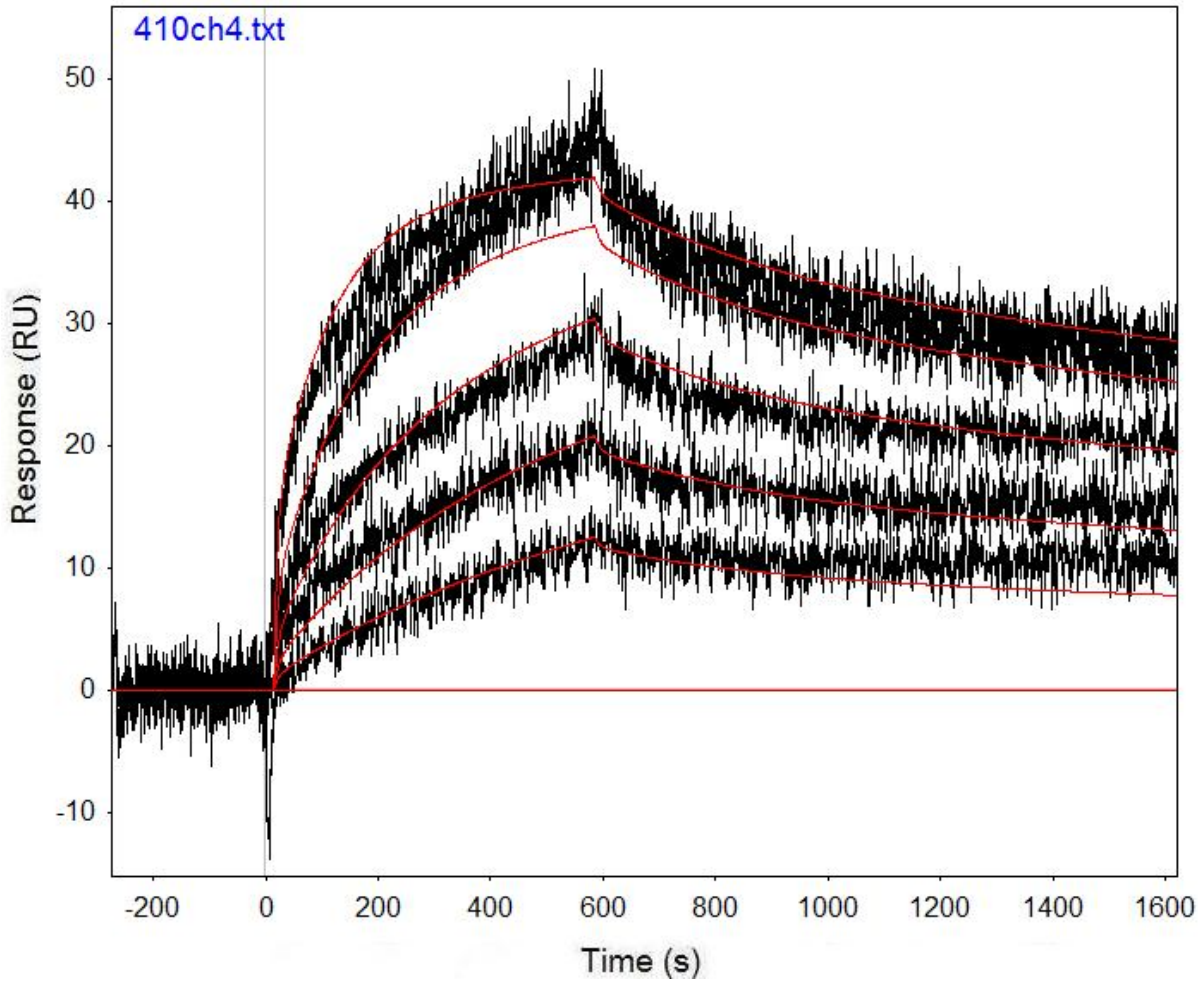

Figure B.103: Run 410, channel 4 model and data graph.

Table B.103: Run 410, channel 4 model parameters.

	kfwd1	krev1	kfwd2	krev2	kfwd3	krev3	ProA (RU)
Value	6919	0.0001738	4134	0.003267	42013	0.1195	14.93
Error (abs)	263.5	2.587E-05	158.9	0.000386	6458	0.01904	0.03019
Error (%)	3.808	14.885	3.844	11.827	15.371	15.933	0.202

Run 421, channel 4: Performed at pH 7.4 in PBST, at an IgG concentration of 3.0 µm. RSSE is 1.093.

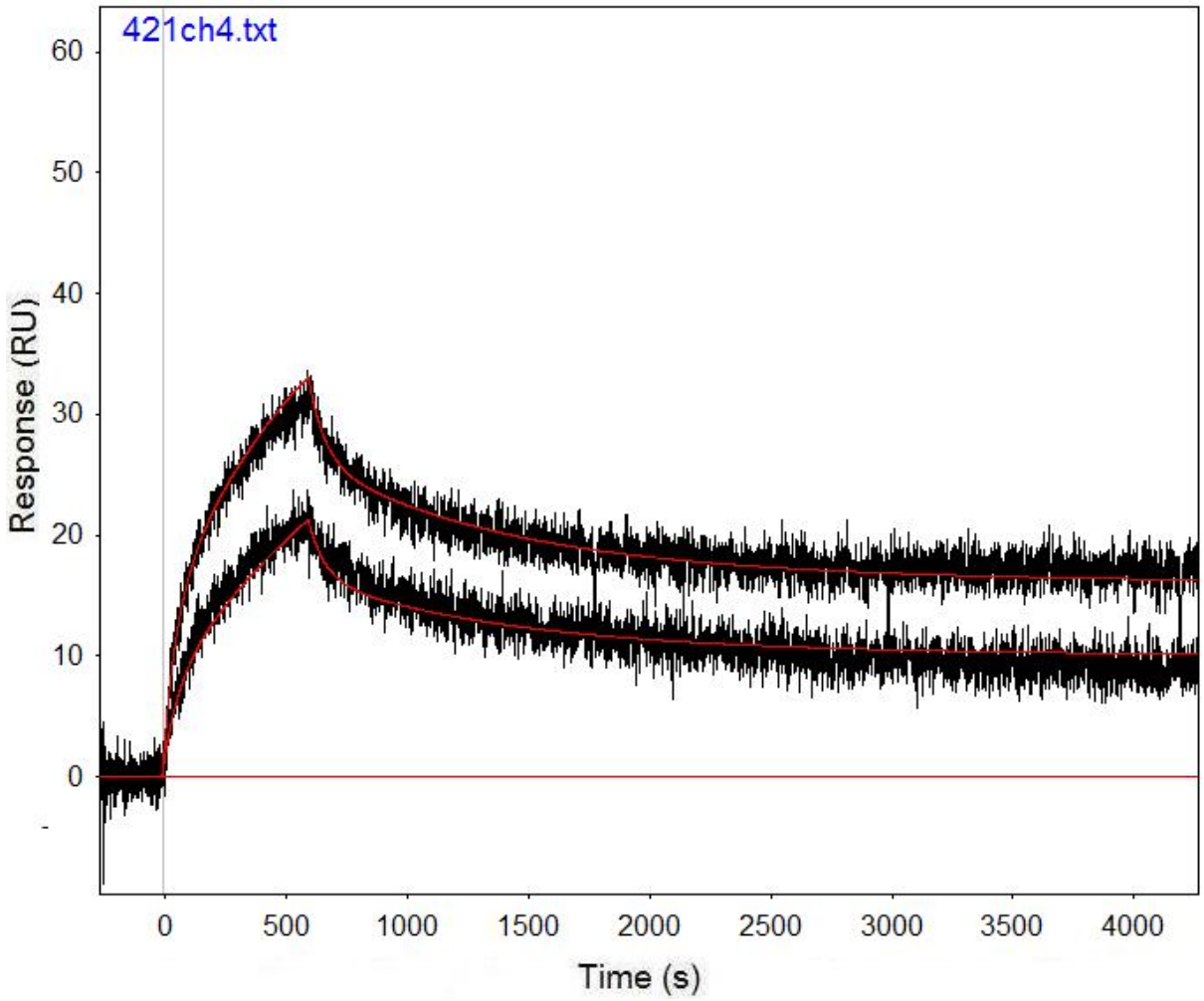

Figure B.104: Run 421, channel 4 model and data graph.

Table B.104: Run 421, channel 4 model parameters.

	kfwd1	krev1	kfwd2	krev2	kfwd3	krev3	ProA (RU)
Value	1682	0.001204	1960	5.82E-06	9273	0.01488	20.28
Error (abs)	34.39	0.0000695	49.57	5.82E-06	316.4	0.000653	0.1274
Error (%)	2.045	5.772	2.529	100.052	3.412	4.389	0.628

Run 426, channel 3: Performed at pH 7.4 in PBST, at an IgG concentration of 3.0 µm. RSSE is 1.784.

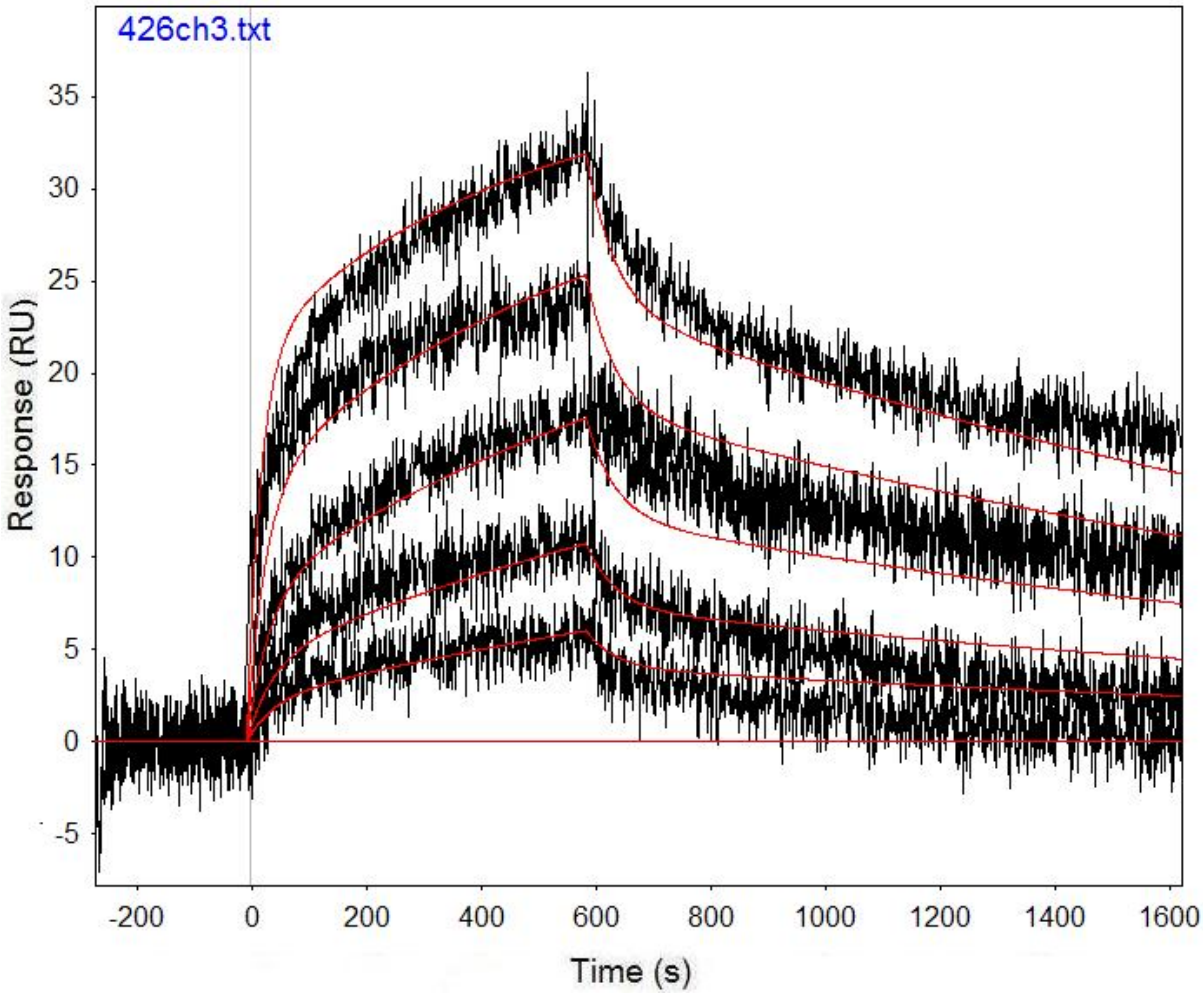

Figure B.105: Run 426, channel 3 model and data graph.

Table B.105: Run 426, channel 3 model parameters.

	kfwd1	krev1	kfwd2	krev2	kfwd3	krev3	ProA (RU)
Value	1157	0.0004721	6295	0.02064	13.45	-8.344	583.5
Error (abs)	13.8	8.485E-06	226.5	0.000806	0.05704	0.5861	1.365
Error (%)	1.193	1.797	3.598	3.904	0.424	-7.024	0.234

Run 426, channel 4: Performed at pH 7.4 in PBST, at an IgG concentration of 3.0 µm. RSSE is 2.896.

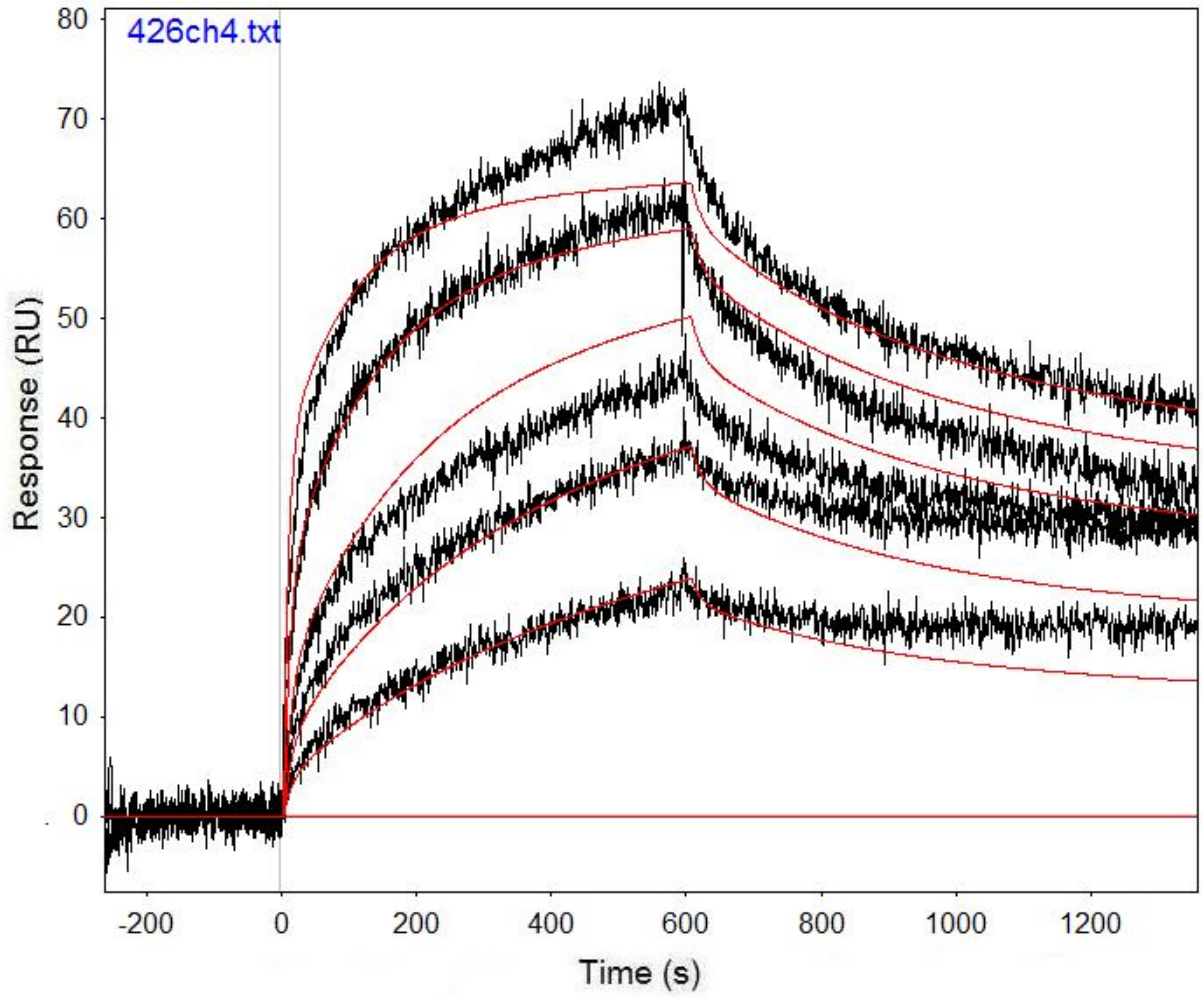

Figure B.106: Run 426, channel 4 model and data graph.

Table B.106: Run 426, channel 4 model parameters.

	kfwd1	krev1	kfwd2	krev2	kfwd3	krev3	ProA (RU)
Value	2993	0.003293	2509	0.000122	20966	0.07029	22.59
Error (abs)	150.9	0.0004878	260.8	7.67E-05	1632	0.006531	0.0417
Error (%)	5.042	14.813	10.395	62.920	7.784	9.292	0.185

Run 434, channel 4: Performed at pH 5.0 in sodium acetate, at an IgG concentration of 1.067 µm. RSSE is 1.688.

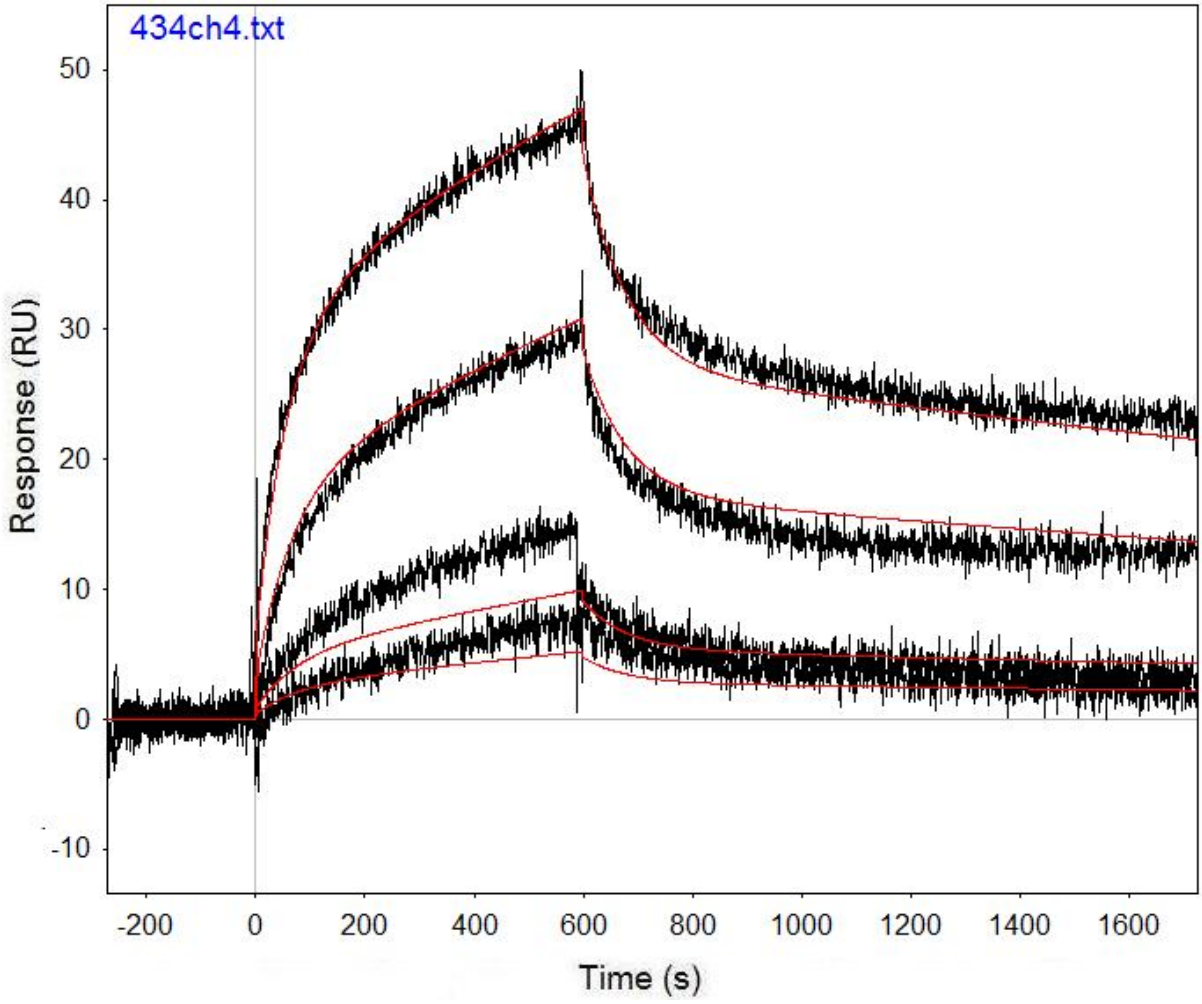

Figure B.107: Run 434, channel 4 model and data graph.

Table B.107: Run 434, channel 4 model parameters.

	kfwd1	krev1	kfwd2	krev2	kfwd3	krev3	ProA (RU)
Value	891.4	0.0002104	4604	0.01284	3350000	46	29.38
Error (abs)	13.38	7.809E-06	279.1	0.000402	73730000	1007	0.2797
Error (%)	1.501	3.712	6.062	3.130	2200.896	2189.130	0.952

Run 439, channel 5: Performed at pH 5.0 in sodium acetate, at an IgG concentration of 1.067 µm. RSSE is 2.804.

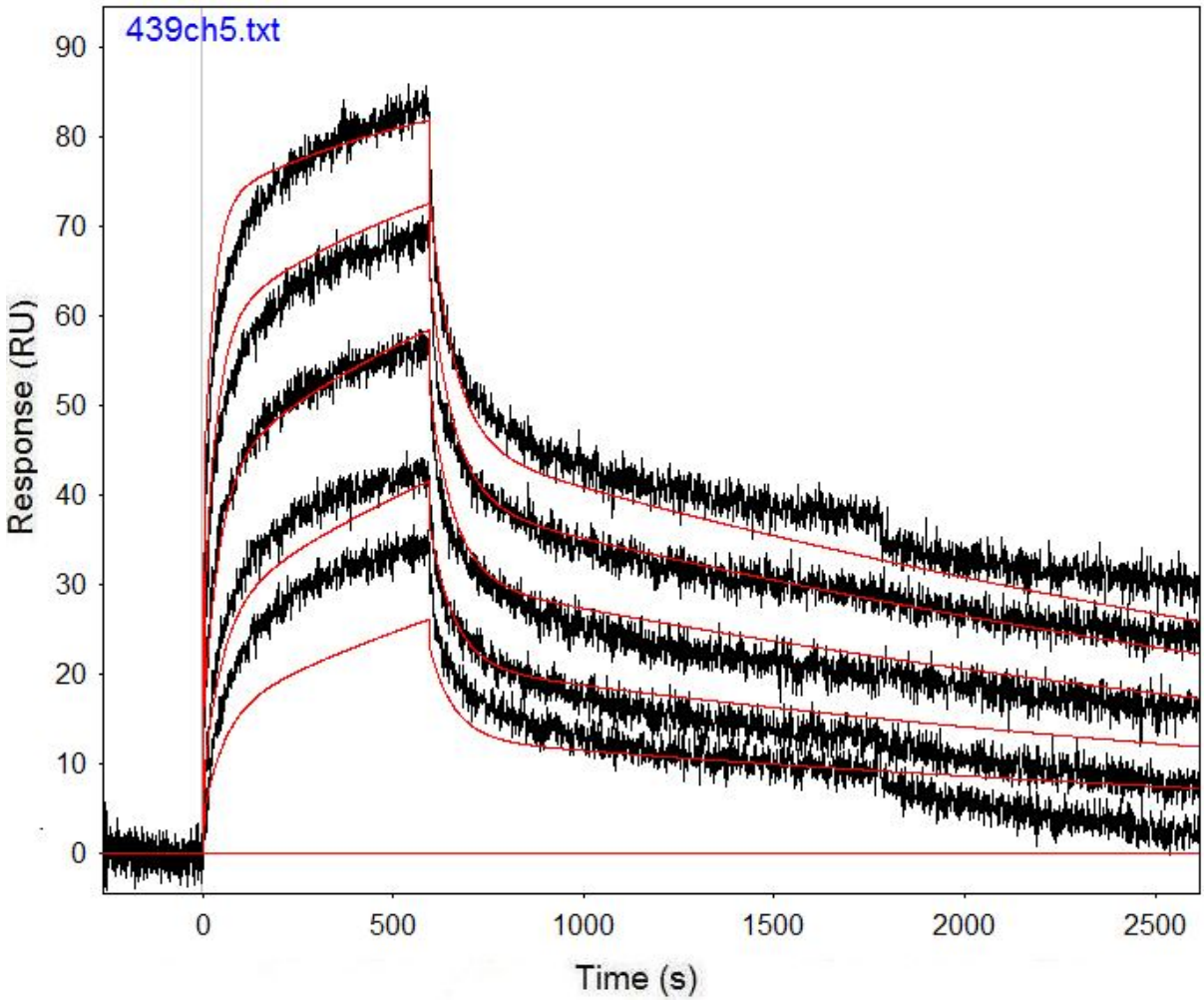

Figure B.108: Run 439, channel 5 model and data graph.

Table B.108: Run 439, channel 5 model parameters.

	kfwd1	krev1	kfwd2	krev2	kfwd3	krev3	ProA (RU)
Value	4878	0.0002813	34457	0.01565	14180000	18.55	30.95
Error (abs)	25.2	2.293E-06	732.5	0.00026	13210000	17.26	0.04883
Error (%)	0.517	0.815	2.126	1.660	93.159	93.046	0.158

Run 444, channel 5: Performed at pH 5.0 in sodium acetate, at an IgG concentration of 1.067 µm. RSSE is 3.81.

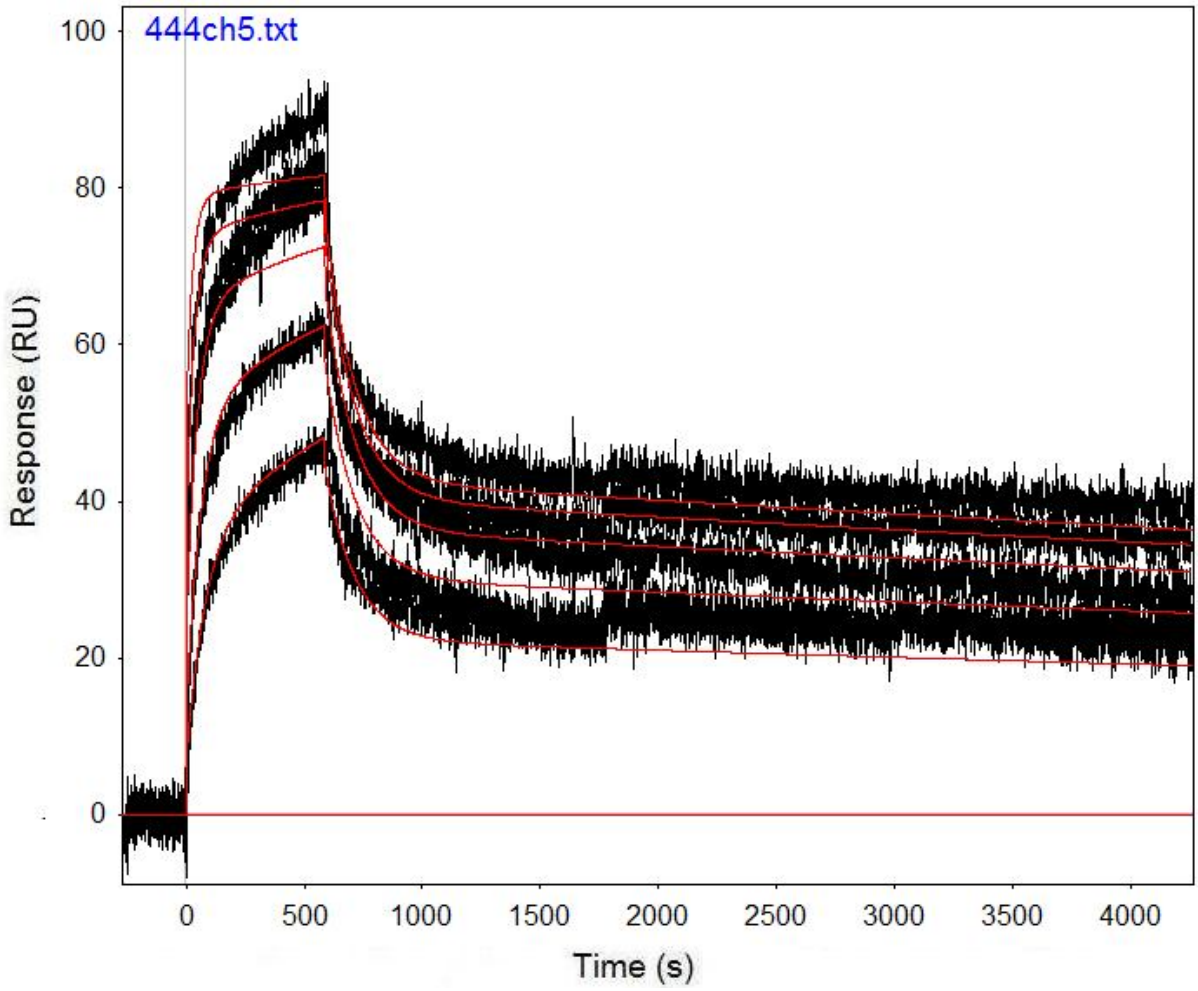

Figure B.109: Run 444, channel 5 model and data graph.

Table B.109: Run 444, channel 5 model parameters.

	kfwd1	krev1	kfwd2	krev2	kfwd3	krev3	ProA (RU)
Value	12534	4.362E-05	66188	0.007776	65730000	42.93	28.27
Error (abs)	66.4	9.543E-07	935.6	9.91E-05	82070000	53.73	0.03707
Error (%)	0.530	2.188	1.414	1.274	124.859	125.157	0.131

Run 460, channel 5: Performed at pH 5.0 in sodium acetate, at an IgG concentration of 0.5 µm. RSSE is 4.641.

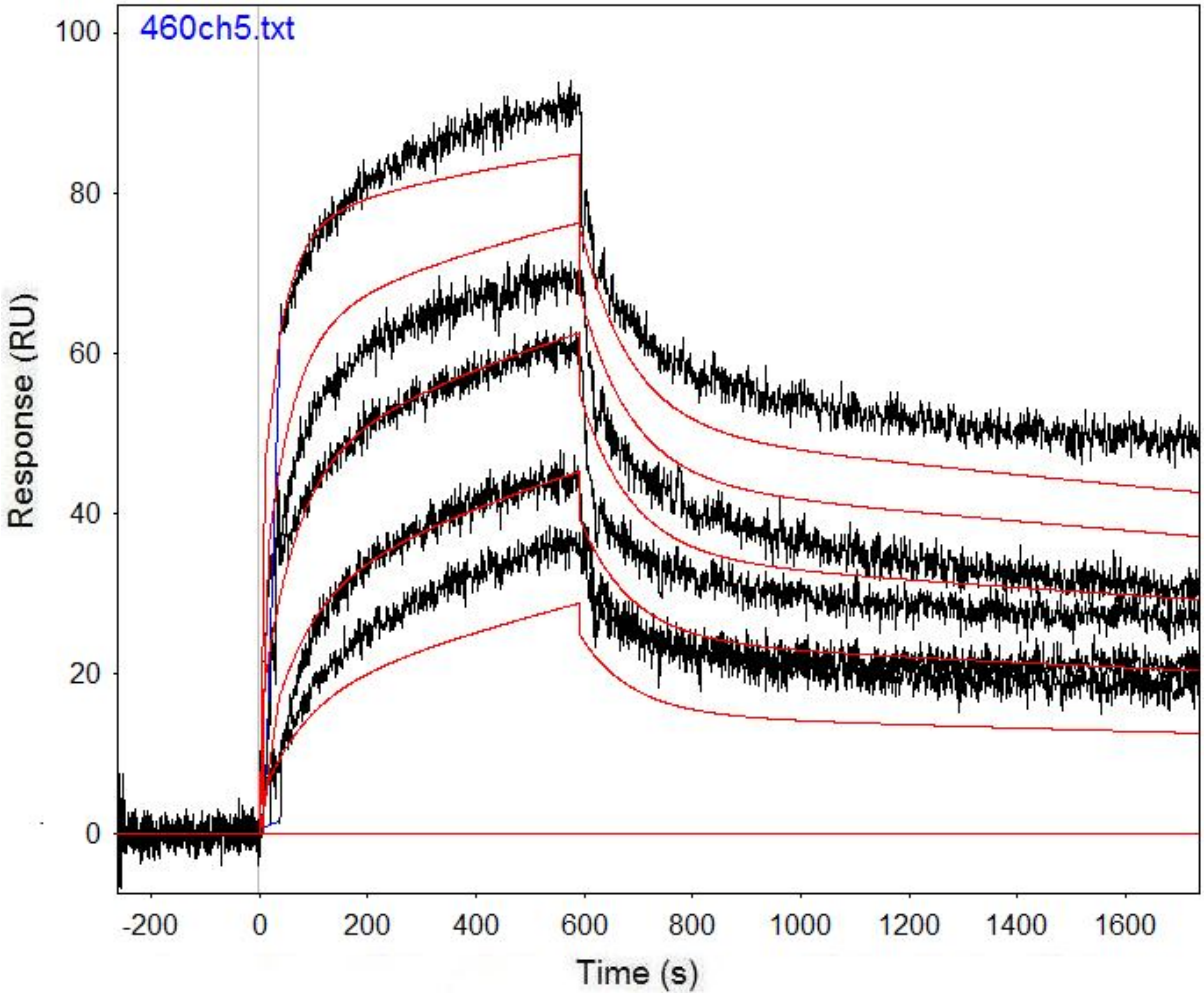

Figure B.110: Run 460, channel 5 model and data graph.

Table B.110: Run 460, channel 5 model parameters.

	kfwd1	krev1	kfwd2	krev2	kfwd3	krev3	ProA (RU)
Value	1934	0.000149	8771	0.01146	6521000	20.62	31.56
Error (abs)	23.61	8.688E-06	365.4	0.00042	90400000	284.6	0.08816
Error (%)	1.221	5.831	4.166	3.668	1386.290	1380.213	0.279

Run 464, channel 4: Performed at pH 5.0 in sodium acetate, at an IgG concentration of 3.0 µm. RSSE is 3.031.

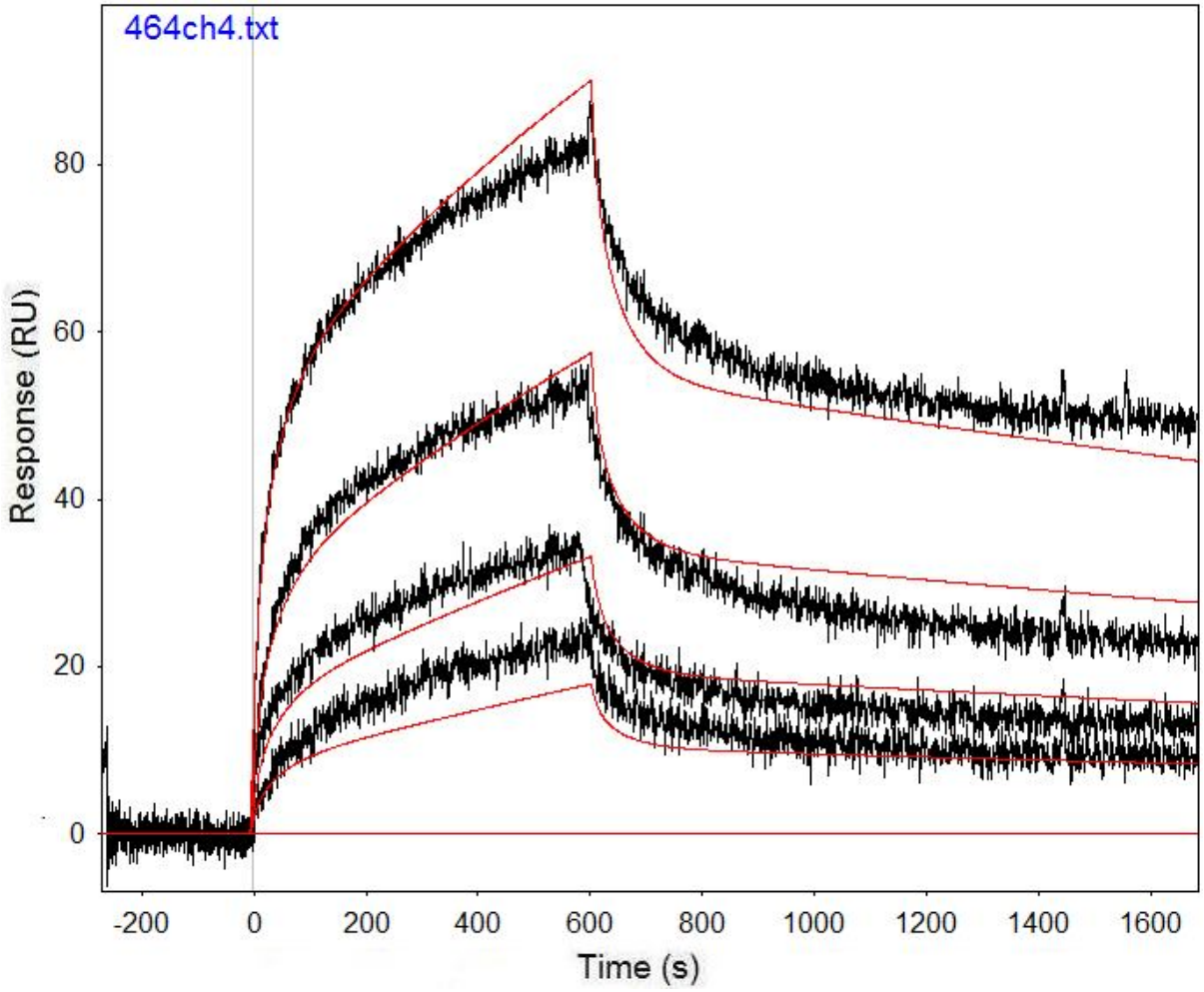

Figure B.111: Run 464, channel 4 model and data graph.

Table B.111: Run 464, channel 4 model parameters.

	kfwd1	krev1	kfwd2	krev2	kfwd3	krev3	ProA (RU)
Value	280.8	0.0001939	1455	0.01857	3798	0.08797	61.42
Error (abs)	3.329	6.459E-06	228.1	0.001427	436.6	0.01876	0.4242
Error (%)	1.186	3.331	15.677	7.684	11.496	21.325	0.691

Run 474, channel 5: Performed at pH 5.0 in sodium acetate, at an IgG concentration of 1.0667 µm. RSSE is 4.299.

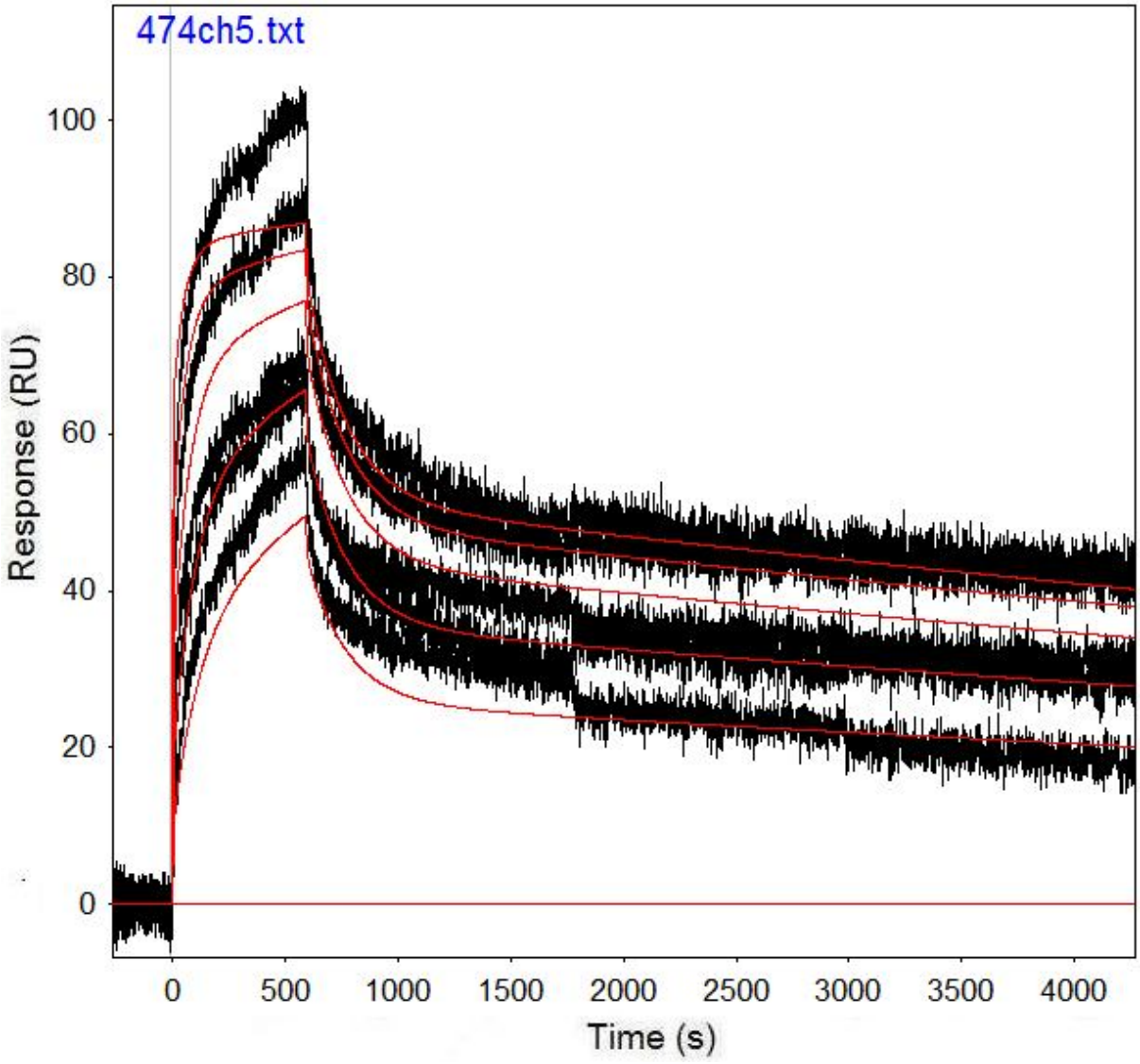

Figure B.112: Run 474, channel 5 model and data graph.

Table B.112: Run 474, channel 5 model parameters.

	kfwd1	krev1	kfwd2	krev2	kfwd3	krev3	ProA (RU)
Value	353000	0.1968	12781	6.88E-05	36303	0.005663	30.07
Error (abs)	34533	0.02008	66.19	1.05E-06	686.5	8.77E-05	0.04156
Error (%)	9.783	10.203	0.518	1.518	1.891	1.548	0.138

Run 479, channel 5: Performed at pH 5.5 in sodium acetate, at an IgG concentration of 1.067 µm. RSSE is 3.717.

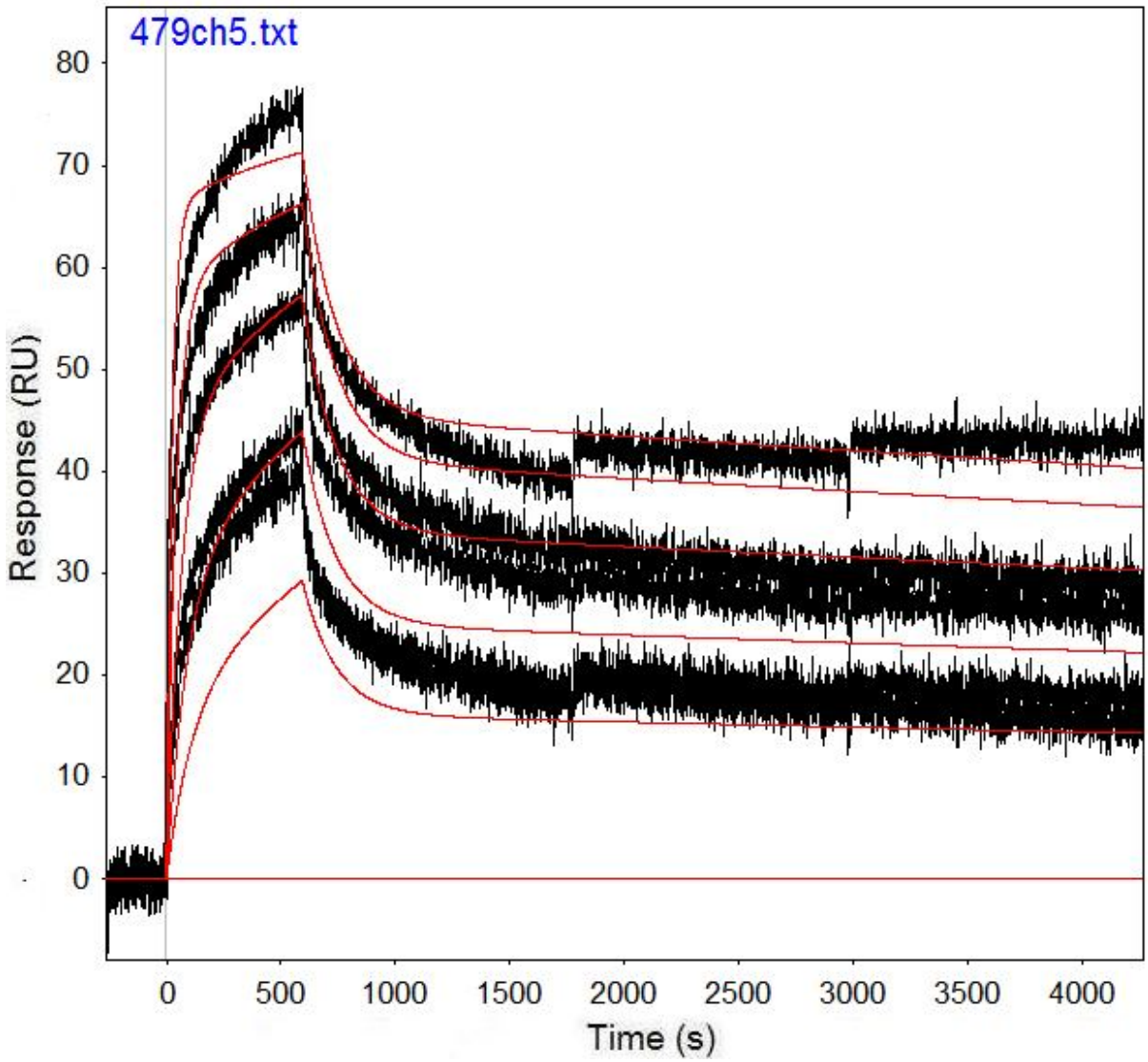

Figure B.113: Run 479, channel 5 model and data graph.

Table B.113: Run 479, channel 5 model parameters.

	kfwd1	krev1	kfwd2	krev2	kfwd3	krev3	ProA (RU)
Value	3876000	3.517	7375	3.32E-05	28271	0.006998	25.42
Error (abs)	1748000	1.585	38.81	1.08E-06	538.6	0.000107	0.04253
Error (%)	45.098	45.067	0.526	3.242	1.905	1.535	0.167

Run 485, channel 5: Performed at pH 5.5 in sodium acetate, at an IgG concentration of 1.067 µm. RSSE is 3.555.

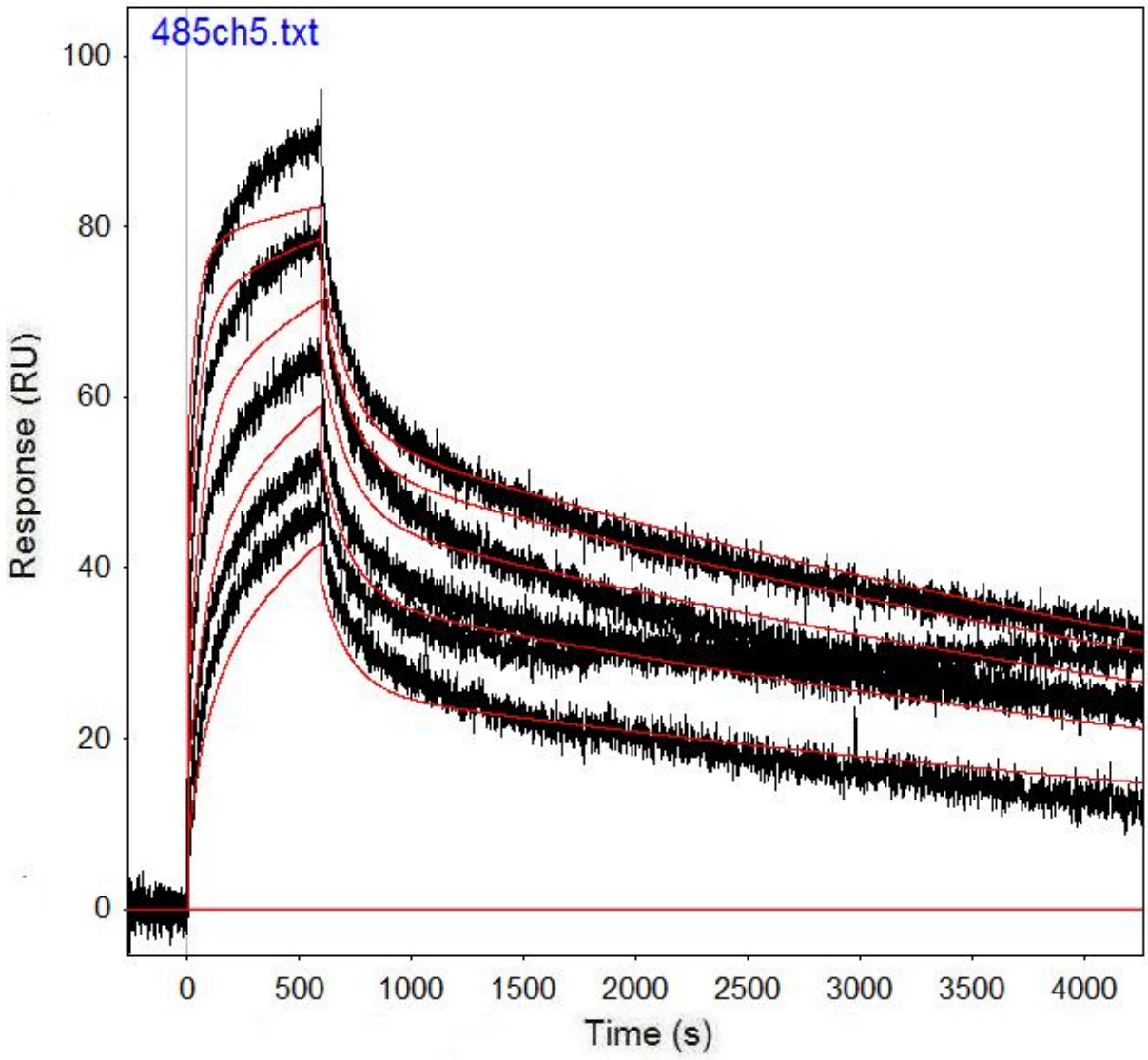

Figure B.114: Run 485, channel 5 model and data graph.

Table B.114: Run 485, channel 5 model parameters.

	kfwd1	krev1	kfwd2	krev2	kfwd3	krev3	ProA (RU)
Value	8.99E+08	815	12187	0.000142	34904	0.006144	27.73
Error (abs)	4.16E+10	37650	63.59	1.04E-06	502.2	0.0001	0.0431
Error (%)	4620.774	4619.632	0.522	0.732	1.439	1.629	0.155

Run 490, channel 5: Performed at pH 5.5 in sodium acetate, at an IgG concentration of 1.067 µm. RSSE is 2.565.

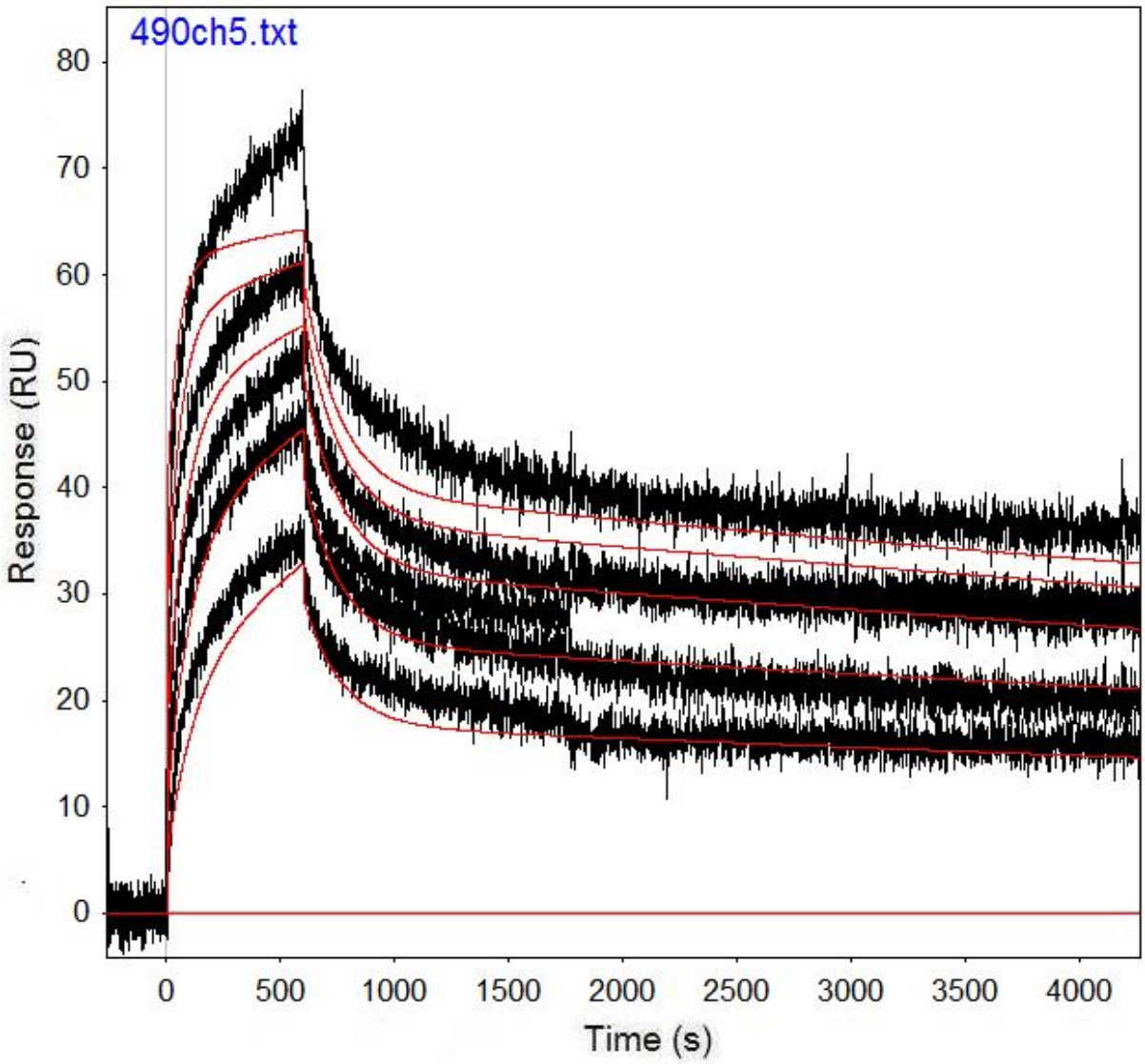

Figure B.115: Run 490, channel 5 model and data graph.

Table B.115: Run 490, channel 5 model parameters.

	kfwd1	krev1	kfwd2	krev2	kfwd3	krev3	ProA (RU)
Value	9.55E+08	663.5	10572	5.18E-05	30184	0.006241	22.45
Error (abs)	4.73E+10	32858	41.27	7.75E-07	426.4	7.49E-05	0.0261
Error (%)	4952.870	4952.223	0.390	1.497	1.413	1.199	0.116

Run 495, channel 5: Performed at pH 5.5 in sodium acetate, at an IgG concentration of 0.5 µm. RSSE is 4.89.

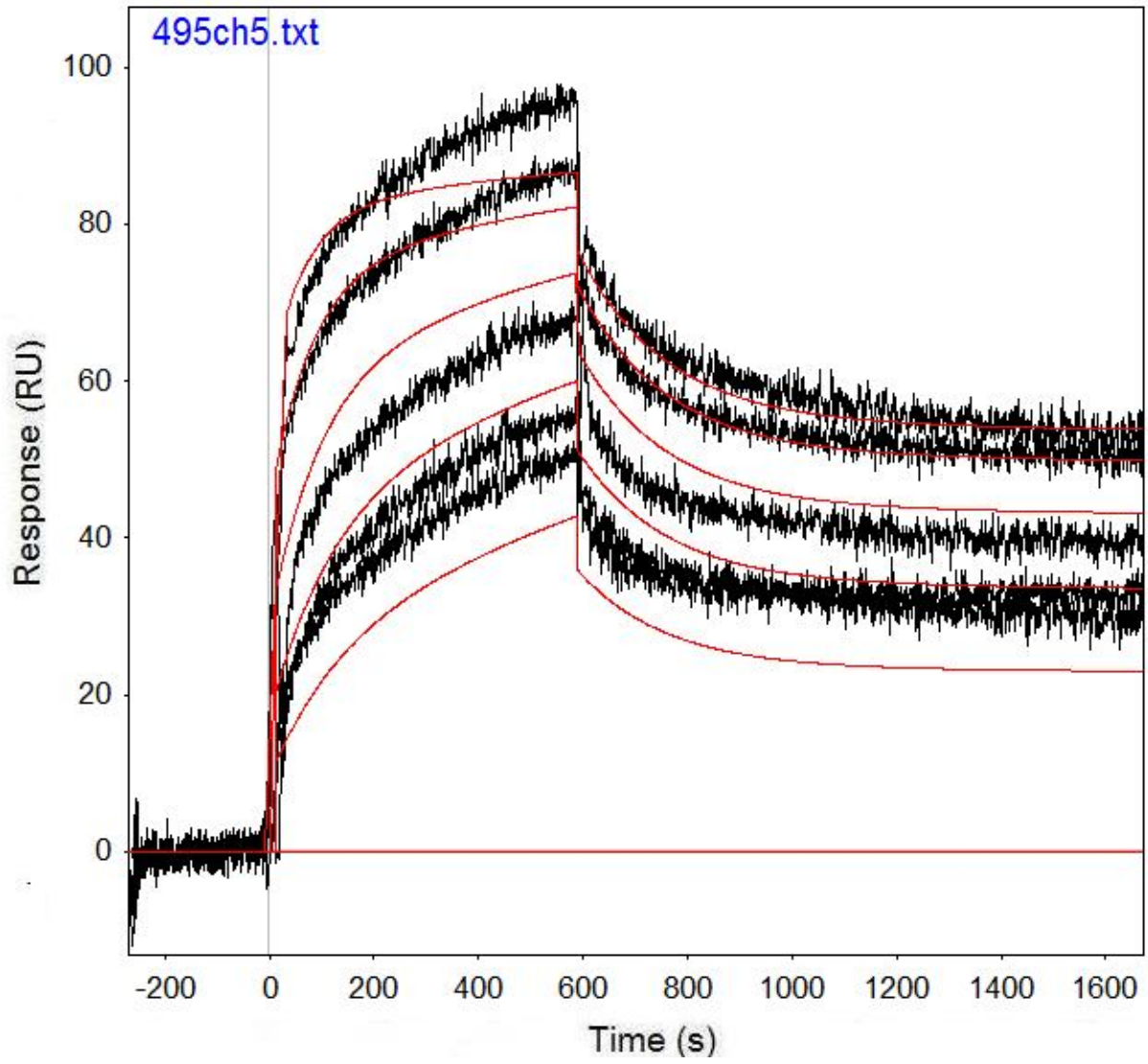

Figure B.116: Run 495, channel 5 model and data graph.

Table B.116: Run 495, channel 5 model parameters.

	kfwd1	krev1	kfwd2	krev2	kfwd3	krev3	ProA (RU)
Value	1.54E+09	340.1	22018	1.49E-05	46780	0.005938	30.33
Error (abs)	8.75E+10	19382	394.8	1.37E-05	1613	0.000289	0.07012
Error (%)	5702.932	5698.912	1.793	92.024	3.448	4.869	0.231

Run 506, channel 5: Performed at pH 5.5 in sodium acetate, at an IgG concentration of 3.0 µm. RSSE is 4.082.

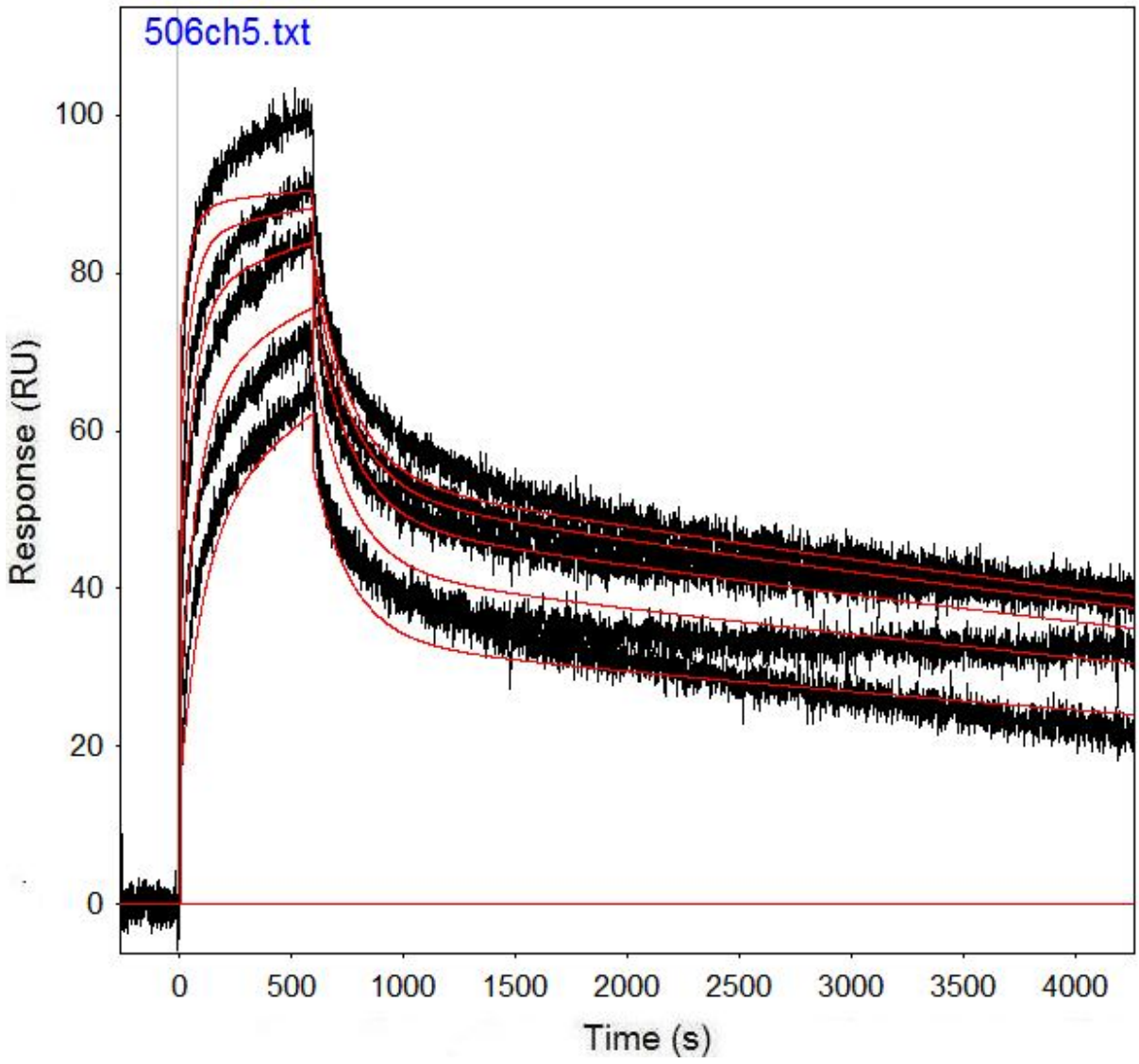

Figure B.117: Run 506, channel 5 model and data graph.

Table B.117: Run 506, channel 5 model parameters.

	kfwd1	krev1	kfwd2	krev2	kfwd3	krev3	ProA (RU)
Value	8.16E+08	742.4	7313	9.1E-05	20900	0.005986	30.89
Error (abs)	7.9E+09	7194	40.07	9.16E-07	340.7	8.88E-05	0.03569
Error (%)	968.861	969.019	0.548	1.007	1.630	1.484	0.116

Run 520, channel 5: Performed at pH 6.0 in PBST, at an IgG concentration of 1.067 µm. RSSE is 3.737.

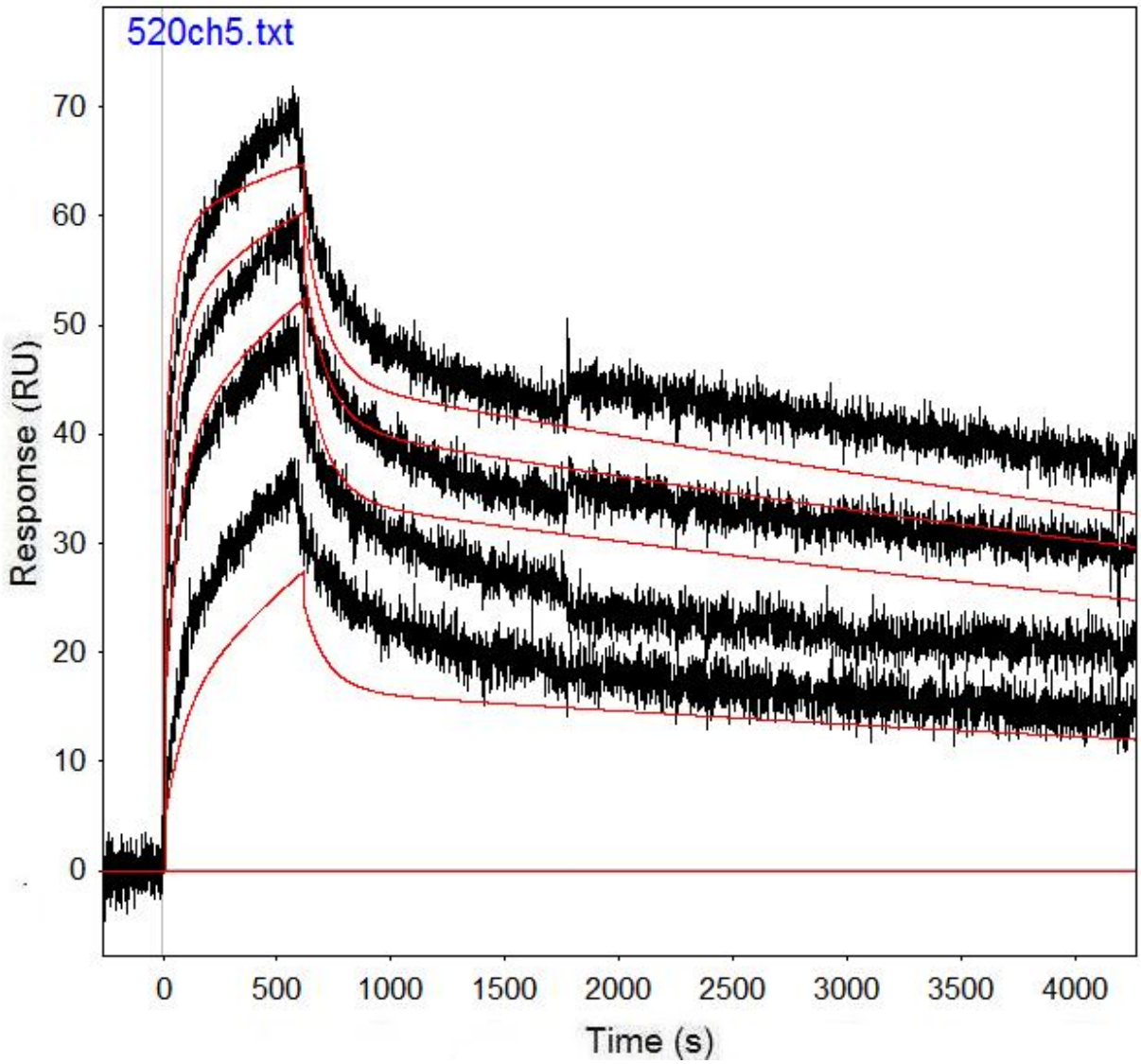

Figure B.118: Run 520, channel 5 model and data graph.

Table B.118: Run 520, channel 5 model parameters.

	kfwd1	krev1	kfwd2	krev2	kfwd3	krev3	ProA (RU)
Value	8.71E+08	768.8	8558	8.72E-05	27383	0.01015	23.03
Error (abs)	5.53E+10	48797	52.84	1.07E-06	1003	0.00029	0.04464
Error (%)	6347.986	6347.164	0.617	1.226	3.663	2.859	0.194

Run 530, channel 5: Performed at pH 6.0 in PBST, at an IgG concentration of 1.067 µm. RSSE is 3.156.

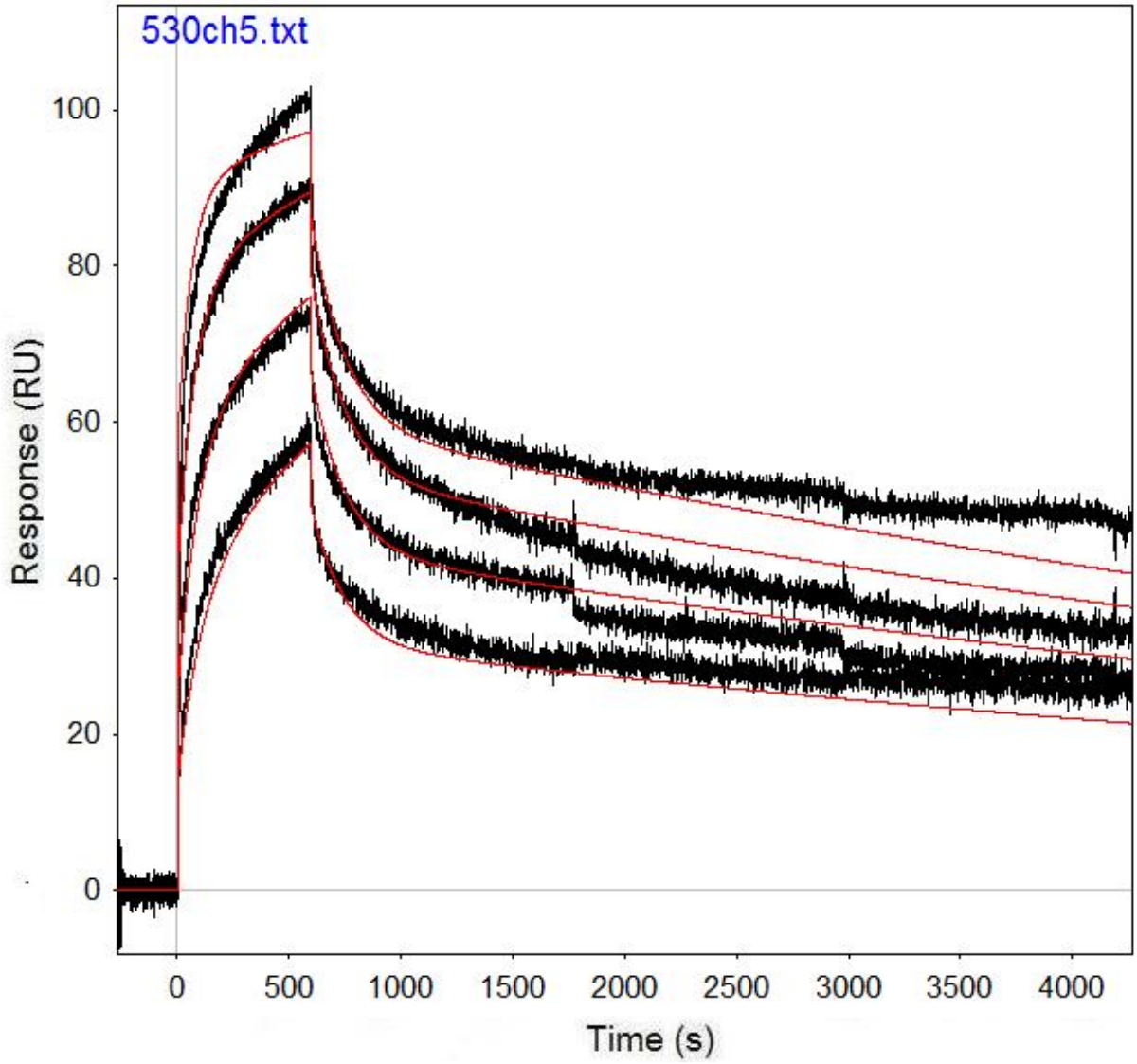

Figure B.119: Run 530, channel 5 model and data graph.

Table B.119: Run 530, channel 5 model parameters.

	kfwd1	krev1	kfwd2	krev2	kfwd3	krev3	ProA (RU)
Value	7.25E+08	601.5	6775	0.000106	17742	0.006777	35.09
Error (abs)	1.97E+09	1630	30.8	7.6E-07	284	9.56E-05	0.04258
Error (%)	271.023	270.989	0.455	0.719	1.601	1.411	0.121

Run 535, channel 5: Performed at pH 6.0 in PBST, at an IgG concentration of 1.067 µm. RSSE is 4.593.

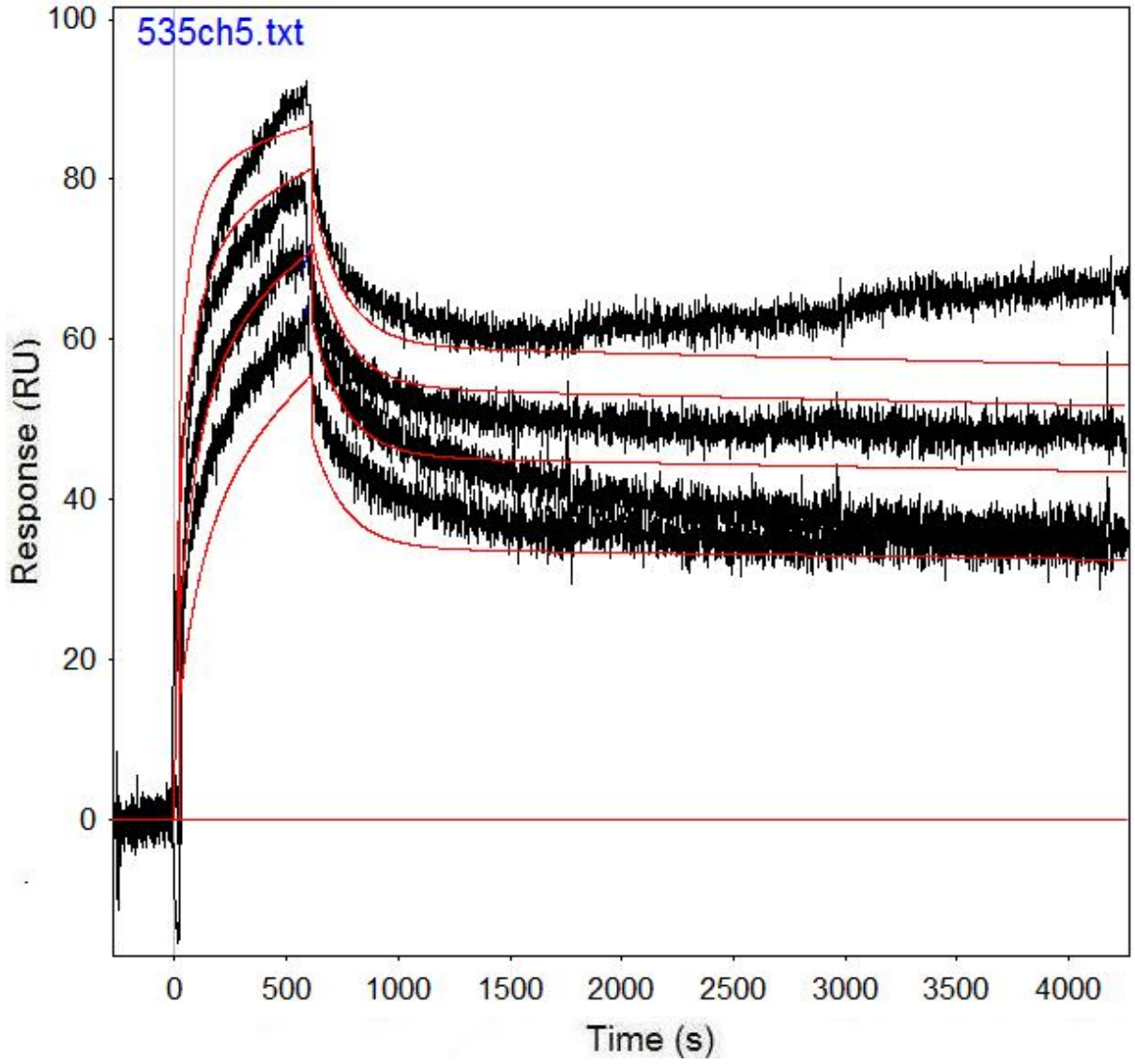

Figure B.120: Run 535, channel 5 model and data graph.

Table B.120: Run 535, channel 5 model parameters.

	kfwd1	krev1	kfwd2	krev2	kfwd3	krev3	ProA (RU)
Value	7.37E+08	476.7	8814	1.18E-05	18251	0.006969	30.69
Error (abs)	1.22E+10	7888	58.62	8.94E-07	597.1	0.000188	0.05334
Error (%)	1654.003	1654.709	0.665	7.587	3.272	2.695	0.174

Run 540, channel 5: Performed at pH 6.0 in PBST, at an IgG concentration of 3.0 µm. RSSE is 2.321.

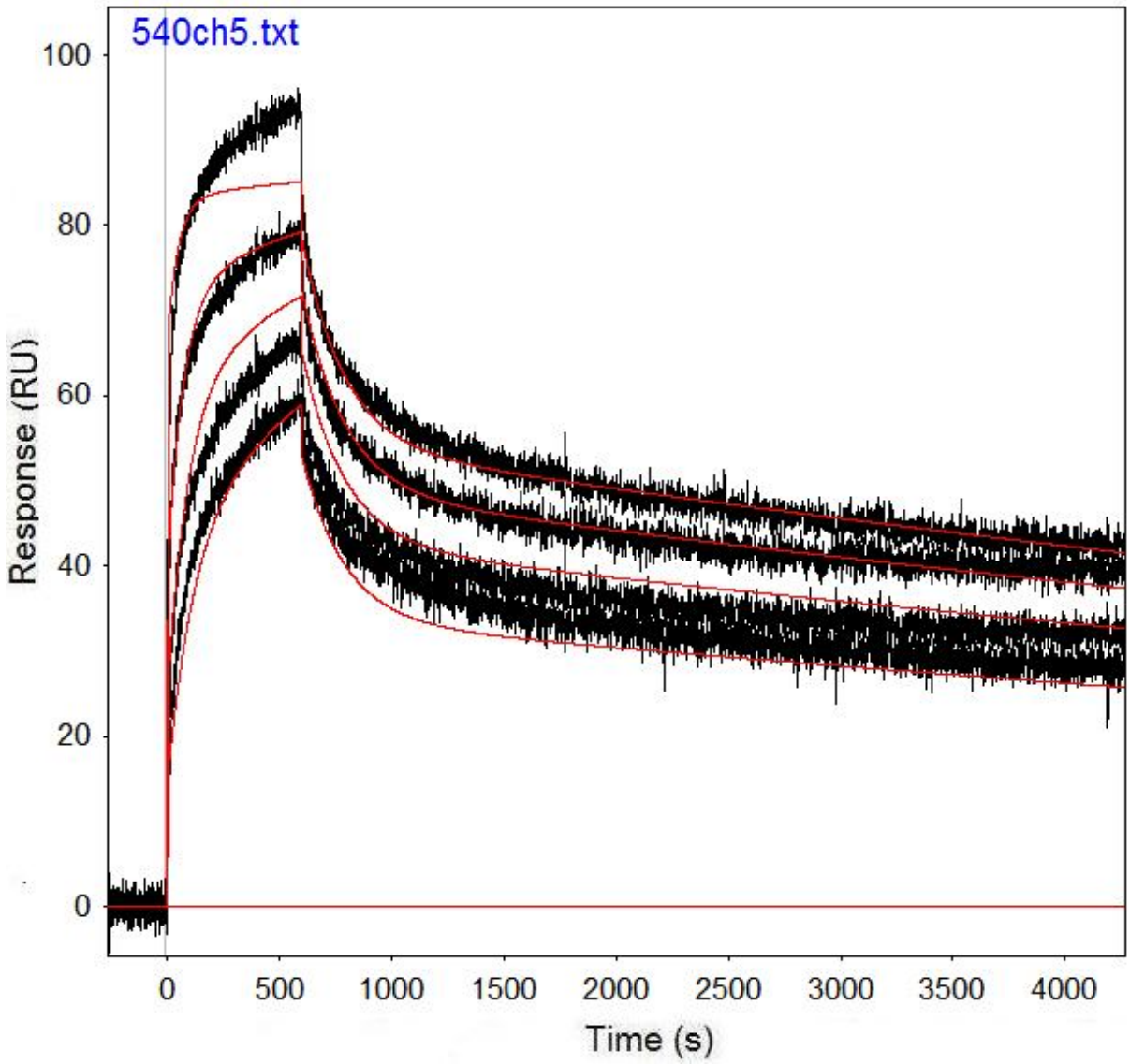

Figure B.121: Run 540, channel 5 model and data graph.

Table B.121: Run 540, channel 5 model parameters.

	kfwd1	krev1	kfwd2	krev2	kfwd3	krev3	ProA (RU)
Value	3.97E+08	358.1	7663	7.33E-05	17346	0.005331	29.01
Error (abs)	2.25E+09	2030	25.46	5.97E-07	191.1	5.27E-05	0.02308
Error (%)	566.675	566.881	0.332	0.815	1.102	0.989	0.080

Run 545, channel 5: Performed at pH 6.0 in PBST, at an IgG concentration of 3.0 µm. RSSE is 5.901.

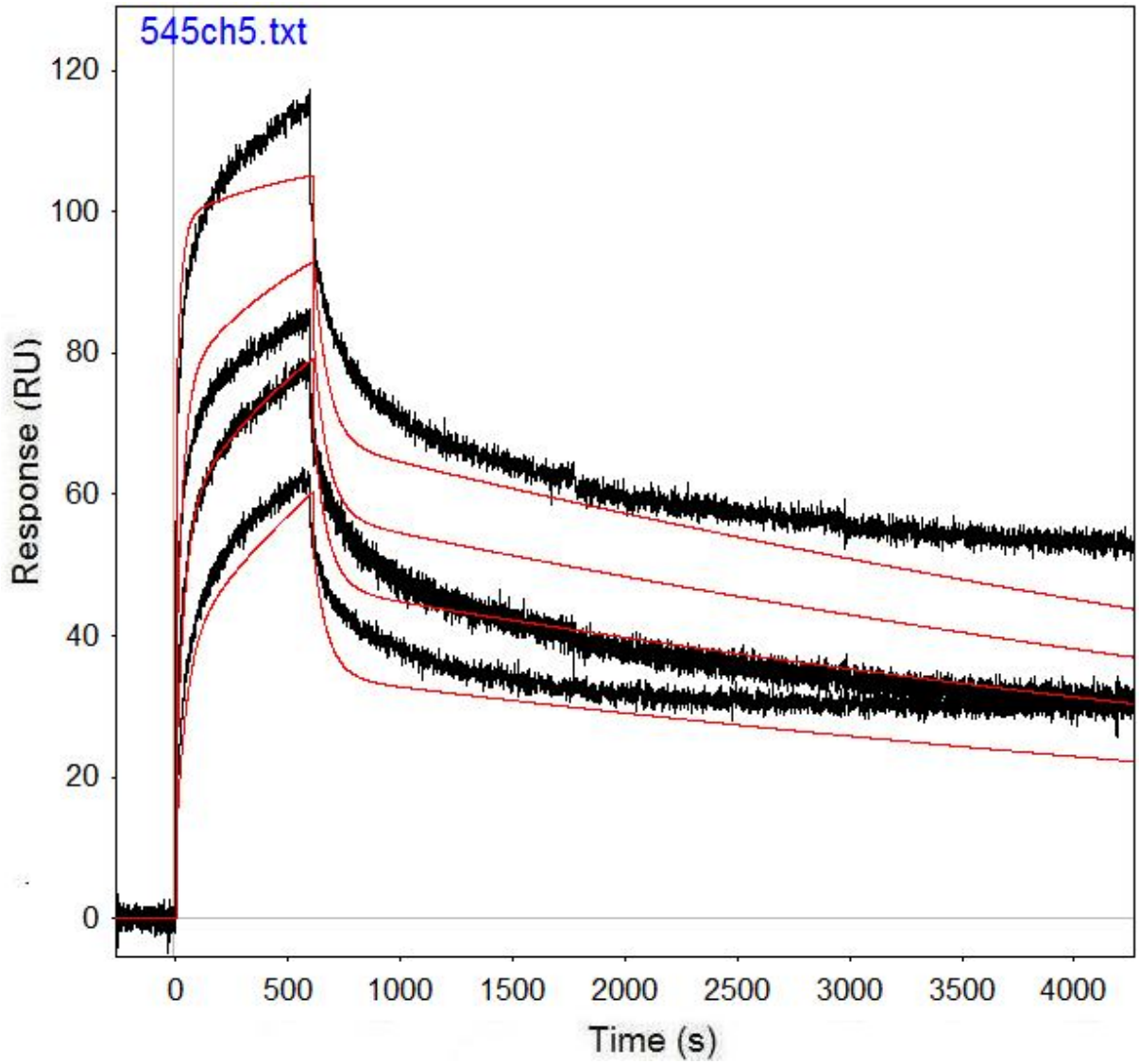

Figure B.122: Run 545, channel 5 model and data graph.

Table B.122: Run 545, channel 5 model parameters.

	kfwd1	krev1	kfwd2	krev2	kfwd3	krev3	ProA (RU)
Value	6.98E+09	8193	5180	0.000119	31191	0.01634	36.48
Error (abs)	1.5E+12	1758000	34.62	1.15E-06	1439	0.000524	0.07068
Error (%)	21461.3	21457.342	0.668	0.962	4.614	3.204	0.194

Run 554, channel 5: Performed at pH 6.5 in PBST, at an IgG concentration of 1.067 µm. RSSE is 3.074.

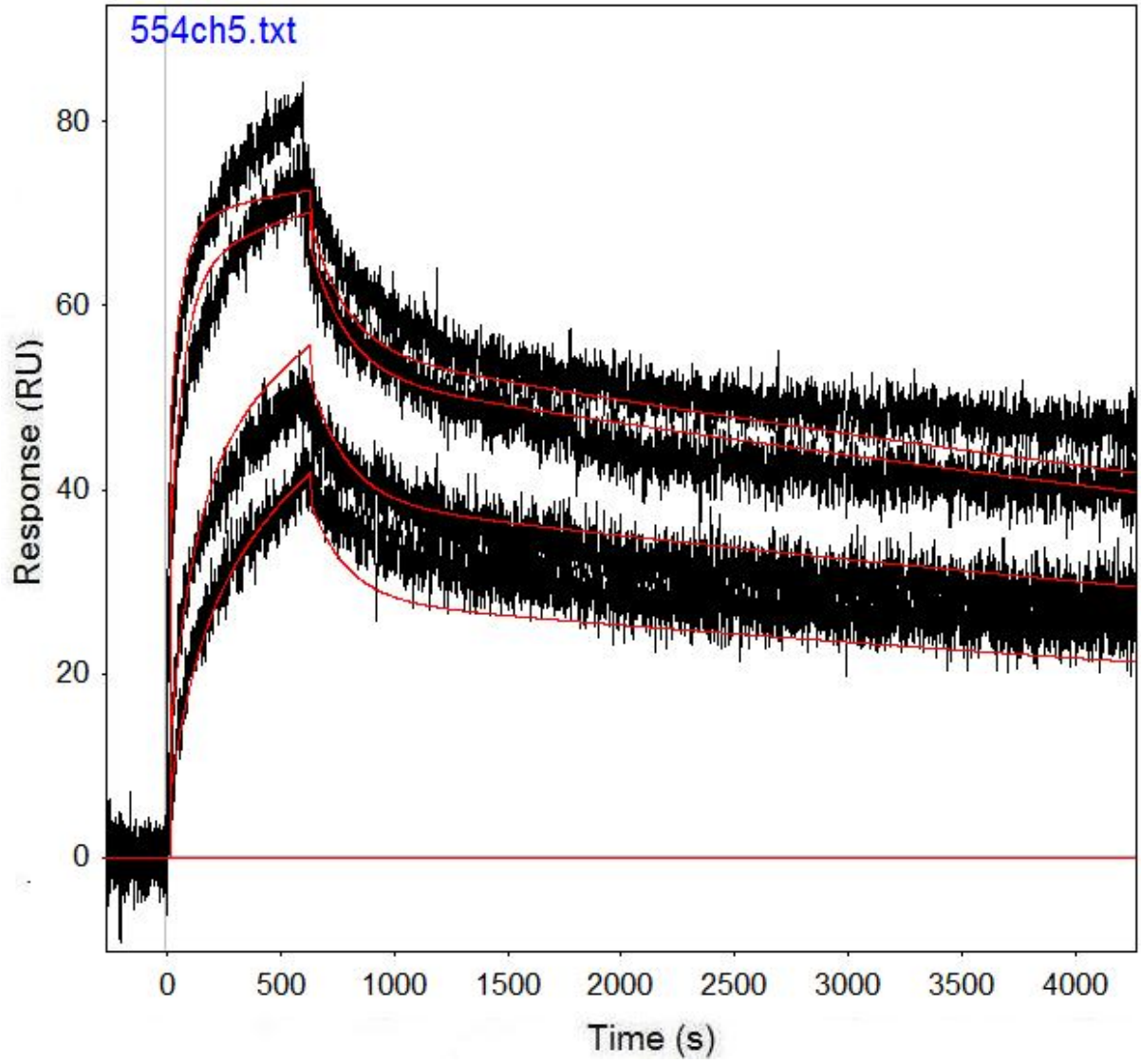

Figure B.123: Run 554, channel 5 model and data graph.

Table B.123: Run 554, channel 5 model parameters.

	kfwd1	krev1	kfwd2	krev2	kfwd3	krev3	ProA (RU)
Value	9E+09	5827	16177	7.87E-05	27394	0.006485	24.93
Error (abs)	3.02E+13	19530000	79.44	7.46E-07	737.9	0.00014	0.02922
Error (%)	335073.3	335163.89	0.491	0.948	2.694	2.163	0.117

Run 559, channel 5: Performed at pH 6.5 in PBST, at an IgG concentration of 1.067 µm. RSSE is 3.832.

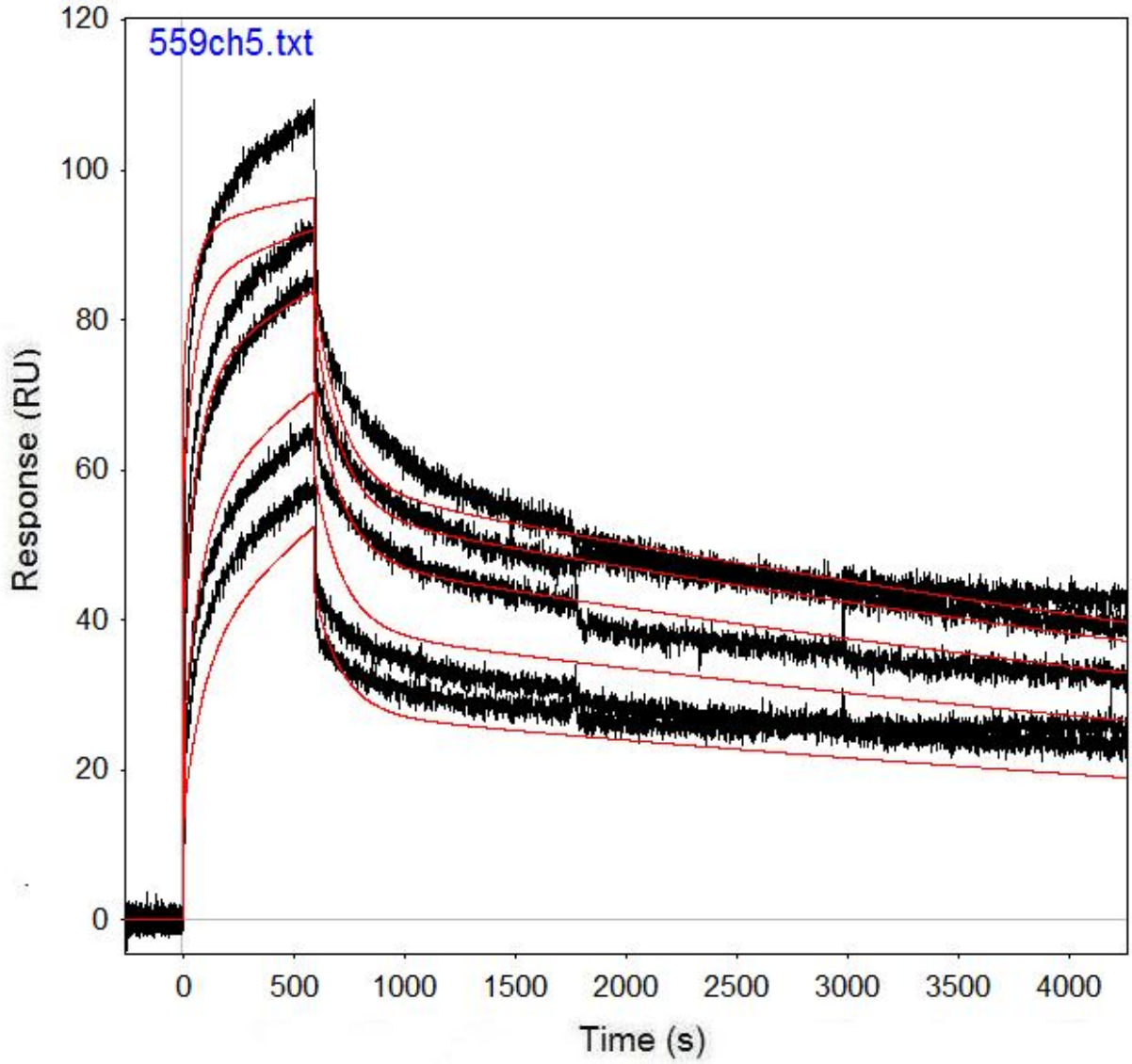

Figure B.124: Run 559, channel 5 model and data graph.

Table B.124: Run 559, channel 5 model parameters.

	kfwd1	krev1	kfwd2	krev2	kfwd3	krev3	ProA (RU)
Value	1.14E+10	4425	12312	0.000104	39421	0.00823	33.56
Error (abs)	1.35E+12	523400	58.68	8.11E-07	840.4	0.000142	0.03929
Error (%)	11836.6	11828.249	0.477	0.782	2.132	1.727	0.117

Run 574, channel 5: Performed at pH 6.5 in PBST, at an IgG concentration of 1.067 µm. RSSE is 3.299.

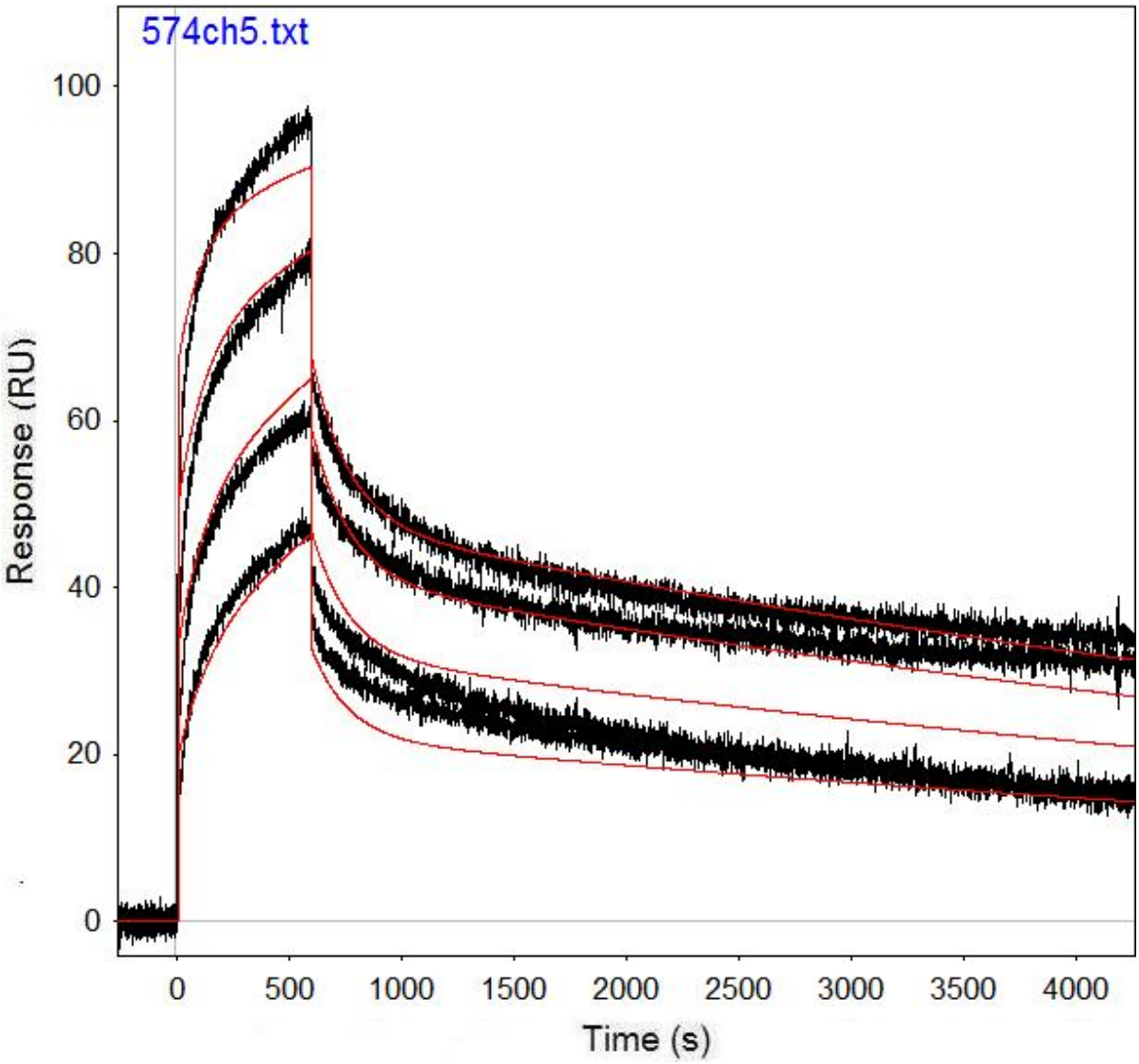

Figure B.125: Run 574, channel 5 model and data graph.

Table B.125: Run 574, channel 5 model parameters.

	kfwd1	krev1	kfwd2	krev2	kfwd3	krev3	ProA (RU)
Value	1.22E+10	3379	8927	0.000116	17386	0.006143	33.96
Error (abs)	5.67E+12	1565000	59.51	1.11E-06	539.2	0.00014	0.06427
Error (%)	46320.5	46315.478	0.667	0.958	3.101	2.281	0.189

Run 579, channel 4: Performed at pH 6.5 in PBST, at an IgG concentration of 3.0 µm. RSSE is 3.11.

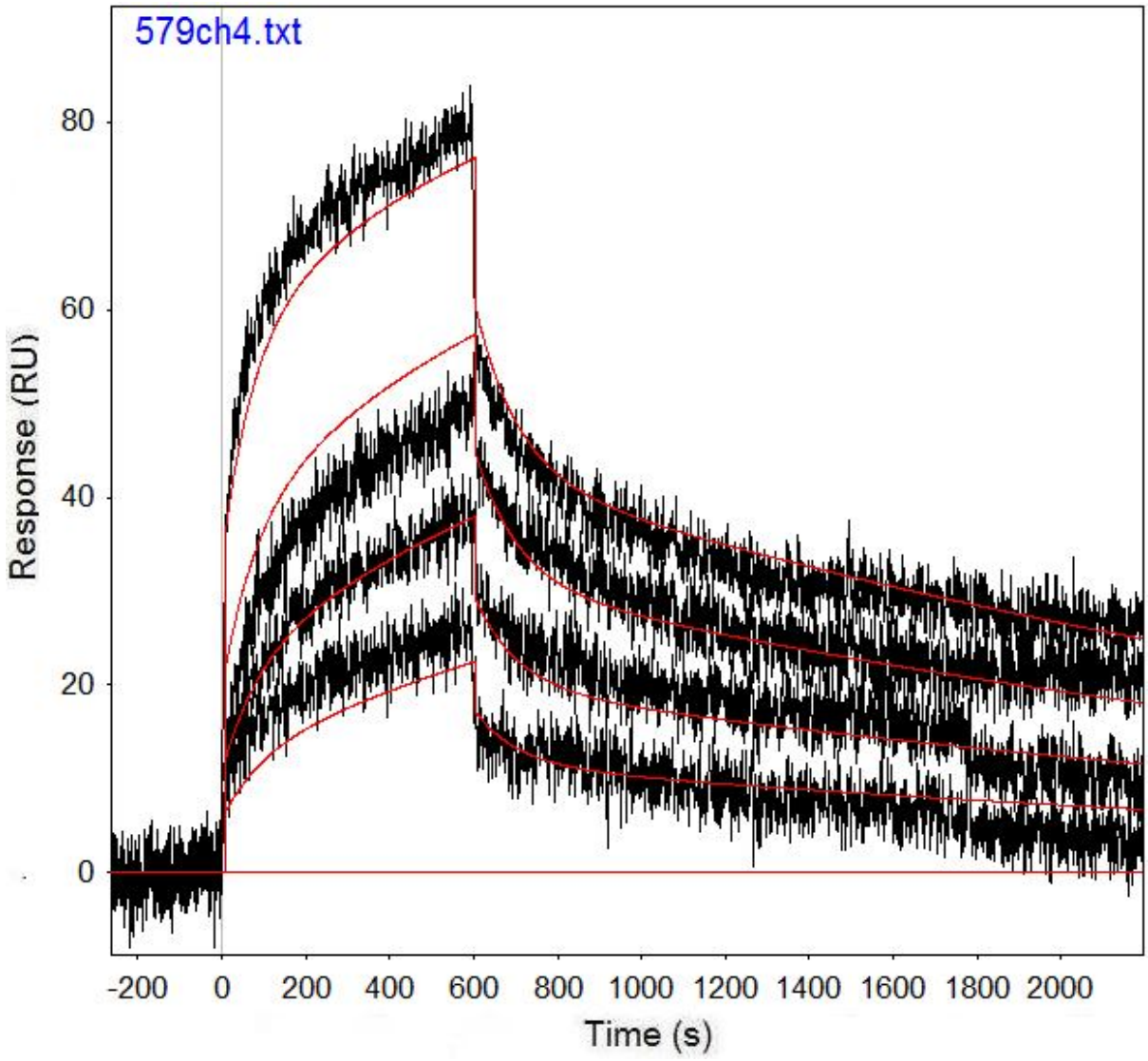

Figure B.126: Run 579, channel 4 model and data graph.

Table B.126: Run 579, channel 4 model parameters.

	kfwd1	krev1	kfwd2	krev2	kfwd3	krev3	ProA (RU)
Value	2.07E+09	12408	626.5	0.000338	1726	0.00996	35.96
Error (abs)	2.62E+12	15710000	7.04	5.73E-06	74.42	0.000357	0.1509
Error (%)	126544.4	126611.86	1.124	1.695	4.312	3.581	0.420

Run 598, channel 5: Performed at pH 7.0 in PBST, at an IgG concentration of 1.067 µm. RSSE is 3.17.

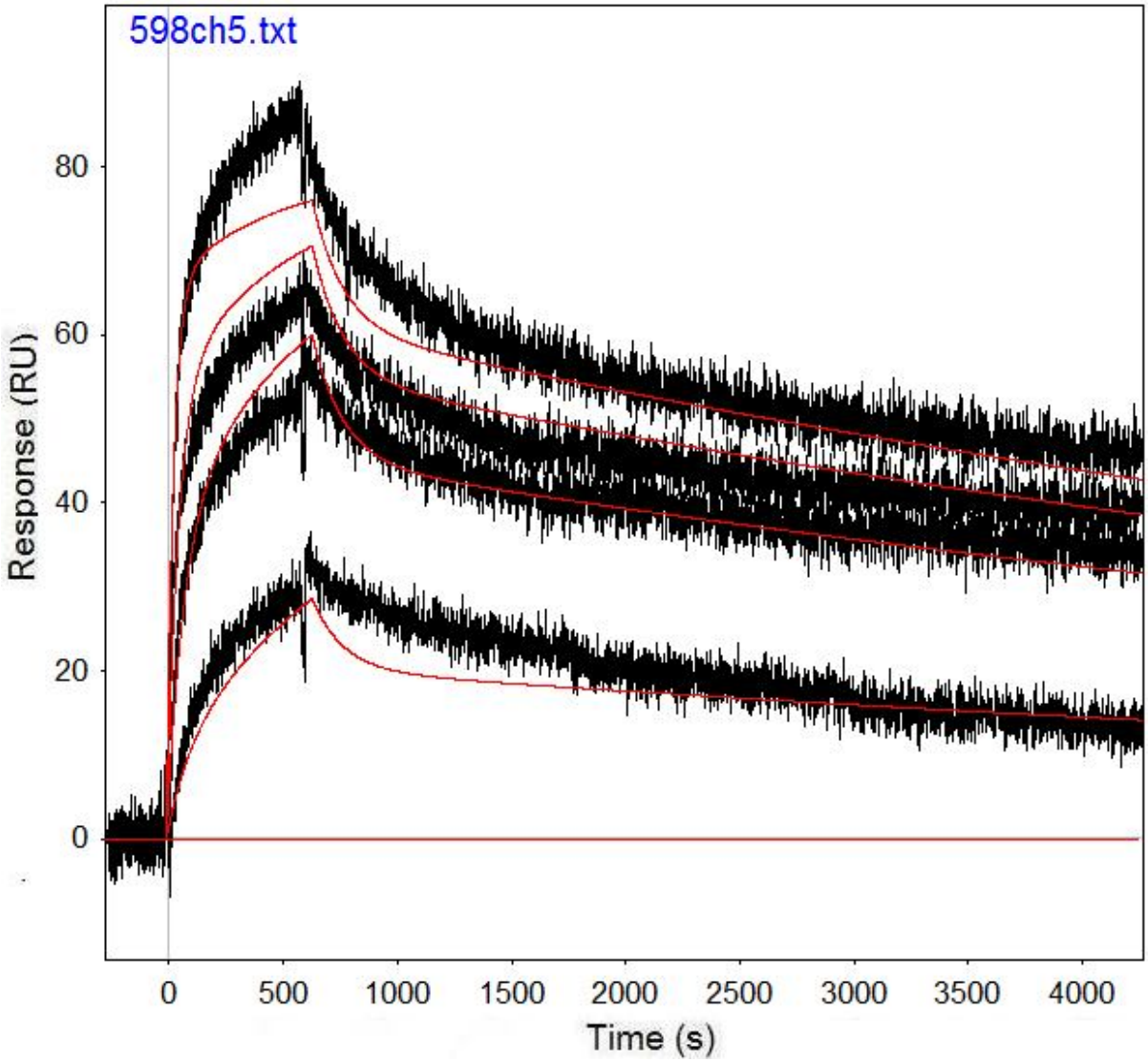

Figure B.127: Run 598, channel 5 model and data graph.

Table B.127: Run 598, channel 5 model parameters.

	kfwd1	krev1	kfwd2	krev2	kfwd3	krev3	ProA (RU)
Value	2553	4.652E-05	5331	0.000127	17242	0.007461	26.93
Error (abs)	186200	0.002667	186100	0.001548	306.5	0.000189	0.03731
Error (%)	7293.4	5733.0181	3490.902	1221.784	1.778	2.536	0.139

Run 603, channel 5: Performed at pH 7.0 in PBST, at an IgG concentration of 1.067 µm. RSSE is 1.765.

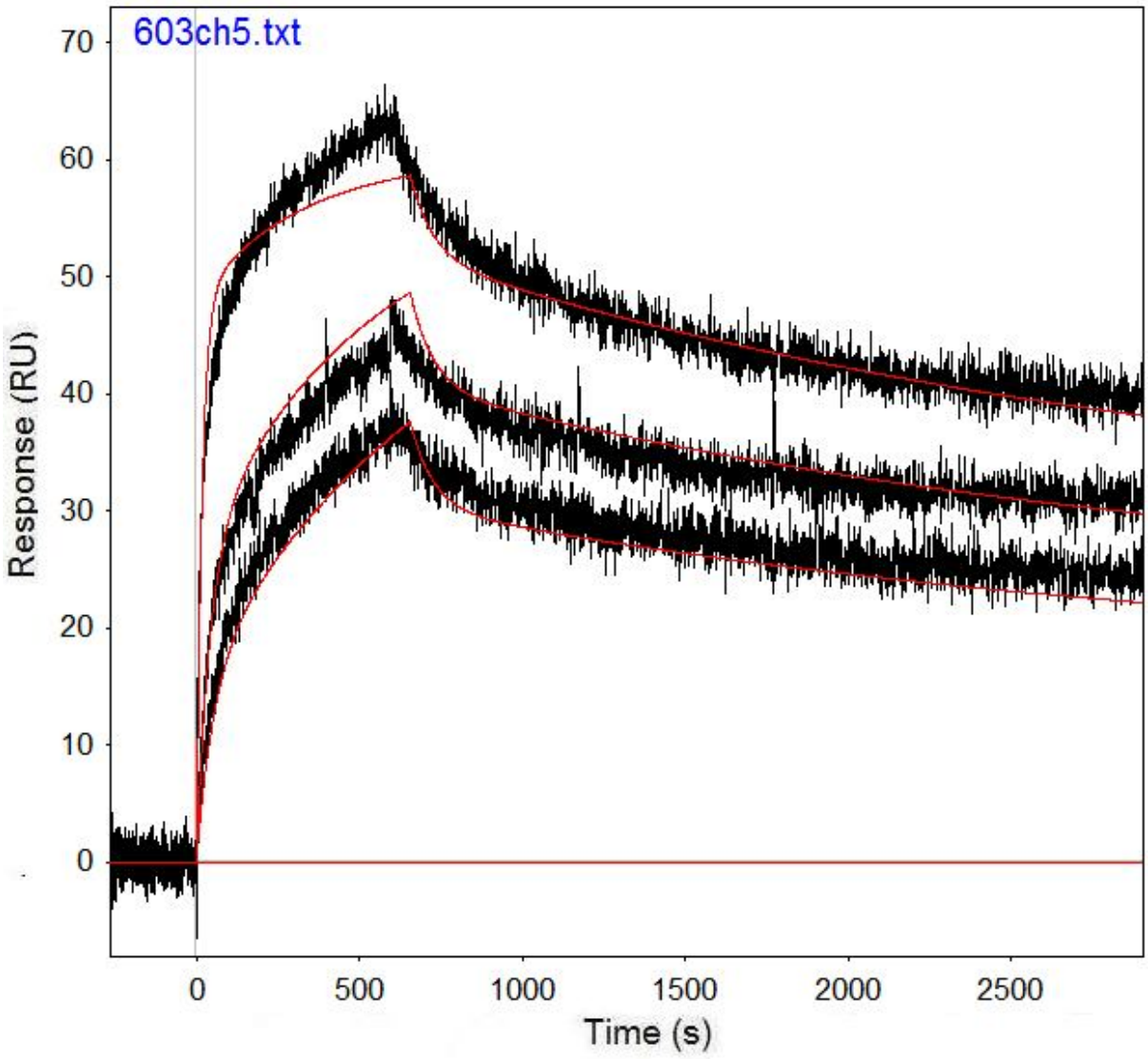

Figure B.128: Run 603, channel 5 model and data graph.

Table B.128: Run 603, channel 5 model parameters.

	kfwd1	krev1	kfwd2	krev2	kfwd3	krev3	ProA (RU)
Value	5539	0	5297	0.000401	31555	0.01451	20.39
Error (abs)	6886	0.0001882	6783	0.000371	664.9	0.000413	0.02231
Error (%)	124.3		128.054	92.377	2.107	2.849	0.109